Thermoreversible Gelation, Crystallization and Phase Separation Kinetics in Polymer Solutions under High Pressure

Jian Fang

Dissertation submitted to the Faculty of

Virginia Polytechnic Institute and State University

in Partial Fulfillment of the Requirements for the Degree of

Doctor of Philosophy

in

Chemical Engineering

Dr. Erdogan Kiran (Chair)

Dr. Richey M. Davis

Dr. Stephen Martin

Dr. Ross J. Angel

Sept, 10th 2008

Blacksburg, VA

Keywords: Phase Behavior, Phase Separation Kinetic, Gelation, Crystallization

Thermoreversible Gelation, Crystallization and Phase Separation Kinetics in Polymer Solutions under High Pressure

Jian Fang

Abstract

This thesis is an experimental investigation of phase behavior, crystallization, gelation and phase separation kinetics of polymer solutions in dense fluids at high pressures.

The miscibility and dynamics of phase separation were investigated in solutions of atactic polystyrene with low polydispersity (M_w = 129,200; PDI = 1.02) in acetone. Controlled pressure quench experiments were conducted at different polymer concentrations to determine both the binodal and the spinodal envelops using time- and angle resolved light scattering techniques. At each concentration, a series of rapid pressure quenches with different penetration depths in a range from 0.1 MPa to 3 MPa were imposed and the time evolution of the angular distribution of the scattered light intensities was monitored. The solution with 11.4 wt % polymer concentration underwent phase separation by spinodal decomposition mechanism for both shallow and deep quenches. Below this critical polymer concentration, phase separation was found to proceed by nucleation and growth mechanism for shallow quenches, but by spinodal decomposition for deeper quenches.

Gelation and crystallization processes and the influence of pressure and the fluid [Cho *et al.* 1993]composition were investigated in solutions of poly(4-methyl-1-pentene) [P4MP1] in n-pentane + CO_2 and in solutions of syndiotactic polystyrene [sPS] in toluene + CO_2, and also in acetophenone + CO_2 fluid mixtures over a pressure range up to 55 MPa and carbon dioxide levels up to 50 wt %.

In pure pentane, P4MP1 undergoes crystallization and leads to Form III polymorph at low pressures, but to Form II at high pressures. In n-pentane + CO_2 mixture fluids, the polymorphic state changes from a mixture of Forms III and II to Form II and eventually to

Form I with increasing CO_2 content. High level of carbon dioxide (≥40 wt %) in the solution was found to lead to gelation instead of crystallization. No liquid-liquid phase boundaries could be observed in any of the P4MP1 solutions.

In contrast to P4MP1 in n-pentane, syndiotactic polystyrene was found to undergo gelation in toluene or acetophenone forming a polymer-solvent compound with the δ crystal form. Also in contrast to P4MP1 systems, addition of carbon dioxide to sPS solutions alters the process from that of gelation to crystallization leading to the β crystal form. In solutions with high CO_2 level, in addition to the gelation or crystallization boundaries, a liquid-liquid phase separation boundary was also observed.

The phase separation path followed was found to influence the eventual morphology and the crystal state of the polymer. In sPS solutions in toluene + CO_2, if the sol-gel boundary were crossed first by cooling the solution at a fixed pressure, the resulting morphology was found to be fibrillar and the polymer displayed the δ crystal form. If instead, the liquid–liquid phase boundary were crossed first by reducing pressure at a fixed temperature, the polymer-rich phase leads to a stacked-lamellar morphology with the β crystal form while the polymer-lean phase leads to a mixed morphology with lamellar layers connected by fibrils with the polymer displaying δ + β crystal forms.

In solutions in acetophenone + carbon dioxide, when the gelation boundary is crossed first, the resulting structure is the δ form as in the toluene + CO_2 case. At comparable CO_2 levels, when the L-L phase boundary is crossed first, in the acetophenone system, polymer-rich phase was found to generate a mixture of δ + β forms while only the δ form was found in the polymer-lean phase, in contrast to the observations in the toluene + CO_2 systems.

Based on crystallographic, spectral and microscopic data, a thermodynamic framework was developed which provides a mechanistic account for the formation of the different polymorphs.

To my wonderful family

for the amazing support they have always provided

Acknowledgements

I would first like to express my deepest gratitude to my advisor, Dr. Erdogan Kiran, for his continuous guidance, support, trust, and encouragement throughout my study and research at Virginia Tech. His influence has been critical to my development as a research scientist. I thank him for being the most influential person in my professional life. I also thank him for being a wonderful professor, mentor, role model, and friend.

I would also like to thank the other committee members, Dr. Davis, Dr. Martin, Dr. Angel, Dr. Marand, and Dr. Marand (Chemistry) for their help throughout this study.

I am grateful to Mr. Michael Vaught and Riley Chan for their excellent help with building and maintaining the experimental equipments. I thank Crystallography Laboratory at Virginia Tech and Professor Oyama's lab for permitting the use of the x-ray facilities. I also thank Mr. Stephen McCartney for the help during SEM measurements. I thank my friends and colleagues in Dr. Kiran's ground, Wei Zhang and Kun Liu. I would also like to extend my acknowledgment to all of my friends in Blacksburg and teammates in the soccer team, without them the life out of lab would become colorless.

Finally, I would like to thank my family for their support throughout this process. I would like to show my sincerest gratitude to my mother, a strong woman, Zhuannan Gao. I want to say thank you to my elder brothers, Hui Wang and Jun Wang, for the support they have provided to me during my growing up years. I am deeply grateful to my wife, Jennifer Bai, for her great patience, encouragement, and dedication, for being the most important person in my life, and for being a wonderful mother of our lovely son, Alexander.

Table of Contents

Page

List of Tables

Page

List of Figures

Page

Chapter 1

Introduction

Understanding phase behavior and phase separation dynamics of polymers in fluids and fluid mixtures is important for many processes encountered in polymer science and engineering, including polymerization, purification, modification and post processing. The thermodynamic aspects such as the location of phase boundaries are important for selecting steady operation conditions. The dynamic aspects of phase separation in polymer systems deal with non-equilibrium relaxation processes that follow a transfer of the system from a thermodynamically stable to a thermodynamically unstable state. These transformations are usually induced by a temperature, composition, or pressure quench. The phase separation may proceed by a nucleation and growth or by spinodal decomposition. The time scale of phase separation and the mechanism influence the final structure of polymer materials, for example in formation of particle or microporous materials [Kiran 2000].

The kinetics of phase separation in "polymer + solvent" systems is of continuing interest [Kuwahara *et al.* 1982; Lal and Bansil 1991; Kojima *et al.* 1999; Hatanaka and Saito 2004; Lee *et al.* 2004; Lee *et al.* 2004]. The phase separation in polymer solutions can be induced by changes in the temperature, the solvent (concentration or composition) or the pressure. Lal and Bansil [Lal and Bansil 1991] studied the kinetics of spinodal decomposition of polystyrene solutions in cyclohexane induced by a temperature jump into the unstable region. Phase separation process was monitored by time- and angle-resolved light scattering at ambient pressures. Lee *et al*.[Lee *et al.* 2004] recently carried out a numerical study of temperature-induced phase separation kinetics of polymer solutions subjected to a linear spatial temperature gradient. Their results showed that anisotropic structures and morphologies can be induced by a gradient temperature jump. In addition to temperature

quench, phase separation can also be induced by exposing the solution to a nonsolvent vapor as antisolvent. An example of this is a study by Lee *et al*.[Lee *et al.* 2004] who reported the kinetics of phase separation in a polymer solution (polysulfone in N-methyl-2-pyrrolidinone) film induced by a nonsolvent vapor, water. The data were analyzed based on Cahn-Hilliard linear theory in the initial stages of phase separation.

In contrast to the situation with phase separation induced by temperature change or by concentration change, relatively little work has been done on the kinetics of phase separation processes induced by a pressure change. With the growing application of supercritical fluids in polymer processing, the effect of the pressure on phase separation is now attracting more interest. Compared to the thermal-induced or solvent-induced phase separation methods, the pressure-induced phase separation gives the distinct advantage in that relatively fast quench rates can be achieved uniformly within the system. In one of the earlier studies, Kojima et al.[Kojima *et al.* 1999] have reported the early stage of spinodal decomposition during phase separation of polypropylene solution in trichlorofluoromethane induced by pressure jump using time- and angle-resolved light scattering system. However, majority of the experimental studies on pressure-induced phase separation from high pressure solution that are in the open literatures appears to have been generated in Professor Kiran's laboratory [Xiong 1998; Xiong and Kiran 1998; Liu and Kiran 1999; Xiong and Kiran 2000; Liu and Kiran 2001].

Much attention has been paid to the phase behavior of polymers in compressed fluids at high pressures [Weidner *et al.* 1997; Chan and Radosz 2000; Kiran and Liu 2002; Zhang *et al.* 2003]. However, these have mostly focused on the liquid-liquid (L-L) phase boundary, with limited data on the solid-fluid (S-F) boundary. For crystallizable polymer-solvents systems, it is possible to observe the S-F boundary as well as L-L phase boundary in a phase diagram. Few specific systems reporting S-F phase boundaries in polymer solutions

in compressed fluid have been listed in an early publication [Kiran and Liu 2002; Zhang *et al.* 2003]. In these systems, both L-L phase boundaries and S-F phase boundaries are observed. In some polymer systems, beside the crystallization, thermoreversible gelation undergoes. In these solutions, instead of the fluid-solid phase transition, a sol-gel phase boundary is observed upon cooling.

Polymer gels are basically a network of flexible chains in which the connectedness is created either by a chemical or physical process. Physical processes which favor association between certain points on different chains lead to formation of physical gels which are often thermoreversible. According to De Gennes [De Gennes 1979], physical gels involve either helical structures with two or more strands, or microcrystals with two or more chains, or they result from the formation of nodules as is the case with block copolymers. In the absence of chemical bonds and specific interactions such as ionic, dipole or hydrogen bonds, crystallization becomes the mode of association [Girolamo *et al.* 1976]. A review by Keller [Keller 1995] provides a comprehensive description of both chemical and physical gels with specific details of those chemical processes such as polymerization and crosslinking, and those physical processes such as phase transitions and crystallization, entanglements, or associations that lead to gelation.

The utilization of super-critical fluids or dense fluids in processing of polymers has rapidly expanded in the past couple of decades. Recent attention has been focused on the morphological modification, as well as crystallization of polymeric material by using high-pressure fluid mixtures [Zhang *et al.* 2003; Zhang and Kiran 2006]. These systems are composed of ternary mixtures that are made up of polymer, organic solvent and CO_2. The binary fluid mixture that consist of an organic solvent (good solvent) and CO_2 (antisolvents) can be employed to dissolve a polymer with flexibility of altering the solvent strength with tuning concentrations or pressures towards the polymer. In addition to temperature and

pressure, manipulation of the concentration of CO_2 in the fluid mixture provides an effective method to control the mixing and demixing processes in the ternary polymer solution. The variation of the solvent strength, and hence the change in polymer-solvent interaction, also affect the conformational state of the polymer chains that are reflected as different crystal structures and morphological features in the polymer samples collect from these systems.

The main goal of this thesis is to further our understanding on the phase behavior and the kinetics of phase separation of selected polymers in fluid and binary fluid mixtures of an organic solvent and CO_2 under high pressure. Specifically, the kinetics of phase separation of polystyrene in acetone and the solid-fluid (S-F) and gel-sol (G-S) phase boundaries of poly(4-methy-1-pentene) (P4MP1) in n-pentane and n-pentane + CO_2 fluid mixtures and syndiotactic polystyrene in toluene, toluene + CO_2 fluid mixtures, acetophenone and acetophenone + CO_2 fluid mixtures fluid mixtures have been studied. The P4MP1 and sPS samples after crystallization or gelation from high pressure solutions were further characterized using solid state XRD, FTIR, NMR, SEM and DSC to obtain information on the crystal structure, melting behavior and morphology formed under pressure.

This thesis has been arranged in the following way. Chapter 2 is a brief review of the general theoretical background. The emphasis is on the theory on spinodal decomposition and on polymorphism in polymers. Chapter 3 presents the results of the experimental work and theoretical analysis on the kinetics of polystyrene solutions in acetone under high pressure. Chapter 4 presents the studies on phase behavior, crystallization and gelation of P4MP1 in n-pentane and n-pentane + CO_2. Chapter 5 and chapter 6 present the experimental results of gelation and crystallization of sPS in toluene with or without CO_2 and in acetophenone with or without CO_2 under high pressure respectively. Chapter 7 provides a broad review on thermoreversible gelation in synthetic polymers and proposes

the possible gelation mechanism for P4MP1 in n-pentane solution and sPS in toluene and acetophenone with addition of CO_2. Conclusions and recommendations are presented in Chapter 8.

The following publications have already appeared based on the present thesis research:

Jian Fang and Erdogan Kiran. Crystallization and Gelation of Isotactic Poly(4-methyl-1-pentene) in *n*-Pentane and in *n*-Pentane + CO_2 at High Pressures. *Journal of Supercritical Fluids* (2006), 38(2), 132-145.

Jian Fang and Erdogan Kiran. Kinetics of Pressure-Induced Phase Separation in Polystyrene + Acetone Solutions at High Pressures. *Polymer* (2006), 47(23), 7943-7952.

The following manuscripts have been submitted for publication based on the present thesis research. One is accepted and the other is under review.

Jian Fang and Erdogan Kiran. Thermoreversible Gelation and Polymorphic Transformations of Syndiotactic Polystyrene in Toluene and Toluene + Carbon Dioxide at High Pressures. Accepted for publication in *Macromolecules*

Jian Fang and Erdogan Kiran. Gelation, Crystallization and Morphological Transformations of Syndiotactic Polystyrene in Acetophenone and Acetophenone + Carbon Dioxide Mixtures at High Pressures. Submitted to the *Journal of Supercritical Fluids*

Chapter 2

Theoretical Background

2.1 Miscibility and Phase Separation in Polymer Solutions

2.1.1 Liquid-Liquid Phase Equilibrium

From a thermodynamic perspective, for complete miscibility of a mixture of two components consisting of a polymer and a solvent, the free energy change upon mixing must be negative ($\Delta G_m < 0$) and for binary mixtures, its second derivative with respect to composition must remain positive ($\left[\partial^2 \Delta G_m / \partial \phi^2\right]_{T,P} > 0$) (curve I in Figure 2.1(a)). In partially miscible systems, even though $\Delta G_m < 0$ for all composition, what shows an upward bend in a specific range of compositions identified by two compositions ϕ_{Ib} and ϕ_{IIb}, where first derivatives become identical ($\partial \Delta G_m / \partial \phi|_{Ib,T,P} = \partial \Delta G_m / \partial \phi|_{IIb,T,P}$). These compositions define the equilibrium compositions or binodal composition points at a specific temperature and pressure. Inside the binodal range, two other points known as spinodal points can be identified where the second derivatives of free energy change become zero ($\left[\partial^2 \Delta G_m / \partial \phi^2\right]_{T,P} = 0$), shown as ϕ_{Is} and ϕ_{IIs} on curve I in Figure 2.1 (a). Within the spinodal range, the second derivatives of ΔG_m become negative and the system become thermodynamically unstable leading to phase separation spontaneously. With a change in temperature or the pressure, the shape of ΔG_m, and consequently the compositions corresponding to binodal and the spinodal points can be changed, and the regions of miscibility and immiscibility can be altered. In Figure 2.1 (a), if T1>T2>T3>T4, the system becomes miscible with increasing temperature (in going from T4 to T1), showing an upper critical solution temperature (UCST), as shown in Figure 2.1

(b) and if T1<T2<T3<T4, the system becomes miscible with decreasing temperature (in going from T4 to T1), showing a lower critical solution temperature (LCST), as shown in Figure 2.1 (c). In Figure 2.1 (b) and (c), the loci of the binodal and spinodal points define the boundaries for the stable, metastable and the unstable regions of the system. The binodal and spinodal curves merge where the binodal and spinodal points become identical at specific temperature defining a critical solution temperature. However, holding temperature constant, complete miscibility is almost invariably achieved by increasing pressure, giving an upper critical solution pressure (UCSP) and the point where the binodal and spinodal curves merge together defines a critical solution pressure. (Also shown in Figure 2.1 (b))

Figure 2.2 shows 6 common forms of phase behavior of polymer solutions. Increasing the system pressure for a given solvent, or improving the nature of solvent at a given pressure may transform the phase behavior from one showing an hour-glass shaped region of miscibility (A) to a system showing LCST (C), UCST(D) or both UCST and LCST(B) and finally to one showing complete miscibility (F). Depending on the system, the extent of shift in the LCST and UCST may be different and the system may display only LCST (C) and UCST (D) in accessible range of temperatures. The scenario in E is less common, and represents an island of immiscibility [Kiran 2000].

In pressure-temperature (P-T) phase diagram, there are essentially only two types of phase diagram that describe the polymer solution at high pressures. As shown in Figure 2.3 (a), it is possible to induce the single phase solution to split into two phases by isobarically lowering temperature and crossing UCST curve or increasing the temperature and crossing LCST curve. Note that the LCST curve is more sensitive to pressure since it is typically at temperatures in the vicinity of solvent critical temperature where the solvent is highly compressible. Hence, increasing pressure decreases the molar volume of the solvent and

reduces the free volume difference between solvent and polymer and enhances the miscibility of polymer in solvent. Since the temperatures are fairly low and the phases below UCST are dense fluids, it is not surprising that the UCST curve is relatively insensitive to the pressure. When the two components in solution differ considerably with respect to their molecular size, the UCST curve shifts to higher temperatures and merges with the LCST curve to give the U-LCST type phase behavior shown in Figure 2.3 (b).

2.1.2 Solid-Liquid Phase Equilibrium

Polymers with sufficiently regular chain structures can exist in the crystalline state. Polymeric materials can rarely be made completely crystalline. When an amorphous polymer melt is cooled, crystallization commences at a temperature dependent on the rate of cooling and, more importantly, crystallization ceases before all amorphous state converts into crystalline state. Thus crystalline polymers are in reality "semi-crystalline". The review on the liquid-solid phase equilibrium in a semi-crystalline polymer solution will be presented in this section.

2.1.2.1 Solid-liquid Equilibrium in Binary System

The melting point of a substance is almost always lowered by the addition of a second component into the system. The phenomenon is well known as melting point depression. Departing from both melting points on each side of composition scale, in the simplest case, the two solubility curves intersect at the 'eutectic' point. The shape of phase diagram is schematically shown in Figure 2.4 [Koningsveld and Stockmayer 2001]. As shown in Figure2.4, the non-variant temperature T_e can be observed for any mixture. Such behavior is often observed in small component systems, such as the mixtures of Cadmium/Bismuth (Cd/Bi) [Aerts and Berghmans 1990]. In contrast with the small component, the eutectic crystallization is less commonly observed in polymeric system. For ideal eutectic system, the solubility curves can be expressed by the equation:

$$\ln x_2 = \frac{L_2^0}{R}\left(\frac{1}{T_{m2}^0} - \frac{1}{T_{m2}}\right) \tag{2.1}$$

where L_2^0 is the molar heat of fusion of pure component 2.

When the liquid phase is not ideal, the solubility curve will resemble a sigmoid shape. The equation 2.1 is modified by

$$\ln x_2 + g x_1^2 = \frac{L_{f,m2}^0}{R}\left(\frac{1}{T_{m2}^0} - \frac{1}{T}\right) \tag{2.2}$$

where $g = h/T$ depends on temperature. The concentration dependence of the melting temperature of component i is then given by

$$T = \frac{\Lambda_i + h(1 - x_i)^2}{\Lambda_i / T_{mi}^0 - \ln x_i} \tag{2.3}$$

where $\Lambda_i = L_{f,mi}^0 / R$. [Koningsveld and Stockmayer 2001]

Due to the low compressibility of solids, the effect of pressure on solubility curve in binary solid/liquid equilibrium is usually small.

2.1.2.2 Solid-Liquid Equilibrium in Polymer Solutions

For a polymeric system, the equation describing solid-liquid phase behavior is modified to:

$$\left(\frac{1}{T} - \frac{1}{T_{m2}^0}\right) = -\frac{R V_{u2}}{L_{u2}^0 V_s}\left[\frac{1}{\mathrm{m}_2}\ln x_2 + \left(\frac{1}{m_2} - \frac{1}{m_1}\right)x_1 + \chi x_1^2\right] \tag{2.4}$$

where V_s is the chosen molar volume of the lattice sites, V_{u2} is the molar volume of repeat unit in component 2. $\chi \equiv g$ (interaction parameter) is a composition independent parameter. This expression reduces under appropriate conditions to special non-polymeric systems presented earlier.

When both components are capable of crystallization, a eutectic point may be found at the

intersection of the two solubility curves. Usually, the pure melting point of a polymer is much greater than that of solvent, the eutectic concentration becomes too small to be detected in a polymer solutions.

If the liquid-liquid critical point is close to T_{m2}^{0} (the melting point of polymer), the melting point depression is small in full composition range, the solubility curve will interfere with the miscibility gap, forming a non-variant three-phase point. This situation is shown in Figure 2.4b which shows the solubility curve (1) representing binary solution in equilibrium with polymer crystals (2) and liquid-liquid miscibility gap (3) (showing a UCST). Upon cooling from a temperature above the miscibility gap, homogenous polymer solutions with a concentration between A and B will separate into two liquid phases l_a and l_b, and finally will reach the non-variant temperature T_3, where the polymer in both phase crystallizes. While cooling a solution from D point at concentration of X_2, instead of the liquid-liquid phase separation, the polymer crystals will appear and till the temperature reaches T_3, and all polymers crystallize. The type of phase diagram has been reported on the system of diphenylether/linear polyethylene [Aerts *et al.* 1993].

2.1.2.3 Solid Solutions

If the exchange of components is allowed in a crystal lattice, solid solution will be formed. In an extreme case, if replacement is possible in any composition in the binary system, the solid solution may be very close to an ideal solid solution, which shows a similar phase diagram as ideal liquid solution. Such complete miscibility in the solid state can be observed in the systems of, H_2O/D_2O, C_6H_6/C_6D_6 and even in a polymeric system isotactic polystyrene/poly(o-fluorostyrene) [Stehling *et al.* 1971]. While it is much more common to find quite limited miscibility in solid phases, since in most cases the two components have different crystal structures and the molecule from one component can not be easily fit into

the crystal lattice formed by the other. In some cases, the invasion of new molecules from one component does break the crystal lattice of the old one and form a new lattice structure, which usually is called as ‘compound’.

2.1.2.4 Compounds

Compound formation involving polymeric reactants has received a growing interest in recent years. The original of the occurrence of thermoreversible gelation in polymer solution has been proposed as the formation of polymer-solvent compounds [Guenet 1986]. To take insight into the mechanism of thermoreversible gelation, the knowledge on compounds is needed.

The formation of crystallizable compounds between the component atoms or molecules will affect the phase behavior of the solution. A compound is said to melt *congruently* at a given pressure, when the composition of the melt is identical to that of the compound. While a compound is defined as *incongruent* one if a new phase is formed during the melting of the compounds. The new phase can be solid, or a second liquid phase. If melting takes place without any dissociation, the compound is completely undissociated in solid, liquid and gas, the system in fact is a ternary system.

Figure 2.4c shows a typical phase diagram of the compound which dissociate congruently upon heating. As shown in Figure 2.4c, the compound S_{12} can melt congruently at T_1, and departure from S_{12}, two solubility curves go both sides. At T_2, the right-side branch of solubility curve of S_{12} intersects with that of S_2, forming a eutectic point $S_{12}/l/S_2$. And at the temperature of T_3, the left-side branch of solubility curve of S_{12} will meet with that of S_1, forming another eutectic point $S_{12}/l/S_1$. Systems showing congruent melting behavior has been known for a long time [Koningsveld and Stockmayer 2001] but have not been widely reported in polymeric systems. An example given by Point and Coutellier [[Point and

Coutelier 1985]] is on p-dibromobenzene/PEO.

If the melting temperature of polymer in Figure 2.4c were much higher, the solubility curve of the polymer might come to intersect the left branch of solubility curve of the compound and the compound S_{12} will melt incongruently. A qualitative representation is given Figure 2.4d. When the compound melts incongruently, the compound separate into two phases: a liquid phase (L) and a polymer crystalline phase (S_2). A well-known example of incongruent melting in the polymeric system is o-xylene/syndiotactic polystyrene [Deberdt and Berghmans 1994].

2.2 Kinetics of Phase Separation in Polymer Solution

The kinetics of phase separation in polymer systems that deal with non-equilibrium relaxation processes that follow a transfer of the system from a thermodynamically stable to a thermodynamically unstable state is the subject of many theoretical and experimental investigations. These transformations are usually induced by a temperature or pressure quench. The study on kinetics of phase separation of polymer mixtures or polymer solutions is important in polymerization and processing, as well as property modifications. Information on the time scale of phase separation coupled with polymer property knowledge provide the critical criteria needed to design and control the final structure of polymer materials in which transient structures can be locked in.

2.2.1 Pressure-Induced Phase Separation

The phase separation in polymer solutions can be induced by changes in the temperature, the solvent (concentration or type) or the pressure. In contrast to the situation with phase separation induced by temperature change or by concentration change, relatively little work has been done on the kinetics of phase separation processes induced by a pressure change. With the growing application of supercritical fluids in polymer processing, the effect of the

pressure on phase separation is now attracting more interest [Kiran 2000]. Compared to the thermally-induced or solvent-induced phase separation methods, the pressure-induced phase separation gives the distinct advantage in that fast quench rates can be achieved uniformly within the system.

In order to illustrate the kinetics of phase separation process, a typical pressure quench experiment is shown in Figure 2.5. The solution that is first homogenized and kept at conditions above the demixing pressures is quickly transferred to two-phase region by a sudden drop in pressure. The line ABC in Figure 2.5 represents just one path at a concentration along which one may enter the metastable region or the unstable region depending on the different penetration depths. In general, if the system is subjected to a shallow quench and brought into the metastable region (path AB), the phase separation takes place via the nucleation growth mechanism. In contrast, if the system is subjected to a deeper quench and brought into an unstable region (path AC), the separation proceeds via the spinodal decomposition mechanism. At the critical polymer concentration, where the binodal and spinodal curves merge together, the phase separation proceeds only by spinodal decomposition for both shallow and deeper quench (path DE).

In the nucleation process, nuclei with different sizes appear as a result of spontaneous concentration fluctuation. Among the new born nuclei, only those exceeding a critical size continuously grow, while those with smaller size dissolve into the bulk phase. Therefore, nucleation is an activated process involving a certain energy barrier. In contrast, spinodal decomposition is a truly spontaneous process and no energy barrier is involved. In this process, the homogeneous phase is unstable against concentration fluctuations with arbitrary amplitude exceeding a critical wavelength. In general, the nucleation and growth process often leads to the formation of droplets within continuous phase (as shown in Figure 2.6a), while spinodal decomposition initially leads to formation of co-continuous

phases (as shown in Figure 2.6b). A detailed review of the nucleation and growth theory is beyond the scope of this proposal. In the next section, the discussions are mainly focused on spinodal decomposition.

2.2.2 Spinodal Decomposition

Time-evolution of phase separation via spinodal decomposition may be classified into three stages: early stage, intermediate stage and late stage as shown in Figure 2.7. In the figure, ϕ_A represents the spatial concentration fluctuation of polymer A in the binary mixture AB at time t. ϕ_{A0} represents the average polymer concentration of polymer A in the whole system. The abscissa r represents characteristic wavelength. During the early stage of spinodal decomposition (SD), the characteristic wavelength L of the domain size does not change with time, only the concentration difference of the polymer A in A-rich phase and B-rich phase increases with time. The phase separation at this stage can be predicted by the Cahn-Hilliard theory [Cahn 1965]. In the intermediate stage, the concentration difference and the characteristic wavelength both increase with time. And in late stage, the concentration fluctuation reaches the equilibrium concentration and the domain size is coarsening without a change in concentration.

2.2.2.1 Cahn-Hilliard Linear Theory

The Cahn-Hilliard linear theory [Cahn and Hilliard 1958; Cahn 1959; Cahn and Hilliard 1959; Cahn 1961; Cahn 1965] was the first theoretical model of spinodal decomposition. Even though this theory is now considered to be only applicable to very short times after the phase separation begins, it provides a very useful intuitive understanding of the long wavelength instability and the nature of spinodal decomposition.

Consider an inhomogeneous solution whose composition everywhere only slightly differs

from the average composition, and with small composition gradients. Its free energy is given by

$$F = \int \left[f(c) + \kappa (\nabla c)^2 \right] dV \tag{2.5}$$

here $f(c)$ is the free-energy density of homogeneous materials of the composition c, $\kappa (\nabla c)^2$ is the additional free energy density if the material is in a gradient in composition, κ is the energy gradient parameter.

Now consider the continuity equation about the concentration fluctuation $c(\mathrm{r},t)$

$$\frac{\delta c(\mathbf{r},t)}{\delta t} = -\nabla.\mathbf{j}(\mathbf{r},t) \tag{2.6}$$

where the interdiffusion current $\mathbf{j}(\mathbf{r},t)$ is proportional to the gradient of chemical potential

$$\mathbf{j}(\mathbf{r},t) = -M\nabla\mu(\mathbf{r},t) = -M\nabla\frac{\partial F}{\partial c(\mathbf{r},t)} \tag{2.7}$$

Here M is the mobility, which is treated as a constant in the linear theory.

Combining equations 2.5, 2.6 and 2.7, one obtains the Cahn-Hilliard diffusion equation

$$\partial c/\partial t = M\nabla^2\left[-2\kappa\nabla^2 c + \frac{\partial^2 f}{\partial^2 c} \right] \tag{2.8}$$

Equation 2.8 can be solved by a simple exponential relation, which leads to

$$\partial c_q(\beta,t) = \partial c_q(\beta,0)\, exp\left[R(\beta)t \right] \tag{2.9}$$

where the growth rate $R(\beta)$ is given by

$$R(\beta) = -M\left(\partial^2 f/\partial c^2\right)\beta^2 - 2M\kappa\beta^4 \tag{2.10}$$

The behavior of $R(\beta)$ as function of β is shown in Figure 2.8. If the system is in the metastable region, where $\partial^2 f/\partial c^2 > 0$, then $R(\beta)$ is negative for all β and the amplitude of any concentration fluctuation decays exponentially. In contrast, if the system is brought

into unstable region inside the spinodal curve where $\partial^2 f/\partial c^2 < 0$, then the $R(\beta)$ is positive for a wavenumber in the range of $0 < \beta < \beta_c = \left(\frac{-\partial^2 f/\partial c^2}{2\kappa}\right)^{\frac{1}{2}}$, and the amplitude of any fluctuation increases exponentially with time. Thus, the system is unstable and phase separation takes place spontaneously. Furthermore, $R(\beta)$ shows a maximum value at a time-invariant wavenumber $\beta_m = \beta_c/\sqrt{2}$ indicating that the concentration fluctuation at wavelength of $2\pi/\beta_m$ has the fastest growth rate. For $\beta_c < \beta$, even though the system is in the unstable region, the concentration fluctuation at wavelength smaller than $2\pi/\beta_c$ decays exponentially.

The structure factor $S(q,t)$ at time t after the quench is:

$$S(q,t) = \langle \partial c_{-q}(t) \partial c_q(t) \rangle \tag{2.11}$$

where the brackets denote an thermal average over sample volume. Then also exhibits a simple exponential relaxation:

$$S(q,t) = S(q,0)\exp[2R(q)t] \tag{2.12}$$

Here $S(q,0)$ is the structure factor at $t = 0$.

The key prediction from Cahn-Hilliard theory is that, the initial stages of the spinodal decomposition should produce an exponential growth in the scattering light intensity for $q < q_c$, with a peak at a time-independent wavenumber $q_m = q_c/\sqrt{2}$; while for larger wavenumber $q > q_c$, the fluctuations are exponentially damped to zero. In fact, the predictions by the linear theory are only valid at the very early stage after the quench is applied. Shortly after the phase separation begins, the linear approximation breaks down.

In the Cahn-Hilliard linear theory, $R(q)$ also depends on q and can be given by:

$$R(q)/q^2 = \mathrm{D}_{\mathrm{app}} q^2 \left(1 - q^2/2q_m{}^2\right) \tag{2.13}$$

where q_m is the wave number corresponding to the maximum growth rate of the fluctuations and $\mathrm{D}_{\mathrm{app}}$ is the apparent diffusion coefficient with the expression:

$$\mathrm{D}_{\mathrm{app}} = M\left(\frac{\partial^2 f}{\partial c^2}\right) \tag{2.14}$$

The plot of $R(q)/q^2$ vs. q^2 shows a linear behavior with a negative diffusion constant. The negative value of the diffusion coefficient is important in early stage of spinodal decomposition phase separation and causes the amplification of long wavelength fluctuation.

2.2.2.2 Cahn-Hilliard-Cook Theory

Based on the Cahn-Hilliard linear theory, Cook [Cook 1970] refined the theory by adding a random thermal noise term to Equation 2.8

$$\frac{\delta c(\mathbf{r},t)}{\delta t} = -\nabla.\mathbf{j}(\mathbf{r},t) + \xi(\mathbf{r},t) \tag{2.15}$$

Cook's modification was made only within context of linear theory, and still failed to predict coarsening process which is expected to happen after initial stage of phase separation. Langer [Langer 1971] later developed the fluctuation theory upon Cook's introduction of random thermal noise into the continuity equation. In order to include non-linear effects, the full expansion of the free energy fluctuation has to be used

$$\begin{aligned}\frac{\delta F}{\delta \mu(\mathbf{r})} &= -K\nabla^2\mu + \frac{\partial f(c_o+\mu)}{\partial \mu} \\ &= -K\nabla^2\mu + \left(\frac{\partial f}{\partial c}\right)_{c_o} + \left(\frac{\partial^2 f}{\partial c^2}\right)_{c_o} \mu + \sum_{n=3} \frac{1}{(n-1)!}\left(\frac{\partial^n f}{\partial c^n}\right)_{c_o} \mu^{n-1}\end{aligned} \tag{2.16}$$

Combining Equation 2.9, 2.15 and 2.16, the equation of motion for the structure factor can

be obtained

$$\frac{\partial S(q)}{\partial t} = -2Mq^2\left[\left(Kq^2 + \left(\frac{\partial^2 f}{\partial c^2}\right)_{c_o}\right)S(q) + \sum_3^{\infty}\frac{1}{(n-1)!}\left(\frac{\partial^n f}{\partial c^n}\right)_{c_o} S_n(q)\right] + 2MK_BTq^2 \quad (2.17)$$

where $S_n(q)$, the higher order structure factor, are the Fourier transforms of the higher order two-point correlation functions

$$S_n\left(|\vec{r} - \vec{r}_o|\right) = \left\langle \mu^{n-1}(\vec{r})\,\mu(\vec{r}_o)\right\rangle \quad (2.18)$$

Here if we neglect all of the higher-order terms in (2.17), we obtain Cook's linear equation of motion for S:

$$\frac{\partial S(q)}{\partial t} = 2R(q)S(q) + 2MK_BTq^2 \quad (2.19)$$

where the amplification factor, $R(q)$, is given by

$$R(q) = -Mq^2\left(Kq^2 + \frac{\partial^2 f}{\partial c^2}\right) \quad (2.20)$$

Langer *et al*. [Langer *et al.* 1975] proposed a truncation scheme (LBM approach). By using the assumption that the one-point probability density function for concentration fluctuation is of the form of two Gaussian functions, they decoupled the equation for the probability density function and the equation of motion equation and generated that

$$\frac{\partial S(q)}{\partial t} = -2Mq^2\left(Kq^2 + A(t)\right)S(q) + 2MK_BTq^2 \quad (2.21)$$

The term, $2MK_BTq^2$, accounts for the thermal noise. Even though the analytical expression for $A(t)$ is not possible, the qualitative behavior of $S(q)$ is still clear. By introducing a time-dependent term $A(t)$ into $R(q)$, the time-independent $R(q)$ in the linear theory now becomes a time-dependent $R(q,t)$, and the growth of $S(q)$ is no longer exponential in time. Then, at a given time t, a maximum in $R\left(q, t = t^*\right)$ still exists but with a

time-dependency $q_m(t) = \sqrt{-\frac{A(t)}{2K}}$. Since $|A(t)|$ decreases with time, $q_m(t)$ shifts to the smaller q numbers, this is the origin of the coarsening due to nonlinear effects.

2.2.2.3 Power Law Approximation and Scaling Analysis

A number of approaches have been taken to describe the coarsening process of phase separation. Among the approaches, power law approximation was usually applied for phase separation dynamics [Hashimoto *et al.* 1986; Binder and Fratzl 2001]. For example, the time (t) dependence of the average concentration correlation length (q_m) is often assumed to be given by

$$q_m(t) \approx t^{-\alpha} \tag{2.22}$$

and the time dependence of the maximum scattered light intensity (I_m) is given by

$$I_m(t) \approx t^{\beta} \tag{2.23}$$

Langer [Langer *et al.* 1975]developed the full set of nonlinear equations which describes the phase separation process, and using numerical techniques to solve the nonlinear equation found that $\alpha = 0.212$ and $\beta = 0.81$. Taking a different approach, Binder [Binder *et al.* 1978] described spinodal decomposition using the reactive cluster model which describes the limit where the kinetic activation barrier to phase separation is finite but much smaller than the available thermal energy. In the low temperature limit, the reactive cluster model predicts $\alpha = 1/(d+3)$ and $\beta = 3/(d+3)$ (where d is the system dimensionality), while in intermediate temperature limit $\alpha = 1/(d+2)$ and $\beta = 3/(d+2)$. Siggia [Siggia 1979] proposed a surface tension driven mechanism, predicting the highest exponent $\alpha = 1$

Besides the length scale of the domain, the structure factor $S(q,t)$ has also been hypothesized to follow a scaling behavior. Furukawa [Furukawa 1985] proposed an idea of the dynamical scaling in that the structure function $S(q,t)$ or the scattering function $I(q,t)$ of the unmixing systems at time t can be scaled with a single length parameter $L(t)$

$$S(q,t) \sim L(t)^d \tilde{S}(qL(t)) \tag{2.24}$$

With a universal scaling function $\tilde{S}(x)$

$$\tilde{S}(x) \sim \frac{x^2}{\gamma/2 + x^{2+\gamma}}, \tag{2.25}$$

where d is the dimensionality of the system, and q is the scattering vector. The quantity x is defined as

$$x = qL(t) = q/q_m \tag{2.26}$$

and γ is defined as

$$\gamma = d+1 \quad \text{for the off-critical mixture} \tag{2.27}$$

$$\gamma = 2d \quad \text{for the critical mixture} \tag{2.28}$$

2.3 Polymorphism in Polymers

Polymorphism is defined as the ability of a substance to exist in more than one crystalline structure. The phenomenon is important technologically in a number of industries including chemical engineering and pharmaceutical development. Polymorphism is also widespread phenomenon in polymers; almost all crystalline polymers are polymorphic, if the right conditions for crystallization for the different crystalline forms can be found [Corradini and Guerra 1992].

The polymorphic crystalline structures of polymers can be formed by packing of polymer chains which having different conformations or by packing of polymer chains having same conformations into different modes corresponding to different unit cells. Most of polymorphic structures in crystalline polymers fall into these two categories [Corradini and Guerra 1992].

This section is organized in the following way. In the first subsection, the polymorphic structures in different polymers are reviewed. In the second subsection, the techniques for characterization of the polymorphic structures in polymer are also reviewed.

2.3.1 Polymorphic Structures in Polymers

2.3.1.1 Syndiotactic Polystyrene

Syndiotactic polystyrene (s-PS) presents a very complex polymorphic behavior [Immirzi *et al.* 1988; Gomez *et al.* 1990; Gomez and Tonelli 1990; Guerra *et al.* 1990]. Mainly, two crystalline forms, α and β, containing planar zigzag chains with an identity period of 5.1 Å and two forms, γ and δ, containing 2_1 helical chains with an identity period close to 7.7 Å (generated by *trans trans gauche gauche* (TTGG) conformational sequence) were formed by crystallization from melts and solutions. Two helical conformational structures are shown in Figure 2.9.

The α form can be obtained by compression moulding, and the β form can be formed by solvent casting at 170 ℃ from o-dichlorobenzene solutions. Both of these forms are characterized by an identity period of 5.1 Å, corresponding to planar zigzag chain conformation. The α form has a hexagonal unit cell, while the β form has an orthorhombic unit cell. And the forms having an identity period of 7.7 Å can be obtained by swelling of samples of the α form in different solvents. The γ form is formed by swelling α form by

dichloromethane and then completely desiccating, while for swelled samples, the structure changes with the different solvents; indicating the inclusion of molecules of the solvent into the crystalline structure. For these variable crystalline structures of s-PS, which include molecules of solvent with formation of a 'polymer-solvent compound', are called the δ form [Rizzo *et al.* 2005]. The DSC [Immirzi *et al.* 1988] and IR [Reynolds *et al.* 1989] observations on the γ form samples show that a solid-solid phase transition from γ form to α form occurs at 190-200 °C and also this transition is irreversible. The α form has a melting temperature at around 270 °C [Gomez and Tonelli 1991].

The s-PS crystalline phases differ greatly in their densities [D'Aniello *et al.* 2005]. In fact, densities difference of the γ form (1.10 g/cm^3), β form (1.078 g/cm^3), α form (1.034 g/cm^3) and δ form (0.977 g/cm^3) phases with respect to the amorphous phase (1.05 g/cm^3), are of nearly +5, +2,5, -1.5 and -7 %, respectively. The unusual large reduction of density of the δ form crystalline phase is due to the presence of well characterized crystalline cavities, in which the solvent molecules can be incorporated.

The detailed unit cell information for the different polymorphic structures is given in table 2.1.

2.3.1.2 Isotactic Polystyrene

Isotactic polystyrene has a polymorphic behavior involving packing of chains having completely different conformations. The classical conformation of iPS is a 3_1 helical structure [Natta and Corradini 1955] that appears in the samples after melting crystallization. Under suitable experimental conditions, iPS can produce crystallization gels, in which the chains assume a nearly extended 12_1 helical conformation [Atkins *et al.* 1977]. The two possible conformations proposal for two crystalline forms of iPS are shown in Figure 2.10.

2.3.1.3 Poly(vinylidene fluoride)

Poly(vinylidene fluoride) PVDF is one of the chemically simplest fluorinated polymers, having the monomer unit CH_2CF_2. PVDF is known to show extensively complex polymorphism. Five different crystalline modifications have been reported [Lovinger 1983].

The most common polymorph of PVDF is the α form, which may be obtained by crystallization from the melt at atmospheric pressure. The chain conformation of the α form has been shown to be TGTG'. The unit cell has been reported as being monoclinic with all unit cell angels equal to 90°, with experimental error and with cell dimension of a = 0.496, b = 0.964 and c = 0.462 nm [Bachmann and Lando 1981]. The unit cell of α form PVDF consists of two chains with same conformations, whose dipole moments normal to the chain axes are antiparallel, thus neutralizing each other, resulting in a nonpolar unit cell.

A polar analog of the α form, so called δ form, can be produced by application of a high electric field to films of α form. In effect, this involves rotation of every second chains by 180° about its axis in each α form unit cell, so that molecules are now packed with their dipole moments pointing to this same direction, resulting in a polar unit cell. It is generally believed that the chain conformation and the unit cell dimension are similar to that of the α phase and that the two chains in the cell pack such that their dipoles reinforce rather than cancel each other.

The third known polymorph of PVDF is known as the β form. It is most commonly prepared by relatively low temperature mechanical deformation of the α form. The β form has been shown to consist of planar (or nearly planar) zigzag chains (TTTT) packed into an orthorhombic unit cell with dimension of a = 0.858, b = 0.491 and c = 0.256 nm.

Another known polymorph of PVDF is known as the γ form. The γ form can be produced directly from α form by annealing at high temperature and pressure or by various temperature-pressure thermal treatments of both α form and β form, or crystallization from dimethyl sulfoxide, dimethylacetamide and dimethylformamide solutions. It was found that γ form has chains conformation of T_3GT_3G' packing in a monoclinic unit cell with a = 0.496, b = 0.967 and c = 0.920 nm and β = 93° [Weinhold *et al.* 1980; Lovinger 1981]. There is a solid-state form α form to the thermodynamically more stable γ form occurring at high temperature ~ 160 °C through limited intramolecular motions. The γ form can be readily transformed to the β form under mechanical deformation. A nonpolar analog of γ form (ε- form) PVDF has also been reported but may exist only within a mixture of phases obtained at very high temperatures.

The structural characterization of different crystalline forms is briefly summerized in Table 2.2.

2.3.1.4 Isotactic Poly(butene-1)

Isotactic poly(butene-1) exhibits four crystalline forms: Form I and Form I', hexagonal with a 3_1 helix [Holland and Miller 1964]; Form II tetragonal with a 11_3 helix [Turner-Jones 1963]; and orthorhombic Form III with a 4_1 helix [Cojazzi *et al.* 1976]. Form I was formed via a solid state transformation from Form II whereas Form I' is the same crystalline structure crystallized from solutions [Holland and Miller 1964]. The difference between Form I and Form I' is that Form I is twined, however the Form I' is untwined. The unstable Form II crystallizes during cooling of the melt, which is kinetically favored. Usually, From III is generated from solutions and is a relatively stable crystalline form in room temperature. The structural characterization of different crystalline forms is briefly listed in Table 2.3.

2.3.1.5 Isotactic Polypropylene

Isotactic polypropylene (iPP), one of the most important semicrystalline commercial polymers, presents a complex polymorphism in the solid state. It has been widely reported that iPP can form three crystalline phases: α, β, γ and the mesomorphic 'smectic' phase [Bruckner *et al.* 1991; Lotz *et al.* 1996; Phillips and Mezghani 1996]. Basically, the chain conformation of each phase is a 3_1 helix. The polymorphism of iPP arises from different packing of the helix into the unit cell.

The prevalent and most widely studied modification is the α form obtained by crystallization from the melt and solutions. The structure of the α form was first proposed by Natta and Corradini (1960) and then confirmed by successive studies [Mencik 1972; Hikosaka and Seto 1973], containing four chains in 3_1 helical conformation with alternating rows of right- and left- hand helices. The four possible chain conformations are given in Figure 3. The α form actually has two variants, the most stable α_2 form ($P2_1/c$) with order in up and down direction of the methyl-groups, and less stable α_1 form (C_2/c) with random up-down direction of the methyl-groups. The transition from α_1 to α_2 can be made by annealing the α_1 form near the melting point.

The β form of iPP was first identified in 1959 by Keith et al.[Keith *et al.* 1959]. The β form is normally referred to as 'hexagonal iPP'. The β form can be obtained by crystallization in a temperature gradient [Lovinger *et al.* 1977], from melt under shear [Leugering and Kirsch 1973] or in presence of nucleating agents [Li and Cheung 1999].

The γ form was first mentioned by Addink and Beintema [Addink and Beintema 1961], who reported some diffraction lines which could not be accounted for by α or β form. The main way of obtaining a virtually pure γ phase in common PP is crystallization at elevated pressures [Teramoto *et al.* 2004]. At atmospheric pressure, the γ phase is produced under

special conditions, in particular, by crystallization of low-molecular-weight fraction of PP [Bruckner and Meille 1989] or polypropylene derived copolymers with a small amount of ethylene [Dean and Register 1998]. As for the β form, all attempts to obtain oriented fibers of γ phase produced only a transformation into the oriented α form crystals.

The structural characterization of different crystalline forms of isotactic polypropylene is summarized in Table 2.4.

2.3.1.6 Poly(4-methyl-1-pentene)

Isotactic poly(4-methyl-1-pentene) (iP4MP1) is a semicrystalline polyolefin which presents a complex polymorphic behavior. Five different crystalline forms have been reported for this polymer when crystallized from semidilute solutions depending on the solvent and thermal history of the crystallization [Charlet and Delmas 1984; Charlet *et al.* 1984].

Form I is the most stable crystalline form which is the only one obtained from melt crystallization. It can be also obtained by crystallization from solutions of high-boiling point solvents, like normal alkanes with number of carbon atoms greater than 9, branched dodecane and branched decane [Charlet and Delmas 1984]. Form I is characterized by chains in 7_2 helical conformation packed in a tetragonal unit cell [Kusanagi *et al.* 1978].

Form II was prepared for the first time by isothermal crystallization at 20 °C from dilute xylene solutions, and later, by crystallization from tetramethyltin solution, or as a minor component in a mixed structure crystallized in carbon disulfide solutions. A tetragonal unit cell and chains in 4_1 helical conformation have been proposed by Takayanagi *et al*. [Takayanagi and Kawasaki 1967] from x-ray diffraction pattern on single crystal mats.

Form III can be obtained from xylene (by isothermal crystallization at 65 °C and decalin

solutions, as well as linear (5-7 carbon atoms) and branched (6-9 carbon atoms) alkanes. It is also obtained in carbon tetrachloride and cycloalkanes containing 6-10 carbon atoms. The crystalline structure of Form III has been determined as a tetragonal unit cell containing chains in 4_1 helical conformation. Form III transforms into Form I by annealing at ca. 100 °C or under stretching [Charlet and Delmas 1984].

Form IV was obtained by annealing Form I above 200 °C under pressure up to 4500 bar [Hasegawa *et al.* 1970]. The same crystalline modification can also be obtained by crystallization from cyclopentane solutions. Stretching of an unoriented sample in Form IV leads to a fiber in Form I; however, partially oriented sample in Form IV and well oriented sample have been obtained by swelling fibers of Form I in saturated cyclopentane vapor at 50 °C. From the X-ray fiber diffraction and solid-state ^{13}C NMR spectrum, a 3_1 helical conformation of the chains has been proposed for Form IV with suggestion of a hexagonal unit cell.

A Form V crystalline structure has been reported for gels formed in cyclopentane and cyclohexane [Charlet and Delmas 1982]. The structure of Form V has not yet been determined.

The chain conformations for different crystalline modifications, Form I, II, III and IV are given in Figure 2.12 and the structural characterization is summarized in Table 2.5.

2.3.2 Techniques for Characterization Polymorphs of Polymers

2.3.2.1 X-ray Diffraction

The X-ray diffraction techniques are unique in providing detailed information on the structural organization at the molecular level in the different crystalline forms of a polymer. Different unit cells or the same unit cell with different packing modes for crystalline

polymer will give different diffraction patterns. Almost all of the polymorphism in polymers is first identified by this method. The X-ray diffraction patterns of the four syndiotactic polystyrene crystalline forms as well as a clathrate form are showed in Figure 2.13 [Rizzo *et al.* 2002].

Even though the X-ray diffraction techniques have their advantage for determination of different crystalline structures, there are other characterization techniques which are sensitive to the chain conformation and in some cases to the chain packing, which can be used more efficiently than diffraction techniques in the recognition and quantification of the different polymorphs in polymeric materials. In the following, the application of Fourier transform infrared (FTIR) spectroscopy to the study of polymorphism in polymers is briefly described, and then solid-state ^{13}C nuclear magnetic resonance (NMR) is introduced.

2.3.2.2 FTIR

Several bands of FTIR spectra are conformationally sensitive. It is easy to distinguish between polymorphic forms displaying different chain conformations. For instance, in the case of the α and γ forms of sPS, having trans-planar and 2_1 helical conformations, respectively, the different FTIR spectra are obtained. Also well-defined differences exist between spectra of samples in the α and β crystalline forms (even though both chains contain trans-planar conformation) in two different regions as shown in Figure 2.14 [Guerra *et al.* 1990].

In the identification of different polymorphs in polymers the FTIR technique presents, with respect to the diffraction techniques, the advantages of easier and more rapid measurement. In particular, the high speed of the measurements allows studying the polymorphic behavior under dynamic conditions. The FTIR technique has also advantage of being easily

associated to other techniques. For instance, the FTIR microscopy, which couples the visible image of samples to the corresponding infrared spectra, allows the selection of microaeras of interest, and thus an easy determination of the crystalline forms corresponding to different regions, in samples in which more than one polymorph is present.

2.3.2.3 ^{13}C Solid-State NMR

As first suggested and demonstrated by Schaefer and Stejskal [Schaefer and Stejskal 1976], combination of the techniques of high-power H^1 dipolar decoupling, rapid magic-angle spinning (MAS), and cross-polarization (CP) of ^{1}H and ^{13}C nuclear spins permits the observation of high resolution ^{13}C NMR spectra for solid samples. This is an important advancement on the characterization of polymers by NMR spectroscopy, because we may now observe their structures and dynamics in the solid state, where they most often stand.

Recording the ^{13}C CPMAS solid state NMR spectra of polymers makes possible the observation of the chemical shift (δ) and the relaxation parameters for each resolvable carbon nucleus. The observations provide information concerning the conformations and packing of solid polymers. As a consequence of restricted internal mobility in molecules in the crystalline state, nuclei in different conformation environment or packing methods, can produce different signals in ^{13}C CPMAS NMR spectra. An example of using this method on the P4MP1 system is given in Figure 2.15 [De Rosa *et al.* 1997].

Table 2.1 Structural characterization for the crystal forms of syndiotactic polystyrene

Form	Crystal System	Helix	Unit Cell				Ref
			a (nm)	b (nm)	c (nm)	γ (°)	
α	Hexagonal	Zig-zag	2.625	2.625	0.5045		[Greis *et al.* 1989]
	Trigonal	Zig-zag	2.626	2.626	0.504		[De Rosa 1996]
β	Orthorhombic	Zig-zag	0.881	2.882	0.51		[Chatani *et al.* 1993]
γ		2_1	no unit cell parameters were reported yet				
δ (toluene)	Monoclinic	2_1	1.758	1.326	0.771	121.2	[Chatani *et al.* 1993]
δ (norbornnadiene)	Monoclinic	2_1	1.75	1.45	0.78	107.8	[Petraccone *et al.* 2005]

Table 2.2 Structural characterization for the crystal forms of poly(vinylidene fluoride)

Form	Crystal System	Chain Conformation	Unit Cell				Ref
			a (nm)	b (nm)	c (nm)	β (°)	
α	Monoclinic	TGTG'	0.496	0.964	0.462	~ 90	[Bachmann and Lando 1981]
β	Orthorhombic	TTTT	0.858	0.491	0.256		[Lando *et al.* 1966]
γ	Monoclinic	T_3GT_3G'	0.496	0.967	0.920	93	[Weinhold *et al.* 1980; Lovinger 1981]

Table 2.3 Structural characterization for the crystal forms of isotactic poly(butene-1)

Form	Crystal System	Helix	Unit Cell			T_m (°C)	Ref
			a (nm)	b (nm)	c (nm)		
I	Hexagonal (twined)	3_1	1.77	1.77	0.65	120-135	[Kaszonyiova *et al.* 2005]
I'	Hexagonal (untwined)	3_1	1.77	1.77	0.65	90-100	[Kaszonyiova *et al.* 2005]
II	Tetragonal	11_3	1.46	1.46	2.12	110-120	[Lotz and Thierry 2003]
III	Orthorhombic	4_1	1.25	0.89	0.76	90-100	[Holland and Miller 1964]

Table 2.4 Structural characterization for the crystal forms of isotactic polypropylene

Form	Crystal System	Helix	Unit Cell				Ref
			a (nm)	b (nm)	c (nm)		
α	monoclinic	3_1	0.665	2.096	0.65	β = 99.3°	[Natta and Corradini 1960]
β	Hexagonal	3_1	0.636	0.636	0.649		[Turner-Jones 1963]
γ	Triclinic	3_1	0.654	2.140	0.650	α = 89.0° β = 99.6° γ = 99.0°	[Morrow and Newman 1968]

Table 2.5 Structural characterization for the crystal forms of poly(4-methyl-1-pentene)

Form	Crystal System	Helix	Unit Cell			ref
			a	b	c	
I	Tetragonal	7_2	1.866	1.866	1.380	[Kusanagi *et al.* 1978]
II	Tetragonal	4_1	1.916	1.916	0.712	[Takayanagi and Kawasaki 1967]
III	Tetragonal	4_1	1.946	1.946	0.702	[De Rosa *et al.* 1994]
IV	Hexagonal	3_1	2.217	2.217	0.650	[De Rosa 1999]

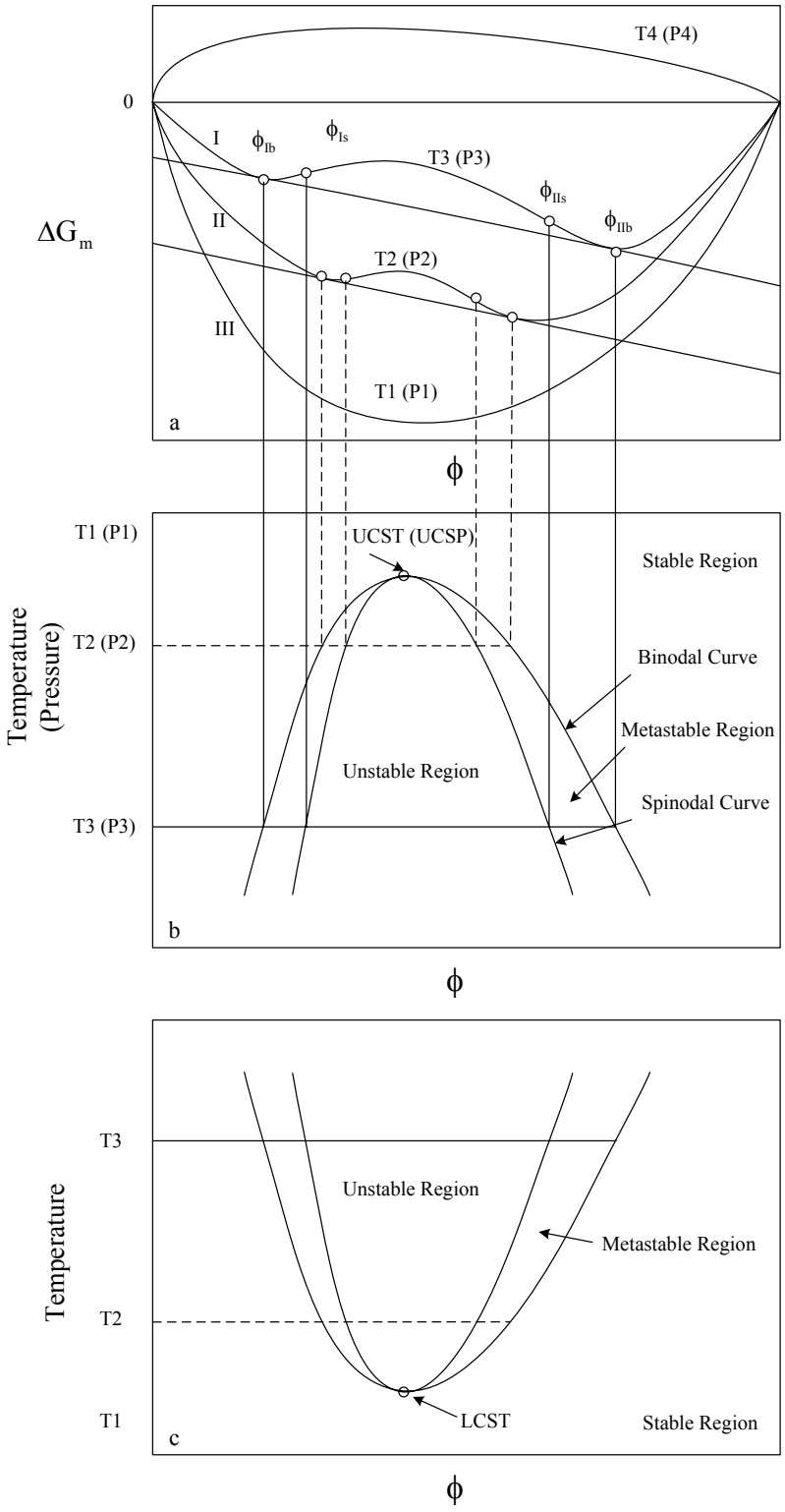

Figure 2.1. Schematic diagram of Gibbs free energy of mixing as a function of polymer concentration. [Utracki 1994]

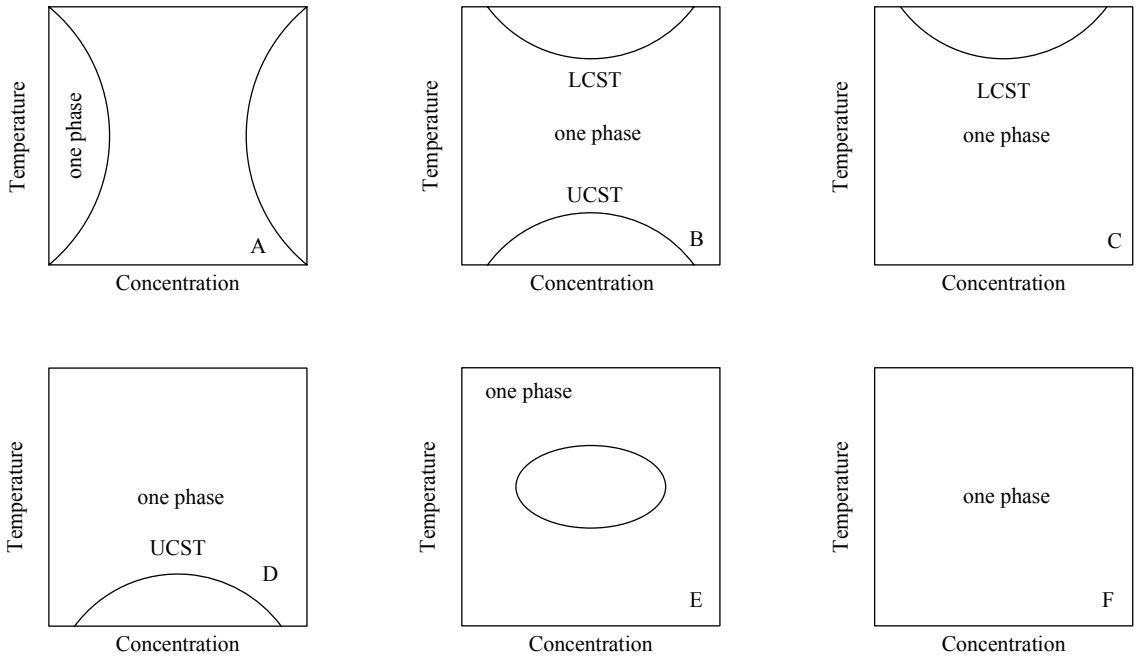

Figure 2.2 Phase behavior in polymer solutions. System displaying (A) hour-glass shaped region of immiscibility; (B) both UCST and LCST; (C) only LCST; (D) only UCST; (E) island of immiscibility; (F) complete miscibility. Adapted from [Kiran 2000].

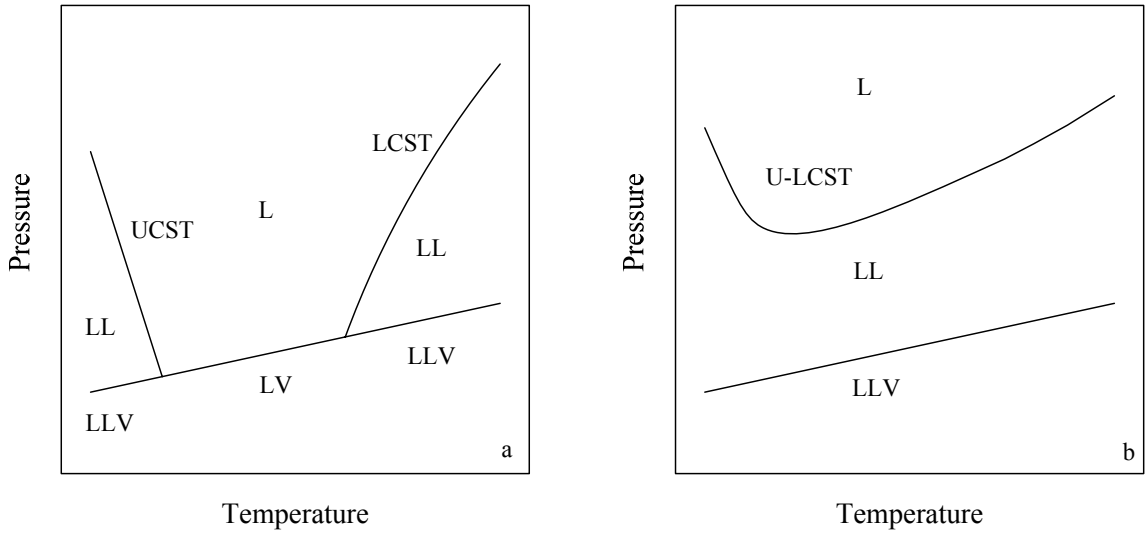

Figure 2.3 Schematic pressure-temperature phase diagrams for amorphous polymer solution. (a) showing both UCST and LCST; (b) showing U-LCST. L: liquid; LL: liquid + liquid; LLV: liquid + liquid + vapor. Adapted from [Kirby and Mchugh 1999].

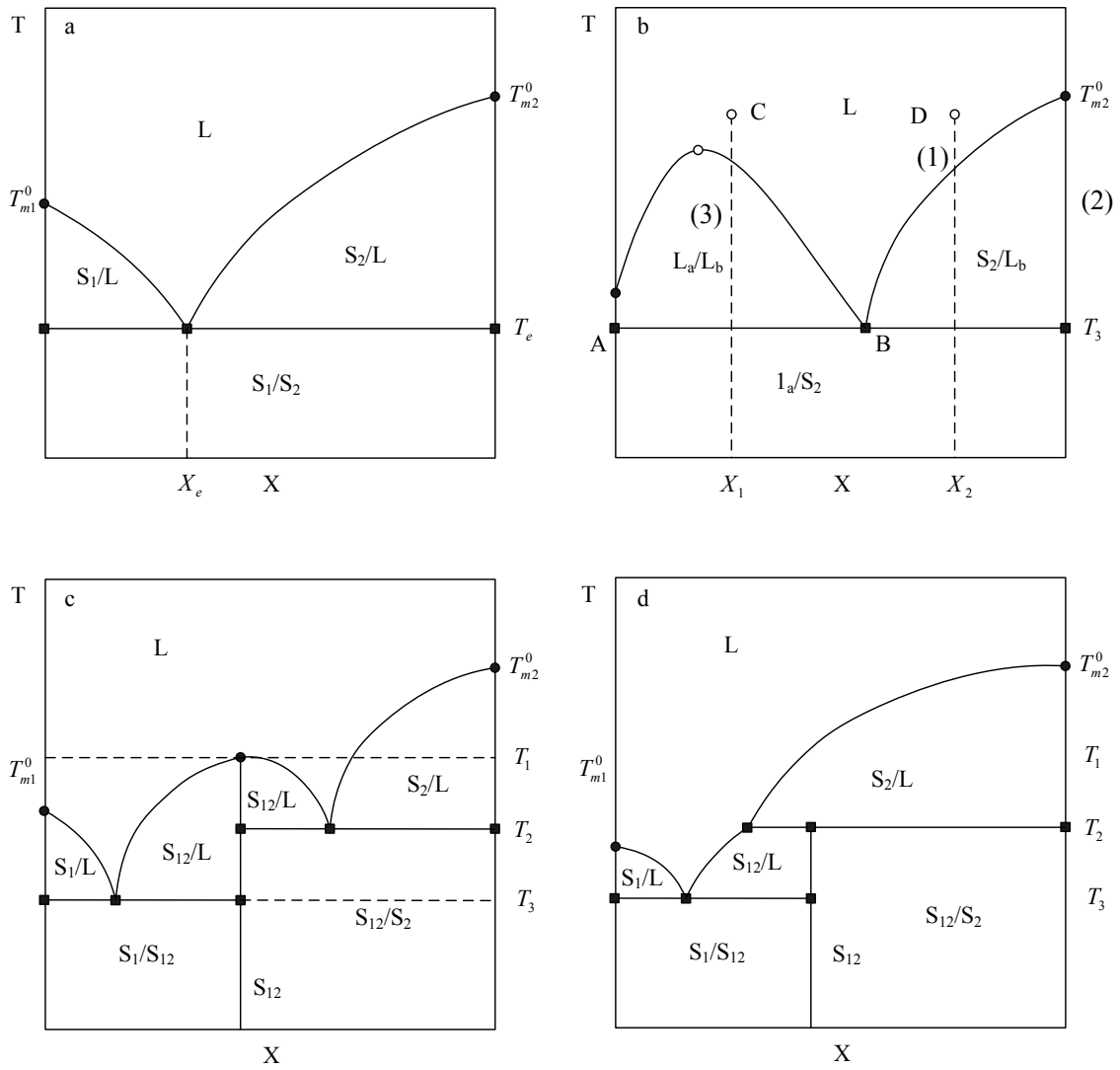

Figure 2.4 Schematic temperature-concentration phase diagrams for solid-liquid equilibrium under constant pressure of: (a) a simple binary mixture; (b) polymer /solvent system showing liquid/liquid (3) and solid/liquid (1) phase equilibrium; (c) the system in which the compound S_{12} dissociates congruently; (d) the system in which the compound S_{12} dissociate incongruently. adapted from [Koningsveld and Stockmayer 2001].

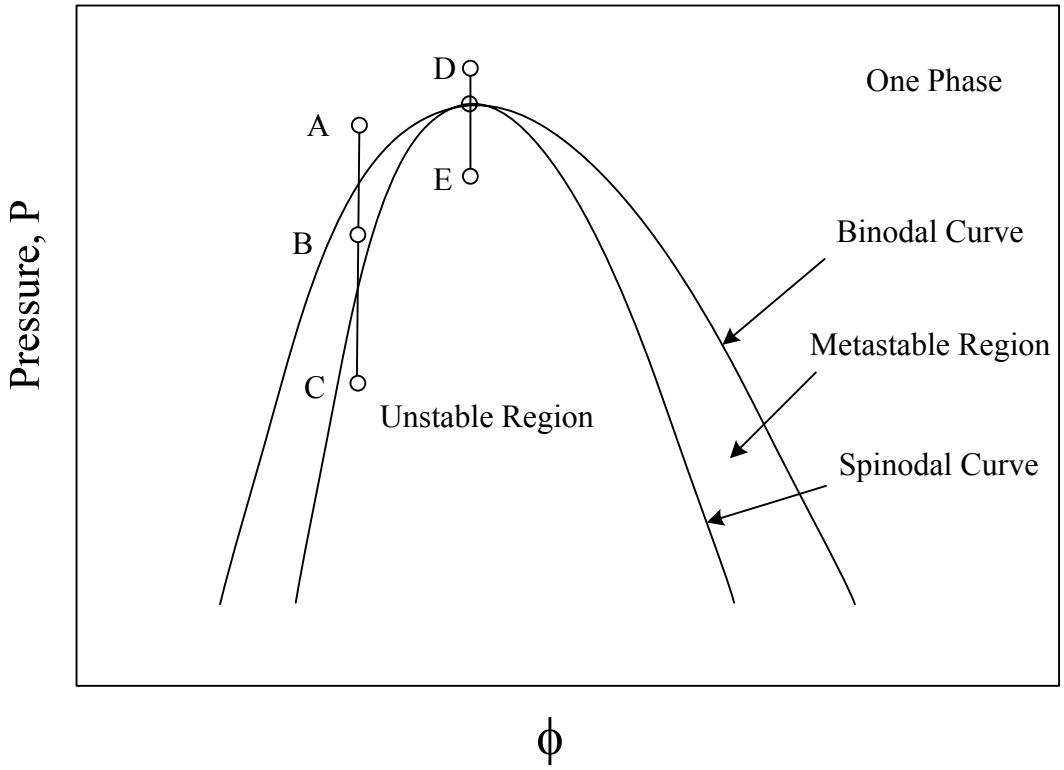

Figure 2.5 Schematic representations of the pressure-induced phase diagram and pressure-quench to different depths of penetration.

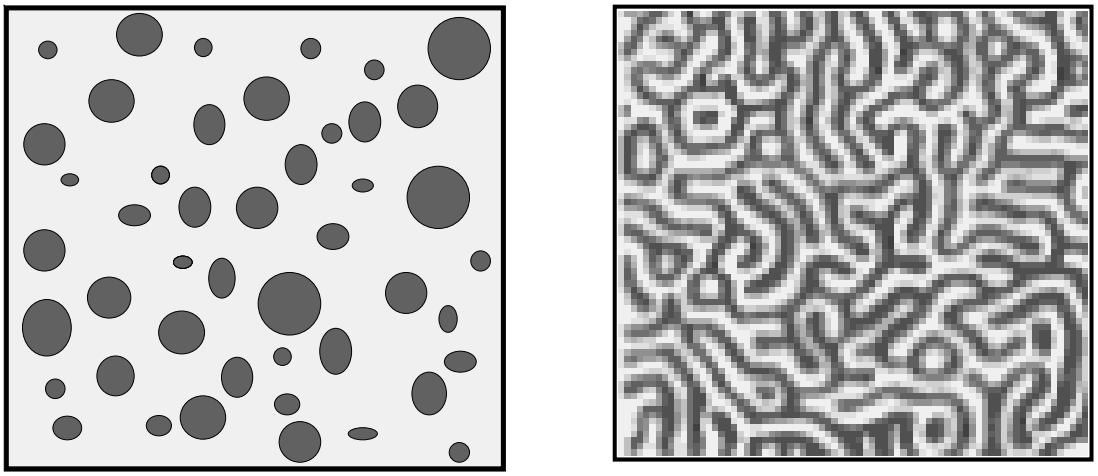

Figure 2.6 Possible morphology of material undergoing phase separation. (a) droplets of minority dispersed in continuous phase. (b) co-continuous morphology with two phases intertwined each other. Adapted from [Xiong 1998].

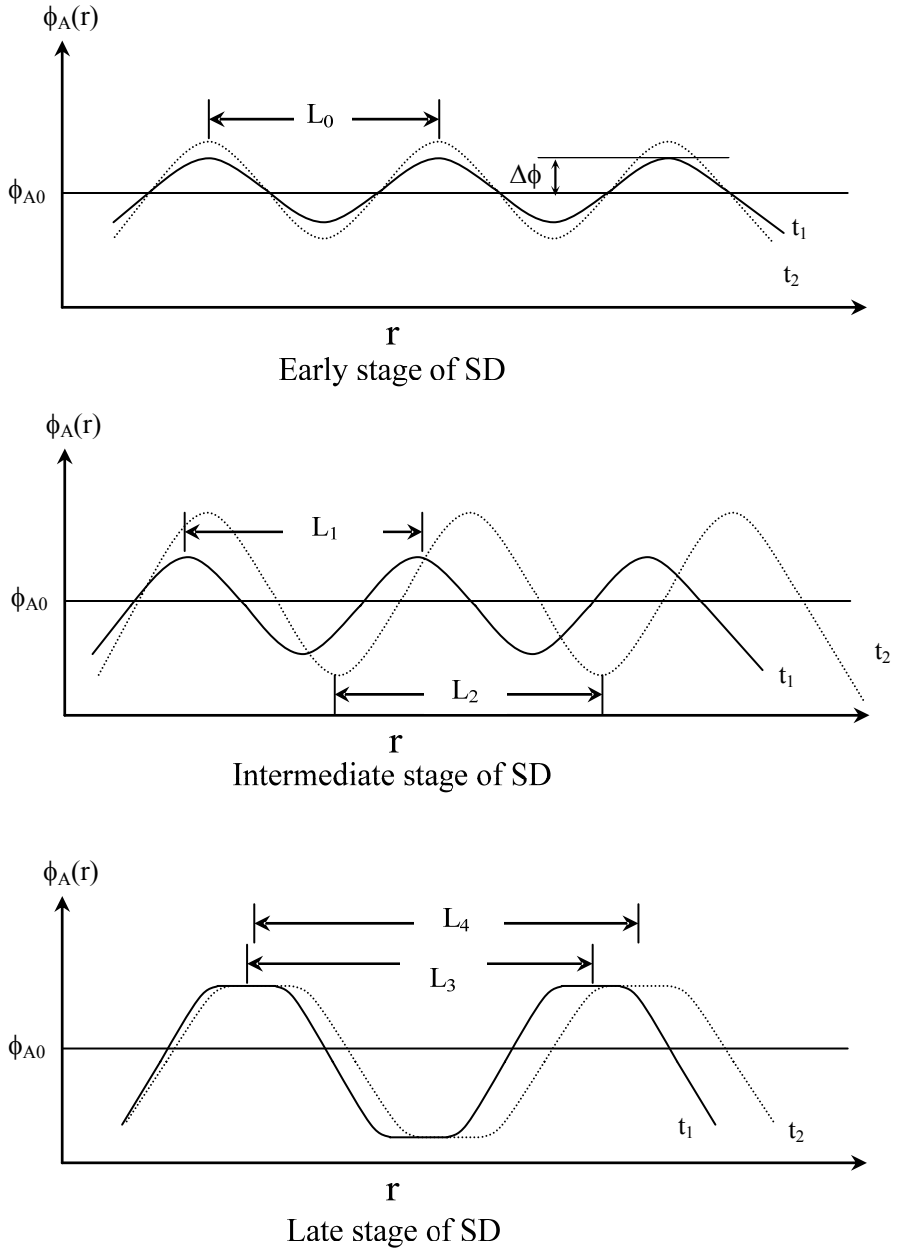

Figure 2.7 The schematic plot of the concentration fluctuation of solution with time in the early stage, the intermediate stage and the late stage (where$L_0<L_1<L_2<L_3<L_4$). adapted from [Hashimoto *et al.* 1986].

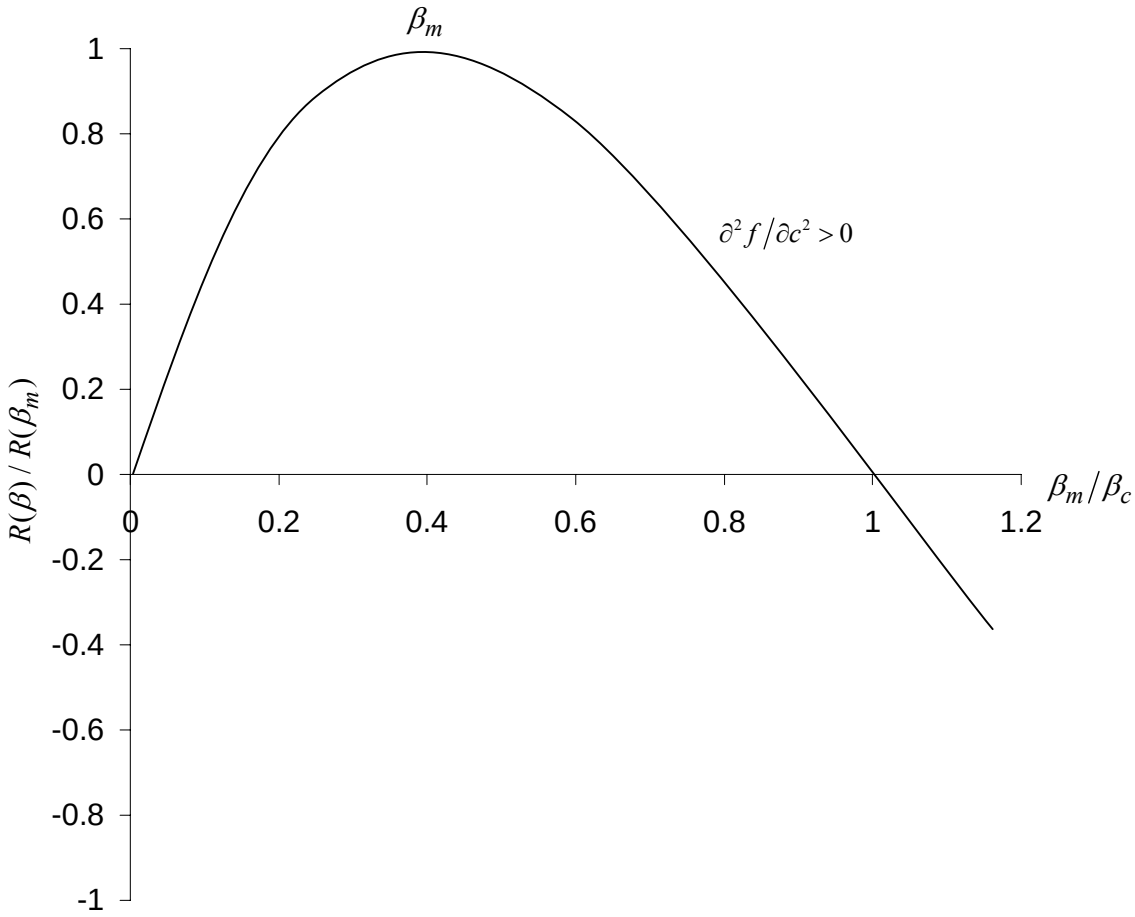

Figure 2.8 Qualitative behavior of reduced growth rate $R(\beta)/R(\beta_m)$ as a function of reduced wavenumber β/β_m [Cook 1970].

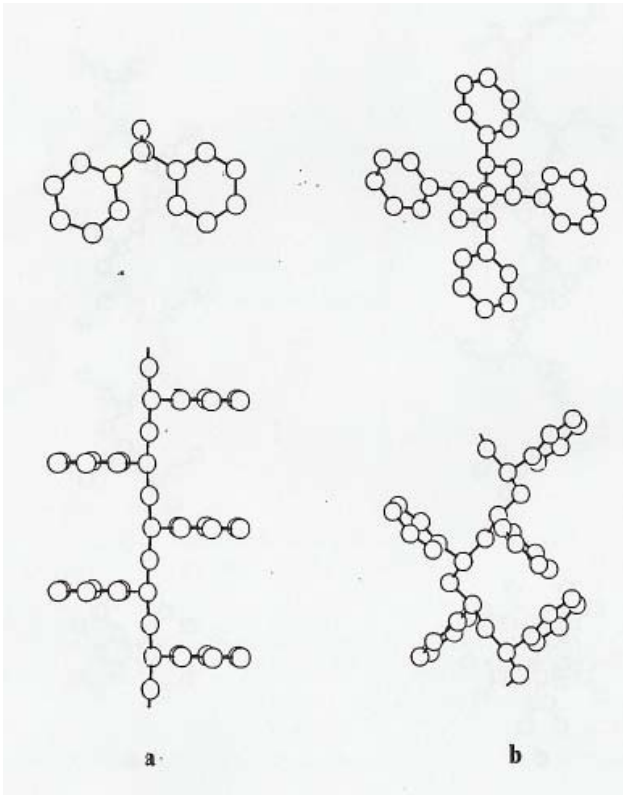

Figure 2.9 Projection along the chain axis and side view of the different conformational structure (a) trans-planar conformation; (b) 2_1 helical conformation [Corradini and Guerra 1992, Advance in Polymer Science;Reprinted with permission from Springer].

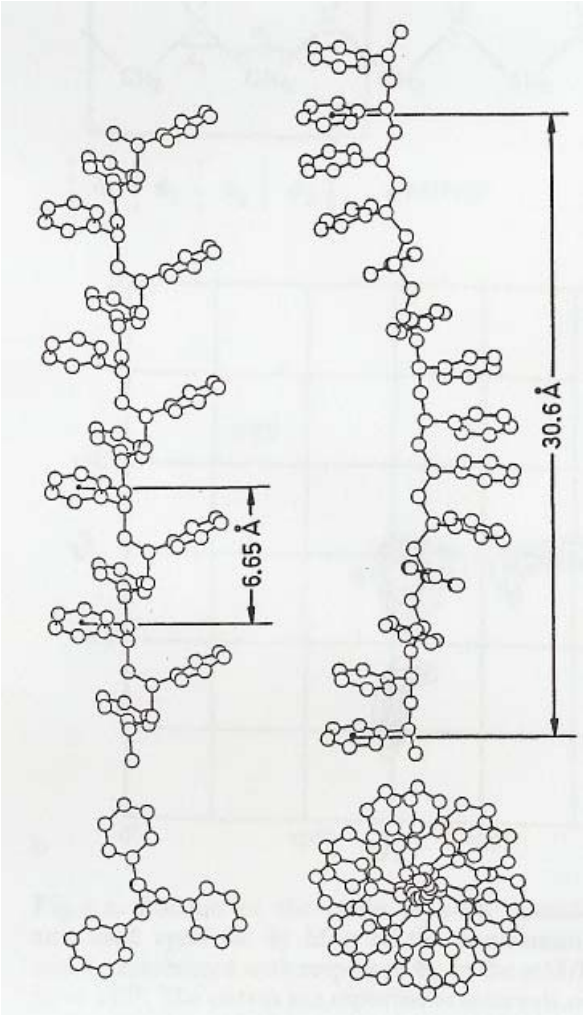

Figure 2.10 The side view and projection along the chain axis of iPS, (a) 3_1 helical structure, (b) 12_1 helical structure [Corradini and Guerra 1992, Advance in Polymer Science; Reprinted with permission from Springer].

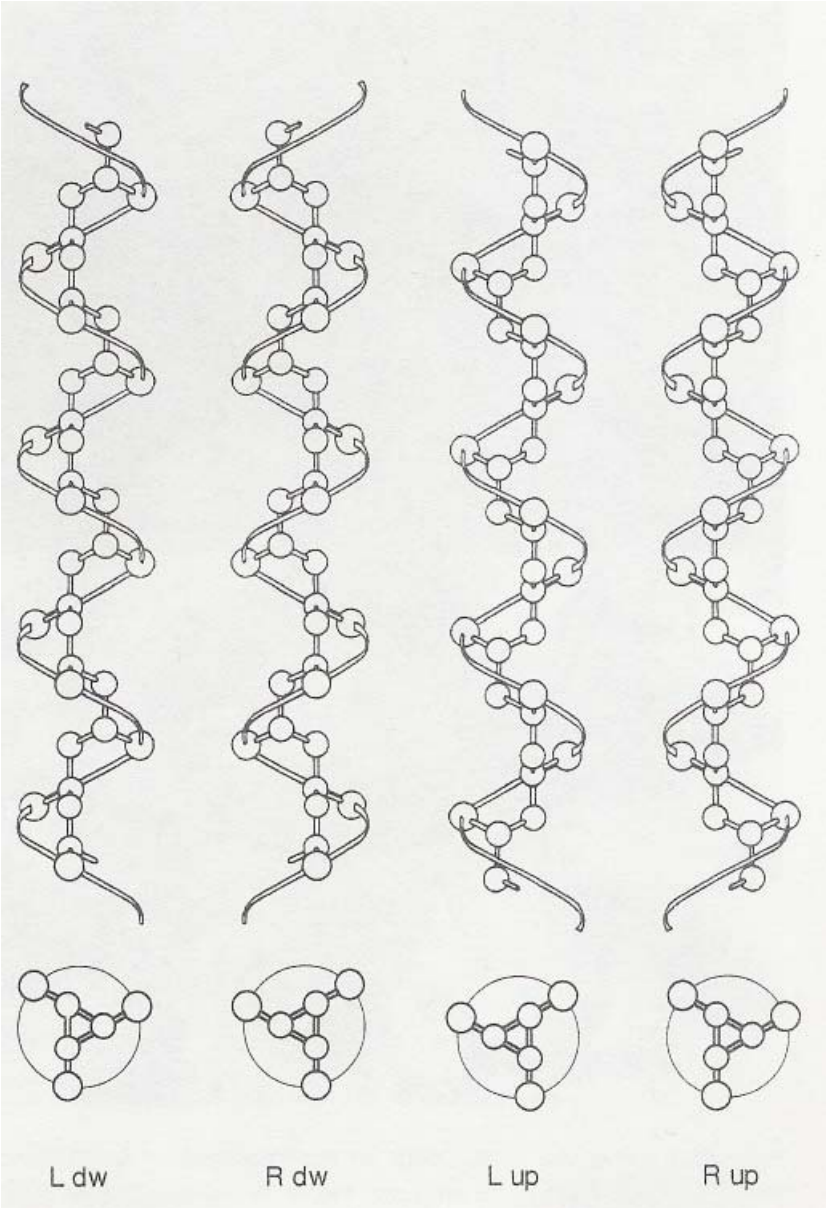

Figure 2.11 Chain configurations in isotactic polypropylene, L and R represent the left-handed and right-handed helix and dw and up represent that the position of methyl group (CH_3) can be either down or up. [Phillips and Mezghani 1996; Polymorphism in Isotactic Polypropylene; Reprinted with permission from CRC press].

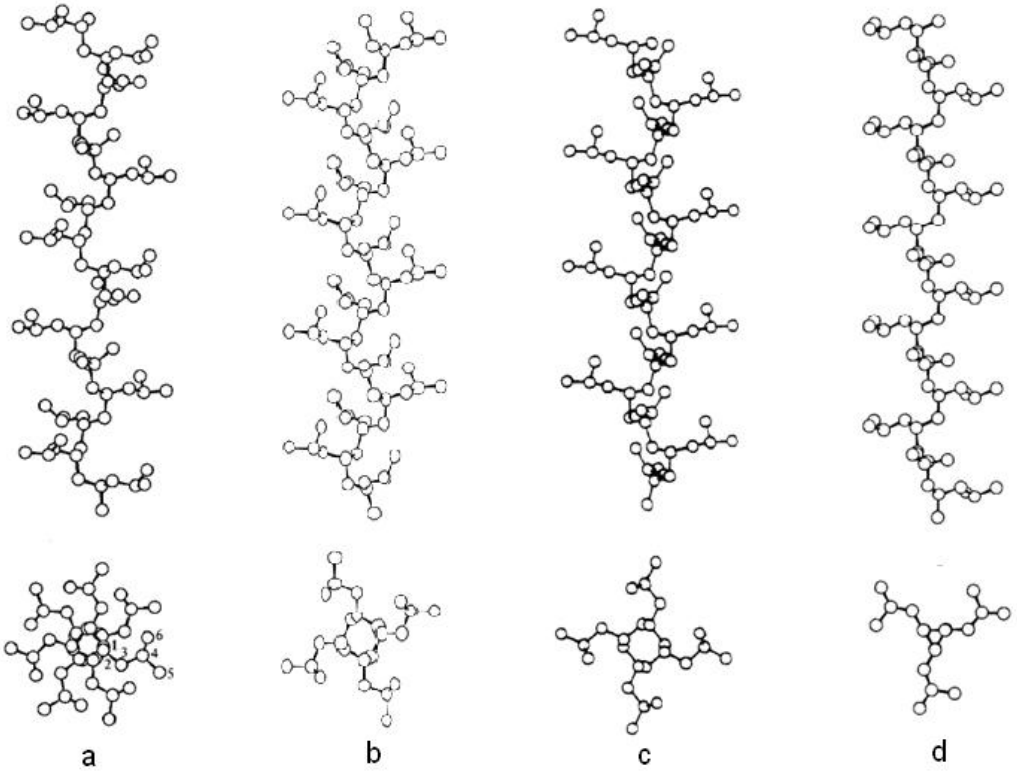

Figure 2.12 The side view and projection along the chain axis of iP4MP1, (a) 7_2 helical structure, Form I; (b) 4_1 helical structure, Form II [De Rosa 2003]; (c) 4_1 helical structure, Form III [De Rosa *et al.* 1994]; (d)3_1 helical structure, Form IV.[De Rosa 1999]

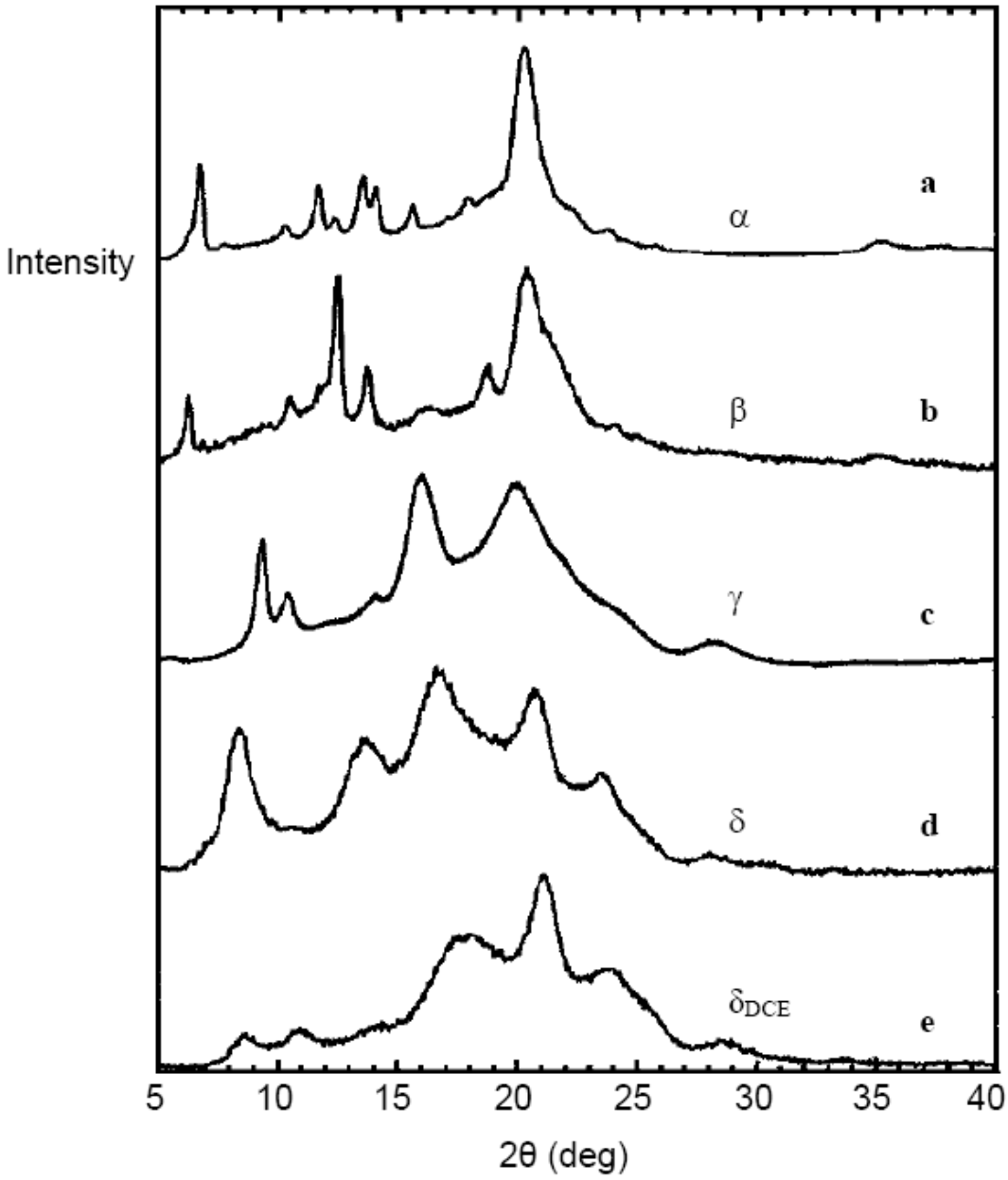

Figure 2.13 Typical X-ray diffraction patterns of the s-PS semicrystalline forms: a) α, b) β, c) γ, d) δ and e) δ clathrate form including 1,2-dichloroethane (DCE). [Rizzo *et al.* 2002, Macromolecules; Reprinted with permission from ACS]

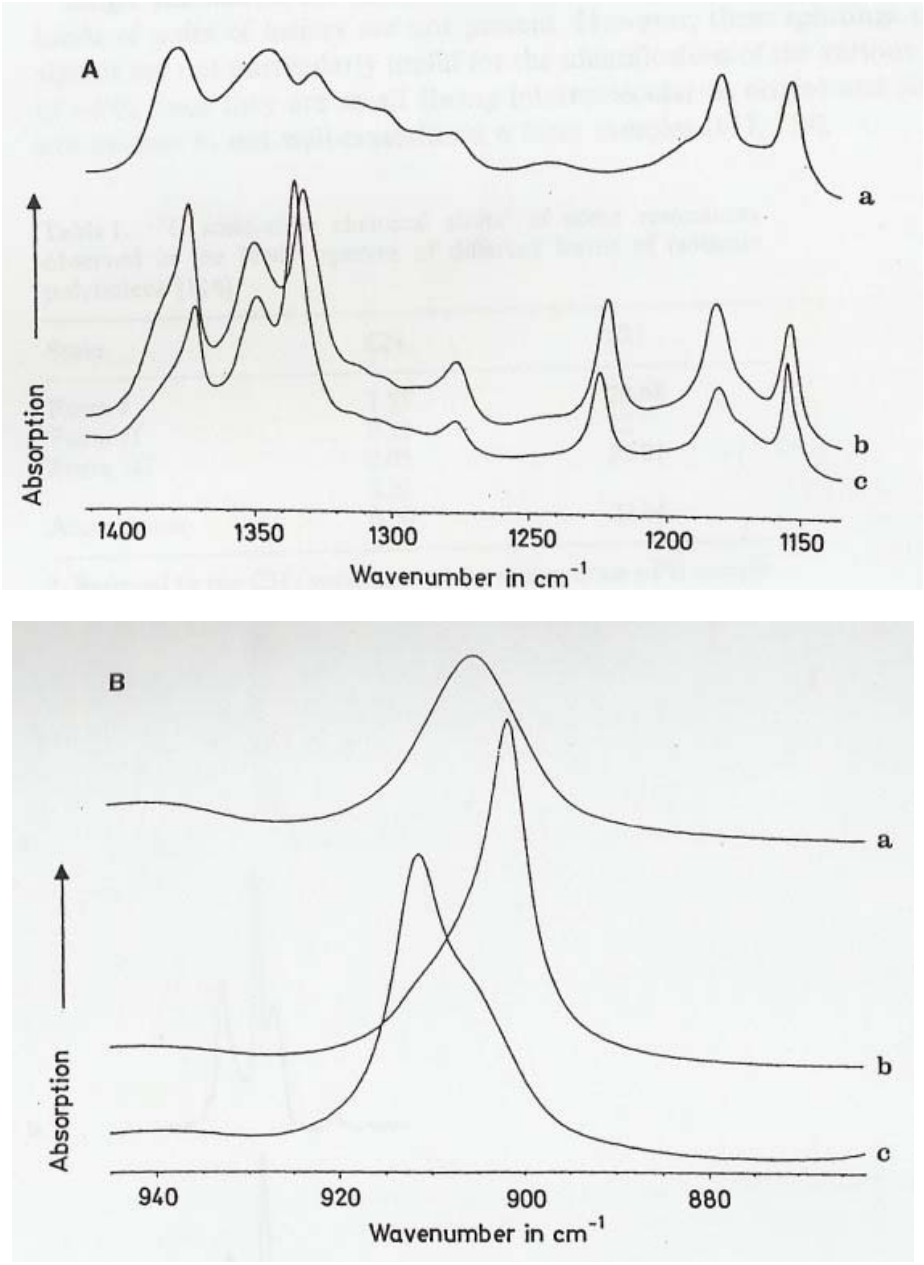

Figure 2.14 Expanded infrared spectra of sPS samples in two different regions: A) 1100-1400cm^{-1}, B) 860-940cm^{-1}; a) amorphous; b) α form; c) β form. [Guerra *et al.* 1990, Macromolecular Chemistry and Physics; Reprinted with permission from WILEY-VCH]

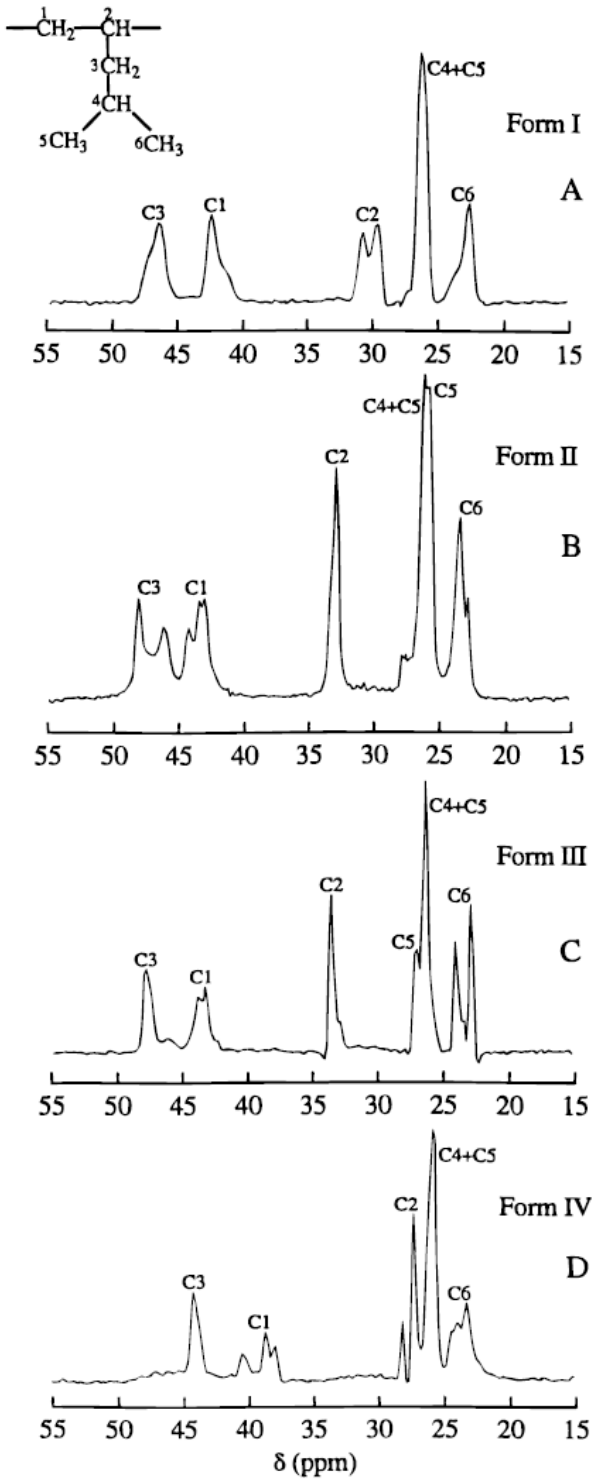

Figure 2.15 Solid-state ^{13}C NMR CP-MAS spectra of four crystalline forms of i-P4MP1: (A) form I; (B) form II; (C) form III; (D) form IV [De Rosa *et al.* 1997, Macromolecules; Reprinted with permission from ACS].

Chapter 3

Kinetics of Pressure-Induced Phase Separation in Polystyrene + Acetone Solutions at High Pressures*

The kinetics of pressure-induced phase separation in solutions of polystyrene (M_w = 129 200; PDI = 1.02) in acetone has been studied using time- and angle-resolved light scattering. A series of controlled pressure quench experiments with different quench depths were conducted at different polymer concentrations (4.0 %, 5.0 %, 8.2 % and 11.4 % by mass) to determine the binodal and spinodal boundaries and consequently the polymer critical concentration. The results show that the solution with a polymer concentration 11.4 wt % undergoes phase separation by spinodal decomposition mechanism for both the shallow and deep quenches as characterized by a maximum in the angular distribution of the scattered light intensity profiles. Phase separation in solutions at lower polymer concentrations (4.0, 5.0 and 8.2 wt %) proceeds by nucleation and growth mechanism for shallow quenches, but by spinodal decomposition for deeper quenches. These results have been used to map-out the metastable gap and identify the critical polymer concentration where the spinodal and binodal envelops merge.

The time scale of new phase formation and growth as (accessed) from the time evolution of scattered light intensities is observed to be relatively short. The late stage of phase separation is entered within seconds after a pressure quench is applied. For the systems undergoing spinodal decomposition, the characteristic wavenumber q_m corresponding to the scattered light intensity maximum I_m was analyzed by power-law scaling according to $q_m \sim t^{-\alpha}$ and $I_m \sim t^{\beta}$. The results show $\beta \approx 2\alpha$. The domain size is observed to grow from 4 μm to 10 μm within 6 s. The domain growth displays elements of self-similarity.

* Published as J. Fang and E. Kiran. "*Kinetics of pressure-induced phase separation in polystyrene + acetone solutions at high pressures*" Polymer (2006), 47(23), 7943-7952.

3.1 Introduction

The kinetics of phase separation in polymer systems deals with non-equilibrium relaxation processes that follow a transfer of the system from a thermodynamically stable to a thermodynamically unstable state. These transformations are usually induced by a temperature or pressure quench. The study on kinetics of phase separation of polymer mixtures or polymer solutions is important in polymer formation and processing, as well as property modifications. Information on the time scale of phase separation coupled with polymer property knowledge provide the critical criteria needed to design and control the final structure of polymer materials in particle formation or formation of microporous materials.

The majority of the studies on phase separation kinetics with polymer systems have been reported on polymer blend systems [Hashimoto *et al.* 1983; Aksimentiev *et al.* 2000; Binder and Fratzl 2001; Henderson and Clarke 2004; Madbouly and Ougizawa 2004; Tang *et al.* 2004; Rappl and Balsara 2005]. Tang *et al.* [Tang *et al.* 2004] studied the temperature induced spinodal decomposition by light scattering in the copolymer blends of poly (styrene-co-methyl methacrylate) and poly(styrene-co-acrylonitrile) which show LCST-type phase behavior. The early stage of phase separation by spinodal decomposition was described in terms of the Cahn-Hilliard linear theory. Madbouly and Ougizawa [Madbouly and Ougizawa 2004] also used time-resolved light scattering technique to investigate the phase separation kinetics of poly(methyl methacrylate) and ploy(α-methylstyrene-co-acrylonitrile) blends which exhibit LCST type phase diagram, near the system's critical polymer concentration. They found that the characterization of the light scattering data for this system can also be described by the linearized Cahn-Hillard theory during the early stage of spinodal decomposition. At the late stages of spinodal decomposition, the scaling structure function was found to be time independent, and could be described by a universal curve.

The kinetics of phase separation in "polymer + solvent" systems is of more recent but growing interest [Kuwahara *et al.* 1982; Lal and Bansil 1991; Kojima *et al.* 1999; Hatanaka and Saito 2004; Lee *et al.* 2004; Lee *et al.* 2004]. The phase separation in polymer solutions can be induced by changes in the temperature, the solvent (concentration or composition) or the pressure. Lal and Bansil [Lal and Bansil 1991] studied the kinetics of spinodal decomposition of polystyrene solutions in cyclohexane induced by a temperature jump into the unstable region. Phase separation process was monitored by time- and angle-resolved light scattering at ambient pressures. Recently, Hatanaka and Saito [Hatanaka and Saito 2004] studied the kinetics of phase separation of polycarbonate and carbon dioxide system by in-situ observation of the light scattering patterns in a special high-pressure cell built to ensure miscibility of the polymer and carbon dioxide. The phase separation process was induced by increasing the temperature above LCST. These authors reported that phase separation proceeded by nucleation and growth mechanism for small temperature jumps, but by spinodal decompositions for large temperature jumps. Their study also showed that the crystallization and liquid-liquid phase separation occur simultaneously at pressures from 5 to 15 MPa and temperatures from 120 to 190 ^{o}C. Lee *et al*. [Lee *et al.* 2004] recently carried out a numerical study of temperature-induced phase separation kinetics of polymer solutions subjected to a linear spatial temperature gradient. Their results showed that anisotropic structures and morphologies can be induced by a gradient temperature jump.

In addition to temperature quench, phase separation can also be induced by exposing the solution to a nonsolvent vapor as antisolvent. An example of this is a study by Lee *et al*. [Lee *et al.* 2004] who reported the kinetics of phase separation in a polymer solution (polysulfone in N-methyl-2-pyrrolidinone) film induced by a nonsolvent vapor, water. The data were analyzed based on Cahn-Hilliard linear theory in the initial stages of phase

separation.

In contrast to the situation with phase separation induced by temperature change or by concentration change, relatively little work has been done on the kinetics of phase separation processes induced by a pressure change. With the growing application of supercritical fluids in polymer processing, the effect of the pressure on phase separation is now attracting more interest. Compared to the thermal-induced or solvent-induced phase separation methods, the pressure-induced phase separation gives the distinct advantage in that the fast quench rates can be achieved uniformly within the system. In one of the earlier studies, Kojima *et al.*[Kojima *et al.* 1999] have reported the early stage of spinodal decomposition during phase separation of polypropylene solution in trichlorofluoromethane induced by pressure jump using time- and angle-resolved light scattering system.

Majority of the experimental studies on pressure-induced phase separation from high pressure solution that are in the open literatures appear to have been generated in our own laboratory. Using a specially designed high pressure time and angle-resolved light scattering system [Xiong and Kiran 2000] suitable to carry out both shallow and deep pressure quenches at pressure up to 70 MPa and temperature up to 413 K, we have reported on the kinetics of pressure-induced phase separation in poly(dimethylsiloxane) + supercritical carbon dioxide [Liu and Kiran 1999], polystyrene + methylcyclohexane [Xiong and Kiran 2000] and polyethylene + n-pentane [Liu and Kiran 2001]. Both the binodal and spinodal envelops and critical polymer concentrations in these systems have been determined by a series of pressure quenches with different quench depths in polymer solutions with different concentrations. We now report on the kinetics of phase separation in polystyrene + acetone system. Polystyrene solutions are one of most frequently studied solutions and acetone has often been used as a model poor-solvent for polystyrene. The

earliest study on the phase behavior of the solutions of polystyrene in acetone was reported by Siow *et al*. [Siow *et al.* 1972]. These solutions display both UCST and LCST phase behavior. The effect of pressure on the phase equilibria for these systems with varying polystyrene molecular weights was later investigated by Zeman and Patterson [Zeman and Patterson 1972] which showed that pressure increases the polymer-solvent miscibility, decreasing the UCST and increasing the LCST. Van Hook and coworkers [Szydlowski and Van Hook 1991; Szydlowski *et al.* 1992; Luszczyk *et al.* 1996] reported a series of investigations on the solutions of polystyrene in acetone system. The effect of pressure, temperature, polymer molecular weight, polymer concentration, and isotope effect on phase separation were investigated. A low angle (2 - 4° range) light scattering system was used to monitor the scattered light intensity and the transmitted light intensity as a function of time. The spinodal points (temperature or pressure) were determined by traditional extrapolation of Debye plots by assigning the spinodal point as the T or P intercept of $1/I_{sc}$ vs T or P curve.s

In this chapter, we report on the kinetics of phase separation in solutions of polystyrene in acetone for different concentrations in terms of the time evolution of the scattered light intensities in a time- and angle- resolved light scattering system. A series of pressure quench experiments have been carried out with different pressure depths to give a complete coverage for each solution, and help map out the binodal and experimentally attainable spinodal envelops.

3.2 Experimental Section

3.2.1 Materials

Polystyrene of low polydispersity (M_w = 129,200, M_w/M_n =1.02) was obtained from Pressure Chemical Company. The HPLC grade Acetone was purchased from Emd Chemicals and used as received.

3.2.2 Apparatus

Figure 3.1 is schematic diagram of the experimental system. The details of construction and operational procedures for this system have already been described in earlier publications [Xiong and Kiran 1998; Liu and Kiran 1999; Xiong and Kiran 2000; Liu and Kiran 2001]. It consists of a solvent delivery line, a pressure generation line, a recirculation pump, a polymer loading and dissolution chamber, a high pressure variable volume scattering cell incorporating a movable position and an air-actuated rod assembly, and the optical light source and data collection and processing facilities. The two sapphire windows in the scattering cell are separated with a very thin stainless-steel spacer giving a path length of 250 μm. Small or intermediate pressure quenches are imposed by manipulating the pressure generator to change the position of the piston and the internal volume. For very fast or deep pressure quenches, the air-actuated expansion rod assembly is used. The optical components consist of a He-Ne laser, a Glan-Thompson polarizer and two convex lenses to collect and transfer the scattered light to a linear image sensor. The linear image sensor has 256 pixels giving a continuous angular coverage of 1.9 - 12.7˚. A beam splitter, placed after the condensing lenses, directs the transmitted light to an Avalanche photo diode detector. The maximum sustainable data acquisition speed of the system is 3.2 ms/scan that permits recording of the temperature, pressure, time, the transmitted light intensities and scattered light intensities over all angles. There are all recorded by a computerized data acquisition software.

3.2.3 Experimental Procedure

The demixing pressure for a given solution is first determined as a reference point to establish the path for the pressure quench. After the desired amount of the polymer and the solvents are loaded into the system, the system is pressurized with the aid of the pressure generator at a given temperature. The high-pressure recirculation pump is activated to

homogenize the contents in the system and achieve dissolution. The homogeneous conditions are verified by visual observations through the sapphire windows. The demixing pressure is determined by decreasing the system pressure until the two-phase region is entered. When the system crosses the phase boundary, the pressure corresponding to the departure from the base value of the transmitted light, or the inverse scattered light is identified as the demixing pressure. These are illustrated in Figure 3.2 for a 7.4 wt % solution, in which pressure was reduced from about 52 MPa to 40 MPa over about 40 s. With the initiation of the pressure reduction, system shows a small but observable temperature reduction which leads to small fluctuations in the transmitted light intensities. The effect is smaller with the scattered light intensities. The scattered light intensities shown in this plot are the average values calculated from the values over the full angle range corresponding to a given time. As shown in the figure, the $1/I_s$ is more stable and thus is preferred in assigning the demixing (binodal) pressure. After the quench is completed, as the system tries to reheat to the initial temperature, a pressure rise is noted from about 39 to 40 MPa.

Once the demixing pressures are determined, the solution is rehomogenized at a pressure about 2 MPa above the demixing pressure. Then, at a given temperature, the pressure is carefully brought to about 0.1 MPa above the demixing pressure. The system is then subjected to a controlled, shallow- or deeper-quench. This is demonstrated in Figure 3.3 for a solution of 8.2 wt % polystyrene in acetone undergoing a pressure quench depth of 0.25 MPa. The total time for the completion of the quench is around 0.5 s, corresponding to a quench rate of 0.5 MPa/s. In the present study, the majority of the quenches were controlled by adjusting the pressure generator. The pressure quench depths were varied from 0.1MPa to 3MPa.

The time evolution and the angular variation of the scattered light intensities show different

trends if the solution is undergoing phase separation by nucleation and growth or by spinodal decomposition. Systems undergoing phase separation by spinodal decomposition show a maximum in the angular variation of the scattering light intensities, while for systems undergoing phase separation by nucleation growth, the angular distribution of scattered light intensities does not display such as a maximum and decrease with angle. The experiments were carried out at each concentration for different quench depths to determine the crossover pressure from one type of phase separation mechanism to another.

3.3 Results and Discussion

The demixing pressures are first determined as the reference points for the quench experiments. Figure 3.4 shows demixing curves for the PS + acetone system at different concentrations in a pressure-temperature (P-T) diagram. For the solution at 4.0 wt %, the data were generated in the temperature range from 331 to 348 K; and for the solution at 8.2 wt %, the experiments were conducted in the temperature range from 337 to 342 K. The demixing pressures for three other concentrations, at 5, 7.4 and 11.4 wt % were determined only at 342 K. In the figure, the region above each curve is one-phase region. The negative slopes of these curves indicate that the systems display upper critical solution temperature (UCST) type phase behavior in this experiment range.

The pressure quench experiments of different quench depths were then conducted at polymer concentration of 4.0, 5.0, 8.2 and 11.4 % by mass at 342 K.

Figure 3.5 shows the time evolution of the scattered light intensities as a function of the wave vector q which is equal to $(4\pi/\lambda)\sin(\theta/2)$ for a quench depth of $\Delta P = 0.70$ MPa at 342 K for 4.0 wt % PS + acetone solution. Here, λ is wave length of the laser light ($\lambda = 632.8$ nm), and θ is the scattering angle. The scattered light intensities increase with time, but

show continual decrease with increasing scattering angles. This is typical of systems undergoing phase separation by nucleation and growth. Figure 3.6 shows the results when the solution was subjected to a greater quench depth of 1.30 MPa. Here, a maximum in angular distribution of the scattered light intensity profile was observed to develop shortly after the quench. The formation of scattering maximum is typical of systems undergoing phase separation by spinodal decomposition. The position of the maximum is noted to move to lower q values with increasing time. The metastable gap that is the quench depth to enter the spinodal decomposition for this solution was observed to be over 0.6 MPa.

Figure 3.7 shows the scattered light intensity profiles during phase separation for 5.0 wt % solution when subjected to 0.15 MPa quench at 342 K. Figure 3.8 shows the results for a deeper quench (0.4 MPa) of this system. Formation of the spinodal ring is distinctly observed after about 4.0 s, which is shortly after the completion of the pressure quench.

Figures 3.9 and 3.10 show the evolution of the scattered light intensity in 8.2 % solutions. The quench depths are $\Delta P = 0.10$ MPa and 0.25 MPa, respectively. The results show the crossover from nucleation and growth to spinodal decomposition in deeper quenches.

Figure 3.11 and Figure 3.12 show the scattered light intensity profile for two different quench depths $\Delta P = 0.10$ MPa and 0.35 MPa, respectively for a solution at a higher concentration of 11.4 wt %. With this solution, the maximum in the scattered light intensity profile is observed to develop shortly after the quench regardless of the quench depth. This observation suggests that the critical polymer concentration must be at or very close to 11.4 wt %.

Table 3.1 summarizes the results of binodal and spinodal pressures (all generated from the quench experiments). Figure 3.13 shows these and the regions where nucleation and

growth was observed in a pressure-concentration phase diagram (P-X). The figure clearly demonstrates the narrowing of the metastable gap in going from 4.0 to 11.4 wt % solutions. The binodal and spinodal curves merge at critical polymer concentration.

3.4 Further Analysis of the Time Evolution of the Scattered Light Intensity and the Characteristic Domain Size

For the early stage of spinodal decomposition, Cahn-Hilliard theory [Cahn and Hilliard 1958; Cahn and Hilliard 1959; Cahn 1961; Cahn 1965] predicts that the scattered light intensity should increase with time exponentially according to

$$I(q,t) = I(q,0)\exp\left(2R(q)t\right) \tag{3.1}$$

Here q is again the wavenumber of growing fluctuations and $R(q)$ is the rate of growth of concentration fluctuations given by

$$q = \frac{4\pi}{\lambda}\sin\left(\theta/2\right) \tag{3.2}$$

$$R(q) = D_{app}q^2\left[1 - \frac{q^2}{2q_m{}^2}\right] \tag{3.3}$$

where D_{app} is the apparent diffusivity and q_m is the wavenumber corresponding to maximum growth rate of fluctuations. The apparent diffusivity can be calculated from plots of $R(q)/q^2$ as the limiting value of $R(q)/q^2$ as q approach to 0, that is

$$D_{app} = \lim_{q\to 0}\left\{R(q)/q^2\right\} \tag{3.4}$$

Linearized Cahn-Hilliard theory is strictly applicable over the time interval in which the location of the maximum in the scattered light intensity does not change with time. However, as shown in Figure 3.8 - 3.11, in the solutions undergoing spinodal decomposition, the spinodal ring is not stationary and the wave number q_m corresponding to

the maximum in the scattered light intensity I_m moves to lower q values with time. Thus the observation times in the present experiments, even though very short compared to observation times encountered in experiments with polymer blends or alloys, is not short enough to capture the new phase formation and evolution in the early stages of the spinodal decomposition.

The intermediate and late stage of spinodal decomposition are often described in terms of power-law relationships [Liu and Kiran 2001; Takenaka *et al.* 2005] of the type

$$I_m(t) \approx t^{\beta} \tag{3.5}$$

$$q_m(t) \approx t^{-\alpha} \tag{3.6}$$

These relationships provide a scaling description in terms of the exponents β and α of the time evolution of the scattered light intensity maximum I_m and the corresponding wavenumber q_m.

Figure 3.14(a) shows the variation of $\log(q_m)$ and $\log(I_m)$ with $\log(t)$ for 8.2 wt % solution subjected to 0.25 MPa quench at 341.9 K corresponding to the data shown in Figure 3.10. Analysis of Figure 3.14 (a) shows that the growth exponent α for q_m is 0.74 and β for I_m is 1.46 which suggests $\beta \approx 2\alpha$. Such dependence has also been observed for polystyrene + cyclohexane [Lal and Bansil 1991] system undergoing temperature-induced phase separation and for polystyrene + methylcyclohexane [Xiong and Kiran 2000], polydimethylsiloxane + carbon dioxide [Liu and Kiran 1999] and polyethylene + *n*-pentane [Liu and Kiran 2001] systems undergoing pressure-induced phase separation. Figure 3.14 (b) shows the results for 11.4 wt % solution subjected to 0.10 MPa quench at 342 K. The growth exponent α is 1.39 and β is 2.18 for this quench, giving a relationship of

$\beta \approx 1.6\alpha$.

The maximum value of the wavenumber q_m is related to the domain size scale, which is expressed as [Hashimoto 1992]

$$L = 2\pi / q_m \tag{3.7}$$

The domain size continuously increases during this time interval of phase separation process. Figure 3.15 shows a plot of the evolution of the characteristic domain size with time in the two solutions shown in Figure 3.14. The domain sizes reach about 5 μm in 1 s after quench is finished and approaches about 15 μm within 5 s for the 11.4 % solution with 0.10 MPa quench, while for 8.2 % solution, the domain size reach 4 μm in 1 s and approaches about 18 μm in 14 s. compared with the two systems, the 11.4 % solution with 0.10 MPa quench shows a faster growth rate than the 8.2 % solution with 0.25 MPa quench. It is worth to mention that even though the stationary q_m region has not been experimentally captured, the data suggests that a domain size of 5 μm is reached in the early stage of phase separation.

For systems that display dynamic similarity, Furukawa [Furukawa 1985] has developed scaling functions given by

$$F(x) = 4x^2 / (3 + x^8) \qquad \text{(critical quench)} \tag{3.8}$$

$$F(x) = 3x^2 / (2 + x^6) \qquad \text{(off-critical quench)} \tag{3.9}$$

Where $F(x)$ is the structure factor expressed as $F(x) \approx I(x)/I_m(t)$ and $x = q/q_m(t)$. In such a system, the plot of $F(x)$ *vs* x should collapse to a single curve for all times. Figure 3.16 shows such a plot for the 8.2 wt % solution at 342 K for a 0.25 MPa pressure quench,

corresponding to the time evolution data shown in Figure 3.10. As shown in the figure, the reduced data points indeed collapse to a single curve, which suggest self-similarity. However the experimental data do not obey the theoretical Furukawa scaling functions. The theoretical curves are also included in Figure 3.16 for comparison purpose. The experimental data deviate more from the theoretical Furukawa scaling expectations as q moves away from q_m.

3.5 Conclusions

The present results show that the mechanisms of pressure-induced phase separation can be differentiated by using time- and angle-resolved light scattering system. The scattered light intensity profile shows a maximum with angle when the polymer solution undergoes phase separation by spinodal decomposition mechanism, while the same profile shows no maximum with angle when the polymer solution undergoes phase separation by nucleation and growth mechanism. For critical or near critical quenches, the spinodal regime is experimentally observed for both shallow and deep quench. However, for off critical quenches, the mechanism of phase separation is found to be varied with quench depths, and the nucleation and growth regimes are observed for shallow quenches and the spinodal regimes are observed for deep quenches. The crossover from nucleation and growth and spinodal is identified. The metastable gap becomes larger when the polymer concentrations are further apart from the critical polymer concentration. The early stage of spinodal decomposition is relatively short. The kinetics of spinodal decomposition in intermediate and late stage is well described by the power-law models

Table 3.1 Binodal and spinodal points of solutions of polystyrene (M_w = 129 200) in acetone. T = 342 K

Polymer Concentration wt %	Demixing Pressure MPa	Spinodal Pressure MPa
4.0	40.15	39.20
5.0	40.70	40.40
8.2	43.30	43.13
11.4	44.80	44.75

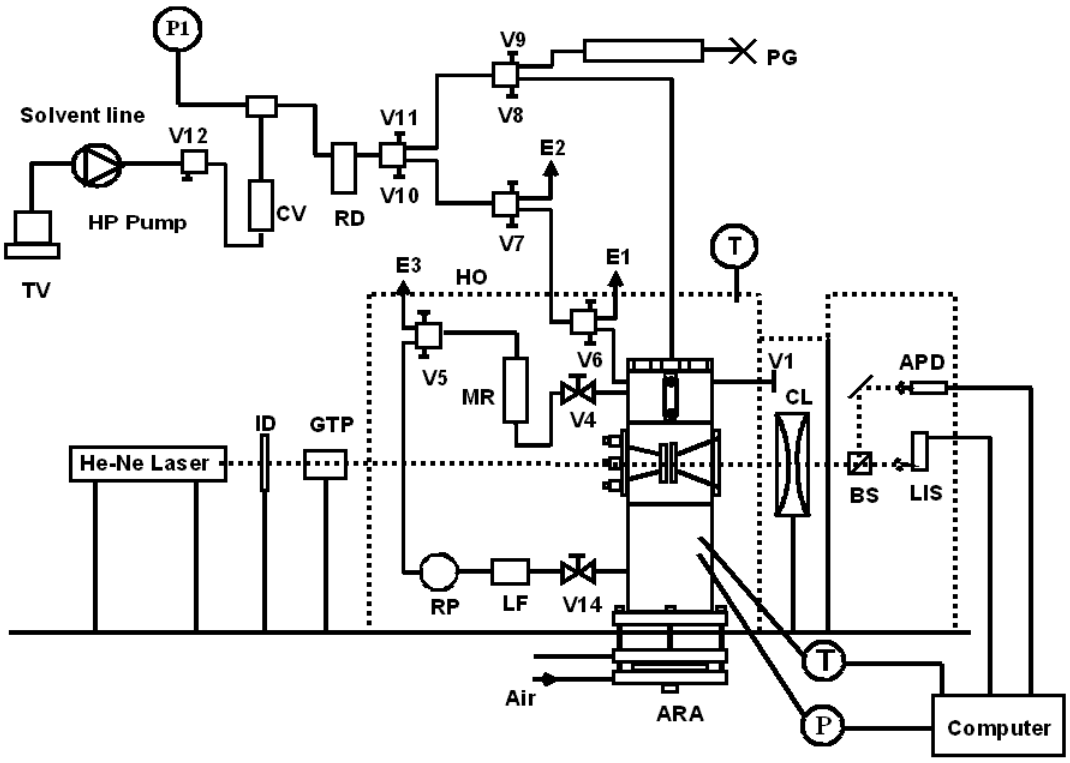

Figure 3.1 Schematic of the high-pressure high-temperature time- and angle-resolved light scattering system. TV = transfer vessel; HP Pump = high pressure pump; CV = check valve; RD = rupture disk; PG = pressure generator; ID = Iris Diaphragm; GTP = Glan-Thompson polarizer; CL = convex lens; BS = beam splitter; APD = avalanche photodiode detector; LIS = linear image sensor; HO = heated over; RP = re-circulation pump; LF = line filter; ARA = air-actuated rod assembly; MR = micro-reactor; T = thermocouple sensor; P = pressure transducer.

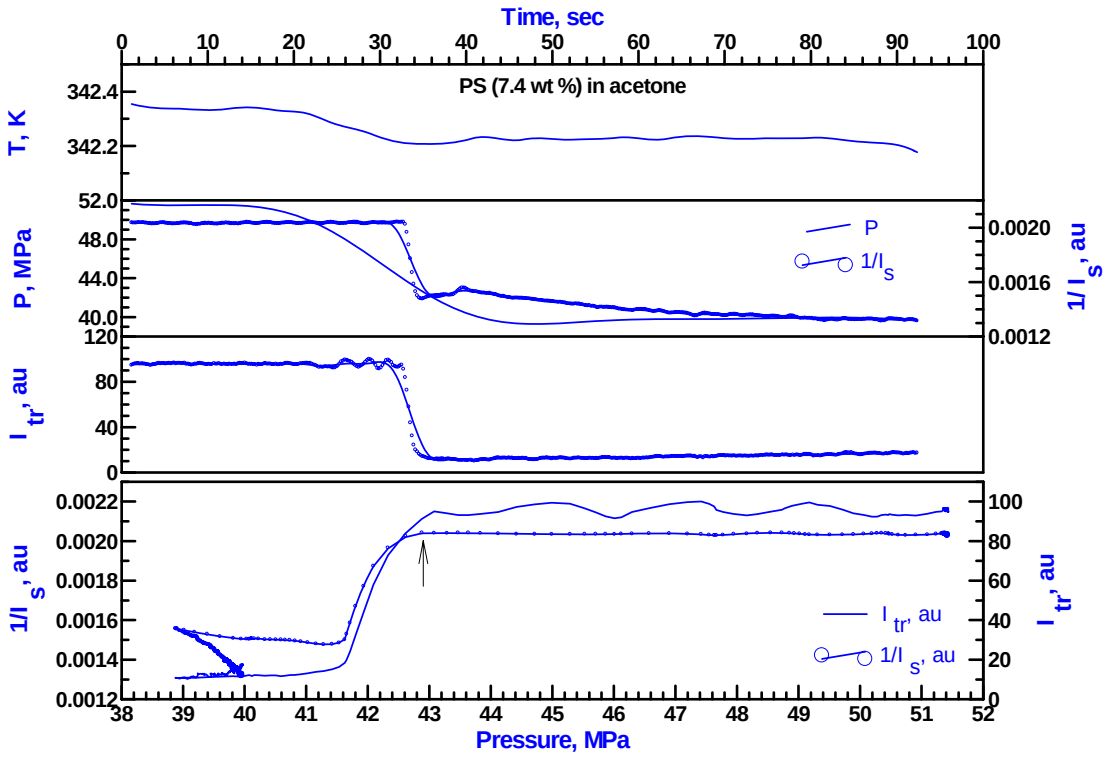

Figure 3.2 Variation of temperature (T), pressure (P), transmitted light intensity (I_{tr}) (in arbitrary units) and inverse average scattered light intensity ($1/I_s$) with time during a pressure reduction. The demixing pressure is determined from the variation of the inverse scattered light intensity with temperature (lower curve in the figure) as the point of departure from the base line intensity as indicated by arrow. The figure represents phase separation in 7.4 wt % solution of polystyrene in acetone and T = 342 K.

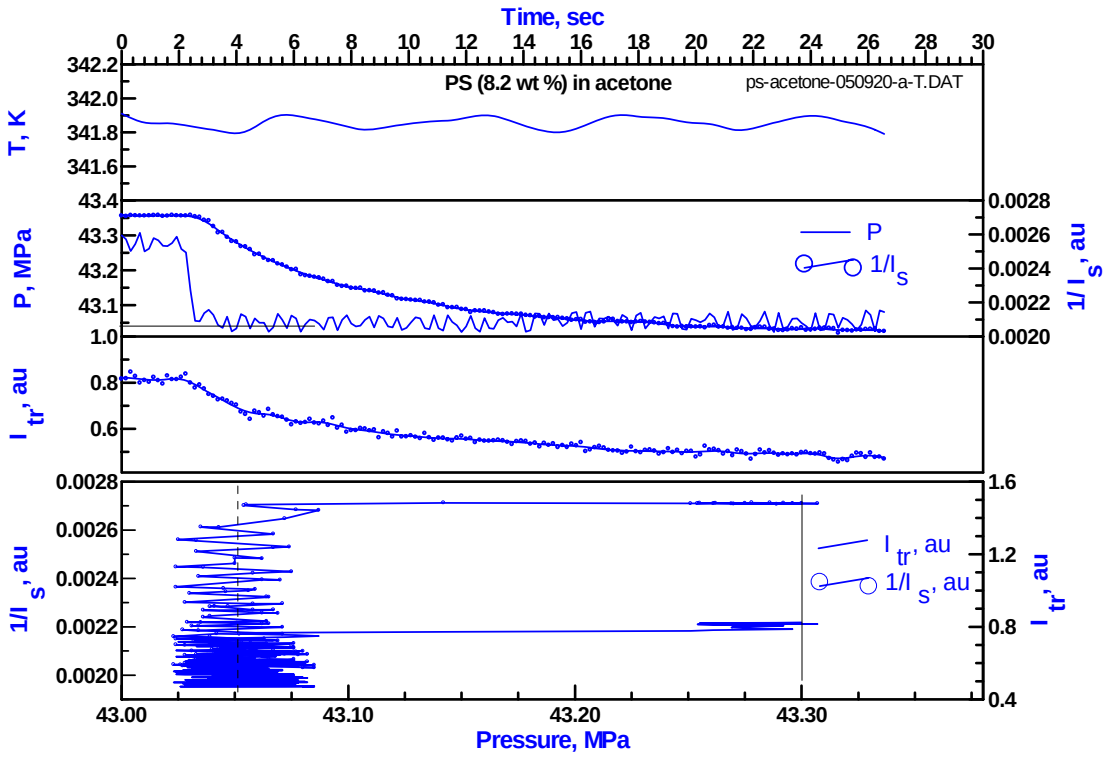

Figure 3.3 Variation of temperature T, pressure P, transmitted light intensity I_{tr}, and inverse averaged scattered light intensity $1/I_s$ with time during a 0.25 MPa pressure reduction in 8.2 wt % solution of polystyrene in acetone.

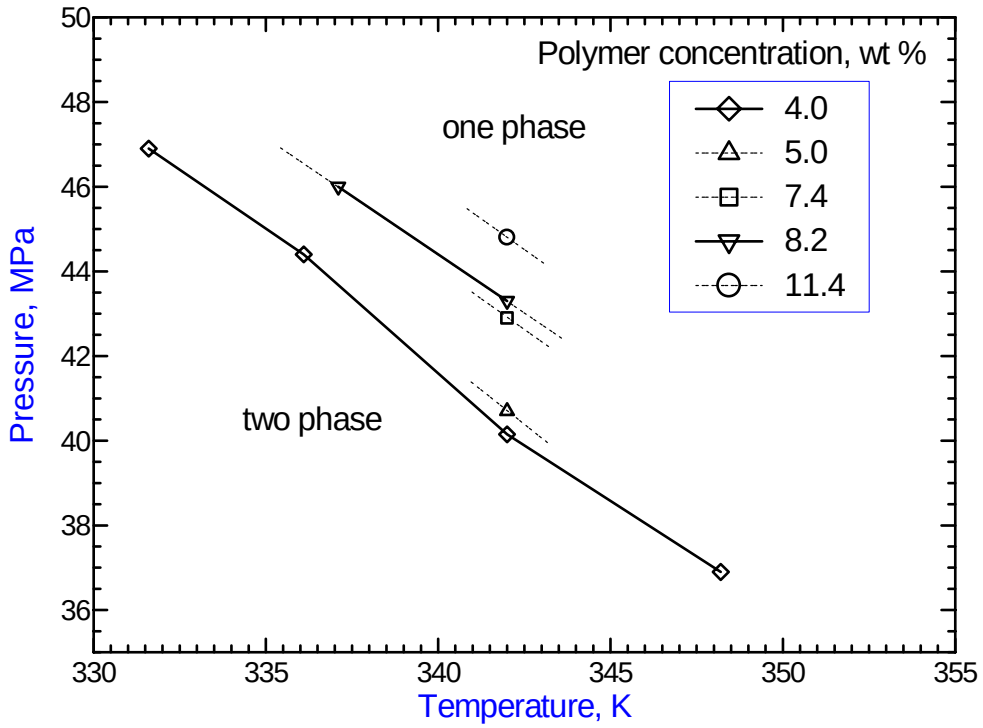

Figure 3.4 Pressure-temperature phase diagram showing the experimentally determined demixing boundaries for 4.0 % and 8.2 % solutions of PS (129.2K) + acetone. The demixing pressure data at temperature of 342 K for 5.0, 7.4 and 11.4 % solutions are also listed in the figure. The system shows a USCT type phase diagram over the experiment temperature range.

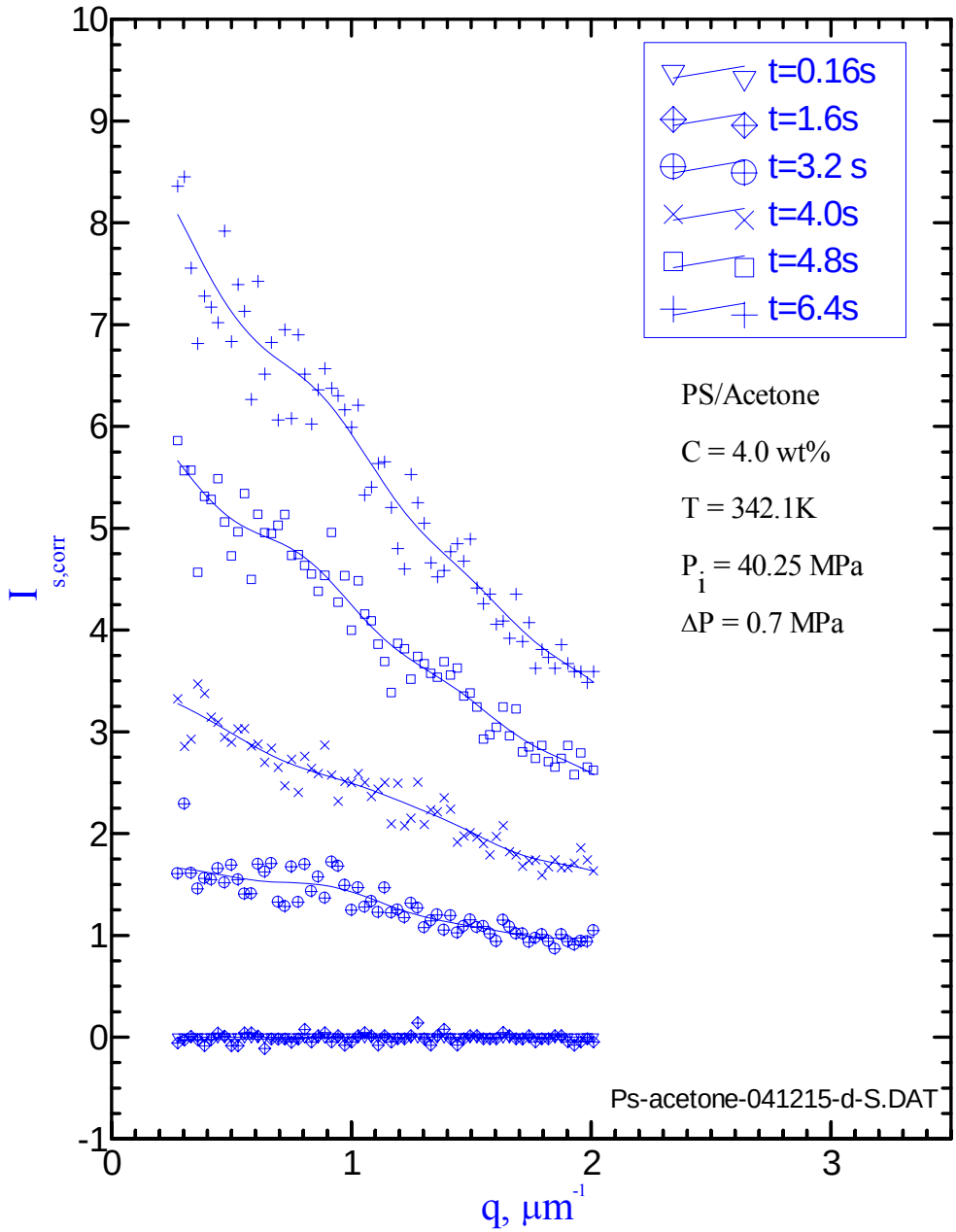

Figure 3.5 Scattered light intensity profiles as a function of wave number (scattering angle) and time for a pressure quench in 4.0 % by mass polystyrene solution in acetone at 342 K. The quench depth $\Delta P = 0.70$ MPa

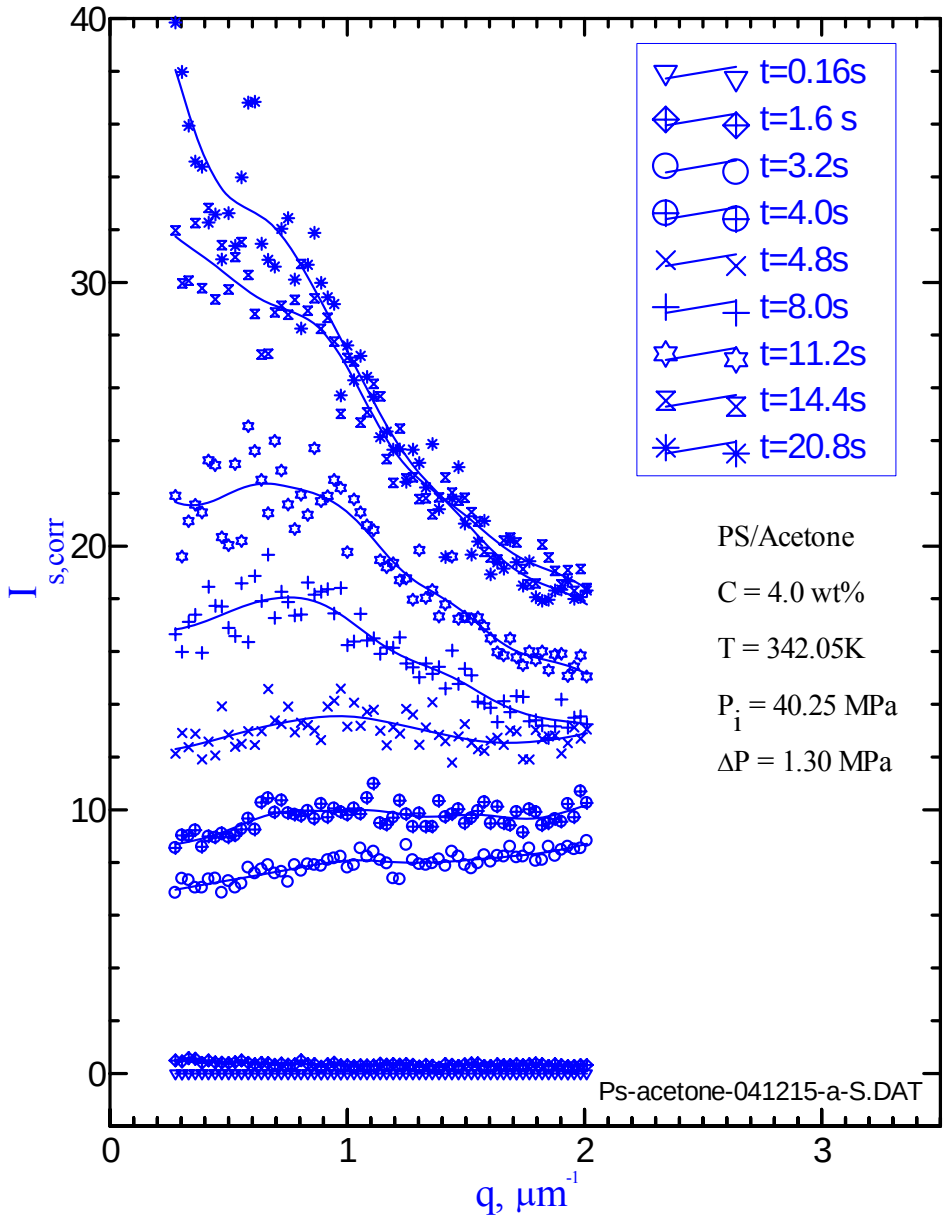

Figure 3.6 Scattered light intensity profiles as a function of wave number (scattering angle) and time for a pressure quench in 4.0 % by mass polystyrene solution in acetone at 342 K. The quench depth $\Delta P = 1.30$ MPa

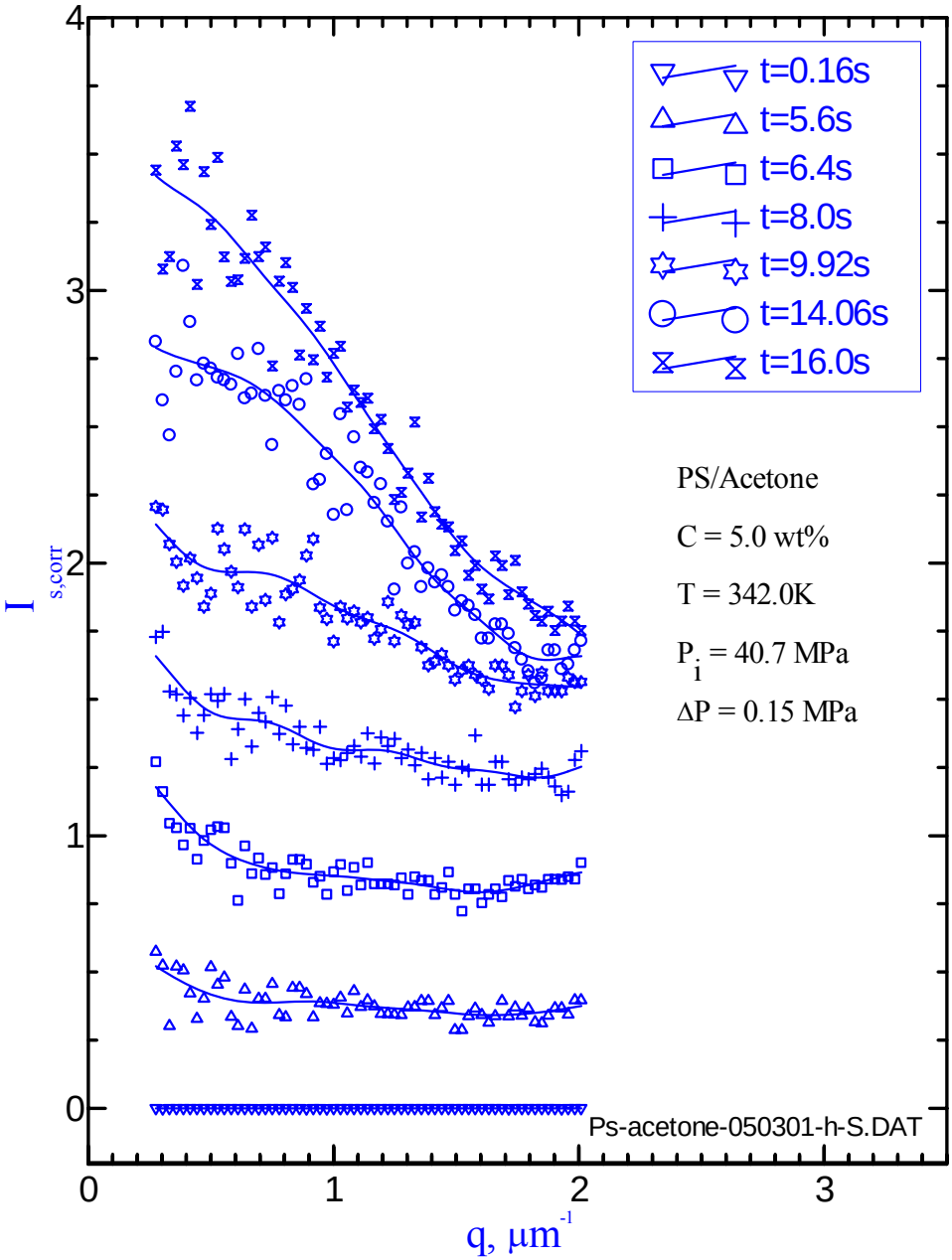

Figure 3.7 Scattered light intensity profiles as a function of wave number (scattering angle) and time for a pressure quench in 5.0 % by mass polystyrene solution in acetone at 342 K. The quench depth $\Delta P = 0.15$ MPa

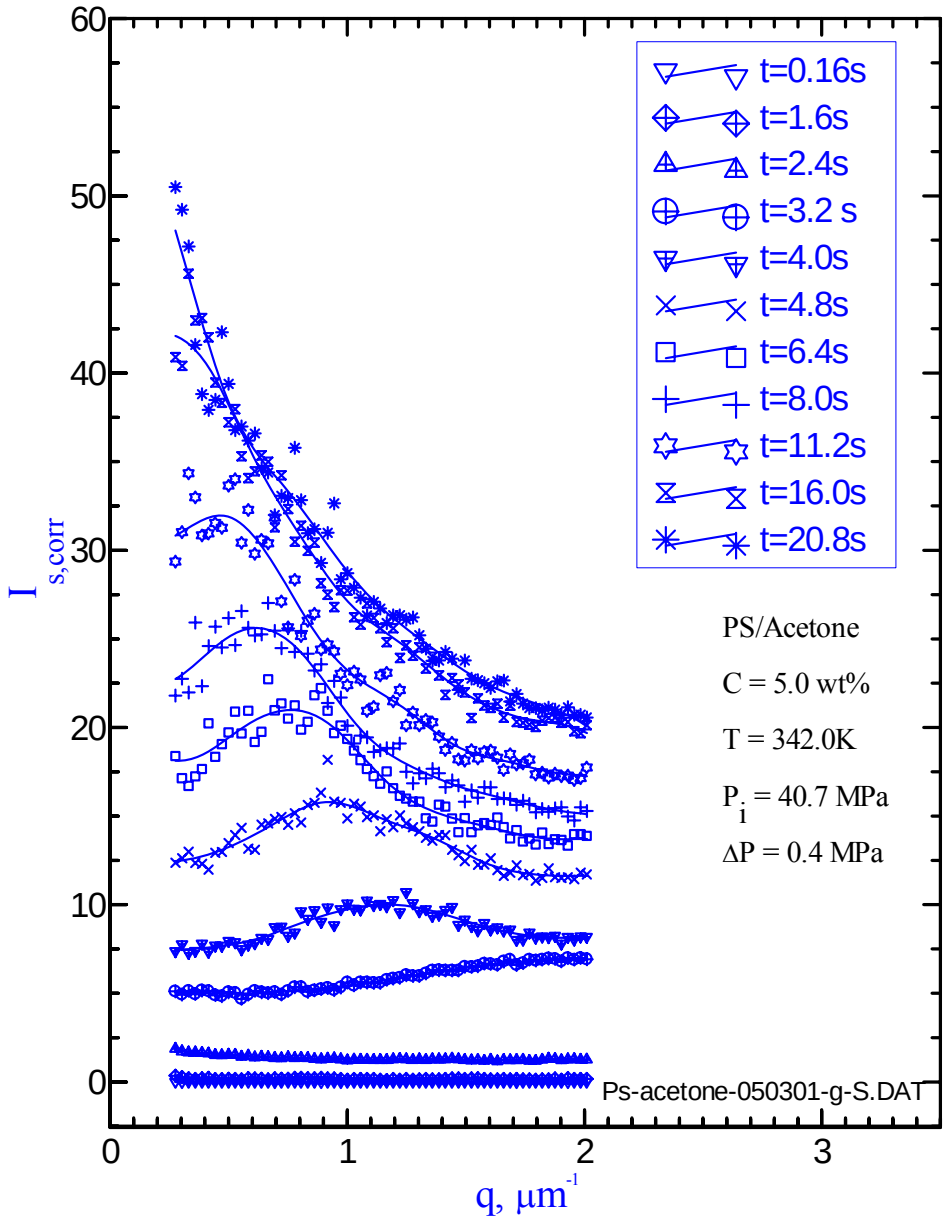

Figure 3.8 Scattered light intensity profiles as a function of wave number (scattering angle) and time for a pressure quench in 5.0 % by mass polystyrene solution in acetone at 342K. The quench depth $\Delta P = 0.50$ MPa

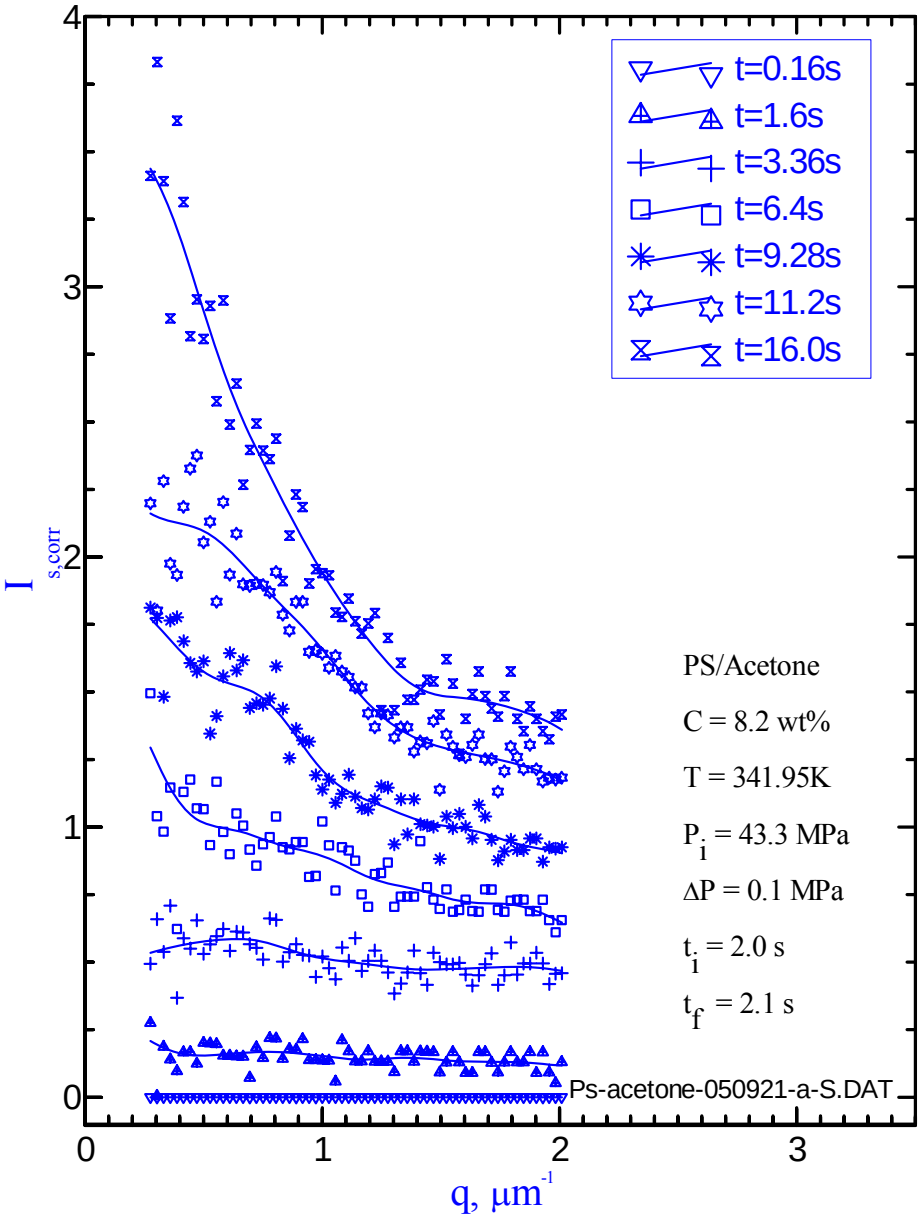

Figure 3.9 Scattered light intensity profiles as a function of wave number (scattering angle) and time for a pressure quench in 8.2 % by mass polystyrene solution in acetone at 342 K. The quench depth $\Delta P = 0.10$ MPa

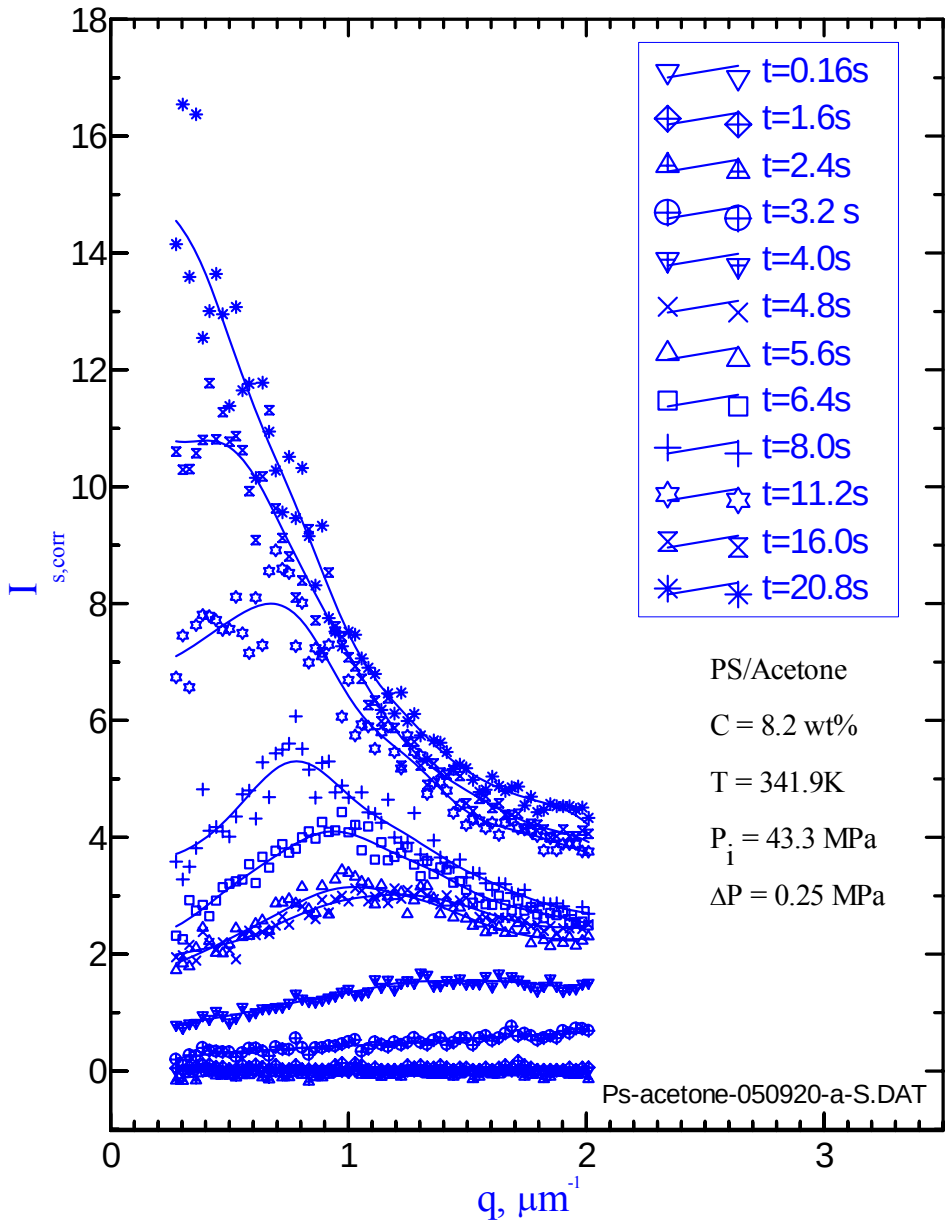

Figure 3.10 Scattered light intensity profiles as a function of wave number (scattering angle) and time for a pressure quench in 8.2 % by mass polystyrene solution in acetone at 341.9 K. The quench depth $\Delta P = 0.25$ MPa

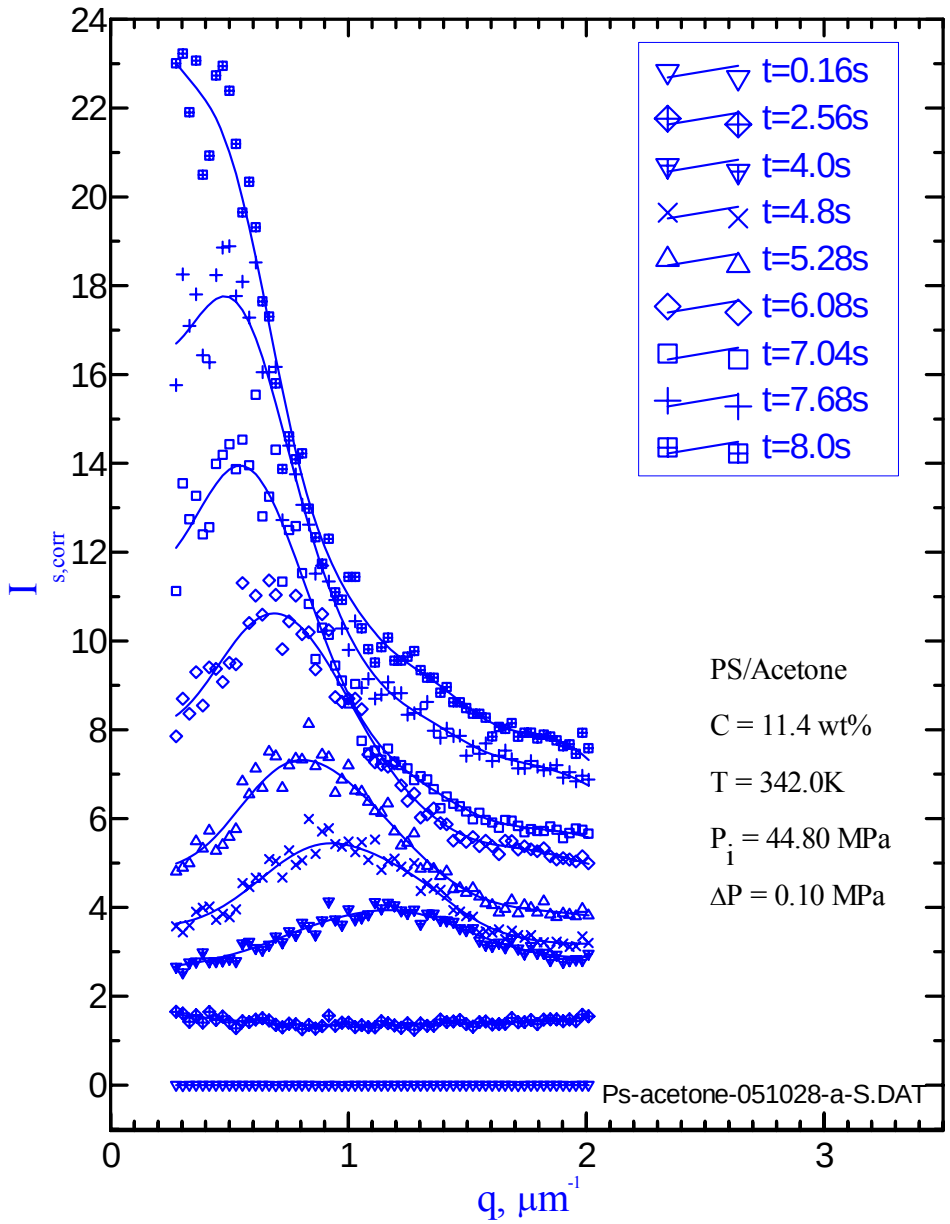

Figure 3.11 Scattered light intensity profiles as a function of wave number (scattering angle) and time for a pressure quench in 11.4 % by mass polystyrene solution in acetone at 342.0 K. The quench depth $\Delta P = 0.10$ MPa

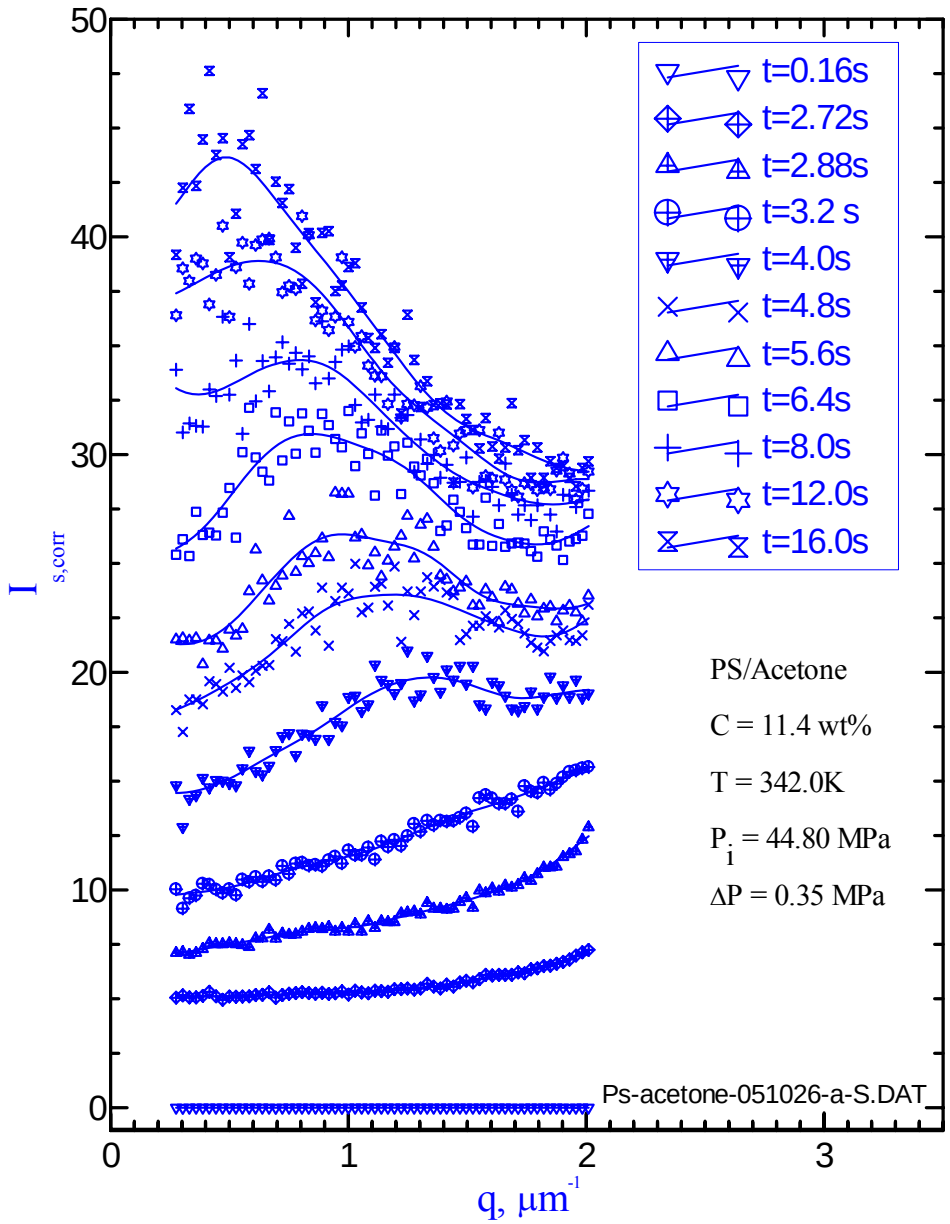

Figure 3.12 Scattered light intensity profiles as a function of wave number (scattering angle) and time for a pressure quench in 11.4 % by mass polystyrene solution in acetone at 342.0 K. The quench depth $\Delta P = 0.35$ MPa

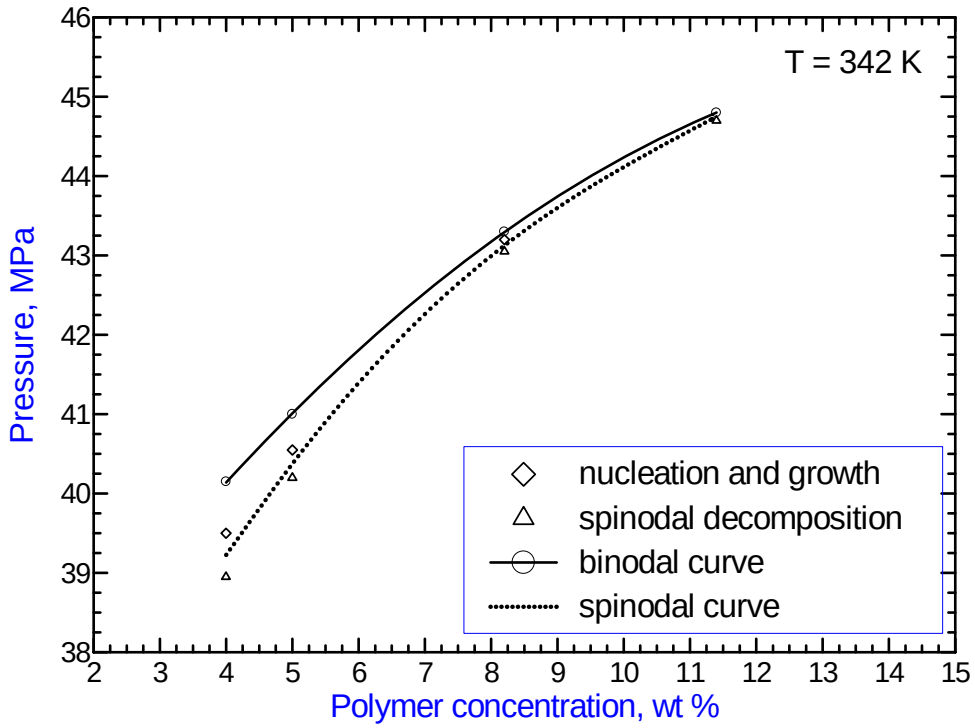

Figure 3.13 Pressure-composition phase diagram and the experimental determined spinodal and binodal curves for PS (129.2K) + acetone system at 342 K

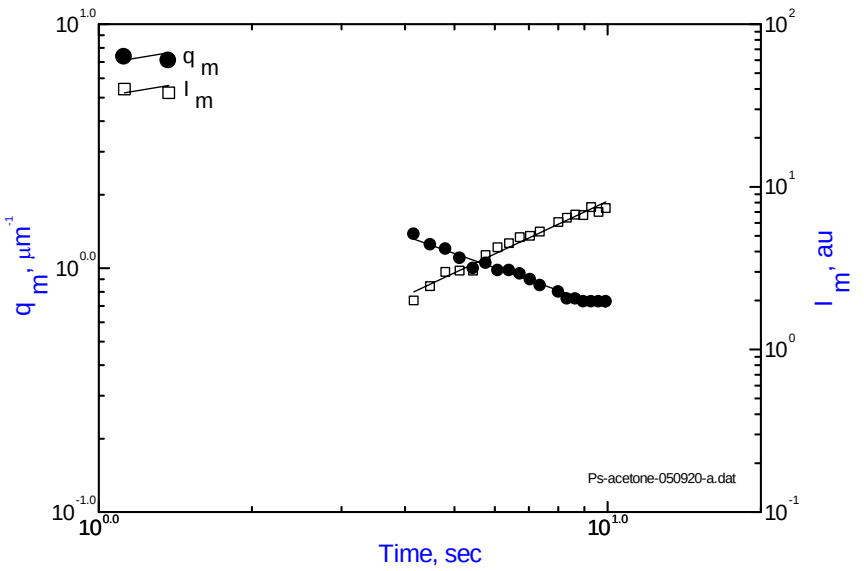

(a)

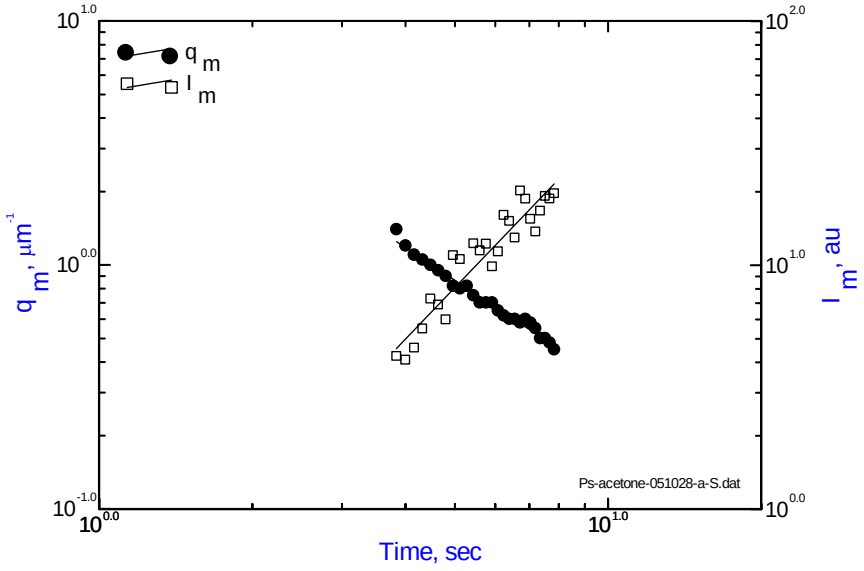

(b)

Figure 3.14 Power-law dependence of q_m and I_m on time. (a): the data correspond to 8.2 wt % solution subjected to 0.25 MPa quench as shown in Figure 3.10. (b): the data correspond to 11.4 wt % solution subjected to 0.1 MPa quench as shown in Figure 3.11.

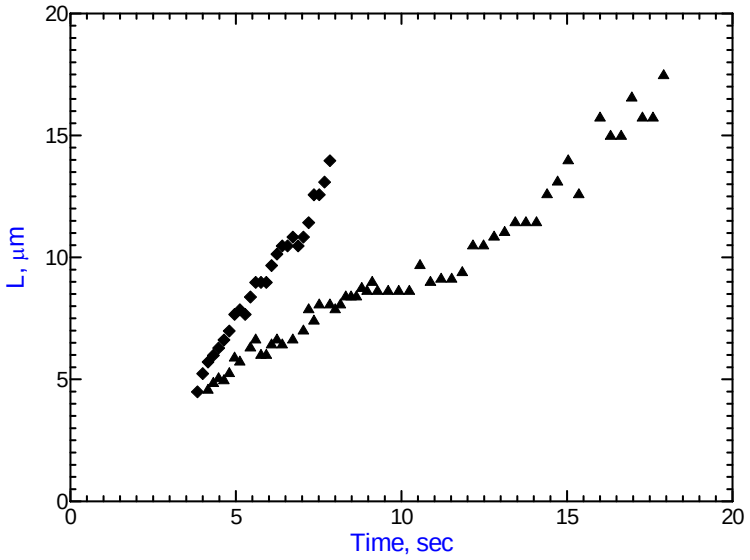

Figure 3.15 Evolution of the domain size with time. The triangle data correspond to 8.2 wt % solution subjected to 0.25 MPa quench as shown in Figure 3.10; the diamond data correspond to 11.4 wt % solution subjected to 0.10 MPa quench as shown in Figure 3.11.

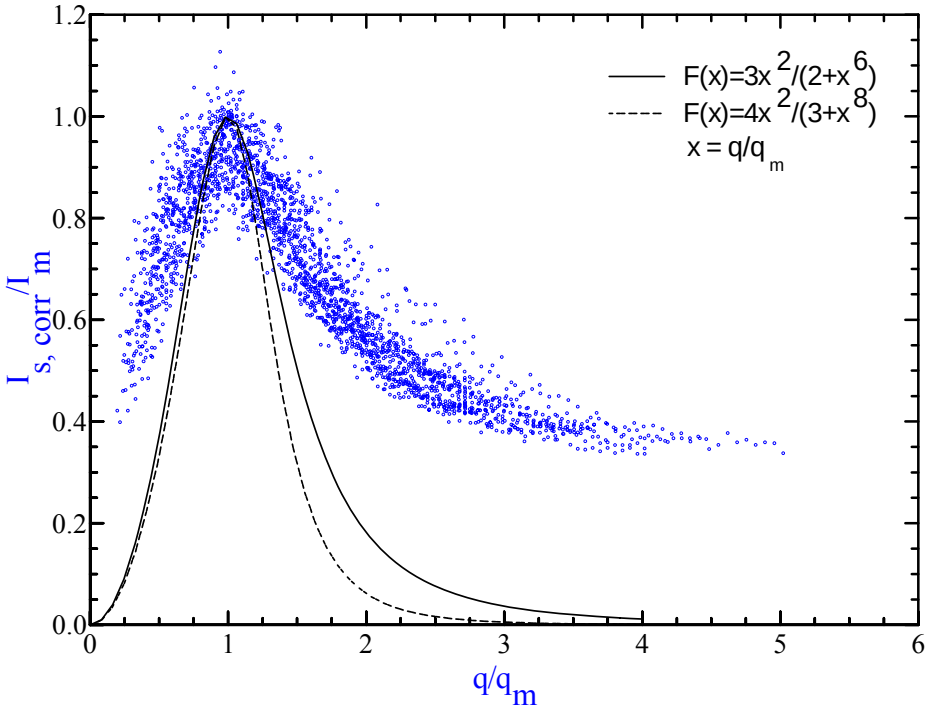

Figure 3.16 Test of dynamic scaling hypothesis for the reduced structure factor. The data correspond to 8.2 wt % solution subjected to 0.25 MPa quench as shown in Figure 3.10. The different time data scale collapse toward a master curve. The solid and dotted curves are the predications from the Furukawa universal scaling functions for off-critical and critical quenches, respectively.

Chapter 4

Crystallization and Gelation of Poly(4-Methyl-1-Pentene) in *n*-Pentane and in *n*-Pentane + CO_2 at High Pressures*

High pressure miscibility and phase separation of isotactic poly(4-methyl-1-pentene) in n-pentane and n-pentane + carbon dioxide mixtures have been studied in the pressure range from 10 to 50 MPa. In n-pentane no liquid-liquid phase separation was observed over the temperature range 298-423 K for solutions containing 1.0, 3.0, 4.6 and 6.5 wt % polymer. The fluid-solid phase boundaries (crystallization and melting temperatures) were determined for these solutions at 10.7, 14.5, 22.0, 29.5, 37.0 and 45.5 MPa. The experiments in n-pentane + carbon dioxide were carried out with the 4.6 wt % polymer solutions, for fluid mixtures containing 5, 10, 20, 40 and 50 wt % carbon dioxide. In the systems containing 5 - 20 wt % carbon dioxide, no liquid-liquid phase separation boundary could be identified, however, compared to the n-pentane solutions, the crystallization and melting temperatures were lowered. In solutions containing 40 and 50 % carbon dioxide in the solvent mixture, instead of crystallization, a new sol-gel type phase transformation was observed, characterized with connectedness of the solution in contrast to particle formation in the case of crystallization. The sol-gel transition temperature was observed to show higher sensitivity to pressure and was observed to move to higher temperatures with increasing carbon dioxide content. The crystals and gel samples collected from the high pressure view cell were characterized by DSC, NMR and SEM to identify the type of crystal modification of the polymer that is promoted in the different solvents and /or pressure conditions, and to assess the resulting morphological changes. This polymer is known to be polymorphic with five different crystal modifications. The original polymer was of Form I with a DSC melting transition at 506 K. When recrystallized from n-pentane

* Published as J. Fang and E. Kiran, "*Crystallization and gelation of isotactic poly(4-methyl-1-pentene) in n-pentane and in n-pentane +CO_2 at high pressures"* J. Supercrit. Fluids (2006), 38 132-145

at ambient pressure it transforms to Form III as verified by NMR results. It displays a DSC endotherm at 347 K, and a multiple melting endotherm clustered around 506 K. When recrystallized in n-pentane at high pressures, it transforms to Form II crystal modification, in which the 347 K endotherm disappears, but an endotherm at 406 K appears. Crystals formed in solutions containing up to 20 wt % carbon dioxide were of Form II. The gels also showed crystalline features corresponding to crystal modification Form I which is further promoted at the higher pressure crystallizations. The SEM results revealed that the polymer inner structure transforms from a lacy appearance in crystals formed in n-pentane to more porous structures in gels formed from n-pentane + carbon dioxide solutions.

4.1 Introduction

Isotactic poly(4-methyl-1-pentene) (iP4MP1) is a semicrystalline polyolefin with a number of interesting properties [Lopez *et al.* 1992]. It is of practical importance as a membrane making polymer. It is the only semicrystalline polymer in which the density of the amorphous fraction is slightly higher than the density of the crystalline fraction at room temperature. Moreover, iP4MP1 presents a complex polymorphic behavior. Five different crystalline forms have been reported for this polymer when crystallized from semidilute solutions depending on the solvent and thermal history of the crystallization [Charlet and Delmas 1984; Charlet *et al.* 1984]. Form I is the most stable crystalline form which is the only one obtained from melt crystallization. Form II and Form III can be obtained from xylene and decalin solutions, as well as linear and branched alkanes [Charlet and Delmas 1984]. Form IV was obtained by annealing Form I above 473K under pressure up to 4500 bar. A Form V crystalline structure has been reported for gels formed in cyclopentane and cyclohexane [Charlet *et al.* 1984].

In this chapter we are reporting on the fluid-solid boundary and specifically the crystallization and gelation behavior of iP4MP1 in n-pentane and n-pentane + CO_2

mixtures. The study was conducted to explore (a) if the crystal modifications could be altered at high pressures in solutions of different carbon dioxide content, and (b) if high pressure conditions would promote gelation and if carbon dioxide would influence the gelation behavior of the polymer. Even though gelation is a well known occurrence in stereoregular polymers at ambient conditions, gelation of iP4MP1 from high pressure solutions, in particular binary in fluid mixtures containing carbon dioxide, to our knowledge has not been previously reported.

Polymer gels are basically a network of flexible chains in which the connectedness is created either by a chemical or physical process. Physical processes which favor association between certain points on different chains lead to formation of physical gels which are often thermoreversible. According to De Gennes [De Gennes 1979], physical gels involve either helical structures with two or more strands, or microcrystals with two or more chains, or they result from the formation of nodules as is the case with block copolymers. In the absence of chemical bonds and specific interactions such as ionic, dipole or hydrogen bonds, crystallization becomes the mode of association [Girolamo *et al.* 1976]. A recent review by Keller [Keller 1995] provides a comprehensive description of both chemical and physical gels with specific details of those chemical processes such as polymerization and crosslinking, and those physical processes such as phase transitions and crystallization, entanglements, or associations that lead to gelation.

Even though literature is limited, crystallization and gelation of polymers at high pressures and in systems containing a supercritical fluid components is of broad interest that range from creation of micro- or nanopartciles [Zhang and Kiran 2006] to microporous materials [Pradhan and Ehrlich 1995; Winter *et al.* 2002], and to generating high viscosity oil displacement fluids in secondary oil recovery operations [Vossoughi 2000]. For example, Pradhan and Ehrlich [Pradhan and Ehrlich 1995] have reported on forming porous

structures by drying the thermoreversible gels that are formed during crystallization of polyethylene and polypropylene from supercritical propane. Winter et al. [Winter *et al.* 2002] has recently reported on generation of porous polymers by first forming a swollen gel state of a cystallizable polymer in supercritical fluid medium and then chemically crosslinking the polymer to provide the connectivity leading to generate open microporous structures. A more recent study reports on the use of CO_2 to trigger chemical transformations in orgaonogels [George *et al.* 2005]. Gelation of biologically important polymers under pressure such as protein modifications is also of great interest in biomedical research as well as in food science such as food preservation [Gekko and Fukamizu 1991; Kanaya *et al.* 1993]. Understanding crystallization and gelation is also important to polymerization reactions [Weidner *et al.* 1997; Giles *et al.* 2003; Yeo and Kiran 2004; Kennedy *et al.* 2005; Tai *et al.* 2005] and formation of particles from high pressure solutions [Knez and Weidner 2003; Yeo and Kiran 2005; Upper *et al.* 2006; Zhang and Kiran 2006].

This chapter, which is a part of our research efforts on polymer miscibility and phase separation in binary fluid mixtures, is focused on the fluid-solid phase boundary; however it reports not only crystallization behavior but also a new sol-gel transition phenomenon. NMR, DSC and SEM results on the crystals and gels that are recovered are presented to describe the effect of the pressure and the fluid composition on the crystal modifications and the resulting morphologies.

4.2 Experimental Section

4.2.1 Materials

The isotactic P4MP1 sample was purchased from Aldrich (cat # 19100-0). It is reported to have a melt index value of 8 g/10 min at 533 K. As shown in the DSC scan in Figure 4.1, under 10 K/min heating and cooling rates, the as-received polymer has a melting transition

at 506 K, and displays two crystallization peaks at 481 and 484 K. The solvent, n-pentane, with a stated minimum purity of "99+%" was purchased from Sigma-Aldrich. Carbon dioxide with a minimum purity of 99.99% was purchased from Air Products. The polymer and the solvents were used without further purification.

4.2.2 Determination of the Phase Boundaries

The determination of phase boundaries was carried out in a variable-volume view-cell system shown in Figure 4.2 [Zhang *et al.* 2003; Upper *et al.* 2006]. The cell is equipped with two sapphire windows for visual observation. A movable piston is used to alter the inner volume of the cell and control the system pressure. A computerized data acquisition system is used to record the temperature, pressure and changes in the transmitted light intensity (I_{tr}) during a phase separation experiment.

In preparation of the polymer solutions in the view cell, pre-weighted polymer (which was in pellet form) is first loaded into the system by removing the variable volume attachment. The solvent(s) are then sequentially (first n-pentane and then CO_2) pumped from a solvent transfer vessel. The amount of solvent charged is recorded with an accuracy of 0.01g from the difference in the mass of the transfer vessel before and after the charge using a Mettler (model 6100) balance. After the desired amount of the polymer and the solvent corresponding to a target composition are loaded, the cell is heated to the desired temperature, and the polymer solution is pressurized by the movable piston to form (if achievable) a clear homogeneous solution phase. The miscibility is verified by observing the solution through the sapphire windows. The magnetic stirrer is used to facilitate the dissolution process.

Phase boundaries were determined along constant pressure paths by either cooling or heating the cell and monitoring the intensity of transmitted light during the process. When

phase separation occurs, the intensity of the transmitted light changes (decreases) rapidly. This is illustrated in Figure 4.3 which represents the data during a cooling experiment from 350 to 310 K at 29.5 MPa in a 4.6 wt % solution of iP4MP1 in n-pentane. The initial phase-demixing temperature is identified as the departure point from the base transmitted light intensity for the homogeneous solution (shown with the arrow in Figure 4.3). Figure 4.4 shows the system behavior during re-heating the phase separated mixture from about 305 to 375 K while holding the pressure still constant at 29.5 MPa. The temperature corresponding to the departure point (shown with the arrow in the Figure 4.4) from the base transmitted light intensity is recorded as the initial remixing or melting temperature. The phase diagram of the solutions with different polymer weight fractions in n-pentane and n-pentane/CO_2 were thus generated by crossing the phase boundary at constant pressure in both the cooling and heating directions.

4.2.3 Differentiation between Crystallization and Gelation

In this study we make a distinction between a solid-fluid transition that is attributed to crystallization, and a sol-gel transition that is attributed to gelation (which may nonetheless be caused by a different mode of crystallization). This distinction is made by visual observations. While the intensity of the transmitted light decreases for both types of transitions, the visual observation through the sapphire windows gives two different pictures. When the system undergoes solid-fluid transition (crystallization), a turbid suspension of particles is observed with no hindrance to the free rotation of the magnetic stirrings bar in the cell. When however the system undergoes a sol-gel transition (gelation), one actually observes a gel in the cell. No suspended solids are observed in the cell, and the stirrer bar gets stuck in the gel and stops turning. The phase boundaries determined from the transmitted light intensity changes are categorized in the following sections as either fluid-solid or sol-gel boundaries as differentiated by such visual observations.

4.2.4 NMR Characterization

^{13}C solid state cross- polarization magic angle spinning (CP-MAS) NMR studies were conducted using a Bruker MSL 300 spectrometer operating at 75.47 MHz on the polymer samples crystallized or gelled in different solvents and different pressures employed in the present study. All spectra were calibrated using adamantine as a standard for the solid CH_2 peak at 38.4 ppm giving shift values referenced to the TMS carbon at 0 PPM. These NMR CP-MAS data were compared with the characteristic NMR patterns reported in the literature [De Rosa *et al.* 1997] for different crystalline forms of this polymer for assignment of the crystalline forms that were generated in a given experiment.

4.2.5 DSC Characterization

A Perkin Elemer (Pyris Diamond) Differential Scanning Calorimeter was used to document the thermal transitions displayed by the initial and treated polymers. Temperatures were calibrated using indium and tin standards. With each sample 4 consecutive scans at 10 K/min heating /cooling rates were generated in inert nitrogen atmosphere. In the first scan the polymer sample was heated to 533 K and then cooled to room temperature which shortly after (about 1 min) was followed by a second heating and a final cooling scans.

4.2.6 SEM Characterization

The morphological features of the samples were investigated using a Leo 1550 Field Emission Scanning Electron Microscope (FESEM). The samples were coated with a 6 nm layer of gold using a Cressington 208 HR sputter coater to reduce the electron charging effects.

4.3 Results and Discussion

4.3.1 iP4MP1 + n-Pentane

4.3.1.1 Phase Boundaries.

Phase boundary determinations were carried out with 1.0, 3.0, 4.6 and 6.5 wt % solution of iP4MP1 in n-pentane by cooling and reheating the system while holding the pressure constant at 10.7, 14.5, 22.0, 29.5, 37.0 and 45.5 MPa. The phase transitions in this system were all fluid-solid (crystallization, during cooling) or solid-fluid (melting, during heating) type transformations. The results are shown in Figure 4.5. The data are tabulated in Table 4.1. As shown in the figure these boundaries are sharp boundaries. The difference in crystallization and melting temperatures is common occurrence which decreases when lower heating and cooling rates are employed [Kiran and Liu 2002]. The difference between crystallization and melting temperatures for this system is however much larger than that we had reported for solutions of high density polyethylene (HDPE) in n-pentane [Kiran and Liu 2002; Upper *et al.* 2006], which is indicative of a slower rate of crystallization for iP4MP1 in n-pentane which may lead to a greater supersaturation. Another difference with the HDPE system is the slightly negative slope of the crystallization line in iP4MP1 solutions which becomes more apparent when polymer concentration is greater than 1.0 wt %. The shape of the fluid-solid boundary typically reflects the competition between a hydrostatic effect that tends to raise the temperature and a solvent effect that tends to decrease the temperature. As shown in Figure 4.1, iP4MP1 has melting and crystallization transitions which are in the 480-506 K range, which in n-pentane are reduced by nearly 200 K to a range in 300-330 K. The solvent effects and high degree of depression of crystallization temperature may be compensating for the hydrostatic effect and lead to the observed negative slope for the boundary.

Figure 4.6 shows the variation of the crystallization temperature with polymer concentration at three different pressures. A crystallization temperature increases up to

about 5 wt %. At concentrations above 6.5 % complete miscibility conditions could not be achieved at the pressures accessible within the view cell.

Additional experiments were carried out with this system by reducing pressure at selected temperatures in the range from 298 to 423 K. No phase change (which would have been a liquid-liquid type phase boundary) could be detected and the system remained homogeneous in the temperature interval indicating that n-pentane is a good solvent for this polymer.

4.3.1.2 Crystal Modifications.

Figure 4.7A shows the NMR spectrum of the original polymer sample. Based on comparisons with literature [De Rosa *et al.* 1997], the crystal modification for the as-received polymer is identified to be Form I. Figure 4.7B is the spectrum of the crystal collected at ambient pressure from n-pentane solution. The crystal modification is identified to be Form III. Figure 4.7C shows the spectrum for the crystal obtained in n-pentane solution at 14.5 MPa. With the appearance of the peak at 22.5 ppm, the crystal modification of this sample is identified to be a mixture of Form II and Form III.

4.3.1.3 Thermal Transitions.

Figure 4.8 shows the DSC scans on the polymer sample that was collected from the view cell after crystallization in n-pentane solution (4.6%) at 14.5 MPa at 301 K for 10 hrs. The first heating scan shows the thermal behavior of the polymer crystals as collected from the view cell. It displays characteristic endothermic peaks at 347 and 406 K and a cluster of three peaks at 489, 498, and 506 K. During the first cooling scan, a doublet crystallization peaks are observed at 484 and 487K. In the second heating scan, only one endotherm at 506 K is observed, all other endothermic peaks disappear. The second cooling scan however reproduces the same doublet crystallization peaks as observed in the first cooling

scan. Once the crystallization history is erased in the first heating scan, the behavior reverts to that of the original iP4MP1 (see Figure 4.1).

Figure 4.9a compares the first heating scans and Figure 4.9b the first cooling scans for the polymers crystallized in 4.6 % solutions in n-pentane at 301 K for 10 hrs at 14.5, 29.5 and 44.5 MPa. Original polymer scan is also included for comparisons. The crystals obtained at 29.5 and 44.5 MPa do not show the endotherm at 347K. In these samples the endotherm at 406 K becomes more distinct. The triplet melting cluster at the high temperature range reduces to a doublet with peak temperatures at 489 and 506K. In the cooling scans, all samples display the double crystallization peaks at 484 and 487 K, however in the samples obtained form higher pressure crystallizations, these appear to merge closer.

Analysis of the DSC data along with the NMR spectra support that the endotherm at 347 K must correspond to transformation of Form III to Form II, and the endotherm at 406 K must represent the transformation from Form II to Form I. The triplet or doublet endotherms in the 489-506 K range represent the melting transition of Form I crystals. In an earlier study on crystallization of iP4MP1 from different dilute solutions, Charlet and coworkers [Charlet and Delmas 1984] had also reported that Form III crystals were formed in n-pentane and they attributed the thermal transformation that they observed in the temperature range from 428 - 441 K as corresponding to Form III-to-Form I solid-solid transition.

The multiplicity of the melting transition is a common phenomenon observed in crystallization from high pressure solutions and the possible reasons leading to such multiplicity of melting peaks has been described in our recent publications[Upper *et al.* 2006; Zhang and Kiran 2006].

4.3.2 iP4MP1 + n-Pentane + CO_2

4.3.2.1 Phase Boundaries

The influence of CO_2 on the phase boundaries were investigated for 4.6 wt % polymer solutions in n-pentane + CO_2 solvents mixture with carbon dioxide levels of 5, 10, 20, 40 and 50 wt % in the solvent mixture. Up to 20 wt % CO_2 levels, the system showed solid-fluid phase transitions. For the fluid mixtures containing 40 % and higher CO_2, the transitions were sol-gel type transitions.

I. Fluid-Solid Transition Figure 4.10 shows the fluid-solid phase boundaries for 4.6 wt solutions in n-pentane + CO_2 mixtures (with CO_2 content $\leq$ 20 wt %) which were determined along a cooling (crystallization) and then a heating (melting) path while holding pressure constant at 10.7, 14.5, 22.0, 29.5, 37.0 and 44.5 MPa. The data are tabulated in Table 4.2. The boundary in n-pentane (i.e., 0 % CO_2) is also included in the figure for comparisons. In the binary fluid mixtures containing carbon dioxide the phase transition temperatures are observed at lower temperatures compared to the transition temperatures in pure n-pentane with majority of the reduction taking place at CO_2 addition levels up to 10 wt % as illustrated in Figure 4.11.

II. Gel-Sol Transition A striking difference has been observed in the phase behavior of iP4MP1 solutions in n-pentane + CO_2 mixtures in which CO_2 content in fluid mixture is high (above 20 wt %). Visual observations through the view cell in these systems indicate that during cooling the solution transforms into a gel.

Figure 4.12 shows the sol-gel transition temperatures for iP4MP1 in binary solvent mixtures containing 40 and 50 wt % CO_2. These boundaries were determined again along cooling and heating paths while holding the pressure constant at selected values as listed in Table 4.2. Comparison with Figure 4.10 shows that the sol-gel boundary is not as sharp as

the fluid-solid boundary, and occurs at higher temperatures. This transition is more sensitive to pressure and shifts to significantly lower temperatures (while still being higher than the fluid-solid transition temperatures) with increasing pressure.

This sol-gel boundary displays characteristics that appear to be a combination of fluid-solid and liquid-liquid phase separation. The high sensitivity of the transition temperature to pressure is a common feature of liquid-liquid phase transitions, while the difference in the observed temperatures of the phase change along the cooling and heating paths is typical of a fluid-solid (crystallization /melting) phase transitions. These features are consistent with the intrinsic characteristics of physical gels in which the connectedness is typically provided by the crystalline (mostly fringed micelles but also in case of very high molecular weight systems chain folded crystals) domains that are linked by amorphous or tie chains [Keller 1995]. This is akin to the notion of a "crystalline –amorphous supermolecular structure" that has been previously proposed to describe P4MP1 films cast from solution [Danch and Gadomski 2000].

It is important to note once again that an exclusive UCST-type L-L phase transition is eliminated for explanation of the phase boundary in Figure 4.12 because of the large temperature gap observed on cooling and heating process, which is the typical feature of fluid-solid (crystallization/melting) type transitions. The sol-gel nature of the transition has been further confirmed by observations of the final state of the samples collected from view cell. When the system undergoes solid-fluid transition (as is the case in the binary mixtures up to 20 wt % CO_2), particles were collected, whereas when the system undergoes sol-gel transition, the polymer in the cell can be removed as a plug.

4.3.2.2 Crystal Modifications

Figure 4.13 shows the NMR CP-MAS spectra of the gels formed in the n-pentane /CO_2

mixtures which have been compared with the NMR spectra of known crystalline forms of the polymers[De Rosa *et al.* 1997]. Figure 4.13 A is the spectrum of the sample obtained from the 4.6 wt % polymer solution in the binary fluid mixture containing 40 % CO_2 at 44.5 MPa. The crystal modification in this sample is identified to be Form II. Figure 4.13 B is the spectra for the sample obtained at the same pressure of 44.5 MPa, but in the binary fluid mixture containing 50 % CO_2. The crystal modification is a mixture of Form II and Form I. The peak at 32 ppm corresponds to the methine carbon of the backbone C2 (as marked in Figure 4.13A) in Form II, while the double peaks at 29 ppm and 29.7 ppm correspond to the methane carbon of the backbone C2 in Form I. Figure 4.13 C is the spectra of the sample obtained in the fluid mixture with 50 % CO_2 but at the lower pressure of 29.5 MPa. This sample displays the crystal modification Form I as is the case for the original polymer sample.

4.3.2.3 Thermal Transitions

Figures 4.14a and 4.15a show the first DSC scans on the samples that were crystallized / gelled from n-pentane + carbon dioxide mixtures at 29.5 and 44. 5 MPa. The scans are shown for samples generated from binary fluid mixtures containing 0, 5, 10, 40 and 50 wt % carbon dioxide. Figures 4.14b and 4.15b are the first cooling scans for the same samples corresponding to each pressure. The sample obtained from the fluid mixtures containing 0-10 % CO2 show similar features with a characteristic endotherm at 406 K and multiple melting peaks in the 489-506 K range. The 406 K endotherm represents the solid-solid transition from Form II to Form I crystal modification. This endotherm is not as observable in systems corresponding to high CO_2. In the cooling scans double crystallization peaks are observed which however appear to merge in samples obtained from fluid mixtures containing 40 and 50 % carbon dioxide.

4.3.3 Further Discussion on the Crystal Modifications

Table 4.3 is a summary of the crystal modifications that have been identified from different crystallization/gelation conditions. Original polymer is of Form I. When re-crystallized from n-pentane at ambient pressure, it transforms to Form III, and at higher pressure crystallizations a transition occurs to Form II, and at 29.5 and 44.5 MPa only Form II is observed. In systems containing carbon dioxide, the crystal modification tends to shift from a mixture of Form III and II to Form II (at 14.5 MPa), or from Form II to Form I (at 29.5 and also in part at 44.5 MPa at the highest CO_2 addition). These results show that the crystallization mostly favors the crystal modification Form II. Gelation on the other hand leads to the Form I crystal modification.

4.3.4 Further Discussion on Gelation

The gelation in iP4MP1 in n-pentane + carbon dioxide mixtures at high carbon dioxide loadings with crystalline features similar to Form I crystal modification as supported by NMR and DSC characterizations is an important observation with practical implications especially in the area of porous material formation. Even though high pressure data are lacking in the literature, the mechanisms by which the solutions of stereoregular polymers in general turn into thermoreversible gels has attracted significant attention over the past several decades. For example, in one of the earlier studies, Lemstra and Challa [Lemstra and Challa 1975] explored the crystallization of isotactic polystyrene [Phillips and Mezghani] in trans-decalin and also in benzyl alcohol. They observed that when solutions were subjected to large undercoolings and when cooled below 273 K, those systems with a polymer concentration greater than 1 wt % would transform to a “rigid gel”. The surface replicas of the freeze-etched gels showed that a fringed-micelle type crystallization was taking place at high undercoolings. The authors then proposed that a transition from a folded-chain type crystallization to a fringed-micelle type crystallization may cause “chain stiffening” of the polymer with a reduced mobility of the phenyl groups leading to the

observed gelation behavior. The fringed micellar bundle-like crystals would then provide the connectedness with "amorphous" chains emanating from these bundles, in contrast to chain-folded lamellae formation which would lead to particle formation. In the case of very high molecular weight polymer systems such as the ultra high molecular weight polyethylene in decalin different portions of a given chain may be linked to different chain folded crystals with interlamellar amorphous tie chains and the chain-folded crystals may also lead to gelation [Keller 1995]. The iPS gels indeed were of crystalline character, displaying sharp melting endotherms and distinct X-ray diffraction patterns (with a 12_1 helix) which were however distinctly different than 3_1 helix displayed by crystals formed by a chain-folding process [Girolamo *et al.* 1976; Sundararajan *et al.* 1982]. The extended 12_1 helix conformation was observed to be promoted in poor hydrocarbon solvents, whereas either the threefold 3_1 conformation or a mixture of three fold and extended conformations were obtained from the aromatic solvents. The influence and the role solvents were explored in a further study by Guenet [Guenet 1986]. DSC studies were conducted on the solvent heat of fusion with different polymer concentrations to assess the amount of solvent molecules adsorbed on the polymer chain at the melting temperature of the solvent. These studies led to the conclusion that the physical cross-links in systems like iPS in trans- or cis-decalin are solvated, that is the solvent is not just located in the amorphous region. The system is a congruently melting "polymer-solvent compound" in which chains are bridged together by solvent molecules, and the extent of the melting point depression depends on the co-crystallized solvent. The formation of a "polymer-solvent compound" has been reported also in the gels of syndiotactic polystyrene [De Rudder *et al.* 2002] and syndiotactic PMMA [Saiani and Guenet 1997]. The concept has been used to describe gel formation in P4MP1 is cyclopentane and cyclohexane [Charlet *et al.* 1984]. In cyclopentane, either crystals or gels were formed when cooling to different temperatures, and there seemed to be a competition between chain-folded crystal formation and gelation in the solution. This was in contrast to the observations in cyclohexane, in which gels were

formed at all conditions. It was proposed that here also the solvent is probably incorporated into the junctions that act as physical cross-links as in a "polymer-solvent compound". Additional support to this notion was later provided by Phuong-Nguyen *et al* [Phung-Nguyen and Delmas 1985] who examined the heat of formation of P4MP1 gels in different solvents. Large exothermic heats of interaction and their dependence on the polymer concentration were interpreted as being indicative of the solvent-induced chain association in this system. Aharoni *et al* [Aharoni *et al.* 1981] based on WAXD studies reported that the gels formed in cyclohexane display the crystalline form IV, but gels formed in cis-decalin display crystal form I, which is usually formed from crystallization from melts. Charlet and Delmas [Charlet and Delmas 1982] have reported on the formation of crystal form V in gels formed in cyclopentane. In a more recent study of gelation of P4M1P in cyclohexane at ambient conditions, a gel that displays crystal modification Form V has been reported [Wegsteen and Berghmans 1998] which is reported to transform to modification III upon drying.

It is likely that in the gels that formed in n-pentane + CO_2, a 'polymer-solvent compound' is also formed. Literature on other systems and present findings emphasize the presence of crystalline domains in the gels and that their crystalline form is influenced by the solvent environment in which they are formed. In the present system form IV and V were not observed which may be dominated in crystals formed in cyclic solvents only. The gels formed in the current study which dried and analyzed by NMR and DSC present Form I or Form II crystalline modification. It is, however, not known which mechanism already leads to the gelation and which crystalline modification is dominated in the gels prior to their collection and drying.

4.3.5 FESEM Result and Morphological Features

The morphology of the polymer samples recovered after recrystallization in n-pentane and

after crystallization or gelation in n-pentane + CO_2 mixtures are shown in Figures 4.16 and 3.17. These samples were obtained after crystallization at 289 K from 4.6 wt % solution in n-pentane at 14.5, 29.5 and 44.5 MPa (Figure 4.16) and in n-pentane + carbon dioxide mixtures with 10, 40 and 50 wt % carbon dioxide at 44.5 MPa. The inner details of the particles formed by crystallization in n-pentane showed a lacy feature with high surface area (Figure 4.16 a) which however appeared to become more dense at higher pressures (Figure 4.16c). Crystallization in binary fluid mixture also leads to formation of particles with a lacy inner structure (Figure 4.17a). The gels show more porous open morphology becoming more porous in gels formed at higher carbon dioxide containing system (Figures 4.17 b and c).

4.4 Conclusions

The present results show that iP4MP1 can be dissolved in and reprocessed from solutions in n-pentane or n-pentane + carbon dioxide fluid mixtures. It is shown that with addition of CO_2 into the solution, the fluid-solid phase separation boundary is shifted to lower temperatures. A unique transformation from crystallization to gelation, takes place in systems that contain high carbon dioxide. The demixing temperatures of gel-sol phase separation are higher than the demixing temperatures associated with fluid-solid phase separation. NMR spectra also reveal that three different crystalline modifications, Form III, Form II and Form I are formed by crystallization from solutions in n-pentane at ambient pressure, in mixture fluids with low content of CO_2 (less than 20 %) and in mixture fluids with higher CO_2 content at high pressures, respectively. The mixtures of Form III + Form II and Form II + Form I were also formed at conditions that are in between the conditions that would lead to pure crystalline modifications. DSC results show that a solid-solid transition of Form III to Form I, and Form II to Form I occur at 347 K and 406 K, respectively. The morphological results on the final crystals show that a more dense structure was formed at higher pressures, while a more porous structure was formed by incorporating more CO_2

into the processing fluid.

Table 4.1 Experimental data for solid-fluid phase separation in iP4MP1 + n-pentane system, crystallization (cooling) and melting (heating) boundary

Polymer Fraction (wt %)	Pressure (MPa)	Crystallization T (K)	Melting T (K)
1.0	44.5	297.2	320.0
	37.0	297.2	321.0
	29.5	297.2	321.5
	22.0	297.2	321.0
	14.5	297.3	320.0
	10.7	297.3	320.0
3.0	44.5	303.8	333.0
	37.0	303.5	332.5
	29.5	302.5	332.5
	22.0	303	331.0
	14.5	304.3	330.5
	10.7	305.2	329.5
4.6	44.5	309.0	337.5
	37.0	309.0	336.0
	29.5	309.0	335.5
	22.0	308.0	335.0
	14.5	309.0	333.5
	10.7	310.0	335.0
6.5	44.5	308.5	337.5
	37.0	308.5	337.5
	29.5	308.4	336.0
	22.0	309.0	336.0
	14.5	309.5	335.0
	10.7	309.7	334.0

Table 4.2 Experimental data for phase separation in 4.6 wt % iP4MP1 in n-pentane/CO_2 system

CO_2 in fluid mixture (wt %)	Pressure(MPa)	Solid-Fluid Transition	
		Crystallization T (K)	Melting T (K)
5	44.5	301.5	330.5
	37.0	301.5	330.5
	29.5	301.8	330.5
	22.0	302.5	331.0
	14.5	303.0	330.0
	10.7	303.5	330.0
10	44.5	299.0	330.0
	37.0	299.2	329.5
	29.5	300.0	329.0
	22.0	300.5	328.5
	14.5	302.5	328.0
	10.7	303.0	326.5
20	44.5	297.3	326.5
	37.0	297.5	327.0
	29.5	298.3	326.5
	22.0	299.5	325.5
	14.5	300.5	325.0
	10.7	304.0	327.5
		Gel-Sol Transition	
		Gelation T (K)	Dissolution T (K)
40	44.5	304.0	328.0
	37.0	310.0	330.5
	29.5	313.0	335.0
	22.0	317.0	341.0
	14.5	327.5	356.0
	10.7	339.0	-
50	44.5	310.0	333.0
	37.0	320.0	342.5
	29.5	325.0	347.5
	22.0	334.0	360.0

Table 4.3 Crystalline structures of iP4MP1 obtained from different solvents at different pressures.

Pressure (MPa)	n-pentane	n-pentane + CO_2, CO_2 wt %			
		5	10	40	50
44.5	II	II	II	II	II+I
29.5	II	II	II	I	I
14.5	III+II	III+II	II	-	-
ambient pressure	III	-	-	-	-

I : crystalline modification Form I
II: crystalline modification Form II
III: crystalline modification Form III

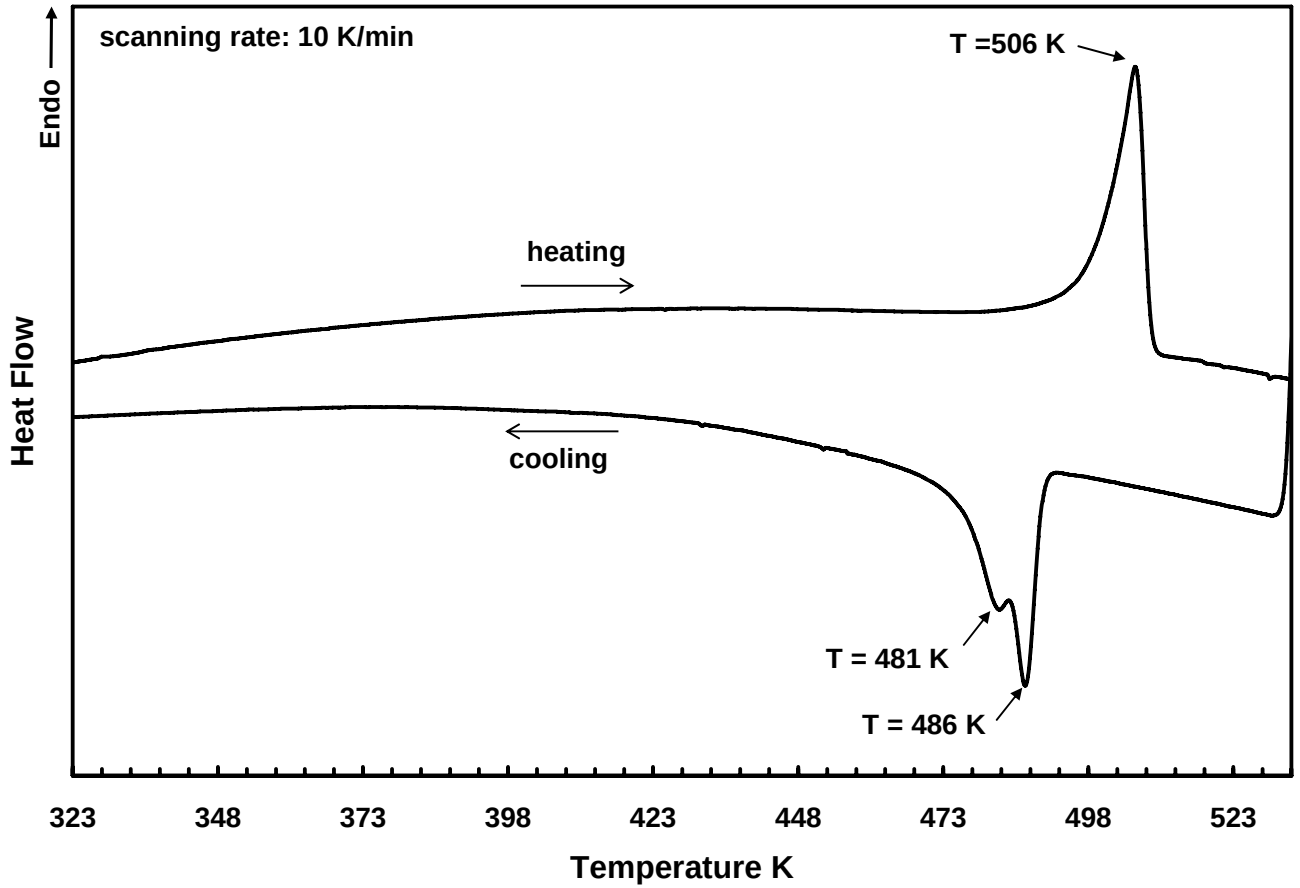

Figure 4.1 DSC scans on original poly (4-methyl-1-pentene) sample. The heating and cooling rates were 10 K/min

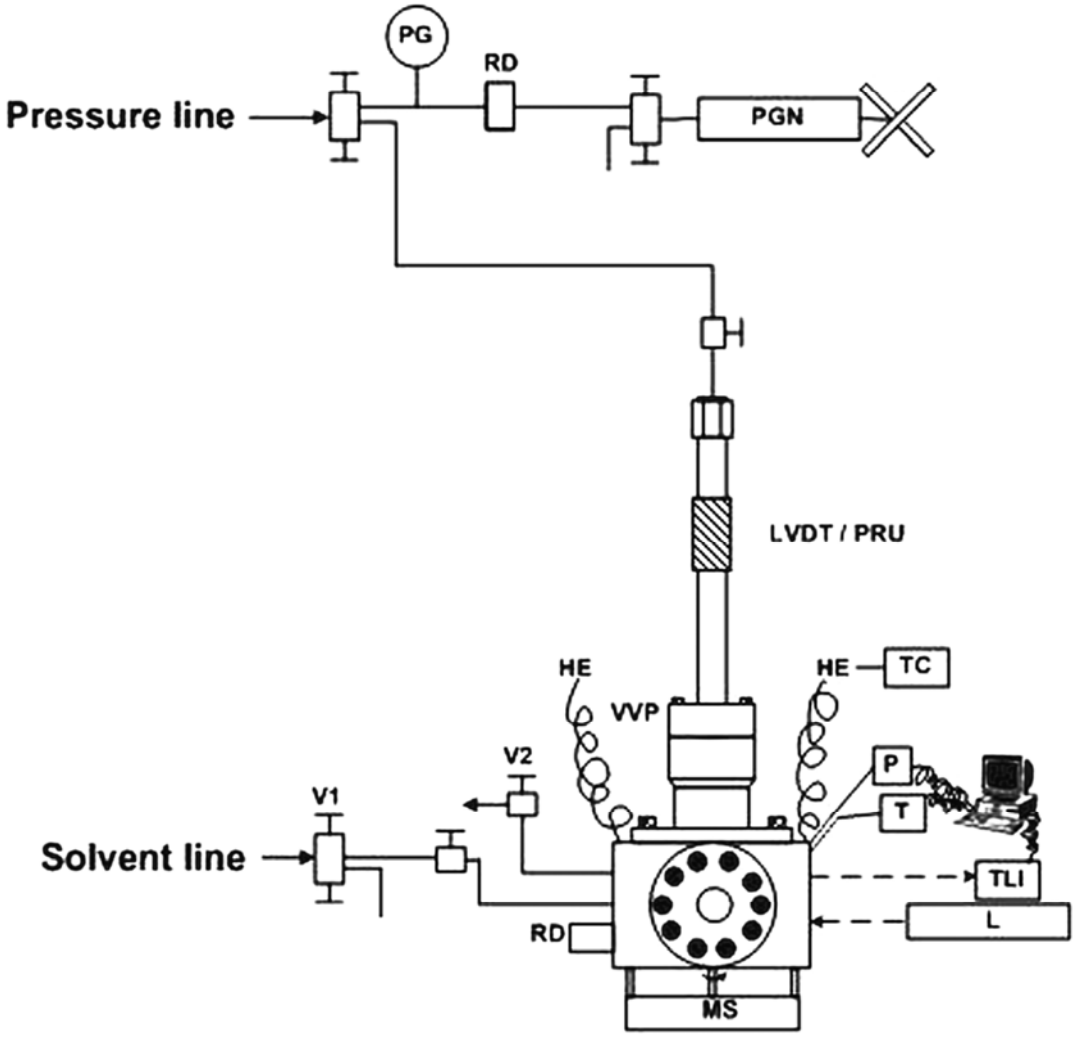

Figure 4.2 Schematic diagram of the view-cell for the determination of S-F phase boundary. PGN = pressure generator; LVDT = linear-variable differential transformer; PRU = position readout unit; TC = temperature controller; HE = cartridge heating elements; VVP = variable volume part housing the movable piston; P = pressure; T = temperature; L = Light Source; MS = magnetic stirrer; RD = Rupture Disk.

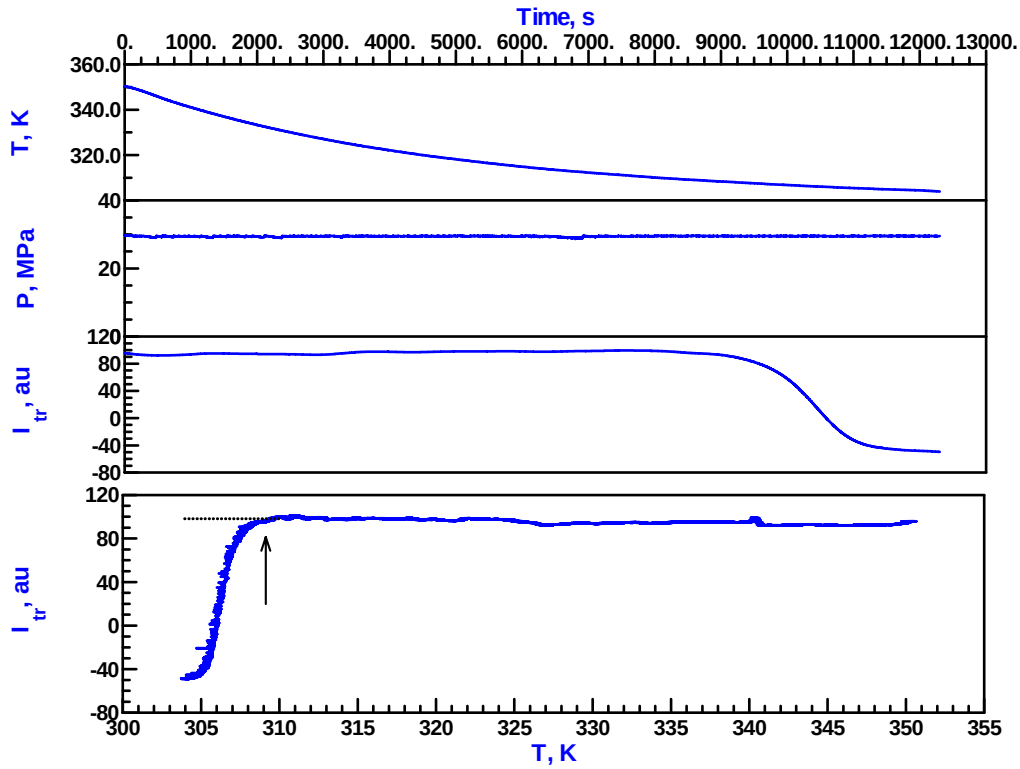

Figure 4.3 Variation of temperature (T), pressure (P), and transmitted light intensity (I_{tr}) (in arbitrary units) with time along a constant pressure path during cooling. The incipient demixing condition is determined from the variation of the transmitted light intensity with temperature (lower curve in the figure) as the point of departure from the base line intensity as indicated by arrow. The figure represents phase separation in 4.6 wt % solution of poly (4-methyl-1-pentene) in n-pentane and P = 29.5MPa.

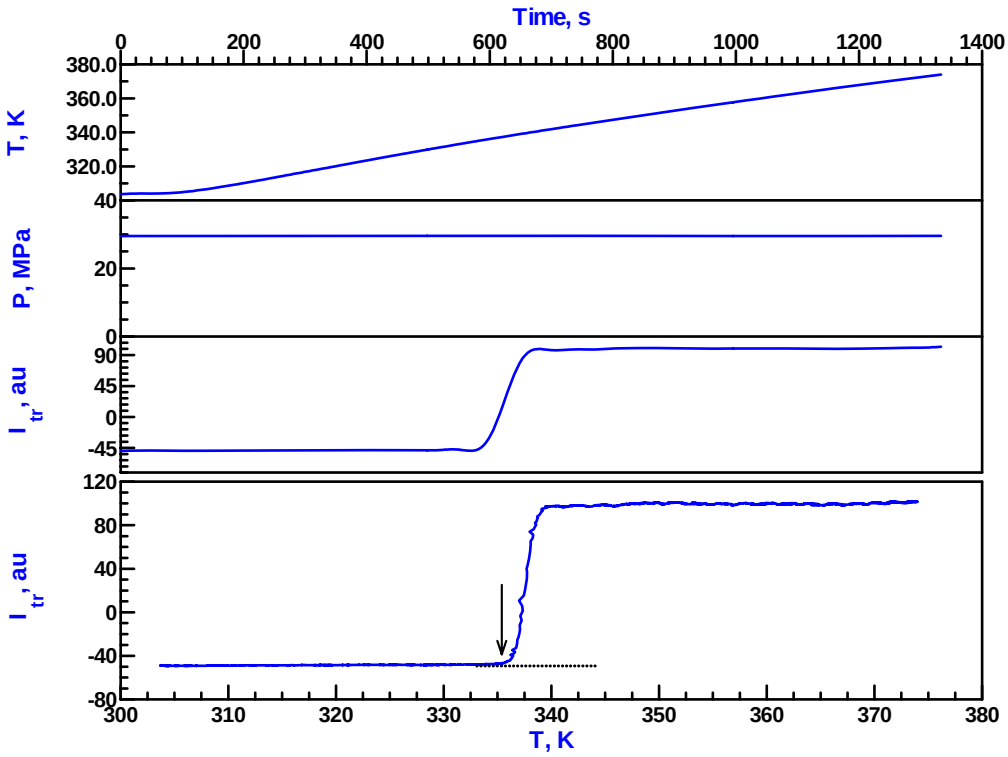

Figure 4.4 Variation of temperature (T), pressure (P), and transmitted light intensity (I_{tr}) (in arbitrary units) with time along a constant pressure path during heating. The incipient demixing condition is determined from the variation of the transmitted light intensity with temperature (lower curve in the figure) as the point of departure from the base line intensity as indicated by arrow. The figure represents phase separation in 4.6 wt % solution of poly (4-methyl-1-pentene) in n-pentane and P = 29.5MPa.

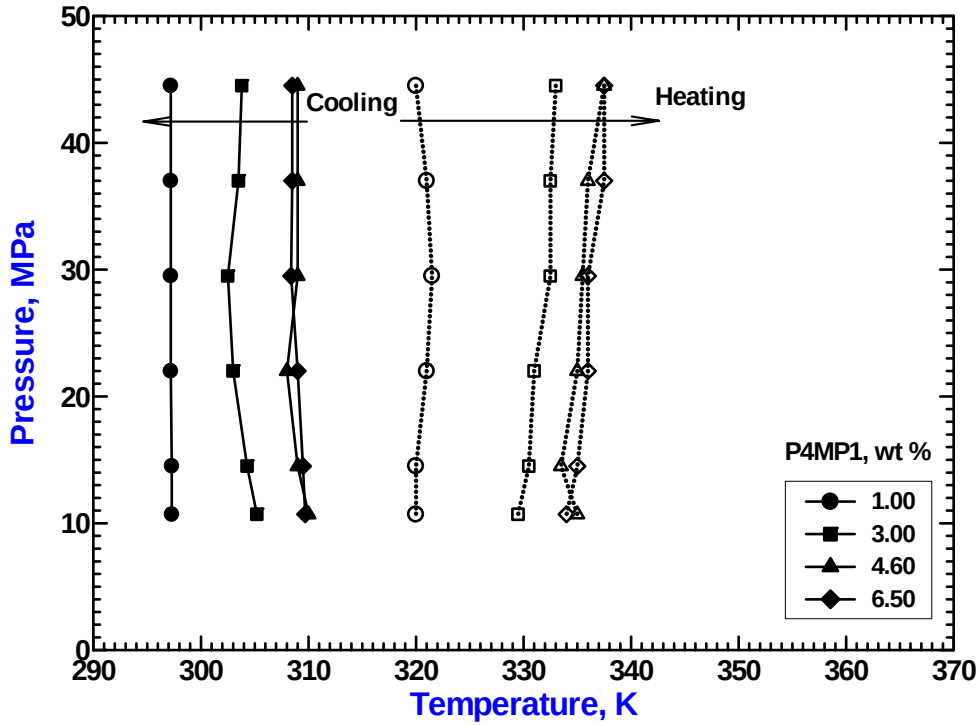

Figure 4.5 The solid-fluid phase boundaries for poly (4-methyl-1-pentene) solution in n-pentane for different polymer concentrations. Filled symbols represent the F-S phase transition (crystallization) temperatures upon cooling, and the open symbols represent the S-F phase transition (melting) temperatures upon heating.

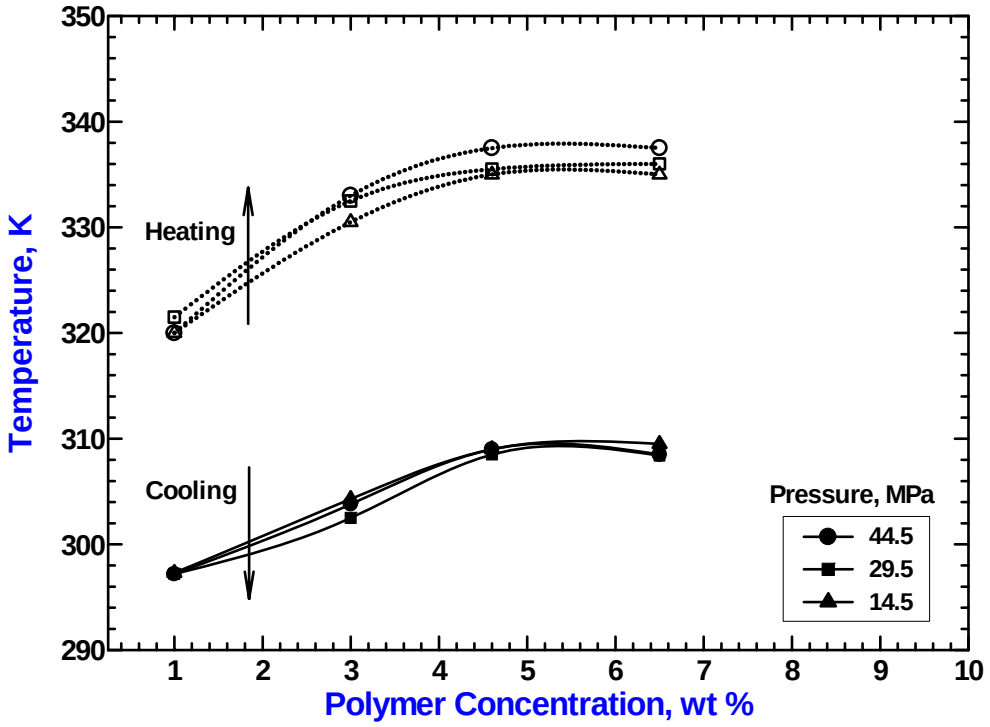

Figure 4.6 Variation of the crystallization (filled symbols) and melting (open symbols) temperatures with polymer concentration for poly (4-methyl-1-pentene) solution in n-pentane at pressures of 14.5, 29.5 and 44.5 MPa.

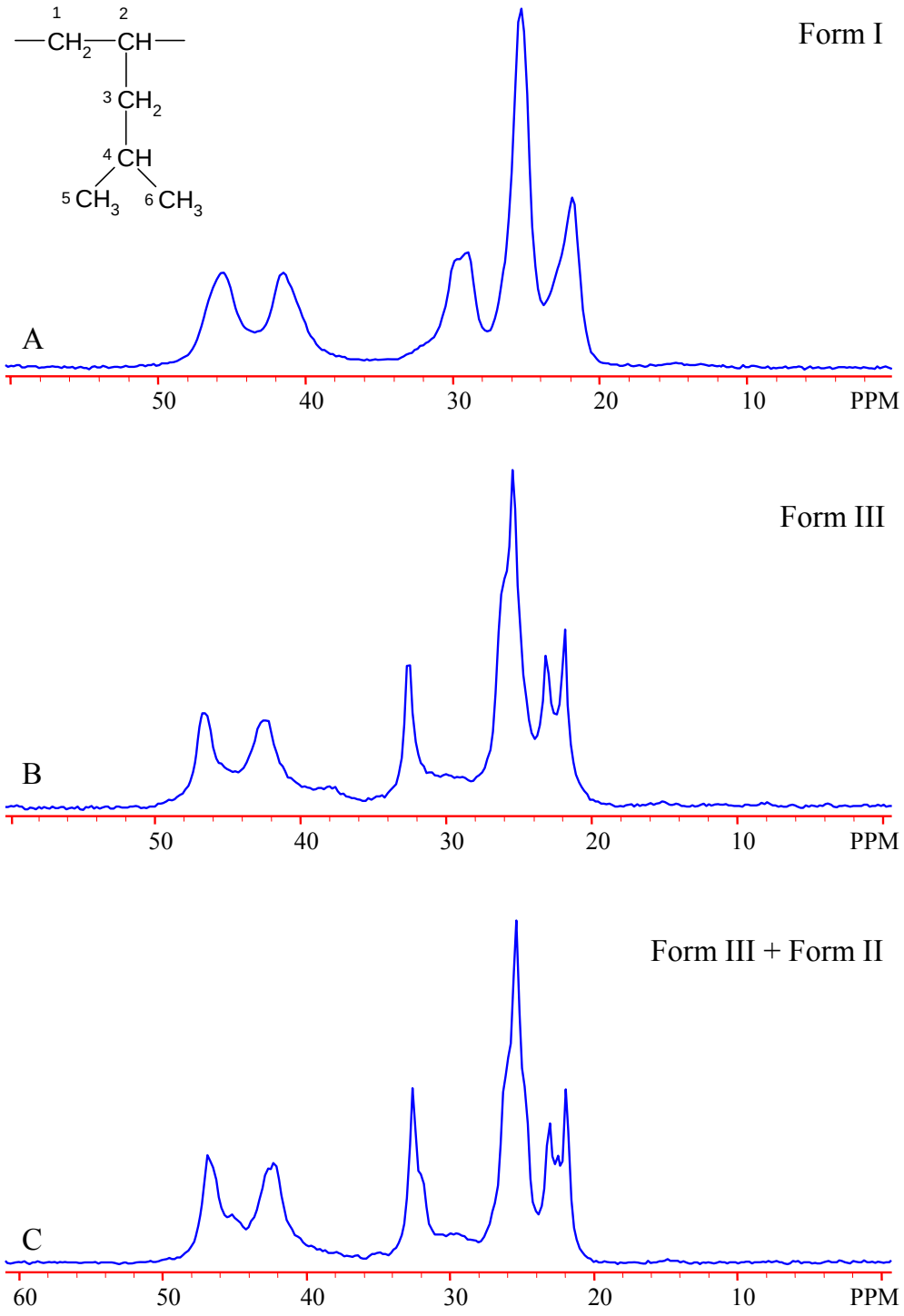

Figure 4.7 Solid-state ^{13}C NMR CP-MAS spectra of i-P4MP1: (A) original iP4MP1 sample; (B) polymer after crystallization in n-pentane solution at ambient pressure; (C) polymer after crystallization in n-pentane solution at 14.5 MPa.

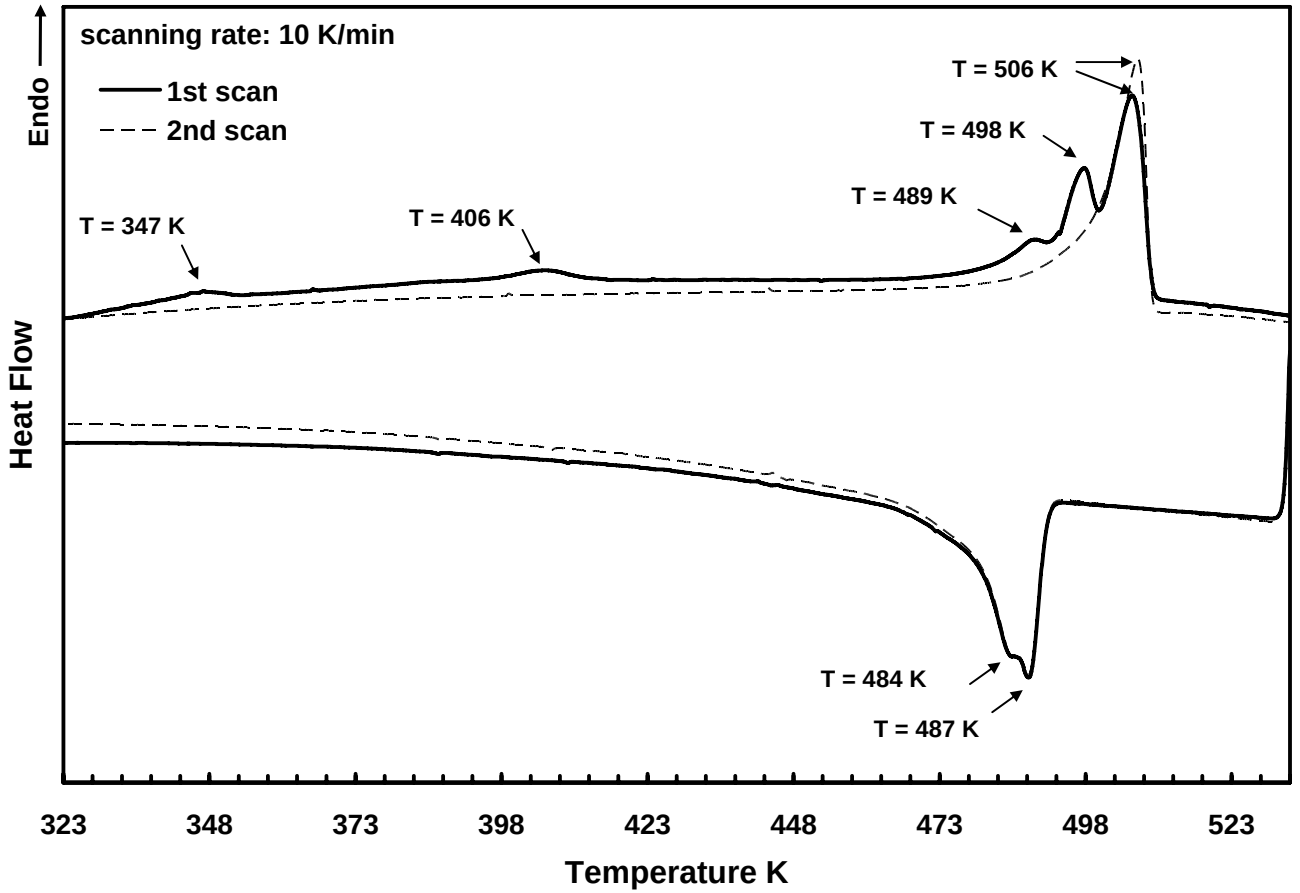

Figure 4.8 DSC scans on Poly (4-methyl-1-pentene) crystallized from a 4.6 wt % solution in n-pentane at 14.5 MPa and 301 K for 10 hours. The heating and cooling rates were 10 K/min. The solid curves are the first heating and cooling scans and dotted curves are the second heating and cooling scans.

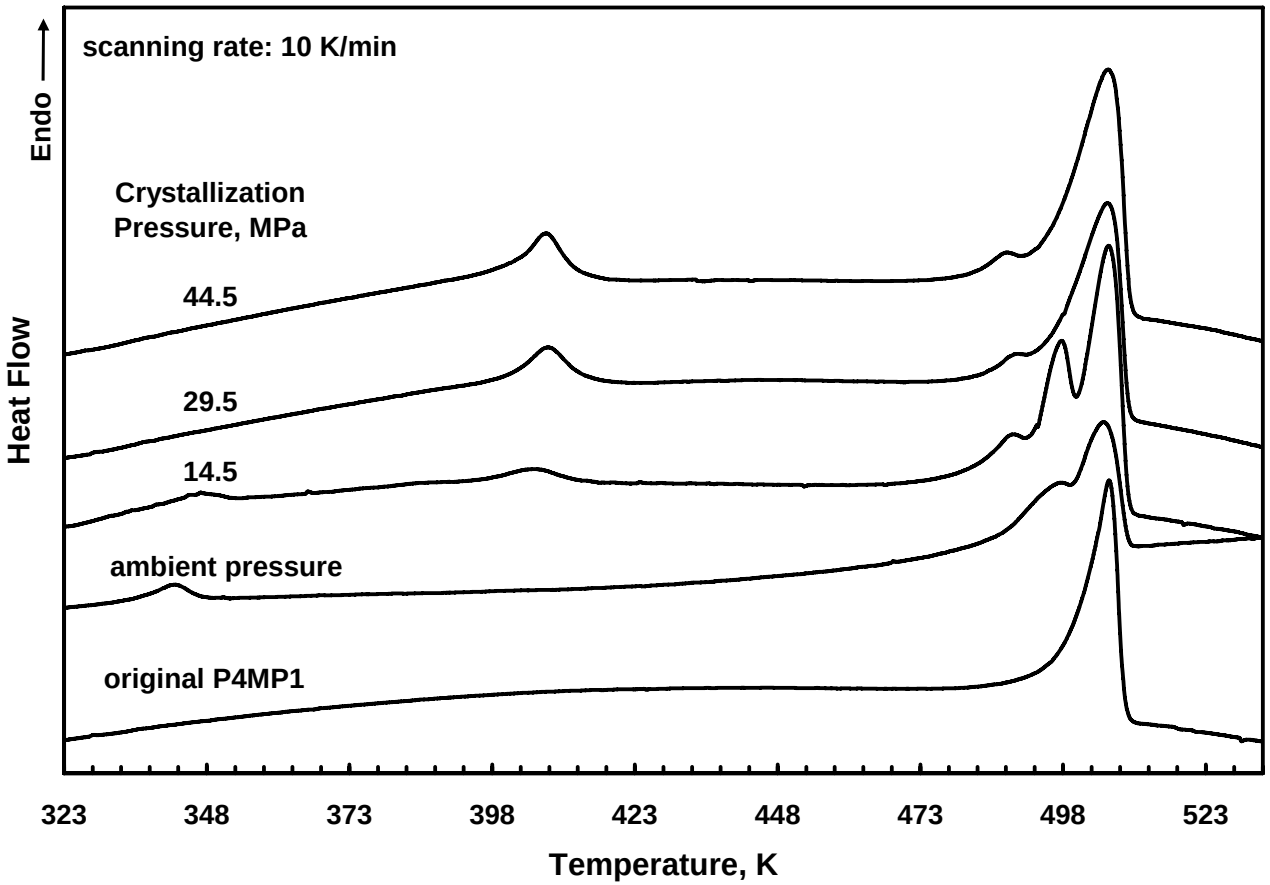
scanning rate: 10 K/min
Endo
Heat Flow
Crystallization
Pressure, MPa
44.5
29.5
14.5
ambient pressure
original P4MP1
323
348
373
398
423
448
473
498
523
Temperature, K

(a)

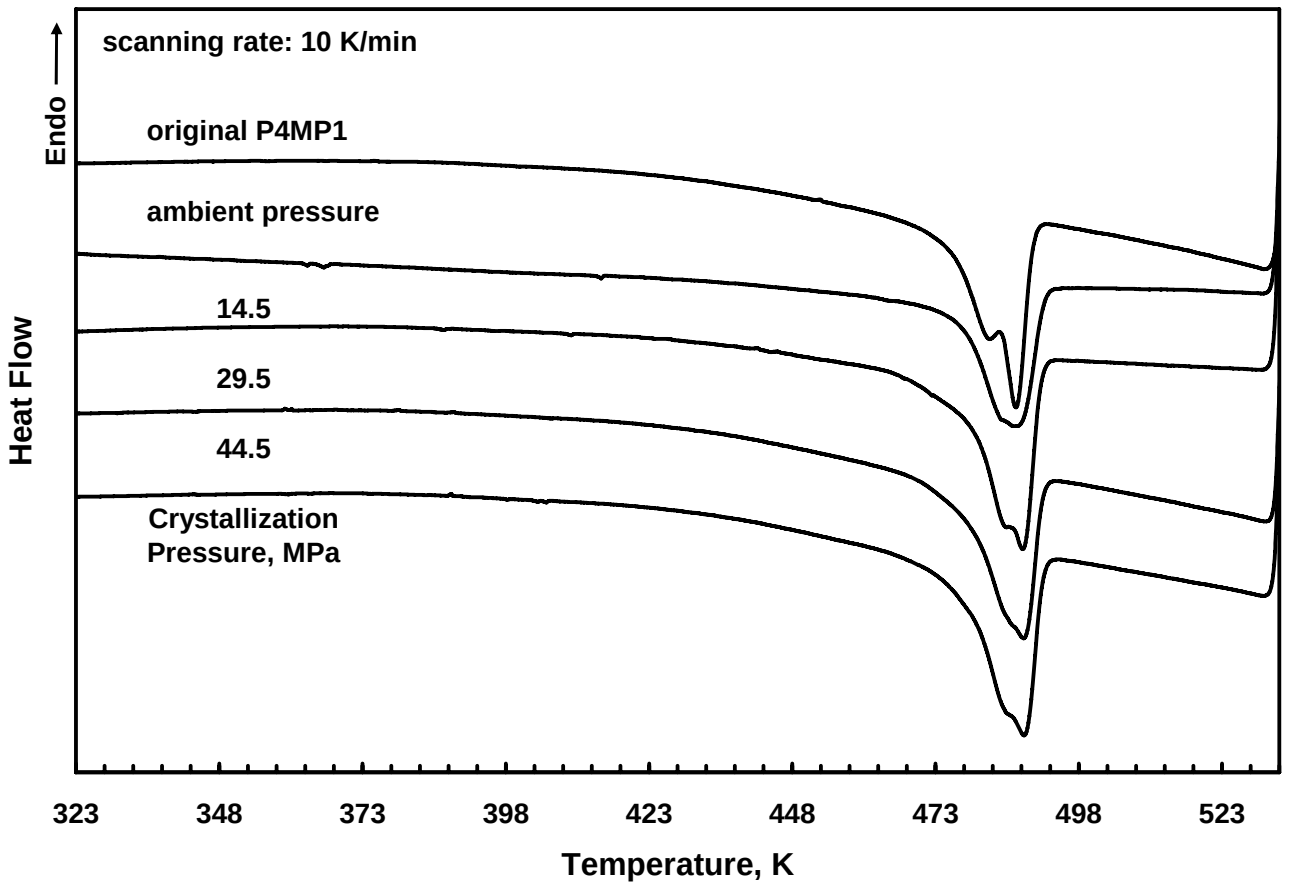

(b)

Figure 4.9 Comparison of the DSC scans of Poly (4-methyl-1-pentene) crystallized from 4.6 wt % solutions in n-pentane at 301 K for 10 hours at the pressures indicated with the original polymer: (a) first heating scans; (b) first cooling scans.

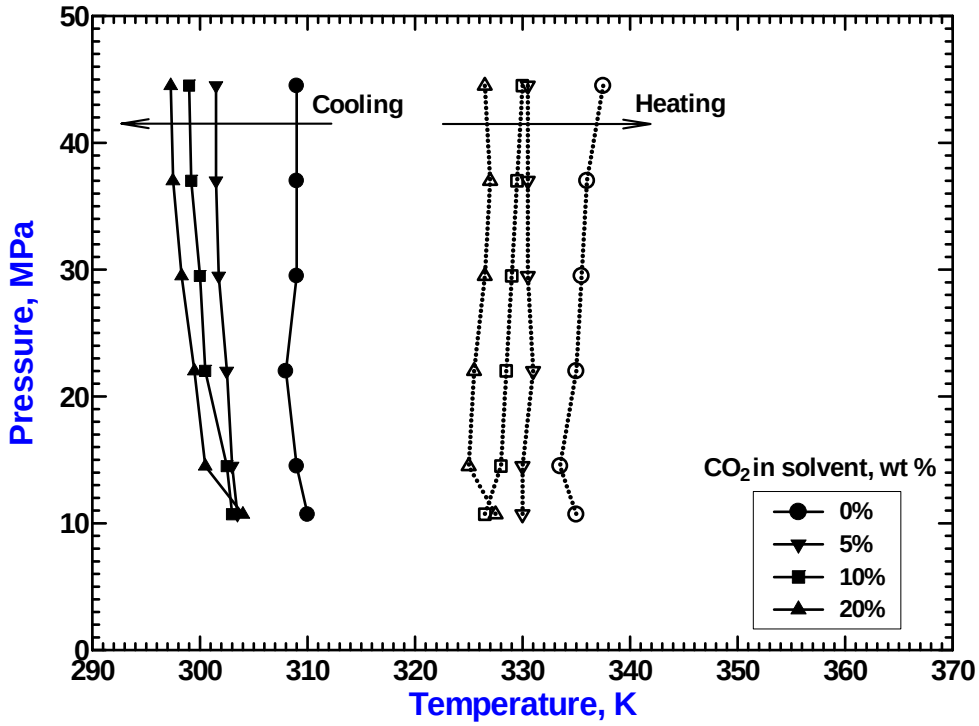

Figure 4.10 The solid-fluid phase boundaries for 4.6 wt % poly (4-methyl-1-pentene) solution in *n*-pentane and *n*-pentane + CO_2 mixture of different CO_2 content. Filled symbols represent the crystallization (cooling) temperatures, and the open symbols represent the melting (heating) temperatures.

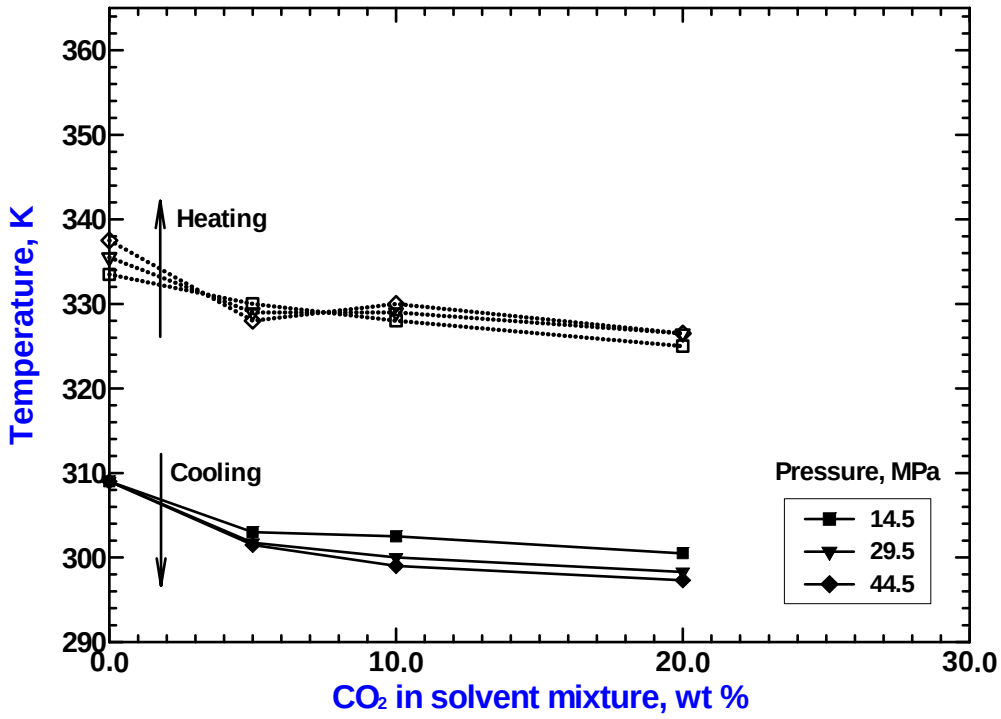

Figure 4.11 Effect of CO_2 level in the solvent mixture on the solid-fluid phase boundaries for 4.6 wt % poly (4-methyl-1-pentene) solutions in n-pentane and n-pentane + CO_2 mixture at 14.5, 29.5 and 44.5 MPa. Filled symbols represent the crystallization and the open symbols represent melting transition temperatures.

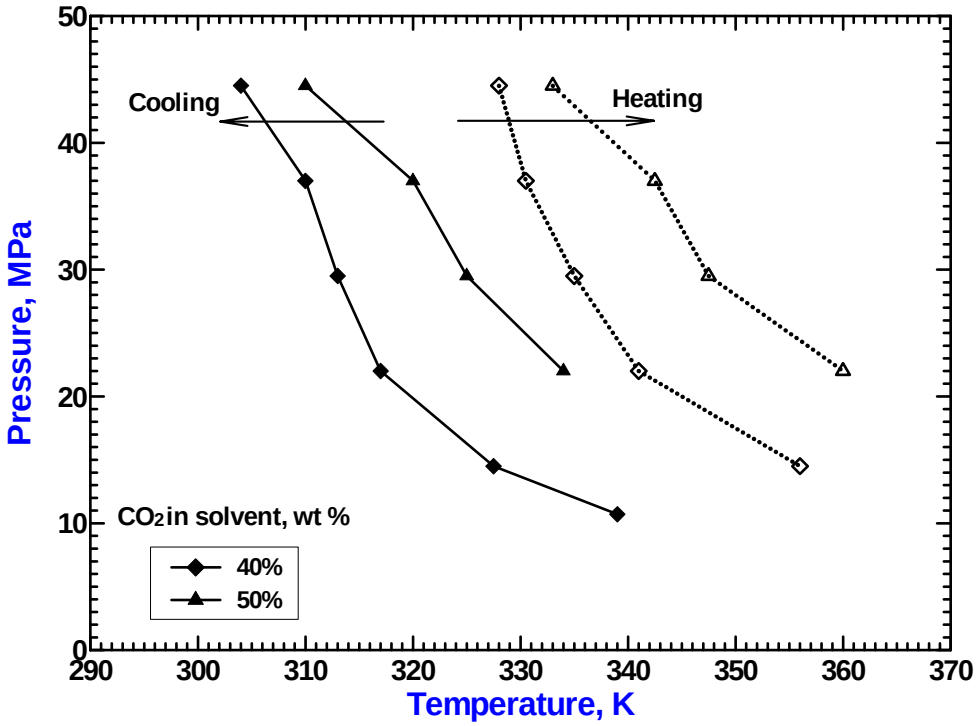

Figure 4.12 The gel-sol phase boundaries for 4.6 wt % poly (4-methyl-1-pentene) solution in n-pentane + CO_2 mixtures. Filled symbols represent the gelation temperatures (cooling), and the open symbols represent the dissolution temperatures upon heating.

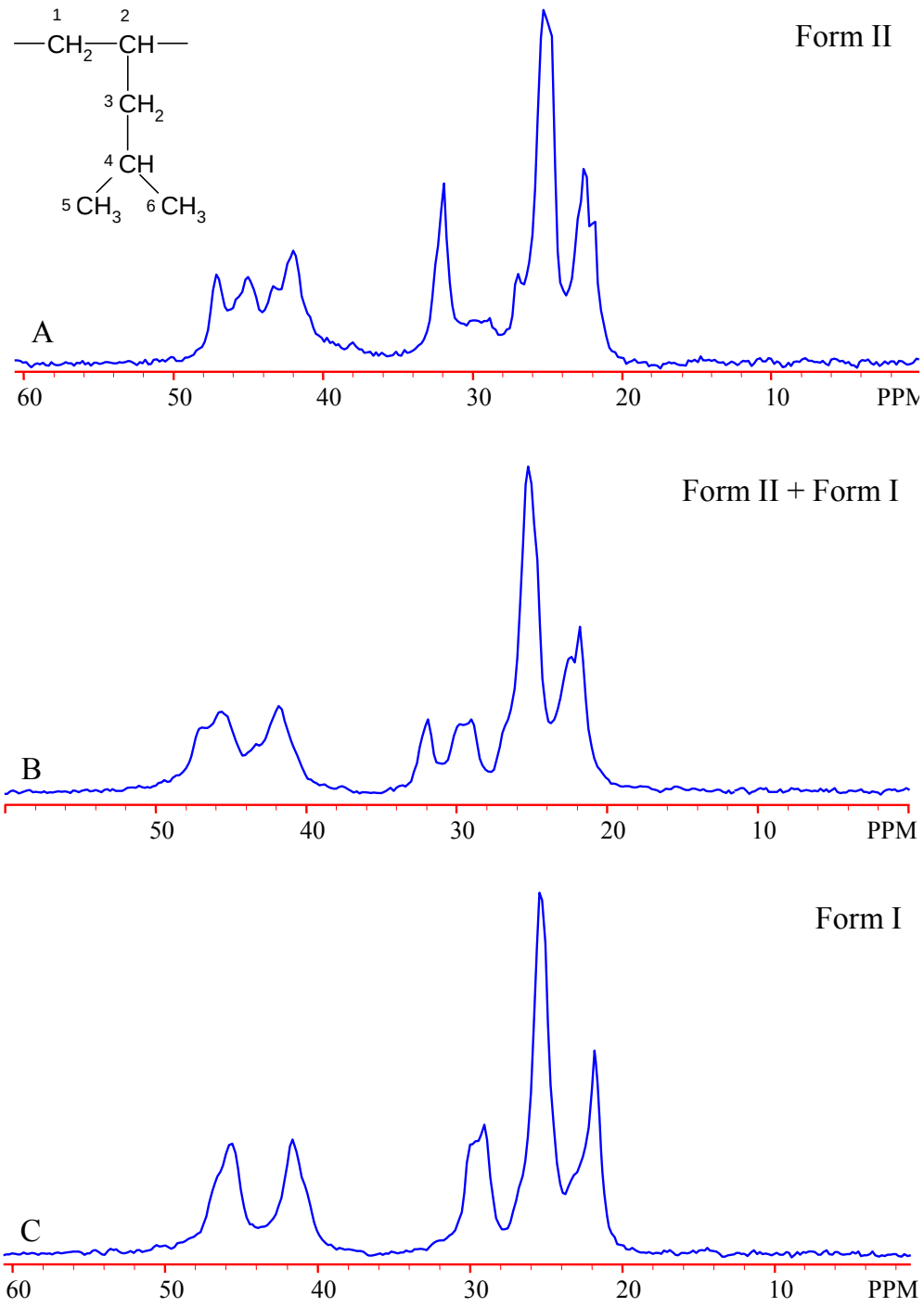

Figure 4.13 Solid-state ^{13}C NMR CP-MAS spectra of i-P4MP1 after crystallization from: (A) 60/40 (wt) n-pentane/CO_2 solution at 44.5 MPa; (B) 50/50 (wt) n-pentane/CO_2 solution at 44.5 MPa; (C) 50/50 (wt) n-pentane/CO_2 solution at 29.5 MPa.

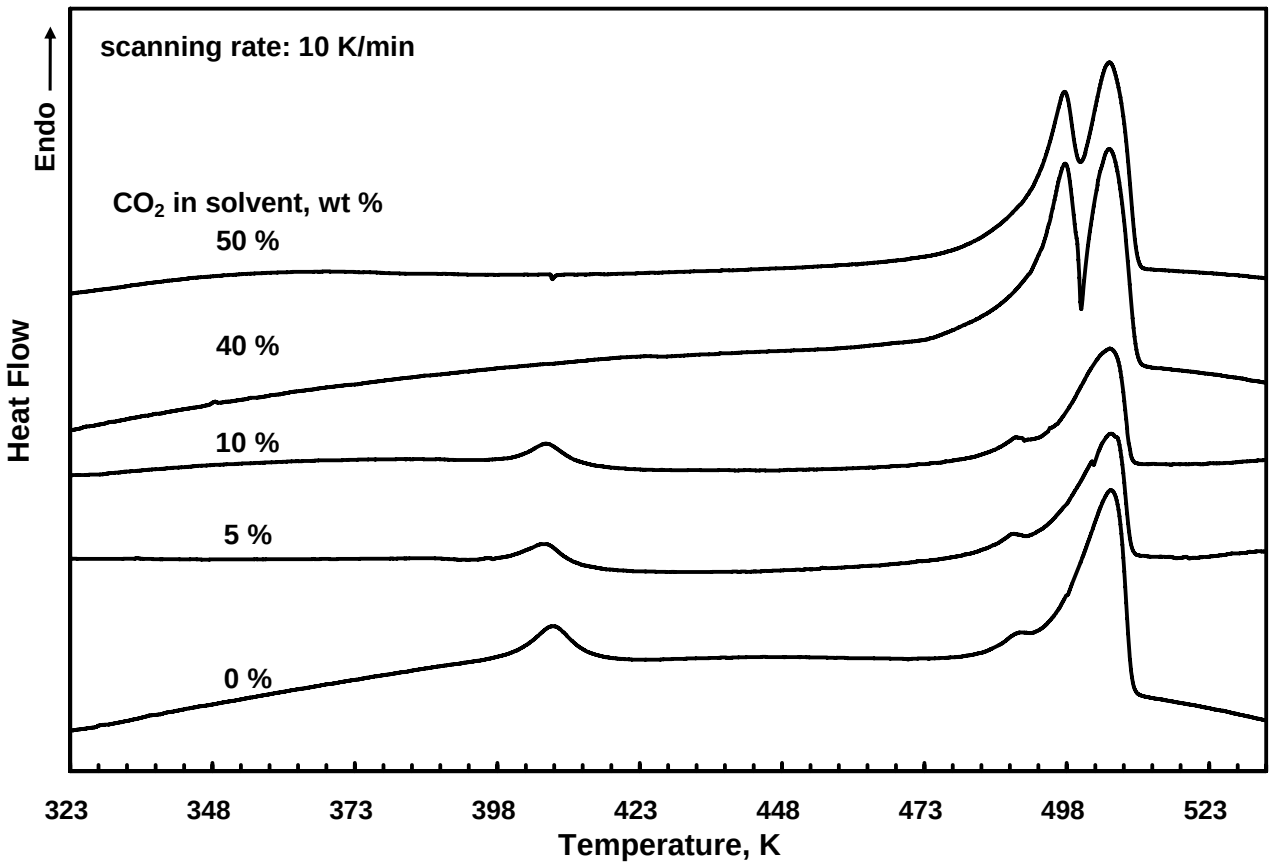
scanning rate: 10 K/min
Endo
CO2 in solvent, wt %
50 %
40 %
10 %
5 %
0 %
Heat Flow
323
348
373
398
423
448
473
498
523
Temperature, K

(a)

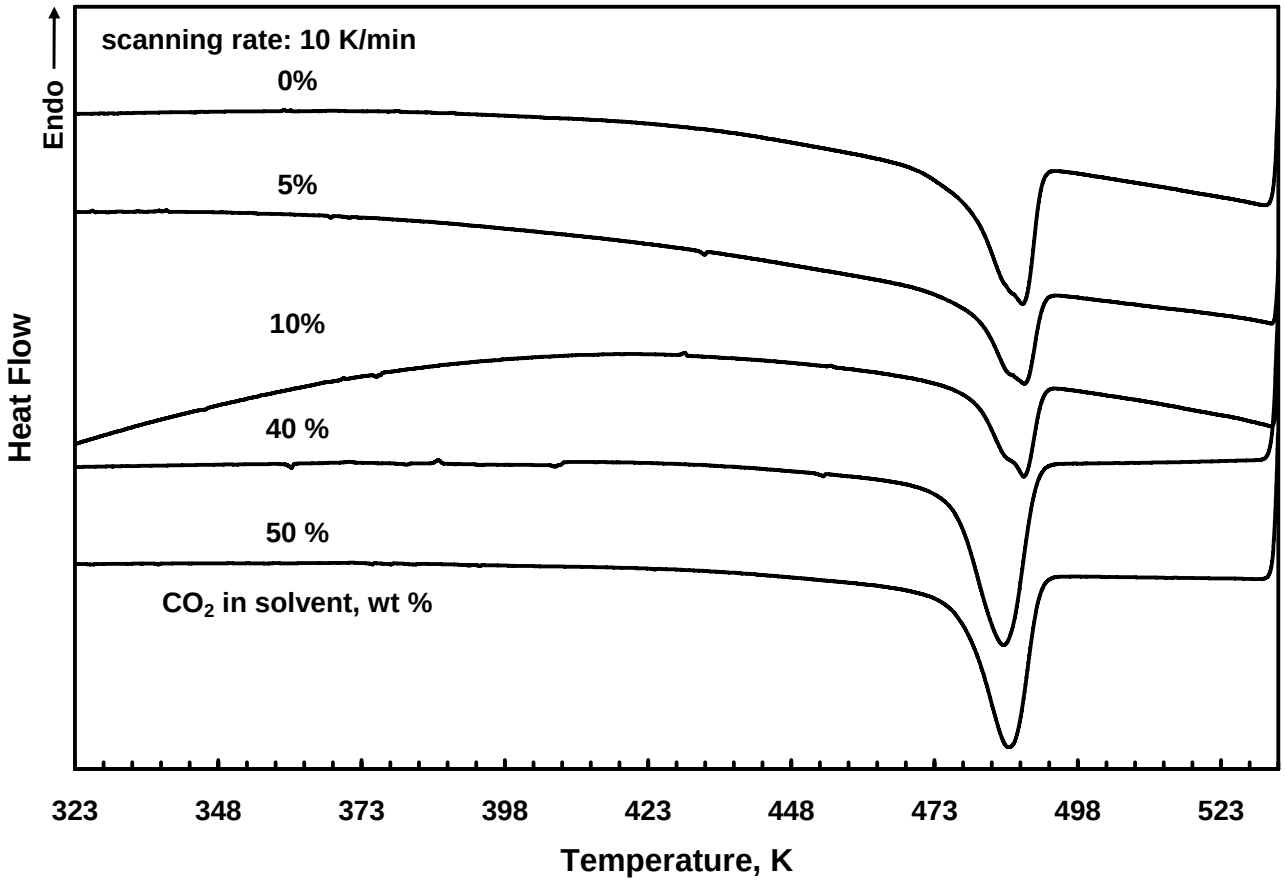

(b)

Figure 4.14 Comparison of the DSC scans for Poly (4-methyl-1-pentene) crystallized from 4.6 wt % solutions in n-pentane + CO_2 solution of different CO_2 content at 298 K and 29.5 MPa for 10 hours: (a) first heating scans; (b) first cooling scans.

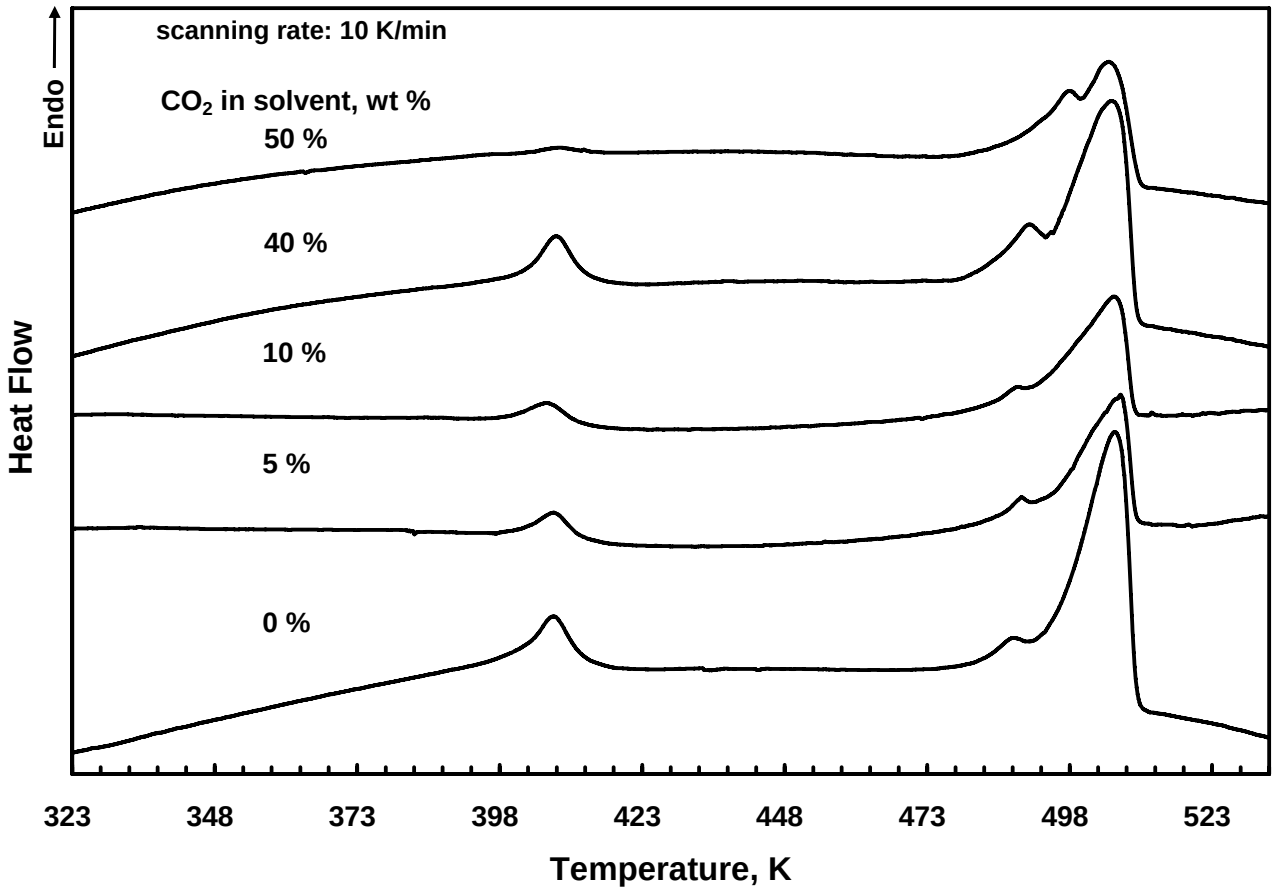
scanning rate: 10 K/min
CO2 in solvent, wt %
50 %
40 %
10 %
5 %
0 %
Endo
Heat Flow
323
348
373
398
423
448
473
498
523
Temperature, K

(a)

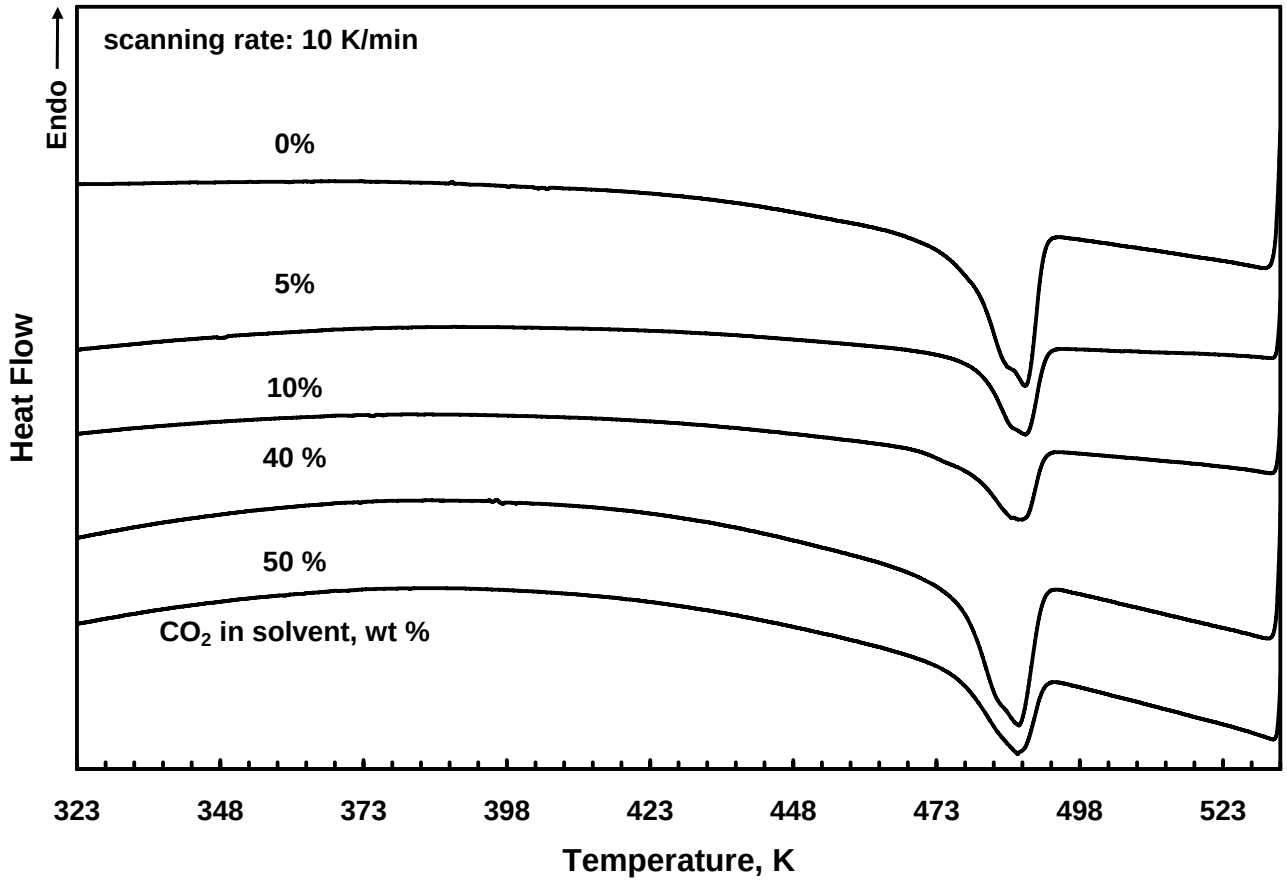

(b)

Figure 4.15 Comparison of the DSC scans for poly (4-methyl-1-pentene) crystallized from 4.6 wt % solutions in n-pentane + CO_2 solution of different CO_2 content at 298 K and 29.5 MPa for 10 hours: (a) first heating scans; (b) first cooling scans.

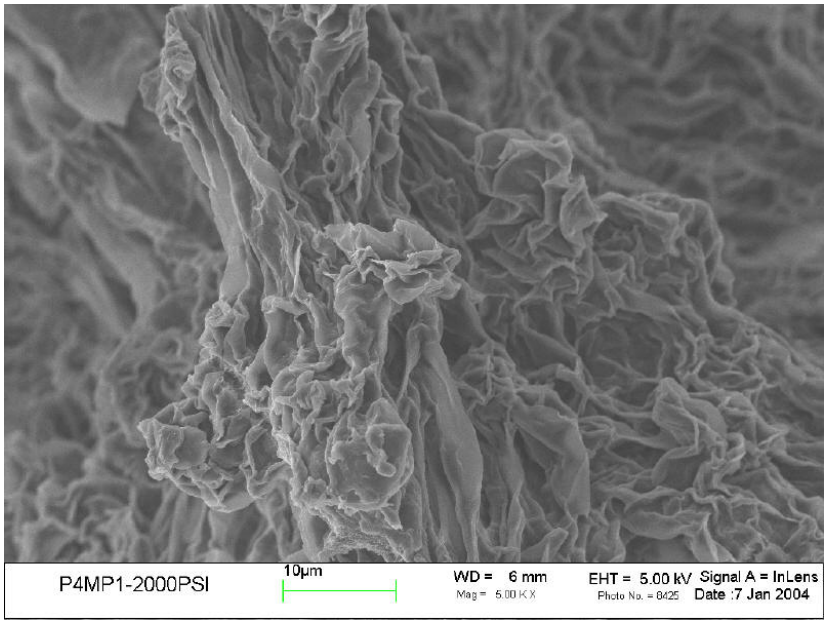
P4MP1-2000PSI
10µm
WD = 6 mm
Mag = 5.00 K X
EHT = 5.00 kV Signal A = InLens
Photo No. = 8425 Date :7 Jan 2004

(a)

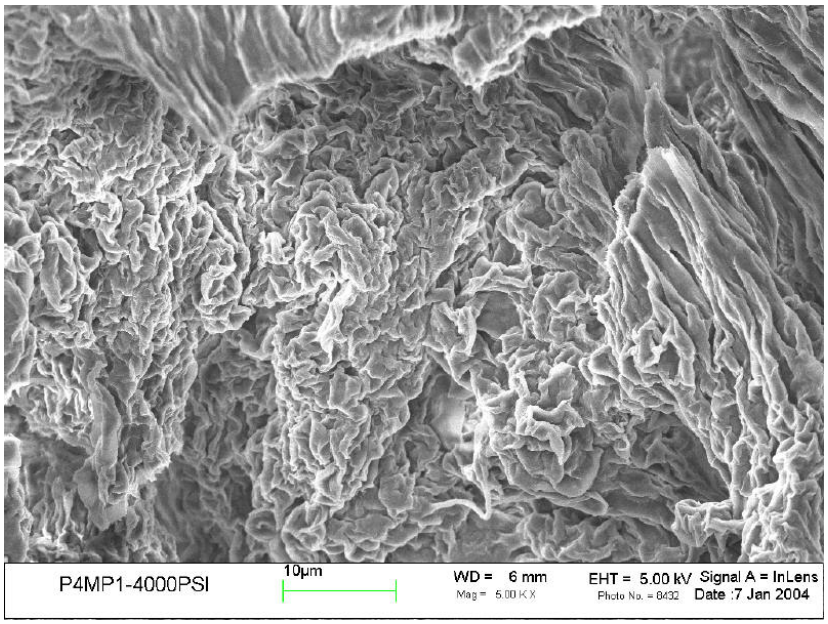
P4MP1-4000PSI
10µm
WD = 6 mm
Mag = 5.00 K X
EHT = 5.00 kV Signal A = InLens
Photo No. = 8432 Date :7 Jan 2004

(b)

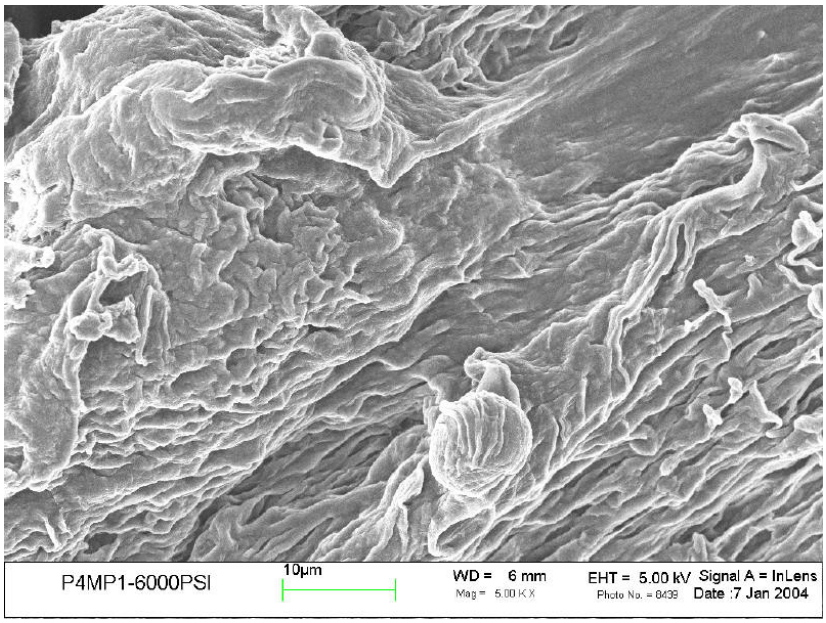

(c)

Figure 4.16 FESEM micrographs of poly (4-methyl-1-pentene) crystals that were formed at 298K for 10 hours from pure n-pentane solution at: (a) 14.5 MPa, (b) 29.5 MPa and (c) 44.5 MPa.

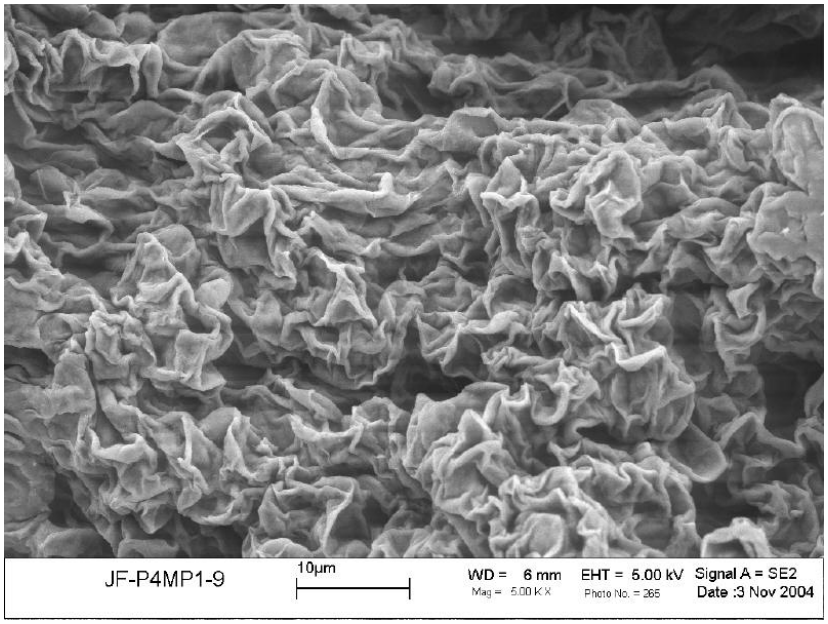
JF-P4MP1-9
10µm
WD = 6 mm
Mag = 5.00 K X
EHT = 5.00 kV
Photo No. = 365
Signal A = SE2
Date :3 Nov 2004

(a)

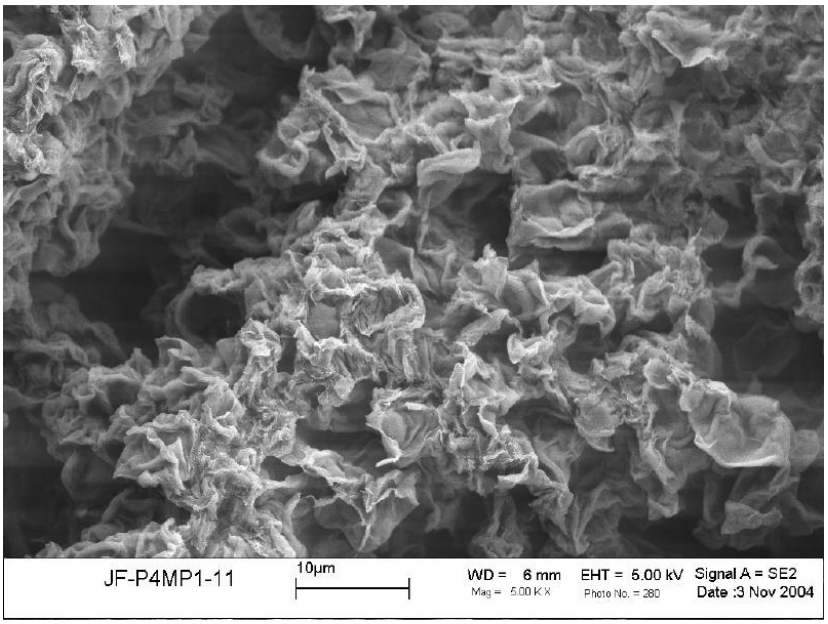
JF-P4MP1-11
10µm
WD = 6 mm
Mag = 5.00 K X
EHT = 5.00 kV
Photo No. = 380
Signal A = SE2
Date :3 Nov 2004

(b)

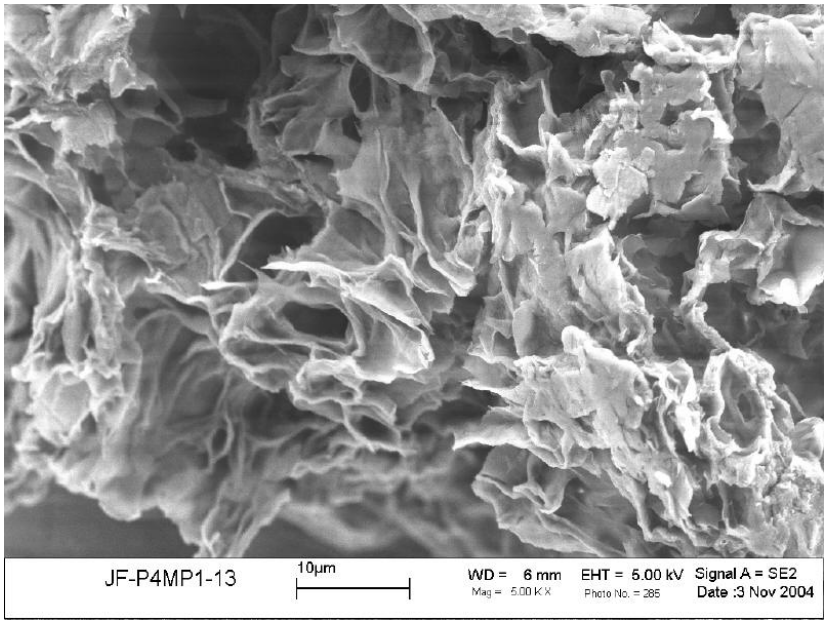

(c)

Figure 4.17 FESEM micrographs of poly (4-methyl-1-pentene) samples that were formed at 298 K and 44.5 MPa for 10 hours from different solutions: (a) n-pentane/CO_2 90/10, (b) n-pentane/CO_2 60/40, (c) n-pentane/CO_2 50/50.

Chapter 5

Thermoreversible Gelation and Polymorphic Transformations of Syndiotactic Polystyrene in Toluene and Toluene + Carbon Dioxide Fluid Mixtures at High Pressures*

The gelation and crystallization processes in solutions of syndiotactic polystyrene in toluene and toluene + carbon dioxide fluid mixtures were studied in a variable-volume view-cell system over a pressure range from 7 - 50 MPa for polymer concentrations up to 25 wt % and for CO_2 concentrations up to 43 wt %. All the solutions in toluene and in toluene + CO_2 mixtures up to 16 wt % CO_2 displayed only a sol-gel boundary. Solutions with 28 wt % CO_2 displayed also a liquid-liquid phase boundary. Solutions in 43 % CO_2 displayed instead a fluid-solid crystallization boundary along with a liquid –liquid phase boundary. Consequences of the phase separation path on the eventual morphology and the crystal state of the polymer were investigated. When solutions are cooled to room temperature while maintaining pressure constant during which the sol-gel boundary is crossed first, the resulting morphology is fibrillar and the polymer displays the δ crystal form with a trace amount of the β form. When the solutions are depressurized instead, holding the temperature constant during which liquid–liquid phase boundary is crossed first, with further cooling the polymer-rich phase (PRP) leads to a stacked-lamellar morphology with the β crystal form. The polymer-lean phase (PLP) leads to a mixed morphology with lamellar layers connected with fibrils and the polymer displays a mixed crystal structure consisting of the δ + β polymorphs. In the absence of gelation at high CO_2 levels, the crystallization leads to only the β polymorph. A mechanistic framework is provided to account for the formation of these different polymorphs from the different phase separation

* Accepted for publication in Macromolecules as "Jian Fang and Erdogan Kiran. *Thermoreversible Gelation and Polymorphic Transformations of Syndiotactic Polystyrene in Toluene and Toluene + Carbon Dioxide Fluid Mixtures at High Pressures*"

paths followed.

5.1 Introduction

Syndiotactic polystyrene (sPS) is a polymer of continuing interests due to its high melting temperature, high crystallization rate and high chemical stability [Malanga 2000]. It has been shown to display a complex crystalline structure with five different polymorphs [Guerra *et al.* 1990; De Rosa *et al.* 1992; Chatani *et al.* 1993]. The α and β forms are all-trans planar zig-zag chain conformations, while the γ, δ and ε forms display 2_1 helical conformations. The δ form refers to clathrate or intercalate cocrystal by incorporating solvent molecules into the crystalline lattice. The γ form is free of solvent molecules in the crystalline lattice, which can be obtained by thermal treatment of δ form [Manfredi *et al.* 1995]. If the solvent molecules in the δ form are extracted by using boiling acetone [Manfredi *et al.* 1995] or supercritical CO_2 [Ernesto Reverchon 1999], a nanoporous crystalline phase δ_e form, "emptied" δ form, can be generated. Recently a new crystalline form of sPS, named ε form, has been reported [Rizzo *et al.* 2007]. The ε form is also a nanoporous crystalline phase, in which pore is in "channel" shape instead of the "cavity" shape in δ_e form [Petraccone *et al.* 2008]. Thermodynamically, the all-trans planar zig-zag conformation is more stable compared to the helical conformation at ambient conditions. The transformation from the helical form to the all-trans form can be achieved by heating or thermal annealing. The helical δ form can be obtained from solutions in suitable solvents, or by sorption of suitable solvents into the amorphous sPS (obtained by rapid quench from melt) or semicrystalline sPS in the α or γ form [Immirzi *et al.* 1988; Vittoria *et al.* 1988]. However, the β form once formed is stable in the presence of solvents and can not be transformed into the δ form [Rapacciuolo *et al.* 1991].

The solid-solid crystal form transitions of sPS have also been studied in carbon dioxide at high pressures [Handa *et al.* 1997; Ma *et al.* 2004]. Carbon dioxide is a well known

plasticizer. Thus polymers can undergo recrytallization at temperatures below their nominal glass transition temperatures. Indeed, it is reported that when exposed to compressed carbon dioxide, sPS undergoes α to β or γ to β transitions in the solid state which otherwise occurs only in the presence of liquid solvents [Handa *et al.* 1997]. It is shown that, in the glassy state, sPS can be transformed directly into the γ form when exposed to CO_2 at about 6 MPa and 363 K [Handa *et al.* 1997] or above the critical pressure and temperature of carbon dioxide in the pressure range from 8 -20 MPa and in the temperature range from 308 – 373 K [Ma *et al.* 2004]. These observations are interesting in that traditionally the γ form is obtained by treating the glassy sPS with solvents such acetone or tetrachloroethane and then removing the solvent by thermal or vacuum techniques [Handa *et al.* 1997; Ma *et al.* 2004]. The γ form obtained with exposure to carbon dioxide transforms into the α form at higher temperatures (i.e., 483 K), with a high degree of crystal perfection. If during thermal annealing at temperatures above 483 K, the amorphous sPS were to be subjected to carbon dioxide at higher pressures (about 12 MPa), it is reported to directly transform to the β form, instead of the α form [Handa *et al.* 1997]. The direct transformation to the β form in carbon dioxide is intriguing in that the β form is normally obtainable by slow cooling from the melt, not from the glassy state.

Beside its complex polymorphism, sPS has also been shown to undergo a thermoreversible gel in a variety of solvents [Deberdt and Berghmans 1993; Deberdt and Berghmans 1994; Daniel *et al.* 1996; Daniel *et al.* 1997; De Rudder *et al.* 2002]. Thermoreversible gels are physical gels and differ from chemical gels which are networks formed through covalent bonds and are heat-irreversible. In thermoreversible gels, the networks are formed through van der Waals interactions. The energy associated with these interactions is of the order of κT and thus these gels are thermoreversible [Guenet 1992]. In water, biopolymers often undergo gelation due to hydrogen bonds [Clark and Ross-Murphy 1987]. Formation of physical gels in synthetic polymers in organic solvents in the absence of hydrogen bonds

can arise as a result of phase separation accompanied by vitrification or crystallization, or as a result of formation of "*polymer-solvent*" compounds [Guenet 1992; te Nijenhuis 1997]. Numerous studies on thermoreversible gelation of sPS in different solvents such as chloroform [Daniel *et al.* 1997], toluene [Daniel *et al.* 1997], benzene [Daniel *et al.* 1996], bromoform [De Rudder *et al.* 2002] have already been reported. In these gels, the polymer-rich phase is characterized as a *"polymer-solvent compound"*, in which the solvent molecules are included in well-defined positions between sPS chains that are in their 2/1 helical conformation. These gels are reported to be stable and strongly elastic. However, studies with bulky solvents such as octadecyl benzoate [Li and Xue 1998] and 1-chlorotetradecane [Daniel *et al.* 2005], have shown that these solvent molecules fail to be incorporated into the cavities created by the helical sPS chain, and in general fail to form a "polymer-solvent compound". The gels formed in solutions in bulky solvents give rise to paste-like, opaque gels with much lower elasticity. In these systems, the polymer-rich phase is found to display ordered all-trans planar chain conformation instead of 2_1 helical conformation.

The phase behavior of sPS in a series of solvents, including chloroform, chlorobenzene, 1,2-dichlorobenzene, o-xylene, 1,2,4-tricholobenzene and decalin, (which represent an order of decreasing solvent quality for sPS), was investigated over the whole polymer concentration range by Berghmans and co-workers [Deberdt and Berghmans 1993; Deberdt and Berghmans 1994; Roels *et al.* 1994; Roels *et al.* 1997] using differential scanning calorimetry (DSC). The solvent quality was found to play a significant role. In good solvents, the melting point depression of the β form with planar zig-zag conformation was observed to be larger than in poor solvents. However, the stability of the δ form was found to increase with increasing solvent quality. In good solvents, the β form was observed to become the thermodynamically stable phase at high polymer concentrations while the δ form becomes the more stable phase at lower polymer concentrations. In poor solvents, the

β form is observed to be the stable phase over the whole polymer concentration range.

The properties of polymeric materials are inherently dependent on their microscopic structure, which is a strong function of their process history. In many cases, phase separation plays a major role. Two modes of phase separation are important for solutions of semi-crystalline polymer. These are the liquid-liquid (L-L) and the fluid-solid (F-S) phase separation, i.e., crystallization. In some systems, instead of the whole system undergoing crystallization, gelation is the prevalent phase separation process which involves crystallization of localized domains that act as anchors. Thermally induced phase separation (TIPS) in combination with crystallization is an important technique for the preparation of polymeric porous membranes [Yave *et al.* 2005; Gu *et al.* 2006; Li *et al.* 2006]. The process is usually initiated by a thermally-induced L-L phase separation, which is then followed by crystallization. The final structure depends on the location of the L-L phase and the F-S (crystallization) phase boundaries. These studies are traditionally carried out at atmospheric pressure. For the solutions of polymers in binary fluid mixtures of an organic solvent with CO_2, the pressure becomes a key tuning parameter to regulate the solvent properties, and consequently the miscibility or phase separation conditions. In these systems, pressure-induced phase separation (PIPS) in combination with crystallization, simply the temperature-induced phase separation that are carried out at high pressures offer new opportunities to form polymers with unique microstructures. In a recent study, Zhang *et al.* [Zhang and Kiran 2006] reported the morphology of polyethylene crystals formed in n-pentane solutions at high pressures. Different morphologies are displayed depending upon the phase separation paths employed and whether or not crystallization is induced directly by crossing the F-S boundary by cooling at high pressure, or is induced by a liquid-liquid phase separation first via a pressure quench which is then followed by cooling to cross the L-S phase boundary.

In the present study, we have investigated the gelation or crystallization process for sPS in toluene and toluene + CO_2 mixtures at high pressures. We are now reporting the phase behavior for these solutions as a function of pressure (up to 50 MPa), polymer concentration (up to 25 %) and CO_2 content (up to 43 %) in the fluid mixtures. The morphology and the crystal habits that are generated by sPS samples after constant pressure cooling, or constant temperature pressure quench followed by cooling are characterized by SEM, DSC and FTIR. The results are discussed in terms of the different paths that are followed. The results are also compared with the ambient pressure phase behavior of sPS in toluene that has been reported in the literature [Daniel *et al.* 1997; Ray *et al.* 2002]. Toluene is known to be a good solvent for sPS. The addition of CO_2 to toluene that is now being presented provides an opportunity to investigate the influence of controlled changes in the solvent quality that can be achieved by adjusting either the pressure, or the temperature, or the amount of CO_2 in the fluid mixture and its consequences in the phase behavior, and the polymer crystal forms that are promoted.

5.2 Experimental Section

5.2.1 Materials

The syndiotactic polystyrene (with 98 % syndiotactic triads) was purchased from Scientific Polymer Products Inc. The polymer had a weight average molecule weight of $M_w = 3.2 \times 10^5$ g/mol and a polydispersity of $M_w/M_n = 3.9$. The solvent, toluene, with a minimum purity of 99.9 % was purchased from AlliedSignal. Carbon dioxide with a minimum purity of 99.99 % was purchased from Air Products. The polymer and the solvents were used as received.

5.2.2 Experimental System

Experiments were carried out in a variable-volume view-cell system described in our

earlier publications [Fang and Kiran 2006]. The cell is equipped with two sapphire windows permitting either visual or optical observations. The cell is heated by four cartridge heating elements. A movable piston coupled with a pressure generator is used to alter the inner volume of the cell and thereby adjust the system pressure. It is operable at pressures up to 70 MPa and temperatures up to 473K. An optical fiber illuminator is used as the light source and the transmitted light intensity is monitored with a fast response photodiode detector. During phase boundary determination, the temperature, pressure and transmitted light intensities are recorded in real-time with a dedicated computer.

5.2.3 Experimental Procedures

In a typical experiment, an accurately weighted amount of polymer is first loaded into the cell. This is followed by the addition of a measured amount of the liquid solvent, i.e., toluene. The cell is then sealed and connected to the CO_2 charge line and the pressure generator. For experiments involving binary fluid mixtures of toluene + CO_2, carbon dioxide is charged from a pre-loaded high pressure transfer vessel. The amount of carbon dioxide charged is assessed from the change in the mass of the transfer vessel. After the loading process is completed, the cell temperature and pressure are brought to the desired conditions for dissolution of polymer, forming a homogenous solution. The miscibility is visually verified through the sapphire windows. A magnetic stirrer is used to facilitate the dissolution process.

Figure 5.1a describes the paths that were followed in determination of phase boundaries. Phase boundaries were approached either by lowering the temperature while keeping the pressure constant (Path 1) or by lowering the pressure while keeping the temperature constant (Path 2). In experiments where temperature was lowered along Path 1, pressure was adjusted with the aid of the pressure generator to compensate for the volumetric change that accompanies temperature reduction and thus maintain constant pressure

conditions. From measurements of the temperature, pressure, and the transmitted light intensities (I_{tr}), graphs depicting the changes in the transmitted light intensity with temperature (along a constant pressure path, Path 1) or with pressure (along a constant temperature path , Path 2) are generated. These are shown in Figure 5.1b. In these plots, the temperature or the pressure corresponding to the departure from the baseline for I_{tr} is identified as the phase separation temperature or pressure. In the present study, the majority of experiments were conducted along Path 1 at different pressures to determine the fluid-solid, or the sol-gel phase boundary that is associated with the crystallization or the gelation of sPS. Once the phase-separated regions were entered, phase boundaries were again determined, but this time in the reverse direction by increasing the temperature (labeled as Path 1' in the figure). In the reverse direction, what is determined is either the melting (S-F) transition for the crystals or the gel-sol transition.

The distinction between gelation and crystallization was made by visual observations. While in systems that undergo crystallization, magnetic stirrer motion remains free, when gelation occurs, it gets stuck in the gel and stops turning. Along Path 1, whenever the gelation occurred during cooling to ambient temperature, the system was held for an additional 24 hrs at the ambient temperature at high pressure to mature the gel. After this maturation time the cell was depressurized and opened to collect the wet gel. Along Path 2, after the pressure-induced L-L phase separation the cell was cooled to ambient temperature while allowing the pressure to decrease, without any further adjustment of the pressure. As before the system was held for an additional 24 hrs to mature the gel at the ambient temperature and the prevailing lowered pressure. After final depressurization to ambient pressure and opening the cell, samples were collected from the upper (representing the polymer-lean phase) and the lower (representing the polymer-rich phase) layers of the cell cavity. The wet gels thus collected were air-dried by exposing to open air flow in a hood for 24 hrs for natural evaporation of the solvent. For some of the samples drying was also

carried out by extracting the wet gel with supercritical carbon dioxide at 313 K and 21 MPa for 24 hrs.

5.2.4 Characterizations by FTIR, SEM and DSC

IR characterizations were carried out with an FTS 3100 (Digilab) FTIR spectrometer. The resolution was 2 cm^{-1} and 32 scans were co-added to obtain a spectrum for each sample. The air-dried gels or crystals were mixed with KBr powder. The transmission spectra were obtained from these prepared KBr disks.

A Leo 1550 field emission scanning electron microscope (FESEM) was used to examine the morphology of the gels or crystals. The air-dried gel samples were freeze fractured after immersing in liquid nitrogen. A 15 nm layer of gold was coated on the samples using a Cressington 208 HR sputter coater to reduce electron charging effects. The morphological features of fractured cross-sectional surfaces were investigated.
X-ray diffraction (XRD) patterns of vacuum-dried polymer samples were obtained with a Scintag XDS-2000 powder diffractometer operated at 45 kV and 40 mA using Cu Kα monochromatized radiation (λ = 0.154178 nm).

The thermal behavior of the gels or crystals was investigated using a Perkin Elemer (Pyris Diamond) Differential Scanning Calorimeter. Due to presence of the resident solvent in the air-dried gels, gold-plated stainless-steel high-pressure capsules were used as sample holders to prevent solvent loss during scans. Thermograms were recorded at heating or cooling rates at 10 K/min in the temperature range 313- 523 K.

5.3 Results and Discussions

5.3.1 Phase Boundaries

5.3.1.1 sPS + Toluene

Figure 5.2 shows the phase boundaries determined under constant pressure cooling and heating experiments (Path 1 and Path 1' in Figure 5.1) in 1.6, 2.8, 4.8, 12.6 and 25.0 wt % solutions of sPS in pure toluene. The experiments were carried out by maintaining the pressure constant at 6.9, 14.5, 22.0, 29.5, 37.0, and 45.5 MPa. The phase transitions were identified as the sol-gel (Path 1) or the gel-sol (Path 1') transitions by visual observation. The magnetic stirrer inside the cell is frozen when the sol-gel phase boundary is crossed but becomes free after crossing the gel-sol phase boundary. As shown in Figure 5.2, the sol-gel and the gel-sol phase boundaries are shifted to higher temperature region with increasing polymer concentration in the solutions. Daniel *et al.* [Daniel *et al.* 1997] studied the temperature-concentration phase diagram for sPS + toluene at ambient pressure using DSC measurement. Their results have shown that the melting temperatures of the gels increase from around 373 K to 423 K when polymer concentration increases from ~ 4 to ~ 50 wt. %. The gel-sol phase boundaries in the present study are in good agreement with these DSC data reported in the literature. Indeed, while for the 4.8 wt % solution the transitions occur in the temperature region from 378 to 390 K, for 25 wt % solution the range is 399-412 K.

Figure 5.2 shows that the temperature difference between sol-gel (gelation) and gel-sol (re-dissolution) phase boundary is over 40 K in these solutions. Large hysteresis in solid-fluid transition temperatures is not uncommon and was also reported for crystallization and melting transitions of polyethylene in high pressure n-pentane solutions [Kiran and Liu 2002] where a 15 K difference was observed. The very large difference between gelation (during cooling) and gel melting (during reheating) observed in present study may arise from the long induction time needed in forming sPS helix conformation for gelation to occur starting from the random sPS coils in solution. Long induction times for

coil-to-helix transformation during gelation of sPS in bromoform solution has been discussed in the literature [De Rudder *et al.* 2002]. Berghmans and Deberdt [Berghmans and Deberdt 1994] studied the phase behavior of sPS in decalin and in o-xylene. The temperatures for formation and melting of helix conformation (δ form) and the zig-zag conformation (β form) have been measured by DSC over the whole polymer concentration range. They report a larger temperature difference for the formation and re-melting of helix conformation (representing gelation and re-dissolution) than for the formation (crystallization) and re-melting of the zig-zag conformation. More recently, an extremely large hysteresis (about 100 K) between gelation and re-dissolution has been reported for gelation of poly(9,9'-dioctylfluorene) in toluene [Kitts and Vanden Bout 2007].

Additional experiments were also carried out along constant temperature paths (Path 2) at selected temperatures higher than gel-sol phase transition temperatures. However, in these experiments in toluene the system remained as homogenous solutions and no liquid-liquid phase separation was detected.

5.3.1.2 sPS + Toluene + CO_2

The influence of CO_2 on the phase boundaries was investigated by adding the CO_2 into sPS solution in toluene. The polymer concentration was at nominal concentration of 4.5 wt % and the compositions of CO_2 in fluid mixture were varied from 0 to 43 wt %.

Figure 5.3 shows the phase boundaries for 4.5 wt % sPS solution in toluene + CO_2 mixture containing 16 wt % CO_2. The phase boundaries for 4.8 wt % sPS solution in pure toluene (0 wt % CO_2) are also included for comparison. As shown in the figure, the sol-gel boundary is shifted to lower temperatures with addition of 16 wt % CO_2. That the addition of CO_2 lowers the fluid-solid transition temperatures was also observed in poly(4-methyl-1-pentene) (P4MP1) solutions in n-pentane + CO_2 (up to 20 wt % CO_2 in

the solvent mixtures) [Fang and Kiran 2006]. The sol-gel or fluid-solid transition temperatures measured in the view cell are the phenomenological observations that reflect the outcome of thermodynamic and kinetic factors for polymer gelation or crystallization which are far from their equilibrium values. Thermodynamically, upon addition of a poor solvent, such as CO_2, the solvent quality of the fluid mixture of toluene + CO_2 for sPS is decreased as compared to the pure toluene. The decreased solvent quality in turn decreases the stability of δ form, and as a result the sol-gel phase boundary corresponding to the formation of δ form (polymer-solvent compound) and the gelation is observed to shift to lower temperatures. Kinetically, for sPS solution in the solvent mixture with 16 wt % CO_2, the rate of toluene intercalation leading to polymer-solvent compound is hindered due to the presence of CO_2, and gelation process is slowed down, thus also shifting the observed sol-gel transition to lower temperatures. Figure 5.3 suggests that the extent of hindrance to gelation of sPS in toluene is greater at higher pressures. Figure 5.3 shows the temperature difference between the sol-gel and the gel-sol phase boundaries for solution with 16 wt % CO_2 is 10 K larger than that for the solution in pure toluene. The augmented hysteresis in solution contain CO_2 is consistent with the notion that CO_2 delays the development of the helical conformation leading to gelation.

The temperature-pressure phase diagrams of 4.8 wt % sPS solution in toluene + CO_2 mixture containing 28 wt % CO_2 and 4.4 wt % sPS solution in toluene + CO_2 mixture containing 43 wt % CO_2 are shown in Figure 5.4. Instead of being at lower temperatures, the sol-gel phase transitions in sPS solution with 28 wt % CO_2 occur at higher temperatures when compared with the solutions in pure toluene and in fluid mixture of 84 wt % toluene + 16 wt % CO_2. The observed phase transition occurring at a higher temperature can be attributed to the appearance of the β form upon cooling. As more CO_2 loaded into system, the solvent quality for sPS becomes poorer. Eventually, the β phase becomes the more stable form than the δ form over the whole polymer concentration range, and the cooling

leads to the transition of the solution to the β form at high temperatures. The transition of the solution to the β form is observed at higher temperatures for the sPS solution containing 43 wt % CO_2 in the solvent. This is in accord with the observation that the melting point depression of β form is decreased as the solvent quality becomes even poorer with further addition of CO_2. Another striking difference in the phase diagram shown in Figure 5.4 is the appearance of the LCST-type liquid-liquid phase boundaries. As would be expected with lowered solvent power [Zhang *et al.* 2003], the L-L phase boundary shifts to much higher pressures when CO_2 amount in the solution is increased from 28 to 43 wt %.

A special heating experiment was carried out for the 4.8 wt % sPS solution in a fluid mixture of toluene (72) + CO_2 (28) following a constant pressure path (as indicated as Path 1' in Figure 5.4). In these experiments, the system was first cooled down to a low temperature below the sol-gel phase boundary to induce gelation. Then it was re-heated while maintaining the pressure constant at 18.5 MPa. As predicted by the phase diagram, the system was observed to first go through the gel-sol phase boundary undergoing re-dissolution and thus entering the homogenous region. With further heating, this was followed by a re-entry into a heterogeneous two-phase region, but this time due to the liquid-liquid phase separation taking place at the higher temperatures (which is typical of systems showing LCST). The transmitted light intensity was monitored during the whole experiment and is shown in Figure 5.5. As shown, initially the transmitted light intensity increases as the gel dissolves and the system becomes transparent. But with continued increase in the temperature, as the liquid-liquid boundary is approached and entered, the new phase domains that develop intermittently block or move away from the light path, leading to the observed series of decrease and increase in I_{tr}. As the phase separation progresses further, the light passage is eventually all hindered and the fluctuations die out as reflected by the lowered $I_{tr.}$

5.3.2 Crystal Structure

FTIR spectroscopy has proven to be a powerful technique to distinguish the different polymorphic forms for sPS [Kobayashi *et al.* 1989; Reynolds *et al.* 1989; Moyses and Spells 1999; Gowd *et al.* 2003; Yoshioka and Tashiro 2003]. There are significant differences in absorption spectrum of the samples whether the planar zigzag form or the 2_1 helix is present [Reynolds *et al.* 1989; Moyses and Spells 1999]. The planar zigzag form shows the characteristic bands at 1349, 1224 and 537 cm^{-1}, while the 2_1 helix form shows the characteristic bands at 943, 934, 572 and 502 cm^{-1}. Figure 5.6 shows the FTIR spectra in the range of 800-1400 cm^{-1} of sPS gel samples formed at 44.5 MPa from different solutions at different polymer concentrations. These spectra are similar to each other. The appearance of characteristic doublet bands at 943 and 934 cm^{-1} indicates helical conformation and that the formation of δ form which incorporates the solvent molecules in these samples.

5.3.3 Morphology

Figure 5.7 shows the FESEM images of the gels (after air-drying and freeze-fracturing) obtained along Path 1 (constant pressure cooling to room temperature and then depressurization) from 1.6, 2.8 12.6 and 25.0 wt % solutions in pure toluene at 44.5 MPa. As shown in the figure, the basic common feature of these gels is a fibrillar network. The network is observed to become denser in gels formed from solutions with increasing polymer concentration reflecting the increased amount of polymer in the gels.

In order to investigate the influence of the method of removal of the solvent from the gel, supercritical CO_2 extraction was also utilized for gels obtained from 4.8 % solutions. The formation of aerogels of sPS by supercritical extraction of traditionally prepared gels has already been reported in the literature [Daniel *et al.* 2005]. Figure 5.8 shows the

comparison of the morphological features of these sPS gel samples which were air-dried, or dried by supercritical CO_2 at 313 K and 21 MPa for 24 hrs. They both show a fibrillar network structure with fiber diameters in the range of 20-30 nm. However, compared to the air-dried sample, the sample after supercritical CO_2 extraction shows a much finer porous structures, which may be viewed as representing the pore structure of the fresh wet gel. Extraction with supercritical fluids is a well recognized technique to alleviate interfacial tension effects and prevent cell collapse during drying.

5.3.4 Path Dependence of the Gel Structure

Figure 5.9 shows the two different paths for collection of the sPS samples at point B starting from a homogenous solution at point A. Path 1 is bringing the system into sol-gel phase separated region at constant pressure as a first step which is then followed by a depressurization process. In the second path, the system is first subjected to a pressure quench into L-L phase separation region upon which the solution phase separates into a polymer-rich and a polymer-lean phase which are then cooled to ambient temperature and depressurized.

The X-ray diffraction patterns for the samples collected at point B following such paths from 4.8 wt % sPS solution containing 28 wt % CO_2 are shown in Figure 5.10. The sPS sample after Path 1displays (Fig 10a) the typical of δ form, as indicated by the diffraction peaks at 2θ = 8.0, 10.3, 13.5, 17.3, 20.1, 23.4 and 28.0° [Manfredi *et al.* 1995]. The X-ray diffraction profile changes dramatically for the sample originating from the polymer-rich phase after Path 2 (Figure 5.10c), which only displays the typical β form indicated by the appearance of the reflections at 2θ = 6.2, 10.4, 12.3, 13.6, 18.6 and 21.1° [De Rosa *et al.* 1992]. The appearance of the both diffraction peaks corresponding to the δ and β forms in the X-ray diffraction pattern for the polymer-lean phase sample after Path 2, as shown in Figure 5.10b indicates the formation of the mixed β + δ crystal forms in this sample. (The

XRD spectrum shown in 10 d is that of a sample obtained from a solution containing 43 % CO_2 and will be discussed later in this section).

Figure 5.11 shows FTIR spectra for these three samples obtained from 4.8 wt % sPS solution in a fluid mixture of toluene (72) + CO_2 (28). The characteristic doublet peaks at 943 and 934 cm^{-1} correspond to the helical conformation and thus the IR spectrum indicates δ form for the sample obtained from Path 1. The intensities of these peaks are altered as Path 1 is changed to Path 2. The peak intensities are lowered for the sample from the polymer-lean phase and disappear for the sample from the polymer-rich phase that is generated following Path 2. The appearance of the peak at 1222 cm^{-1} and the shoulder peak at 911 cm^{-1} in the spectrum of the sample from the polymer-rich phase in Path 2 indicates the presence of the planar zig-zag β form [Roels *et al.* 1997]. The intensities of these peaks are observed to decrease in the sample from the polymer-lean phase. These peaks that are characteristic of the β form are absent in the sample from Path 1. As shown in Figure 5.11, while only the δ form is observed in the sample from Path 1 and the β form is observed in the sample from the polymer rich phase in Path 2, the polymer-lean phase in Path 2 leads to a mixture of δ and β forms. These results are consistent with the results from the XRD measurements discussed above.

Similar observation can be deduced from analysis of the DSC scans (obtained at 10 K/min) of these three samples illustrated in Figure 5.12. The DSC scans of the samples with δ form (Path 1 and Path 2 polymer-lean phase) show a broad endothermic peak in the temperature range 353 - 473 K. This is a typical feature reported in the literature for the δ form in the presence of a guest solvent for which the boiling point is in the range of 373 - 423 K [Chatani *et al.* 1992; Rastogi *et al.* 1998]. Normal boiling point of toluene is 383.6 K. The transformation peaks from δ to γ, and from the γ to α forms are usually masked by the gradual evaporation of the solvent during the scan. The transition of from δ to γ form in a

DSC scan is reported to be more apparent for higher boiling point solvents [Galdi *et al.* 2006]. The DSC scan of the sample showing the planar zig-zag β form displays only the endothermic melting peaks at temperature greater than 523 K corresponding to the crystalline melting of the β form. The multiplicity of the melting peaks for polymer crystals formed from high pressure solutions is common and is often attributed to the multiplicity of the crystal sizes formed in the process as discussed earlier in connection with the crystallization of polyolefins from high pressure solutions [Zhang *et al.* 2003; Zhang and Kiran 2006].

The morphology of sPS samples collected through Path 1, as shown in Figure 5.13a, is a fibrillar network structure which is very similar to the sPS gel structure formed from pure toluene solution, as shown in Figure 5.7. However, a closer examination of Figure 5.13a indicates the presence of aggregates of lamellar structures corresponding to the β form, dispersed within the fibrillar network. This is more clearly illustrated in Figure 5.13b, which is an enlargement of the small framed area of Figure 5.13a. The appearance of the β form dispersed in the δ form in the gel samples, even though the portion is relatively small and not detected in the IR spectra, is a good indicator of the trend that the β form is beginning to become the more stable crystal form as solvent quality becomes poorer with the addition of more CO_2. The presence of the β form in this sample can also account for the observation of the sol-gel phase transition occurring at higher temperatures compared to the sPS solutions in pure toluene, or in fluid mixtures with lower (i.e., 16 wt %) CO_2 content. Figure 5.13c shows the sPS samples recovered from polymer-rich phase after Path 2. Instead of a fibrillar network, a strikingly different morphology, lamellar-disk structures, that is indicative of chain-folded crystals is displayed. The fibrillar network is the typical feature for sPS gels that are generated via formation of the "polymer-solvent compound" which prevents chain folding. In contrast, the lamellar structure is the typical chain folded crystal morphology arising from the planar zig-zag chain conformation.

The morphology of the sample from the polymer-lean phase from Path 2 is shown in Figure 5.13d. A combination of high levels of both fibrillar and lamellar structures is displayed. The lamellar layers corresponding to the β form are actually interconnected by fine fibers corresponding to the δ form. These FESEM observations are in good agreement with the FTIR and DSC results.

The micrograph of sPS samples collected from the polymer rich phase after Path 2 in a mixture of toluene (57) + CO_2 (43) is shown in Figure 5.14. The morphology generated from this solution with much higher carbon dioxide content (43 *vs* 28 %) displays denser stacked-lamellar structures with spherulitic attributes. The XRD diffraction pattern of this sample which is shown in Figure 5.10d, is similar with that of the polymer-rich phase sample from the solution containing 28 wt % CO_2, indicating that only β form was generated in the sample. Even though not included in the present manuscript, both the FTIR and the DSC results on these samples also showed presence of only the β crystalline form. The difference in the samples generated from 28 and 43 % CO_2 containing solutions is thus only in the morphological appearance, and not the actual crystalline form which is the β in both cases.

5.3.5 Further Discussion on Path Dependence of the Crystalline Forms

The path dependence of the gel structures in terms of the different crystalline forms can be understood from a close examination of the phase diagrams. Figure 5.15 a and b are schematic representations of the T-x phase diagrams for sPS solutions in good and poor solvents at ambient pressure that is adapted from the literature [Deberdt and Berghmans 1993; Berghmans and Deberdt 1994; Rastogi *et al.* 1998]. In good solvents, the melting point depression of the β form is large and the melting curve intersects with the L + δ boundary. This is due to the solvent quality being good and the stability of the polymer-solvent compound (i.e. the δ form) being also improved with improved solvent

quality. In good solvents, the β form is the thermodynamically stable phase at high polymer concentrations, while the helical δ form is the thermodynamically stable phase at lower polymer concentrations. At high polymer concentrations, a metastable "β + δ" region is reported at lower temperatures.

In poor solvents, with decreased solvent quality, the melting point depression is reduced, and the melting curve moves to higher temperatures. The stability of δ form is also decreased. As shown in Figure 5.15b, in poor solvents, the β form becomes the thermodynamically stable phase in the whole concentration range and the "L + δ" and the "β + δ" regions depicted at lower temperatures below the "L + β" region are metastable.

Figures 5.16a and b are the schematics for the phase diagram and the phase separation paths in toluene + CO_2 mixtures at relatively high CO_2 content that we propose as being applicable at high pressures in the present study. These are based on the observations in the view cell and the results obtained from the XRD, FTIR and SEM of the samples collected after different paths. [DSC type calorimetric measurements that are generally used to generate phase diagram at ambient pressures are not experimentally amenable to high-pressure measurements in ternary systems that consist of polymer + solvent + carbon dioxide].

For simplicity, the system is viewed as a two-component system composed of the polymer and the pseudo-solvent (the mixture of toluene + CO_2). At the higher temperatures the LCST-type two phase region (L + L) is depicted which is supported by the experimental data in Figure 5.4. The present study shows that these fluid mixtures at high pressures indeed behave as relatively good solvents, leading to completely homogeneous solutions over a wide temperature range at all pressures investigated for mixtures containing up to 16 wt % CO_2. In the case of the system containing 28 wt % CO_2, the solvent quality becomes

poorer, and at lower pressures a liquid–liquid phase separation is observed upon an increase in temperature.

The region below the homogenous liquid (L) region is viewed to be more like the poor solvent case shown in Figure 5.15b, but somewhat modified to account for high pressures and the improved solvent quality that accompanies higher pressures. .Thus the diagram depicts a picture that describes the system as being in an intermediate solvent. The lower temperature portion of the phase diagram is based on the SEM observations on the gel samples that we have presented in the previous sections. The micrographs of the gels formed from the mixture of toluene (72) + CO_2 (28) indicate the presence of the β form over the whole polymer concentration range. Thus, in Figure 5.16, the region below the homogenous liquid phase is the "L + β" region corresponding to the coexistence of the solution and the β crystal phase (representing the zig-zag chain conformation) over the full polymer concentration range. The "L + β" region is depicted as narrowing at lower polymer concentrations due to the larger melting point depression of the β crystal form with the increasing amount of the solvent in the system. Below the "L + β" region is "L + δ" region corresponding to the coexistence of the solution and the "polymer-compound" phase (δ phase) observed at the low polymer concentrations. There is a metastable "β + δ" region at higher polymer concentrations, where β and δ forms coexist.

As already noted, the sPS solutions in toluene + CO_2 for solutions containing 28 % CO_2 also display a LCST-type L-L phase behavior in the high temperature region. In Figure 5.16, along Path 1, upon reduction of temperature the homogenous solution at point A enters the "L + β" region which is then followed by entry into the "L + δ" region where the polymer forms "the polymer-solvent compound" and solution undergoes gelation. Final depressurization stage to ambient pressure (see Figure 5.9) does not alter the structure of the compound. The samples collected through Path 1 show primarily the δ crystal form and

fibrillar morphology. Presence of a small fraction of the β form was also indicated in the SEM micrographs (Figure 5.13). The presence of the β form is understandable since the system traverses the narrow "L + β" region during the cooling process. The system experiences an early stage of crystallization that would lead to the β form. Further development of the β form is however hindered upon entering the "L + δ" region with continual cooling where the δ form rather than the β form is promoted.

In Figure 5.16, along Path 2, the homogenous solution at point A enters the L-L phase separated region upon reduction of pressure which moves the LCST to lower temperatures. The solution which was homogenous at T_1 is now in the immiscible region and the system phase separates into two coexisting phases, a polymer-lean phase (L_1) and a polymer-rich phase (L_2). In the second step along Path 2 (see Figure 5.9) where temperature is reduced, these two phases undergo a process similar to Path 1. The polymer-rich phase enters the "L +β" region first and then goes into a metastable "β + δ" region, while the polymer-lean phase crosses "L +β" region and enters the "L + δ" region. For the polymer-rich phase, the rate of crystallization of the β form is promoted and progresses to completion. As shown in the figure, at higher polymer concentrations the temperature range for the stable L + β region is larger. There is sufficient time during the cooling process that the system remains in the "L + β" region which leads to the effective formation and completion of the stable zig-zag β form. With further cooling, the system enters the metastable "δ + β" region, but the stable β that was generated in the higher temperature range remains with no transformation to the. δ form. This is consistent with the experimental observation that only the β form was collected for the polymer-rich phase. For the polymer-lean phase L_1, during reduction of temperature to room temperature the system first enters the "L + β" region and then the "L + δ" region. One then expects the final crystal form to be predominantly the δ form with presence of a minor β component, as was the case for Path 1. This is actually in contrast to the experimental observations. What is actually observed is a mixture of δ + β

forms with relatively large amount of β (see Figure 5.13d). This discrepancy may be attributed to the different level of CO_2 in the polymer-lean phase and polymer-rich phase after the L-L phase separation. In the ternary system of Polymer (sPS) + Good solvent (toluene) + Poor solvent (CO_2), the polymer-lean phase tends to have more CO_2 compared to the polymer-rich phase after the L-L phase separation [Kiran 1994]. An increase in CO_2 content in the polymer-lean phase leads a decrease in the solvent quality which results in destabilization of the polymer-solvent compound (δ phase) and promotion of the formation of the β form. This would then lead to a mixture of β + δ forms with a relatively large amount of the β form, as is experimentally observed.

Figure 5.17 presents a schematic of T-x diagram for sPS solution in the mixture solvent with higher (43 %) CO_2. As compared to Figure 5.16 for the mixture solvent containing 28 % CO_2, Figure 5.17 includes features that account for the higher reduction in solvent power. The L + β phase boundary is shifted to higher temperatures since the extent of melting point depression of β crystal form would be further decreased due to further reduction of the solvent quality. The "L + δ" phase boundary is shifted to lower temperatures due to decreased solvent quality. The L-L phase boundary is shifted to lower temperatures (reducing the homogeneous region) due to reduced solvent quality. As also indicated in the T-P phase diagram shown in Figure 5.4, the LCST type L-L phase boundary shifts to higher pressures with increasing the CO_2 content in the solvents. This actually leads to a deeper pressure quench below the phase boundary for the solvent with 43 wt % CO_2 compared to the solution with 28 wt % CO_2 even when the same pressure jump (~ 35 MPa) is imposed.

The T-x diagram corresponding to a lower pressure P_2 is also shown in Figure 5.17. The solution which was homogonous at point A at P_1 when pressure is lowered to P_2 undergoes phase separation into the polymer-rich and the polymer-lean phases that coexist. Due to the deeper pressure quench experienced in this higher CO_2 containing solution, the

polymer-rich phase at L_2 has a higher polymer concentration, and the polymer-lean phase at L_1 has a lower polymer content compared with that in Figure 5.16 depicting the case for the lower CO_2 containing solution. Further cooling from L_2 leads to the crystallization in the β form from polymer rich phase at this high polymer concentration resulting in the denser spherulitic structures that were observed in Figure 5.14. The polymer lean phase L_1 has extremely low polymer content which prevented sampling for characterization. But Figure 5.17 would suggest that if a sample could have been collected the polymer in the polymer lean phase would also have been dominated by the β crystal form.

The relative amount of the β form and the crystal morphology observed in the SEM of the different samples can be viewed as reflecting the different stages of the crystallization of the β form. The small β crystal domains dispersed within fibrillar network formed from sPS solutions in toluene (72) + CO_2 (28) through Path 1, which could only be observed in SEM micrograph and not detected in XRD and FTIR measurement, may be regarded as reflecting the early stage of crystallization, the further growth of which is prevented due to entry into the "L + δ" region where the δ form is promoted instead. The β crystal morphology observed in the polymer-rich phase obtained from sPS solutions in toluene (72) + CO_2 (28) through Path 2 may be viewed to represent the middle stage of crystallization in which higher crystallization rates and longer crystallization times permit the development of the lamellar disks. The β crystal morphology observed in samples collected from the polymer-rich phase generated from sPS solutions through Path 2 in toluene + CO_2 with higher amount of CO_2 (43 wt %) may be viewed as reflecting the late stage of crystallization. The higher supersaturation and crystallization rate and longer crystallization time available in the wider "L + β" region lead to the formation of denser, spherulitic structures.

5.4 Conclusions

Only the sol-gel phase boundary was observed in solutions of sPS in pure toluene and toluene + CO_2 mixtures up to 16 wt % CO_2. In solutions with more than 28 wt % CO_2, both sol-gel and liquid-liquid phase separations were observed. The liquid-liquid phase boundary shifted to higher pressures with increasing amount of CO_2 in the solution. The gel samples formed from the sPS solutions in pure toluene and toluene + CO_2 with a CO_2 level up to 16 wt % show a fibrillar network morphology with δ crystal structure. The sPS samples collected from the solutions with higher level of CO_2, i.e., 28 wt % CO_2 in solvent mixture, depending upon the paths followed, are found to display different crystalline structures and morphological feature. The samples collected through constant pressure cooling show a fibrillar structure with a small portion of β form. While the system containing high level of CO_2 first undergoes L-L phase separation by constant temperature pressure quench. The samples recovered after the L-L phase separation show different structures. For the polymer-rich phase, the samples show stacked-lamellar morphology and the β form crystalline structure, and for the polymer-lean phase, the morphology is that of lamellar layers connected with fine fibers displaying a mixture of δ and β phase crystalline structures. With even higher CO_2 content in system, i.e., 43 wt % in solvent mixture, samples collected from polymer-rich phase display a denser stacked-lamellar morphology with spherulitic attributes and β crystalline structure.

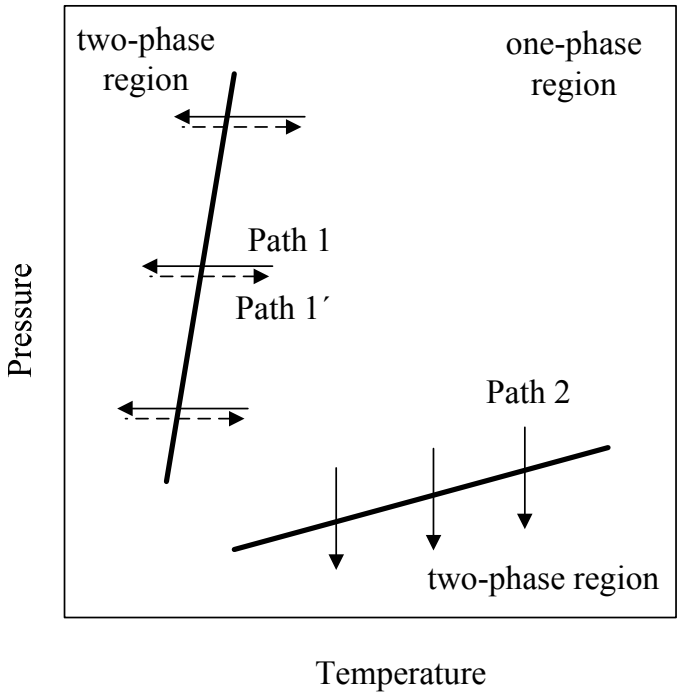

(a)

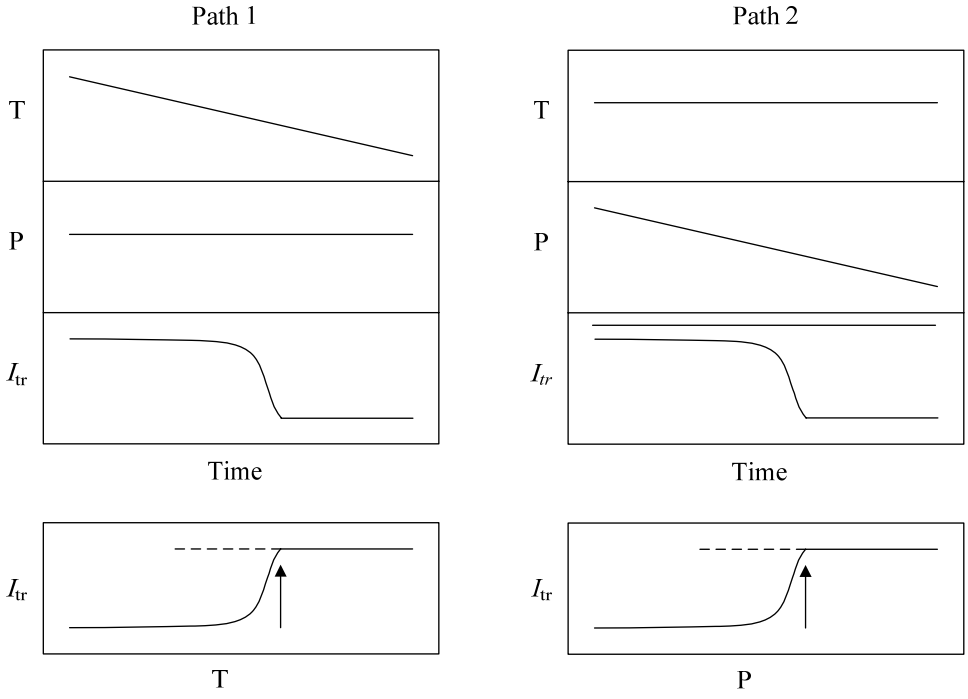

(b)

Figure 5.1 Schematic representation of different paths followed to determine the phase boundaries and the corresponding changes in T, P, and I_{tr} with time.

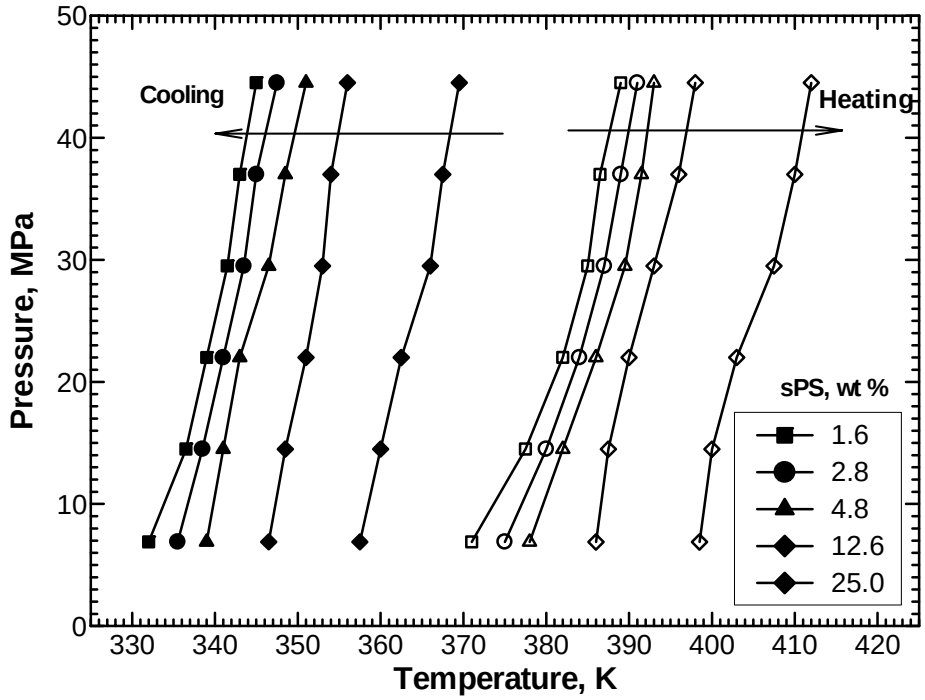

Figure 5.2 The sol-gel phase boundaries for syndiotactic polystyrene solutions in toluene at different polymer concentrations. Filled symbols represent the gel formation points upon cooling and opened symbols represent the gel melting points upon heating.

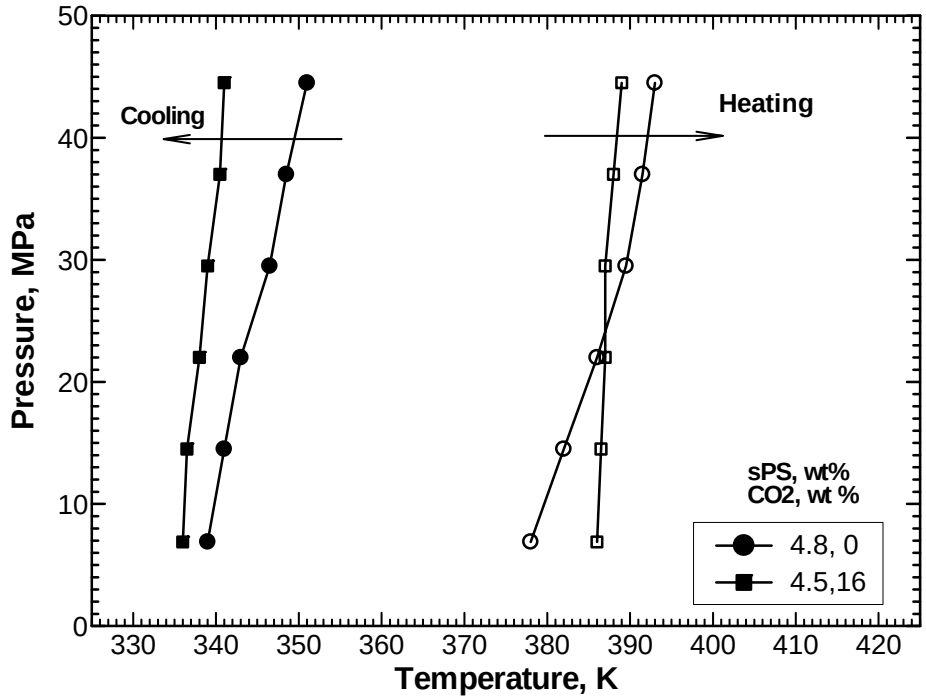

Figure 5.3 The sol-gel phase boundaries for syndiotactic polystyrene solutions in pure toluene and toluene + CO_2 mixture with 16 % CO_2 in the solvent mixture. Filled symbols represent the gel formation points upon cooling and opened symbols represent the gel melting points upon heating.

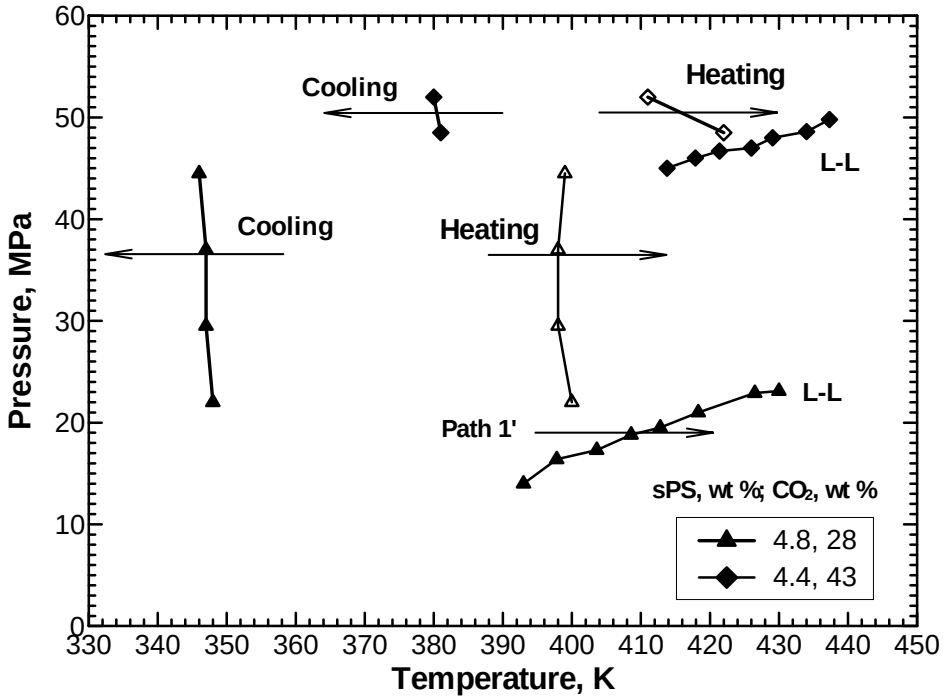

Figure 5.4 The sol-gel and L-L phase boundaries for syndiotactic polystyrene solutions in toluene + CO_2 mixture with 28 % CO_2 and fluid-solid and L-L phase boundaries in toluene + CO_2 mixture with 43 wt % CO_2 in the solvent mixture. Open symbols represent the gel melting (28 % CO_2) or crystalline melting (43 % CO_2) points upon heating.

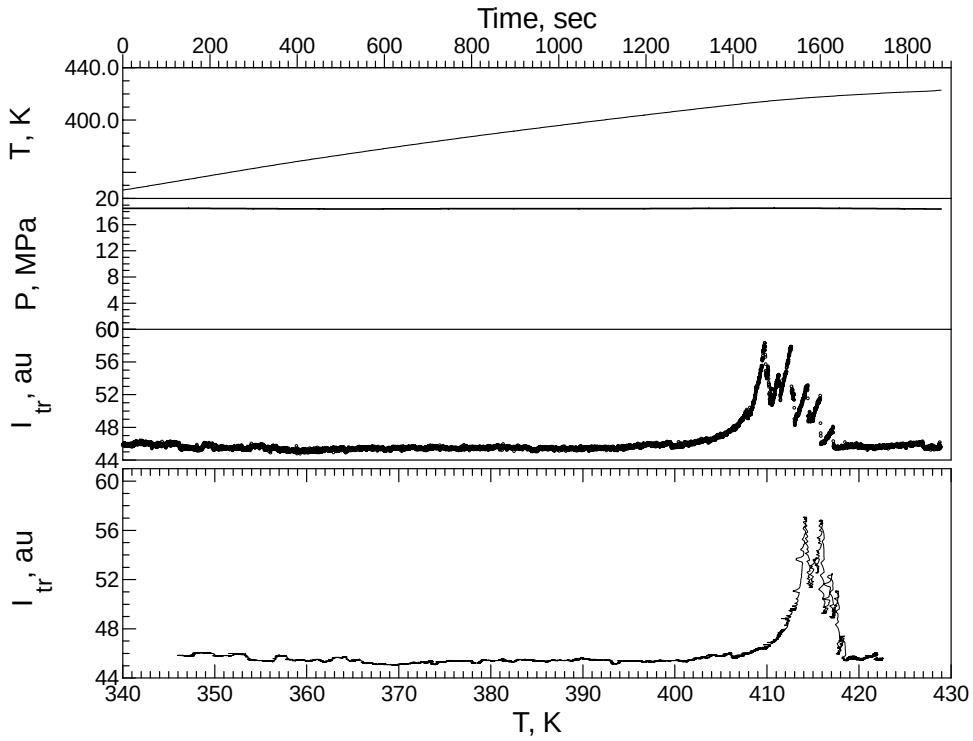

Figure 5.5 Variation of temperature T, pressure P, and transmitted light intensity I_{tr} with time and I_{tr} with temperature along the constant pressure heating path (as indicated as path B' in Figure 4) in 4.8 wt %sPS solution in 72 wt % toluene + 28 wt % CO_2 at 18.5 MPa.

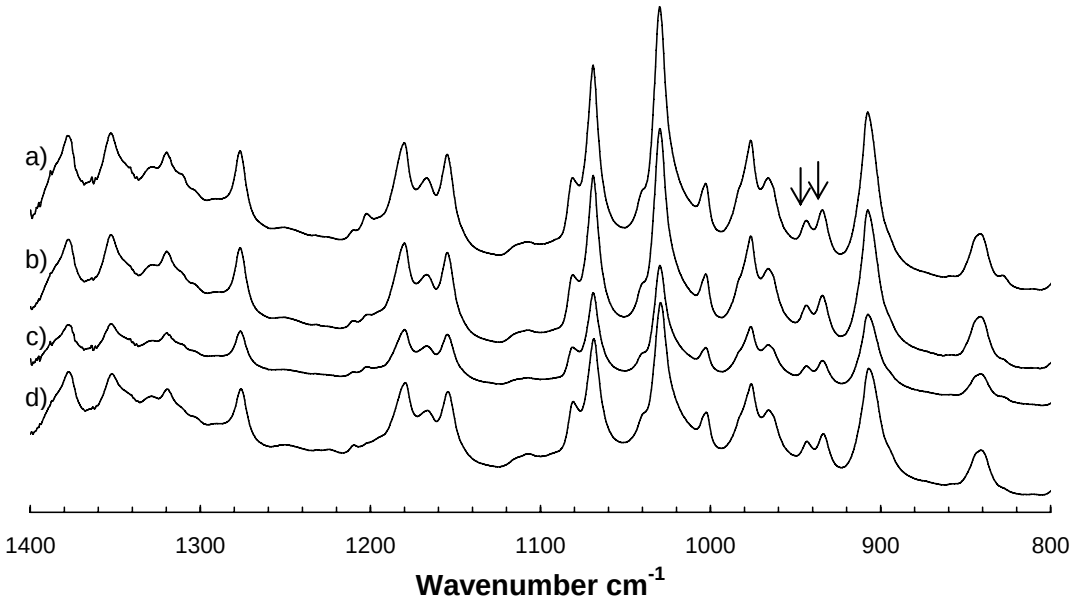

Figure 5.6 FTIR spectra of syndiotactic polystyrene (sPS) gel samples collected from sPS solutions in pure toluene with different polymer concentrations: (a) 2.8 wt %; (b) 4.8 wt %; (c) 12.6 wt % and (d) 25.0 wt %.

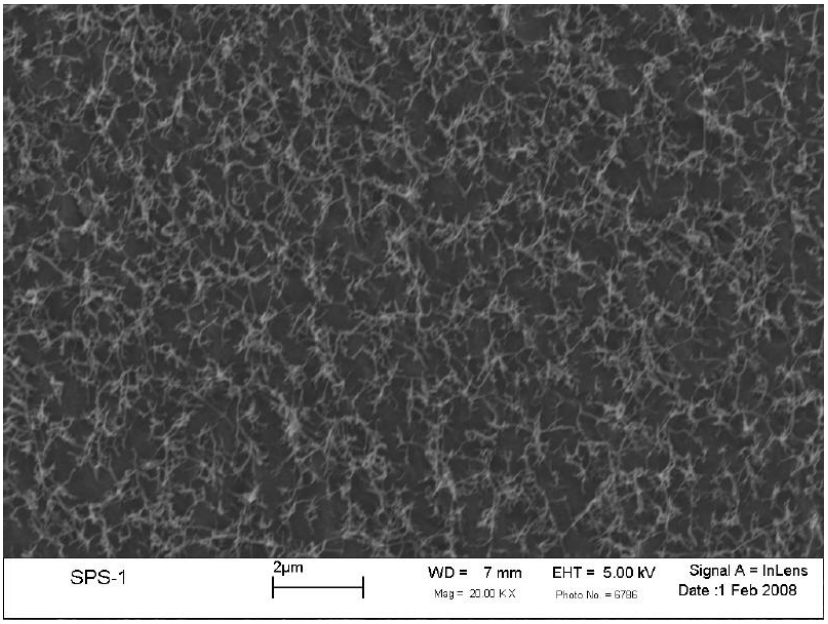
SPS-1
2µm
WD = 7 mm
Mag = 20.00 K X
EHT = 5.00 kV
Photo No. = 6796
Signal A = InLens
Date :1 Feb 2008

(a)

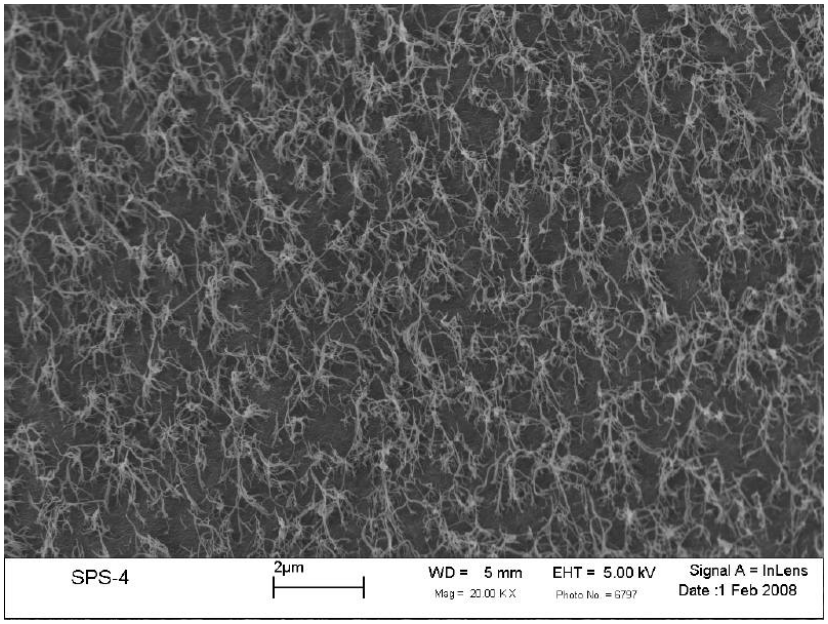
SPS-4
2µm
WD = 5 mm
Mag = 20.00 K X
EHT = 5.00 kV
Photo No. = 6797
Signal A = InLens
Date :1 Feb 2008

(b)

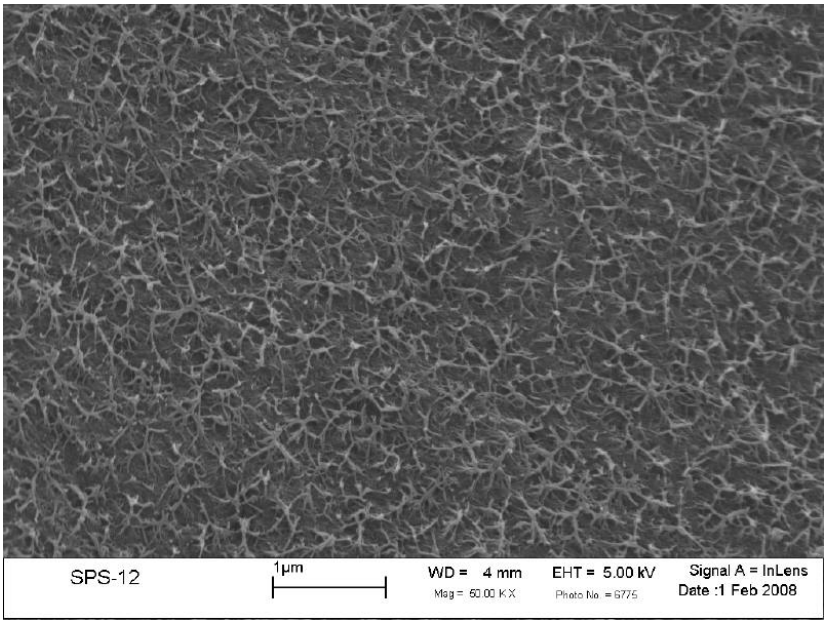

(c)

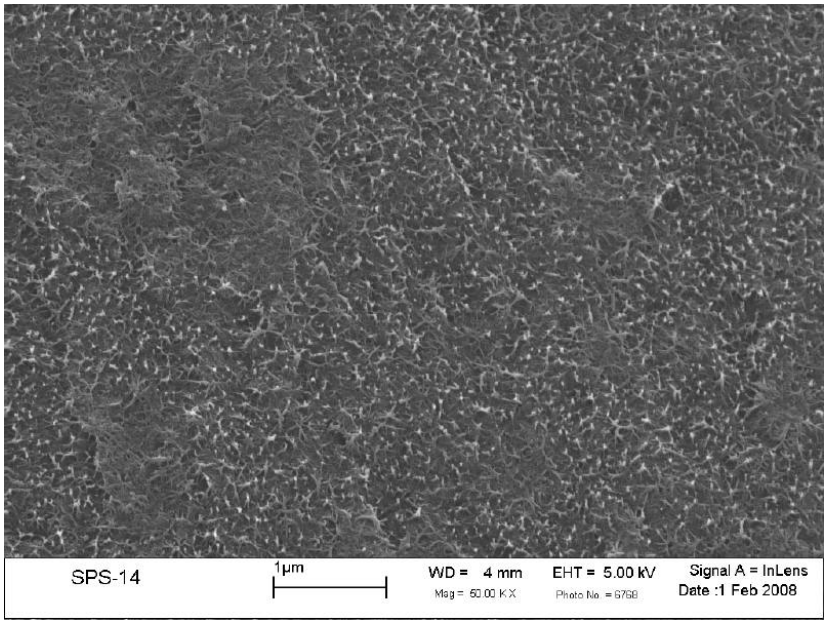

(d)

Figure 5.7 FESEM micrographs of sPS gel samples that were formed at 298K and 44.5 MPa from the solutions with different polymer concentrations: (a) 1.6 wt %; (b) 2.8 wt %; (c) 12.6 wt % and (d) 25.0 wt %. The scale bars are 2 μm in (a) and (b) with the magnification of 20,000 ×; and 1 μm in (c) and (d) with the magnification of 50,000 ×.

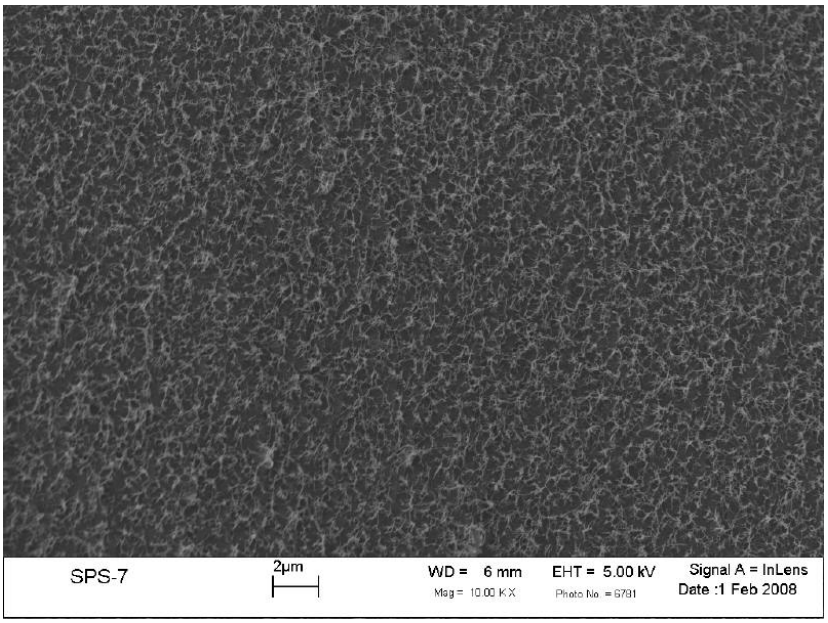
SPS-7
2µm
WD = 6 mm
Mag = 10.00 K X
EHT = 5.00 kV
Photo No. = 6791
Signal A = InLens
Date :1 Feb 2008

(a)

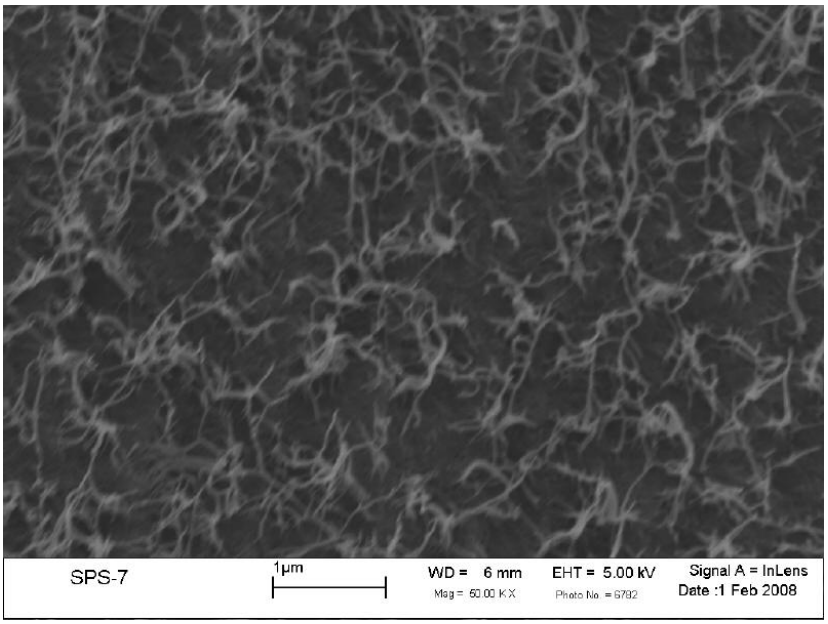
SPS-7
1µm
WD = 6 mm
Mag = 50.00 K X
EHT = 5.00 kV
Photo No. = 6792
Signal A = InLens
Date :1 Feb 2008

(b)

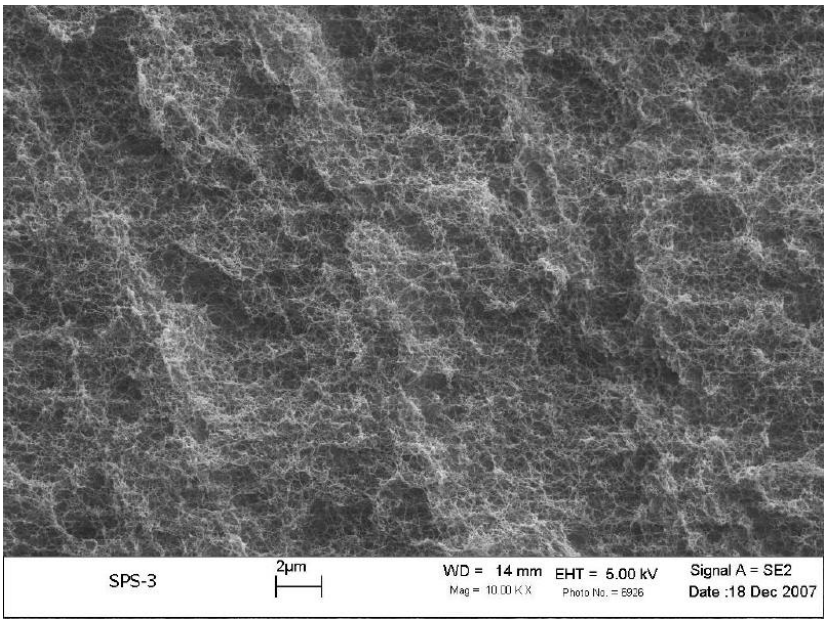

(c)

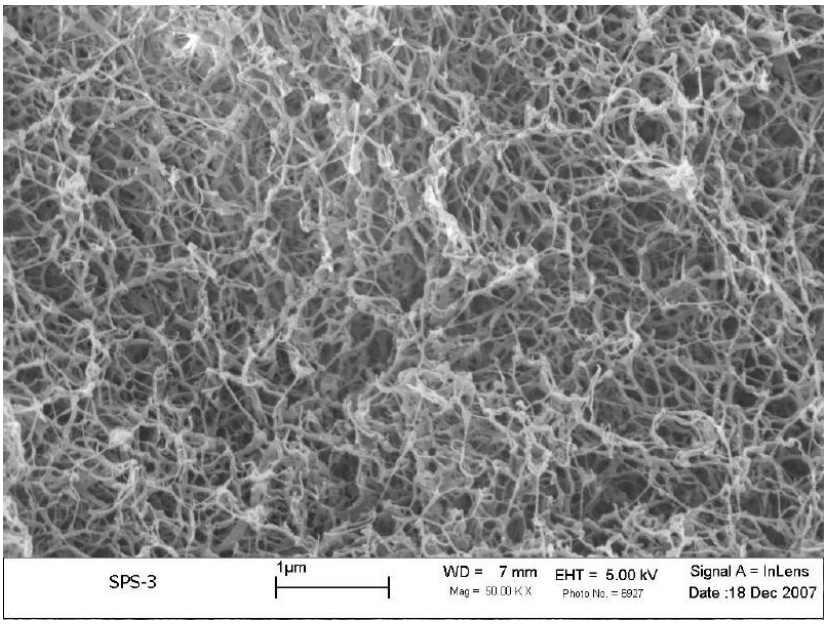

(d)

Figure 5.8 FESEM micrographs of sPS gel samples that were formed at 298 K and 44.5 MPa from the 4.8 wt % solution in pure toluene: (a) (b) after air dried; and (c) (d) after 24 hr supercritical CO_2 extraction at 313 K and 21 MPa. The scale bars are 2 μm in (a) and (c) with 10,000 ×; and 1 μm in (b) and (d) with 50,000 ×.

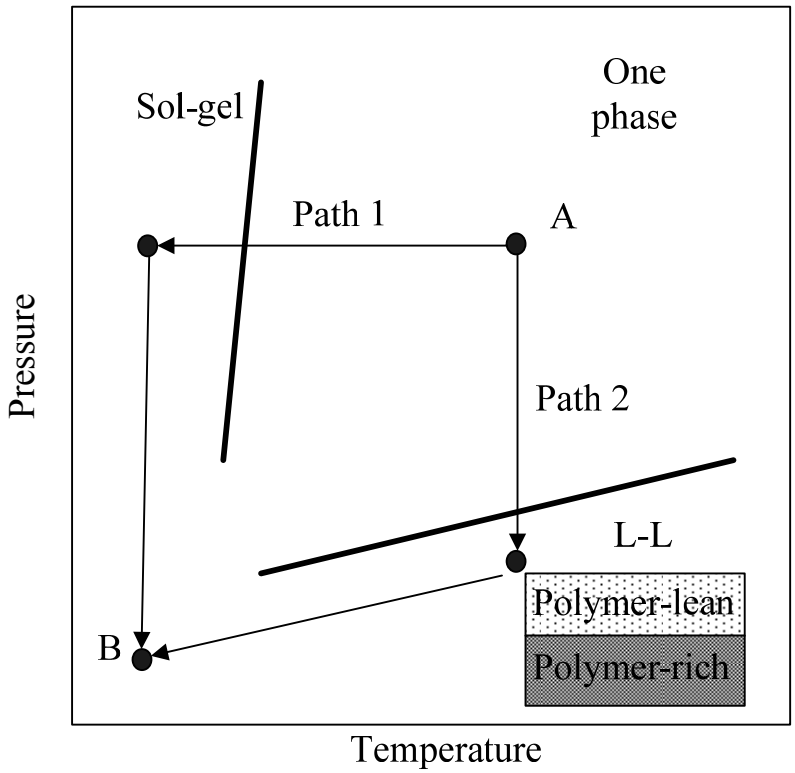

Figure 5.9 Schematic representation of two different phase separation pathways on a T-P phase diagram; path 1: constant pressure cooling process to room temperature followed by further depressurization; and path 2: a pressure quench into L-L phase separation region at a given temperature followed by further cooling to room temperature.

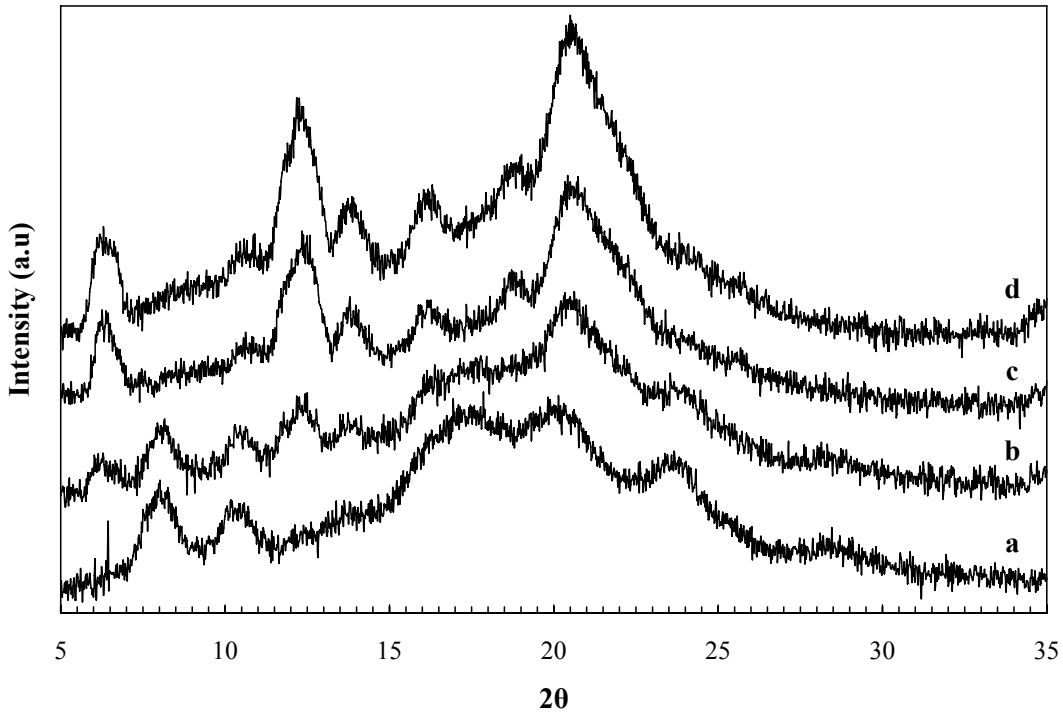

Figure 5.10 X-ray diffraction patterns in the 2θ range 5° - 35° for syndiotactic polystyrene (sPS) samples collected from 4.8 wt % sPS solutions in 72 wt % toluene + 28 wt % CO_2 solution: (a) Path 1; (b) Path 2 polymer-lean phase; (c) Path 2 polymer-rich phase; The XRD pattern shown in (d) is of a sample collected from the polymer-rich phase after Path 2 in a 4.4 wt % solution with higher (43 %) CO_2.

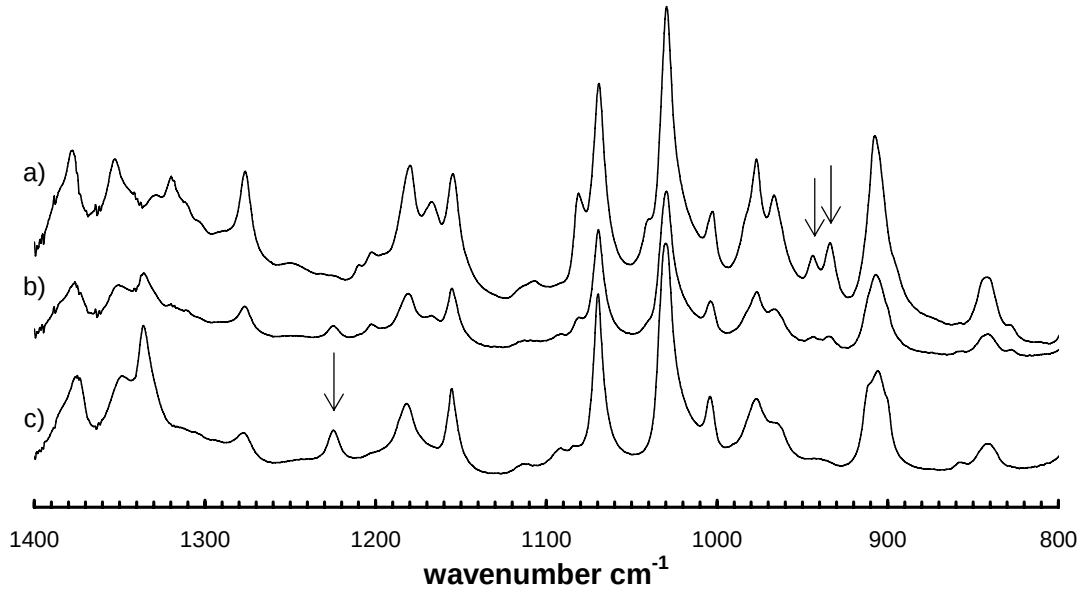

Figure 5.11 FTIR spectra of syndiotactic polystyrene (sPS) samples collected from 4.8 wt % sPS solutions in 72 wt % toluene + 28 wt % CO_2 solution: (a) Path 1; (b) Path 2 polymer-lean phase; (c) Path 2 polymer-rich phase.

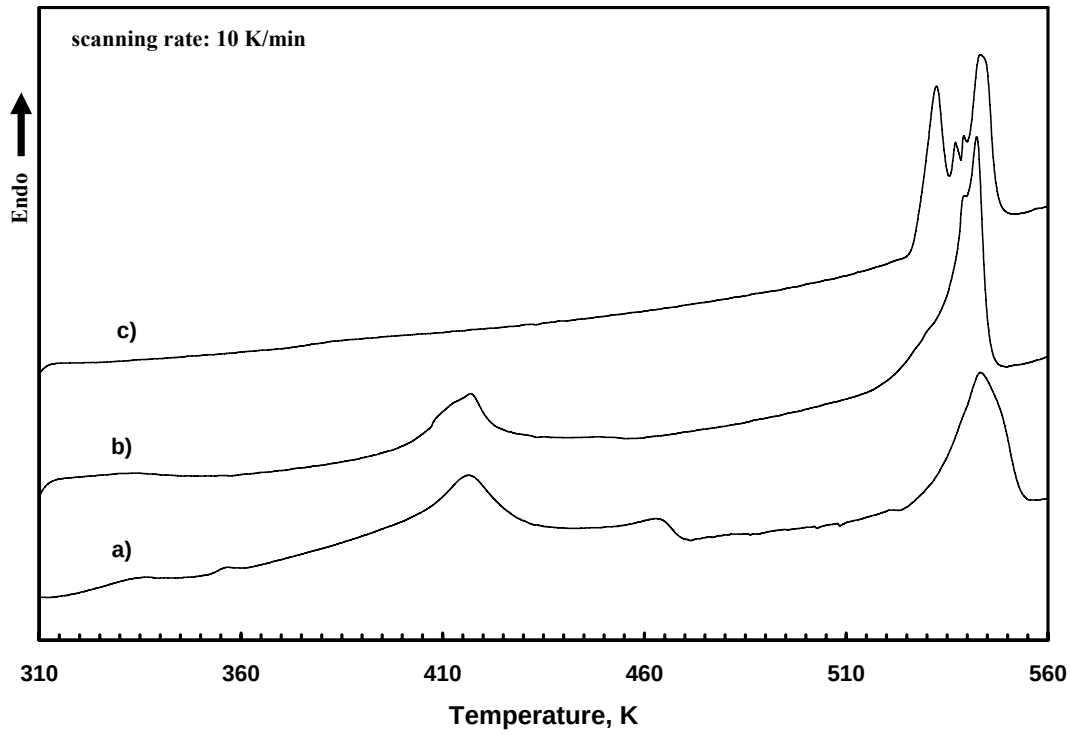

Figure 5.12 Comparison of the DSC scans for sPS samples from 4.8 % solutions in 72 wt % toluene + 28 wt % CO_2: (a) samples collected through Path 1; (b) samples collected from the polymer-lean phase through Path 2; and (c) samples collected from the polymer-rich phase through Path 2.

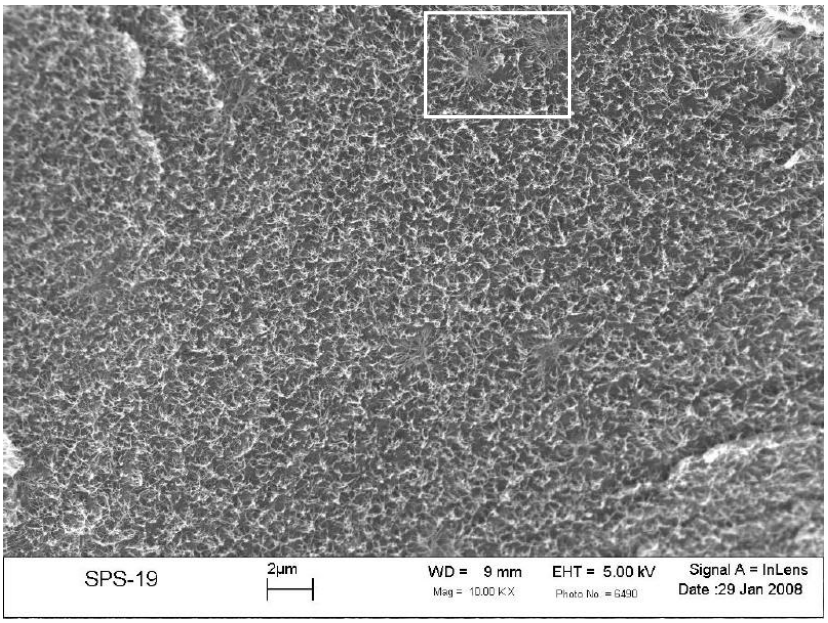
SPS-19
2µm
WD = 9 mm
Mag = 10.00 KX
EHT = 5.00 kV
Photo No. = 6490
Signal A = InLens
Date :29 Jan 2008

(a)

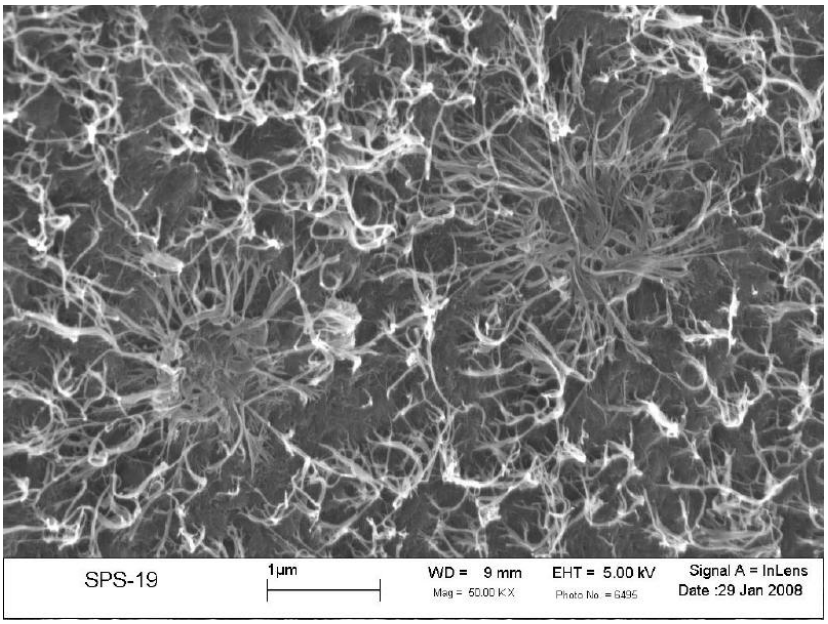
SPS-19
1µm
WD = 9 mm
Mag = 50.00 KX
EHT = 5.00 kV
Photo No. = 6495
Signal A = InLens
Date :29 Jan 2008

(b)

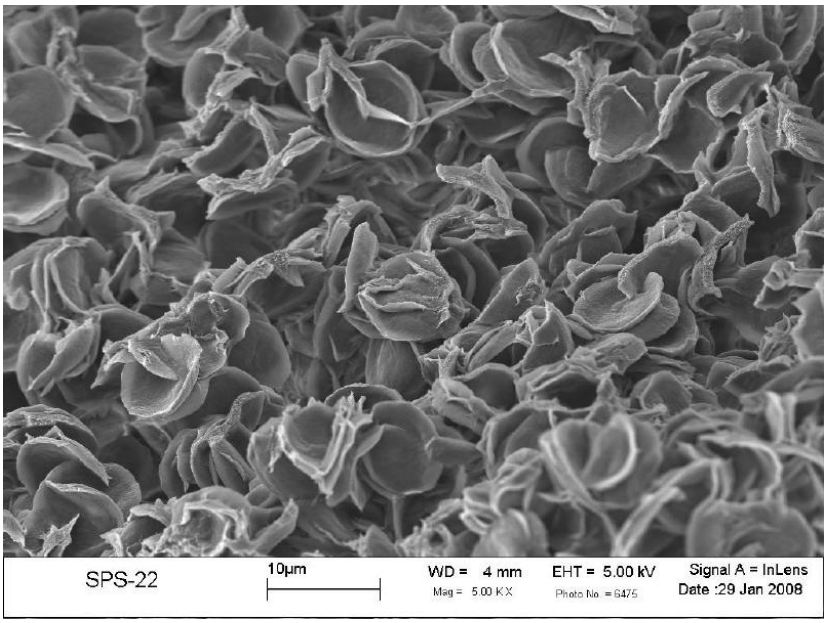

(c)

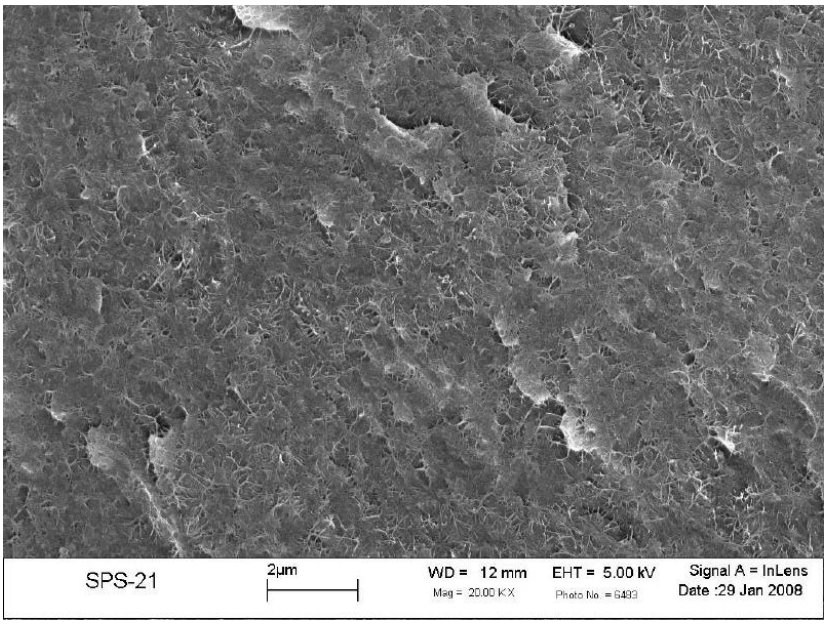

(d)

Figure 5.13 FESEM micrographs of sPS samples that were collected from 4.8 wt % sPS solutions in 72 wt % toluene + 28 wt % CO_2 solution after: (a) Path 1; (b) Enlarged area of (a); (c) Path 2, polymer-rich phase; (d) Path 2, polymer-lean phase. The scale bars and magnifications are: (a) 2 µm, 10,000 ×; (b)1 µm, 50,000 ×; (c) 10 µm, 5,000 ×; and (d) 2 µm, 20,000 ×.

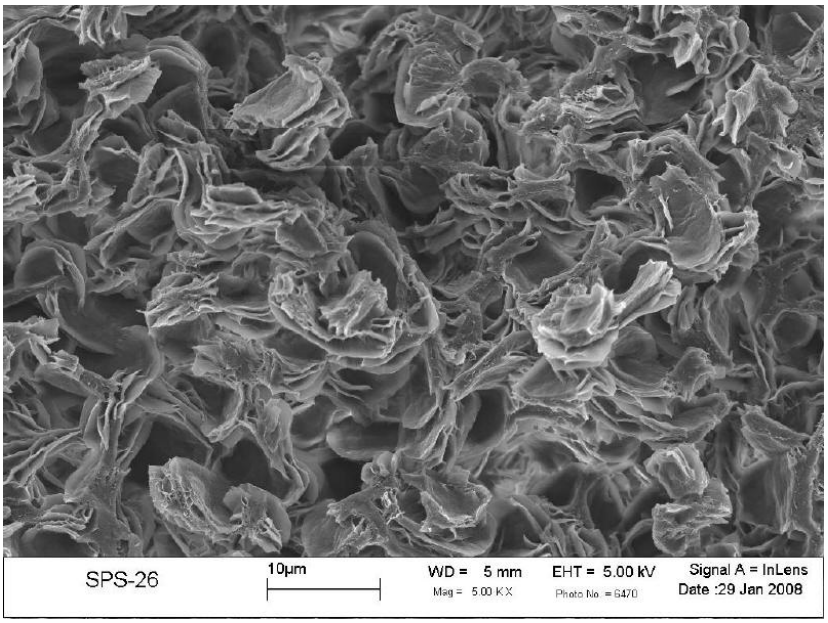

Figure 5.14 FESEM micrographs of sPS samples that were collected from 4.4 wt % sPS solutions in 57 wt % toluene + 43 wt % CO_2 after path 2, polymer-rich phase. The scale bar and magnification are 10 µm, 5,000 ×.

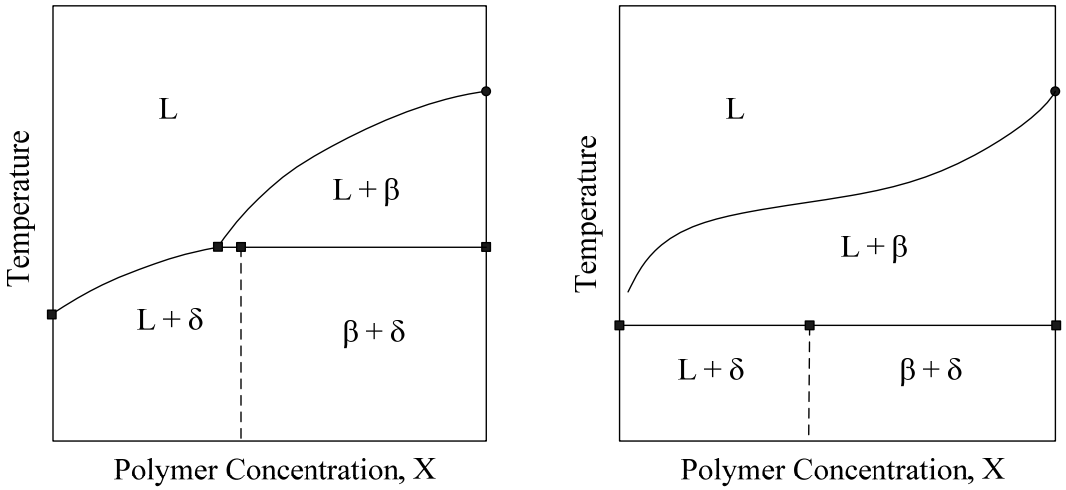

Figure 5.15 Schematic representation of temperature-concentration phase diagrams for sPS in good (a) and poor (b) solvents at ambient pressure. L: liquid phase; β: β crystal form of sPS; δ: δ crystal form.

Path 1:

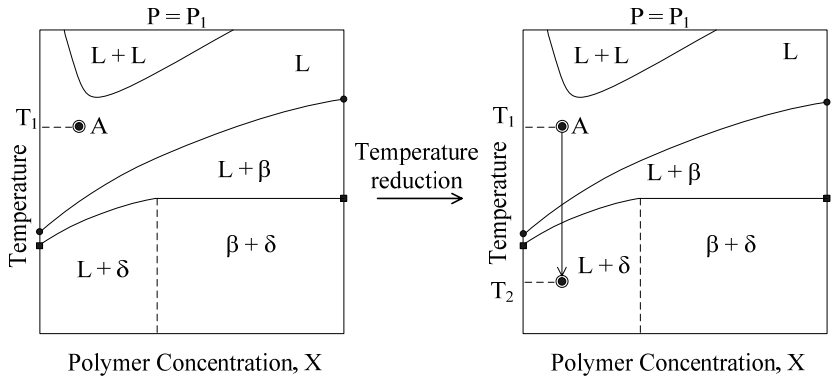

Path 2:

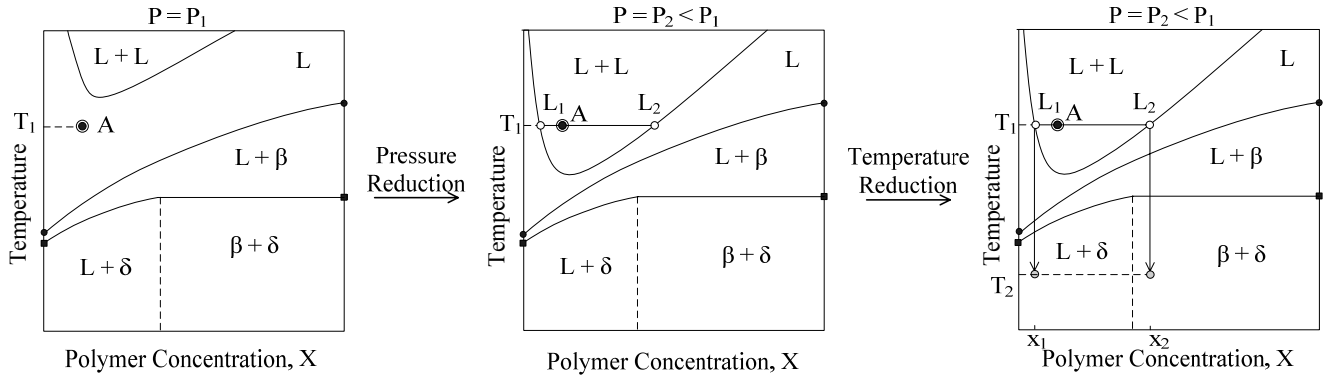

Figure 5.16 Schematic representation of the T-x phase diagrams for sPS in toluene + CO2 at high pressures and the consequence of paths followed on the eventual crystalline forms that are generated. P is pressure, L_1, and L_2 are the polymer - lean and the polymer - rich phases. Other symbols are as in Figure 5.15.

Path 2:

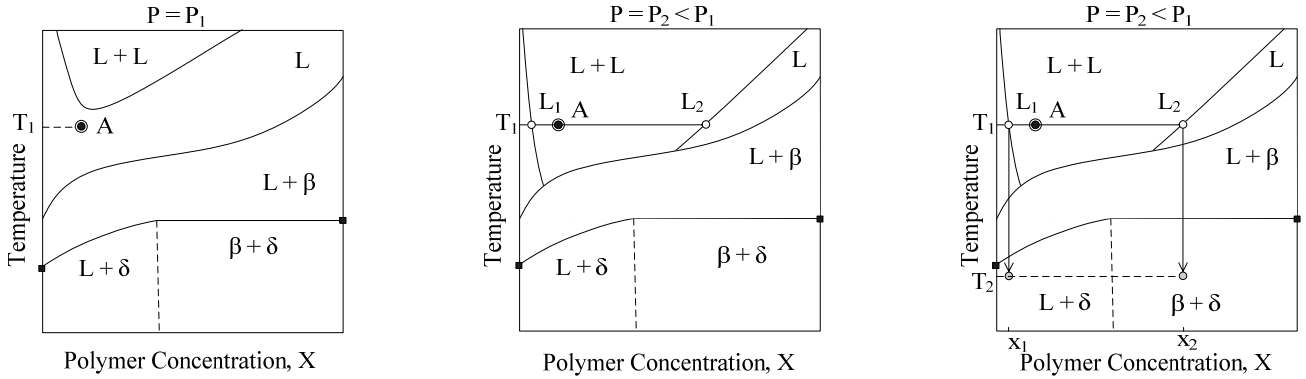

Figure 5.17 Schematic representation of the T-x phase diagram for sPS in toluene + CO_2 with higher CO_2 content at high pressures Symbols are as in Figure 5.16.

Chapter 6

Gelation, Crystallization and Morphological Transformations of Syndiotactic Polystyrene in Acetophenone and Acetophenone + Carbon Dioxide Mixtures at High Pressures*

The gelation and crystallization processes in 5 wt % solutions of syndiotactic polystyrene in acetophenone and acetophenone + carbon dioxide fluid mixtures were studied in a variable-volume view-cell system over a pressure range from 7 - 50 MPa for CO_2 concentrations up to 40 wt %. The solution in pure acetophenone displayed only a sol-gel (gelation) phase boundary. Solutions containing 25 wt % CO_2 displayed both a sol-gel and a liquid-liquid phase boundary. Solutions containing 40 % CO_2 displayed instead a fluid-solid (crystallization) and a liquid-liquid phase boundary. The consequences of crossing the gelation, crystallization or the liquid-liquid demixing boundaries first on the eventual morphology and the crystal structures that develop were investigated. It is shown that when the gelation boundary is crossed first, the resulting crystal structure is the δ form. When the L-L phase boundary is crossed first, polymer rich phase leads to a mixture of δ + β crystal forms while only the δ form is found in the polymer-lean phase from solutions with 25 wt % CO_2. In solutions with 40 wt % CO_2, crossing the crystallization boundary first leads to the β form with no presence of the δ crystal form. However, when the liquid-liquid phase boundary is crossed first, the polymer-rich phase forms only the β crystal form and the polymer-lean phase leads to a mixed crystal structure containing the β and δ forms. Formation of the different crystal structures are

* Submitted for publication in the Journal of Supercritical Fluids as "Jian Fang and Erdogan Kiran. *Gelation, Crystallization and Morphological Transformations of Syndiotactic Polystyrene in Acetophenone and Acetophenone + Carbon Dioxide Mixtures at High Pressures*"

verified by XRD, FTIR and SEM characterizations and are rationalized with a phase diagram describing the paths followed as a result of a change in pressure an/or the temperature.

6.1 Introduction

Syndiotactic polystyrene (sPS) is a polymer of continuing industrial interest because of its high crystallization rate, high melting temperature and good chemical resistance [Ishihara *et al.* 1986; Zambelli *et al.* 1987; Ishihara *et al.* 1988; Malanga 2000]. It is also of great scientific interest due to the many polymorphic states it displays [Grassi *et al.* 1989; Reynolds *et al.* 1989; Gomez and Tonelli 1990; Guerra *et al.* 1990; Chatani *et al.* 1992; De Rosa *et al.* 1992; De Rosa 1996; De Rosa *et al.* 1997; Moyses and Spells 1999; Yoshioka and Tashiro 2003; Albunia *et al.* 2006; Rizzo *et al.* 2007; Petraccone *et al.* 2008]. There are five known polymorphic states, namely the α, β, γ, δ and more recently the ε forms. The α and β forms that are typically obtained from the melt are in planar zigzag chain conformations. While the γ, δ and ε forms which are normally formed in the presence of solvents are in 2_1 helical chain conformation. In the δ crystal form, the solvent molecules are entrapped via formation of a "polymer-solvent compound", whereas the γ form is a solvent-free crystal form obtained by thermal treatment of the δ crystal form. If the solvent molecules in the δ crystal are extracted with for example supercritical carbon dioxide, a nanoporous "emptied" crystalline phase known as the δ_e crystal form is generated in which the pores are in the shape of cavities. The ε form is also a nanoporous crystalline phase, but with pores that are in "channel" shape instead of cavities [Petraccone *et al.* 2008].

The δ form can also be obtained from the α and γ form by sorption of suitable solvents [Immirzi *et al.* 1988]. However, the β from is stable and does not transform to the δ form in the presence of solvents [Rapacciuolo *et al.* 1991]. The systematic studies carried out

by Berghmans and coworkers [Deberdt and Berghmans 1993; Deberdt and Berghmans 1994; Roels *et al.* 1994; Roels *et al.* 1997] on the relative stability of δ and β forms as a function of polymer concentration have shown that in good solvents the β form is the more stable form at high concentrations, while the δ form is the more stable form at low polymer concentrations. The relative stability of the β and δ forms is however altered when the solvent strength is changed. With decreasing solvent quality [Deberdt and Berghmans 1993], the β form becomes the more stable form over the whole polymer concentration range while the δ form becomes metastable.

The use of the fluid mixtures of organic solvents with CO_2 as solvents is an attractive approach to tune the properties of the solvent , in particular the solvent quality [Kiran *et al.* 1993; Zhang *et al.* 2003; Fang and Kiran 2006], and thereby influences the crystal form and morphology of sPS. The outcome can be altered by changing not only the fluid composition, but also by changing the pressure or the temperature for a given fluid composition as we have already demonstrated for gelation or crystallization processes for sPS in toluene + CO_2 mixtures [Fang and Kiran 2008]. In the present paper we are now reporting on the gelation and crystallization of sPS in acetophenone + CO_2 solvent mixtures. Acetophenone (C_6H_5-CO-CH_3) differs from toluene (C_6H_5-CH_3) by a carbonyl group which may interact with carbon dioxide as is the case in acetone + CO_2 systems [Liu and Kiran 2007], and thus is of interest in gaining further insight on the influence of the nature of the solvent on promotion of different crystals forms. As in the case of toluene + CO_2 mixtures, we are providing new information on the effect of the phase separation path followed on the outcome in terms of the morphological features and the crystal forms generated. To our knowledge this is the first ever study of gelation and crystallization of sPS in acetophenone or acetophenone + CO_2 mixtures.

6.2 Experimental Section

6.2.1 Materials

The syndiotactic polystyrene (with 98 % syndiotactic triads) was purchased from Scientific Polymer Products Inc. The polymer had a weight average molecule weight of $M_w = 3.2 \times 10^5$ g/mol and a polydispersity of $M_w/M_n = 3.9$. The solvent, acetophenone, with a minimum purity of 99 % was purchased from Aldrich. Carbon dioxide with a minimum purity of 99.99 % was purchased from Air Products. The polymer and the solvents were used as received.

6.2.2 Experimental System and Procedure

Experiments were carried out in a variable-volume view-cell equipped with two sapphire windows for visual or optical observations which has been previously described [Fang and Kiran 2006; Fang and Kiran 2008]. A movable piston coupled with a pressure generator is used to alter the inner volume of the cell and thereby adjust the system pressure. An optical fiber illuminator is used as the light source and the transmitted light intensity is monitored with a fast response photodiode detector. During phase boundary determination, the temperature, pressure and transmitted light intensities are recorded in real-time with a dedicated computer.

Experimental procedure is similar to that described in our earlier publication [Fang and Kiran 2008]. Briefly, an accurately weighted amount of polymer is first loaded into the cell. This is followed by the addition of a measured amount of the liquid solvent, i.e., acetophenone. The cell is then sealed and connected to the CO_2 charge line and the pressure generator. After the loading process is completed, the cell temperature and pressure are brought to the desired conditions for dissolution of polymer, forming a homogenous solution as verified through the sapphire windows. A magnetic stirrer is used

to facilitate the dissolution process. Once homogeneous conditions are achieved, phase boundaries are determined either by lowering the temperature while keeping the pressure constant (Path 1) or by lowering the pressure while keeping the temperature constant (Path 2) which are illustrated in Figure 6.1. In experiments where temperature is lowered along Path 1, pressure is maintained constant by changing the position of a movable piston in the cell using a pressure generator to compensate for the volumetric changes that accompany changes in the temperature. From measurements of the temperature, pressure, and the transmitted light intensities (I_{tr}), graphs depicting the changes in the transmitted light intensity with temperature (along a constant pressure path, Path 1) or with pressure (along a constant temperature path , Path 2) are generated. The temperature or the pressure corresponding to the departure from the baseline for I_{tr} is then identified as the phase separation temperature or the phase separation pressure.

In the present study, the majority of experiments were conducted along constant pressure paths (Path 1) at different pressures to determine the fluid-solid (crystallization), or the sol-gel (gelation) phase boundaries. In systems that undergo crystallization the magnetic stirrer motion in the view cell remains free, while in systems that undergo gelation the stirrer gets stuck in the gel and stops turning. Once the phase-separated regions were entered, phase boundaries were again determined, but this time in the reverse direction by increasing the temperature (labeled as Path 1' in the figure). In the reverse direction, what is determined is either the melting of the crystals or the dissolution of the gel, i.e., the gel-sol transition.

The polymer samples were collected after gelation or crystallization. Along path 1, after phase separation and cooling to ambient temperature at constant pressure, the system was held for 24 hrs to mature the gel or the crystal while still maintaining the high pressure conditions. After this maturation time at ambient temperature, the cell was depressurized

and opened to collect the wet gel (at T_a and P_a in Figure 6.1). Along Path 2, after the L-L phase separation which leads to a polymer-lean and polymer rich phase, the cell was cooled to ambient temperature while allowing the pressure to decrease, without any further adjustment of the pressure. As before the system was held for an additional 24 hrs to mature the gel or the crystal at the ambient temperature and the prevailing (lowered) pressure. Then the cell was fully depressurized and opened at T_a and P_a. Samples were collected from both the upper (representing the polymer-lean phase) and the lower (representing the polymer-rich phase) layers of the cell cavity. The wet gels or the crystals thus collected were air-dried by exposing to open air flow in a hood for 72 hrs for natural evaporation of the solvent. These samples were further vacuum-dried (at 100 mtorr) for an additional 72 hrs for removal of the solvent due to low volatility of acetophenone.

6.2.3 Characterizations by XRD, FTIR and SEM

X-ray diffraction (XRD) patterns of vacuum-dried polymer samples were obtained with a Scintag XDS-2000 powder diffractometer operated at 45 kV and 40 mA using Cu Kα monochromatized radiation ($\lambda = 0.154178$ nm).

IR characterizations were carried out with an FTS 3100 (Digilab) FTIR spectrometer. The resolution was 2 cm^{-1} and 32 scans were co-added to obtain a spectrum for each sample. The vacuum-dried gels or crystals were mixed with KBr powder. The transmission spectra were obtained from these prepared KBr disks.

A Leo 1550 field emission scanning electron microscope (FESEM) was used to examine the morphology of the gels or crystals. The vacuum-dried gel samples were freeze-fractured after immersing in liquid nitrogen. A 15 nm layer of gold was coated on the samples using a Cressington 208 HR sputter coater to reduce electron charging effects. The morphological features of fractured cross-sectional surfaces were investigated.

6.3 Results and Discussions

6.3.1 Phase Diagrams

Figure 6.2 shows the actual changes in temperature, pressure, and transmitted light intensity (I_{tr}) with time during a constant pressure cooling experiment in 4.8 wt % sPS solution in pure acetophenone at the pressure of 29.5 MPa. The temperature dependence of I_{tr} is shown in the lower part of Figure 6.2. The plot shows two different stages reduction in I_{tr} during a cooling experiment. The first stage of decrease in I_{tr} starts to take place when temperature reaches 380 K (marked as T_1 in the figure). This is followed by a very sharp decrease in I_{tr} when temperature reaches 342 K (marked as T_2 in the figure).

The samples collected from the solution after cooling to room temperature shows, as will be discussed later, only one crystal structure, the δ form. This removes the possibility of the two stage change in I_{tr} being due the formation of different polymorphic structures of sPS, unless the form generated at T_1 is later transformed at T_2. A second possibility is a two-stage gelation process, for which there is literature evidence. By monitoring the changes in IR spectra during a cooling experiment with sPS solution in bromoform, De Rudder *et al.*[De Rudder *et al.* 2002] have reported a two-step change. They observed a small increase beginning at 333 K and a sharp increase at 295 K in the absorbance of the IR peak at 770 cm^{-1} which is related to the formation of 2_1 helix conformation. Based on additional evidence provided by H-NMR and rheological measurements, these authors proposed a two-step process for the gelation mechanism for sPS solutions in bromoform. The initial small increase in the IR absorbance was attributed to the transition of the coil to a single helix and the sharp increase at lower temperature was attributed to the aggregation of single helices into helix association units which eventually lead to the formation of the gel network. In sPS solution in acetophenone, similar to bromoform, it is plausible that the initial decrease in I_{tr} at T_1 arises from polymer chains undergoing a coil-to-helix transition and the sharp decrease in I_{tr} after T_2 arises from the association of

these helices. It should be noted that in reheating experiments in acetophenone only one sharp increase in I_{tr} is observed suggesting that the transition of the associated helices back to coils occurs in just one step. If cooled again the two-step reduction is once again displayed. Even though not explicitly shown, this is demonstrated in Figure 6.3 that shows the T_1 (coil-to-helix), T2 (association of helices and gelation) transitions during cooling and the dissolution (gel-sol transition) boundaries during heating determined in a 4.8 % sPS solution at different pressures. After carrying out the cooling experiment at a given pressure to determine T_1 and T_2, the system was reheated to homogeneous conditions and the gel-sol transition temperature was determined. Then the pressure was changed to a new value and the next cooling experiment was carried out, which were once again characterized by the T_1 and T_2 transitions. The phase boundaries shown in Figure 6.3 were determined at 6.9, 14.5, 22.0, 29.5, 37.0 and 44.5 MPa. The boundaries were found to shift to higher temperatures at higher pressures.

In the temperature range from 350 to 440K, additional experiments were carried out by reducing the pressure to determine if a liquid-liquid phase boundary existed. In these experiments no liquid-liquid phase separation boundary could be observed in solutions in pure acetophenone.

Observation of a two-step reduction in the transmitted light intensity in acetophenone differs from the behavior of sPS solutions in toluene that we reported in our previous study [Fang and Kiran 2008], where only one sharp decrease in I_{tr} was observed during cooling at a temperature closer to T_2. The coil to helix transition that occurs at higher temperatures in acetophenone was either not detectable in toluene by optical means, or delayed and occurs simultaneously with helix association, or does not take place in toluene in contrast to acetophenone.

Figure 6.4 shows the actual changes in temperature, pressure, and transmitted light intensity (I_{tr}) with time during a constant pressure cooling experiment in 4.9 wt % sPS solution in the acetophenone + CO_2 fluid mixture containing 25 wt % CO_2 at 29.5 MPa. Instead of the two-stage changes in I_{tr} observed in pure acetophenone, only one sharp decrease starting from 376 K is observed in this mixture which is close to T_1 in acetophenone. The transition from coil-to-helix and the transition of association of these helixes appear to occur together in the presence of CO_2.at a temperature closer to the coil-to-helix transition in acetophenone. Compared to acetophenone, the solvent quality is deceased with the presence of CO_2 in the fluid mixture. It is reasonable to think that the poorer solvent conditions accelerates the association of solvated sPS helixes, bringing closer the two transformations by shifting T_2 towards T_1.It is important to note that in toluene which is a better solvent for sPS the system undergoes gelation with one reduction in I_{tr} but at the lower temperature [Fang and Kiran 2008], that is at a temperature closer to T_2 rather than T_1.

Experiments were also carried out in a fluid mixture with higher CO_2 content. In solutions with 40 wt % CO_2, cooling leads to crystallization (leading to the β from as will be discussed later) instead of gelation. Figure 6.5 shows the phase boundaries for the 4.9 wt % polymer solution in acetophenone + CO_2 mixture solvents with 25 and 40 wt % CO_2. Open symbols show the gel dissolution (in 25 % CO_2 system) and crystal melting (in 40 % CO_2 system) temperatures. In contrast to pure acetophenone, these solutions in acetophenone + CO_2 mixtures also display liquid-liquid (L-L) phase separation upon pressure reduction. The L-L boundaries are also shown in the figure. Below the L-L boundary, the system is a two-phase system. Observation of the L-L demixing in acetophenone + CO_2 mixtures is an outcome of the decreased solvent quality compared to acetophenone, and the boundary shifts to higher pressures with increased CO_2 content. The liquid-liquid phase boundary in these solutions is a LCST-like boundary, that is, at a

fixed pressure, the system will phase separate with increasing temperature if this boundary is crossed. Experiments were also conducted in solutions with 50 wt % CO_2. However, complete miscibility in this solution could not be achieved for temperatures up to 448K and pressures up to 55 MPa.

Another difference in the phase boundaries in pure acetophenone and acetophenone + CO_2 mixtures is in pressure dependence of the phase separation temperature which is reflected by the slopes of the boundaries. The gelation (solution) and crystallization (melting) phase boundaries in acetophenone + CO_2 solutions have a relatively large negative slope, while the gelation(dissolution) boundaries in pure acetophenone has a positive slope. In CO_2 containing systems, increasing the pressure improves the solvent quality and lowers the transition temperatures, bringing them closer to the temperatures observed in pure acetophenone. Similar trends, even though not as large, were also observed in toluene vs toluene+ CO_2 systems [Fang and Kiran 2008].

6.3.2 Polymorphic Structures

Figure 6.6 shows the X-ray diffraction patterns of the sPS samples obtained after high pressure (44.5 MPa) gelation in pure acetophenone and acetophenone + CO_2 mixture with 25 % CO_2, and after crystallization (at 50 MPa) in acetophenone + CO_2 with 40 wt % CO_2. The presence of the diffraction peaks at $2\theta = 8.2°$, 10.8°, 18°, 21° and 29° for the samples generated from solution in pure acetophenone (curve a) and in acetophenone + CO_2 with 25 wt % CO_2 (curve b) indicates the existence of the δ crystal form in these samples[De Rosa *et al.* 1999]. However, the X-ray diffraction pattern changes dramatically for the sample generated from the solution with high level of CO_2. As shown in the figure (curve c), new peaks at $2\theta = 6.3°$, 12.5° and 13.8° appear which are characteristic of the β crystal form [De Rosa *et al.* 1992]. The disappearance of the characteristic peaks (at $2\theta = 8.2°$ and 10.8°) of δ crystal form indicates that the crystal

form changes from δ form to β form with increasing amount of CO_2 in the solution. A similar transition from the δ form to the β form was also observed in sPS samples generated in solutions in pure toluene and toluene + CO_2 with different levels of CO_2 [Fang and Kiran 2008]. The decreased solvent quality with CO_2 addition into the solutions promotes the formation of the β form, and decreases the stability of the polymer-solvent compound which otherwise would lead to the formation of the δ form.

The FTIR spectra in the range of 800-1400 cm^{-1} of the samples in Figure 6.6 are shown in Figure 6.7. The IR spectrum of the sample from pure acetophenone solution (the spectrum a) shows the strong absorption bands of the solvent at 1078, 927 cm^{-1} indicating that the sample still holds some solvent even after extensive vacuum drying [Gambi *et al.* 1980] (Acetophenone has a relatively high boiling point at 475 K). The characteristic peak of 2_1 helical confirmation at 934 cm^{-1} [Reynolds *et al.* 1989] appears as a shoulder peak. It is masked by the solvent peak at 927 cm^{-1}. For the sample generated from solution containing 25 wt % CO_2, the peaks associated with the solvent decrease dramatically, indicating the more efficient removal of acetophenone in the presence of CO_2 , and the band at 934 associated with the formation of 2_1 helical confirmation of the polymer chain becomes distinct. Despite the interference with the solvent peaks, the FTIR spectra of the samples generated in acetophenone or acetophenone + CO_2 with 25 wt % CO_2 show that only the δ form is present in these samples. The FTIR spectrum changes dramatically for the sample generated from the acetophenone + CO_2 mixture containing 40 wt % CO_2 with the appearance of the peaks at 1337 ,1222 and 911 cm^{-1} which are the characteristic peaks of the β crystal form (spectrum c) [Reynolds *et al.* 1989]. These results from FTIR spectra are in good agreement with XRD in showing the formation of the β crystal form in solutions with high CO_2 content.

It is worth noting that the two peaks at 1214 and 1050 cm^{-1} in spectra a and b in Figure

6.7 disappear in the spectrum (c) of the sample in the β crystal form. These peaks are known to be absent in the spectra of pure acetophenone [Gambi *et al.* 1980] solvent and in the δ crystal form generated in other solvents.[Daniel *et al.* 1996; Daniel *et al.* 1997; Fang and Kiran 2008] The intensity of these peaks show a significant increase with removal of the solvent (compare spectra a and b), which indicates that these peaks are not related to the free solvent molecules. The absence of these peaks in the samples that is in β crystal form shows that these bands are conformation sensitive. In the absence of further studies to elucidate their origin, these peaks appear to be related to the formation of the polymer-solvent compound between sPS and acetophenone, that is, the δ crystal form.

As shown in Figure 6.5, both solutions containing 25 wt % and 40 wt % CO_2 display a L-L phase boundary at the high temperature region. From these solutions, samples were also generated by crossing these L-L phase boundaries through a pressure reduction stage at a fixed temperature, and then cooling the system to ambient conditions (see Figure 6.1, path 2). When the L-L phase boundary is crossed, the solution phase separates into a polymer-rich and a polymer-lean phase. After the final cooling and depressurization, samples were collected from both the upper (representing the polymer –lean phase) and the lower layer (representing the polymer –rich phase) of the view cell.

The X-ray diffraction patterns of the samples collected from the polymer-rich phase generated in these solutions are shown in Figure 6.8. The diffraction pattern shown by the sample generated in solution containing 25 wt % CO_2 (curve a) displays the reflections located at $2\theta = 8.2°$, 10.8°, 18°, 24° and 29°, corresponding to the δ crystal form and also the reflections located at $2\theta = 6.3°$, 12.5° and 13.8°, corresponding to the β crystal form, indicating that the sample is a mixture of δ + β crystal forms. In contrast, the sample generated in the solution with 40 wt % CO_2 displays the reflections corresponding to only

the β crystal form (curve b). XRD measurements could not be carried out on samples from the polymer-lean phase due to very low polymer concentration in this phase and the difficulty of recovering sufficient amount of polymer to carry out the analyses. However, the amount of sample recovered permitted their characterization by FTIR.

The FTIR spectra of the samples from both the polymer-rich and the polymer-lean phases generated from the solutions with 25 wt % and 40 wt % CO_2 are shown in Figure 6.9. The spectrum of sample from the polymer-rich phase from 25 wt % CO_2 solution (curve a) displays the characteristic peak of the δ form at 934 cm^{-1} and the characteristic peaks of the β form at 1222 cm^{-1} and 911 cm^{-1}, indicating that this sample is a mixture of the δ + β forms as was also indicated by the XRD results. However, the spectrum of the polymer-lean phase sample from this solution (curve b) displays only the characteristic peak at 934 cm^{-1} corresponding to δ crystal form, the characteristic peaks of the β form being absent. The spectrum of the polymer-rich phase sample generated in solution containing 40 wt % CO_2 (curve c) only shows the characteristic peak associated with the β crystal form in agreement with the XRD results. The peaks related to the δ form are absent. Curve c in Figure 6.9 is the spectrum of the polymer-lean phase sample from the 40 % CO_2 solution. The appearance of the characteristic peaks corresponding to both the δ form at 934 cm^{-1} and to β form at 1222 cm^{-1} in the spectrum indicates this sample is a mixture of the δ + β forms. It is worth noting that the characteristic peak at 1337 cm^{-1} related to β form (seen in curve a, c and d) and the characteristic peak at 1214 cm^{-1} related to δ form (seen in curve a, b, and d) are also confirmation sensitive and the intensity of these peaks changes dramatically for different samples.

6.3.3 Morphology

Figure 6.10 shows the FESEM images of the samples generated in acetophenone (micrograph a) and in acetophenone + CO_2 mixtures with 25 wt % CO_2 (micrograph b)

and 40 wt % CO_2 (micrographs c and d) following the phase separation paths that involve cooling at constant pressure. The fracture surface of the sample generated from pure acetophenone solutions show a grainy morphology. The polymer is in the δ crystal form as indicated by the XRD and FTIR results. The δ crystal form of sPS usually manifests itself in fibrillar morphology [Daniel *et al.* 2005; Fang and Kiran 2008]. The absence of the fibrillar morphology may be due to the presence of somewhat large amount of resident solvent in the sample as was indicated also from the IR spectra., The sample from the solution containing 25 wt % CO_2 (micrograph b)) is also of the δ crystal form based on XRD and FTIR results and shows a clear fibrillar network with fiber diameters in the range of 20 nm. These SEM results further show that solvent removal is more effective in this CO_2 containing system. Carbon dioxide which alters the solvent quality, may act as a carrier of acetophenone, or as a plasticizer for the polymer that facilitates the diffusion of acetophenone through the polymer. A different morphology is displayed in the sample generated from acetophenone + CO_2 as shown in micrograph c. This is a sample in the β crystal form and displays a stacked-lamellar morphology. Micrograph d is an enlargement showing more clearly the lamellar morphology.

The micrographs of the two polymer-rich phase samples generated from solutions containing 25 and 40 wt % CO_2 by crossing the L-L boundary via pressure reduction are shown in the Figure 6.11. As shown in micrograph a, the sample generated from the 25 wt % CO_2 solution displays a fibrillar-looking network (expected from a δ crystal from) with however presence of lamellar edges (that would suggest presence of the β crystal form). The results from XRD and FTIR measurements had indeed indicated this sample to be a mixture of the δ + β crystal forms. The morphology of the polymer-rich phase generated in the solution with 40 wt % CO_2 shown in micrograph b is that of lamellar morphology that is typical of the β crystal form generated in this higher CO_2 content solution.

Experiments conducted with an acetophenone + CO2 mixture containing 50 wt % CO_2 did not lead to formation of complete dissolution of sPS at temperatures up to 448 K and pressures up to 55 MPa. The L-L phase boundary in this system was clearly above 55 MPa. This partially miscible system was held at 443 K and 51 MPa for 24 hrs. Phase information shown in Figure 6.5 for the 25 and 40 wt % CO_2 cases would indicate that at 443 K and 51 MPa, the 50 wt % CO_2 system would be below the corresponding L-L phase boundary. One may view this system as having been generated by lowering the pressure at 443 K from a high pressures (likely to be much higher than 55 MPa) that would be above the L-L boundary to generate a polymer-rich and a polymer –lean phase. Further cooling of this two-phase system and sampling of the polymer –rich and polymer lean-phases would therefore present another example in which morphology and crystal forms can be explored. The micrographs in Figure 6.12 show the FESEM results for the polymer-rich phase sample generated in this 50 wt % CO2 system. The micrographs are at different magnifications, namely at 50 ×, 200 ×, and 2,000 ×. At low magnification, a porous structure with pore size from 20 to over 300 um is displayed. The morphology is characteristic of a polymer foamed with supercritical CO_2 or with a solvent containing high level CO_2. The pores are not connected. A closer look at higher magnifications show that the dense polymer domain is actually a lamellar crystalline domain with similarity to the morphology of the polymer-rich phase sample (that is in the β crystal form) generated from the 40 wt % CO_2 solution. In the 50 wt % case however, there is less stacking of the lamellar structures. Even though not shown in the paper, the results of XRD and FTIR analyses show that the sample from the 50 % CO_2 solution is also β crystal form without presence of the δ form. The result also shows that the transition from the α crystal form of the initial polymer to the β form has taken place without the polymer being completely dissolved first in the solvent with 50 wt % CO_2. Recently, the solid-solid phase transition of sPS from the α form to the β form was reported by treatment in supercritical CO_2 +

acetone by Liao *et. al*. [Liao *et al.* 2007] They reported that higher treatment temperature and pressure promote the formation of the β and the addition of acetone into the supercritical CO_2 favors this transition. The present results show that such transformations are also occurring in acetophenone + CO_2 at high temperature/pressure conditions.

6.3.4 Influence of the Phase Separation Path on the Crystal Form

The results presented above show that the pressure, fluid composition and the phase separation path followed in gelation and crystallization processes in sPS solutions in acetophenone or acetophenone + CO_2 influence the outcome in terms of the morphology and the crystal form generated. A strong influence of these factors was also shown in our earlier publication for gelation and crystallization of sPS in toluene and toluene + CO_2 solutions where we provided a thermodynamic scheme that provides a mechanistic description of how one crystal form is preferred over the other. The thermodynamic phase diagrams are proposed based on the experimentally observed crystal forms as determined from XRD, FTIR and SEM observations, and the expected trends on how the phase boundaries are altered in going from good to poor solvents with inclusion of carbon dioxide in the solutions. Direct determination of phase boundaries using traditional calorimetric measurements by DSC as applied to solutions in organic solvents at ambient pressures is not amenable to these gelation and crystallization studies that are at high pressures and involve a supercritical fluid component. Nonetheless Figure 6.13 provides a reasonable qualitative picture for solutions of sPS in acetophenone and acetophenone + CO_2 mixtures.

In acetophenone, no L-L phase boundary was observed over the T/P range investigated in the present study. Direct cooling of 4.8 wt % polymer solution at a given pressure leads to gelation in which we have demonstrated that the polymer is in its δ crystal form. Thus the

region at temperatures below the gelation temperature (with T_f in Figure 6.13 being less then T_2 in Figure 6.3) in the low polymer concentration range is depicted as L + δ, corresponding to liquid solvent plus the polymer in its δ form. The higher polymer concentration range of the T-x diagram in acetophenone (Figure 6.13 a) is assumed to be similar to the behavior described in literature in good solvents at ambient pressure with the L + β region being observed at the higher temperatures above a certain polymer concentration, and the β + δ region observed at the lower temperatures.[Fang and Kiran 2008] As was shown in Figure 6.3, the effect of pressure on the gelation boundary in acetophenone is not very large, and the extension of the qualitative phase diagram to high pressures can be reasonably made. In good solvents the β crystal form is the stable form at high polymer concentrations.

Unlike acetophenone, in acetophenone + CO_2 mixtures, the solvent quality is reduced and an LCST-type liquid-liquid phase boundary is observed. This L-L two-phase region is included in Figures 6.13b and 13c. Due to the decreased solvent quality compared to pure acetophenone, when the CO_2 content is increased, the LCST moves further to lower temperatures as shown in Figure 6.13c. With decreased solvent quality, in the CO_2 containing solutions, the L+ β boundary is depicted as shifting to somewhat higher temperatures and the L+ δ shifts to lower temperatures, with L+ β boundary extending over the whole composition range in the system with the higher carbon dioxide content as in Figure 6.13c. In poor solvents, the β crystal form becomes the most stable form over the whole polymer concentration range and the δ form becomes a metastable region below the "L + β" region at low polymer concentrations. Indeed, as shown in the previous sections, cooling the polymer solution in acetophenone + CO_2 mixture containing 25 wt % CO_2 at constant pressure (from T_i to T_f) leads to gelation and the polymer assumes its δ crystal form. Whereas in acetophenone + CO_2 mixtures with 40 % CO_2, cooling from T_i to T_f leads to crystallization with only the β crystal form being observed, confirming that

the β form that is formed first in the cooling process remains as the stable form.

Comparison of the influence of CO_2 on the solvent strength of acetophenone with that of toluene displays subtle but important differences. In the absence of CO_2, the toluene is a better solvent for sPS than acetophenone as reflected by the somewhat lower gel dissolution or crystal melting temperatures in toluene [Fang and Kiran 2008]. As also noted earlier in toluene the early stage of phase separation (reflected by T_1 in Figure 6.3) is not observed. With addition of about 25 wt % CO_2 into the solution, the polymer sample generated in acetophenone + CO_2 mixture is in pure δ crystal form. Whereas the polymer samples generated from toluene + CO_2 solution with 28 wt % CO_2 was found to display a mixture of δ + β crystal forms. This difference indicates that the mixture of acetophenone + CO_2 (25 wt %) must have a higher solvent power for sPS than toluene + CO_2 (28 wt %) fluid mixture, suggesting that CO_2 addition at comparable levels decreases the solvent quality of toluene to a greater extent than that of acetophenone. This difference is most likely arising from the carbonyl group in the acetophenone molecules which provides a potential interaction site for CO_2 [Liu and Kiran 2007]. Indeed, an earlier study [Liu and Kiran 2007] has shown that, in ternary system of poly(ε-caprolactone) + acetone + CO_2, the degree interaction of CO_2 with the -C=O group in the polymer versus the solvent acetone alters the observed miscibility characteristics in the system. The association of CO_2 with the carbonyl group in acetophenone delays the occurrence of the decrease in the solvent power compared to toluene in which such interactions do not exist.

The consequences of crossing the L-L phase boundary first before gelation or crystallization takes place are illustrated in Figure 6.14. When the pressure is reduced (along Path 2 in Figure 6.1) solvent quality decreases, the L-L phase boundary shifts to lower temperatures, and the solution at T_i (point A in the figure) enters the L-L two-phase

region as illustrated in Figure 6.14a.. The solution undergoes phase separates into a polymer-lean (L_1) and phase-rich phase (L_2). Being at different polymer concentrations, each phase traverses different phase domains during further cooling to ambient conditions (i.e., T_f) leading to different crystal forms. For the solution containing 25 wt % CO_2, as discussed in the previous sections, the polymer lean phase leads to δ, but the polymer rich phase leads to a mixture of the β + δ crystal forms. Figure 6.14a is a phase diagram consistent with these observations. For the polymer-lean phase, upon cooling, the phase directly enters to the "L + δ" region where the δ crystal form should be only form generated. While for the polymer-rich phase located at high polymer concentration, upon the reduction of temperature, enters the "L + β" region first before entering into the metastable "L + δ" region. As a result, the competition of the formation of β and δ crystals leads a mixture of the β + δ crystal forms.

Figure 6.14b represents the system with an even higher CO_2 content where the solvent quality is further reduced, lowering the LCST to lower temperatures, and shifting the demixing pressures to higher pressures. Reducing the system pressure in such a system enlarges the two phase region further, and the solutions splits once again into a polymer-lean and polymer-rich phase, but this time with a polymer rich phase of higher polymer concentration than in Figure 6.14a. This figure describes the behavior in the acetophenone+ CO_2 mixture with 40wt % CO_2 in which we have shown that polymer lean phase leads to a mixture of β+ δ crystal forms, while polymer rich phase leads to the β crystal form. As shown in Figure 6.14b, after L-L phase separation, with further reduction of temperature the polymer lean phase enters first the L + β and then the L + δ region. The L + β region being narrow at low polymer concentrations, the distance crossed in the L + β region is short which limits the time for formation of the β crystal, and thus leads to the formation of a mixture of β + δ form. The polymer-rich phase (L_2) on the other hand traverses a longer distance in the L + β region and the competition of

the formation of the β and the δ forms leads only to the formation of the thermodynamically stable β form.

6.4 Conclusions

High pressure gelation and crystallization in solutions of sPS in acetophenone + CO_2 solutions depend on the carbon dioxide content of the mixture fluid. In pure acetone only a sol-gel phase boundary is observed. In solutions containing 25 wt % CO_2, both sol-gel and liquid-liquid phase separation boundaries were observed. In solutions with 40 wt % CO_2, fluid-solid (crystallization) and liquid-liquid phase separation are observed. The gel sample generated from pure acetophenone solutions shows only the δ crystal form. The samples collected after gelation in solutions with 25 wt % CO_2 display δ crystal form when phase boundary is crossed along a constant pressure cooling path. If liquid-liquid phase boundary is crossed first, polymer-rich phase leads to a mixture of δ + β crystal forms, while the polymer-lean phase leads to only the δ form. In solutions containing 40 wt % CO_2 constant pressure cooling leads to crystallization with β crystal form. Along a liquid-liquid phase separation path as the first step, polymer-rich phase leads to a lamellar morphology with β crystal structure, and the polymer-lean phase leads to a β + δ mixture crystal structure. The formation of the different crystal forms along different paths is understandable in terms of T-x phase diagrams that incorporate the influence of the solvent quality on the phase boundaries.

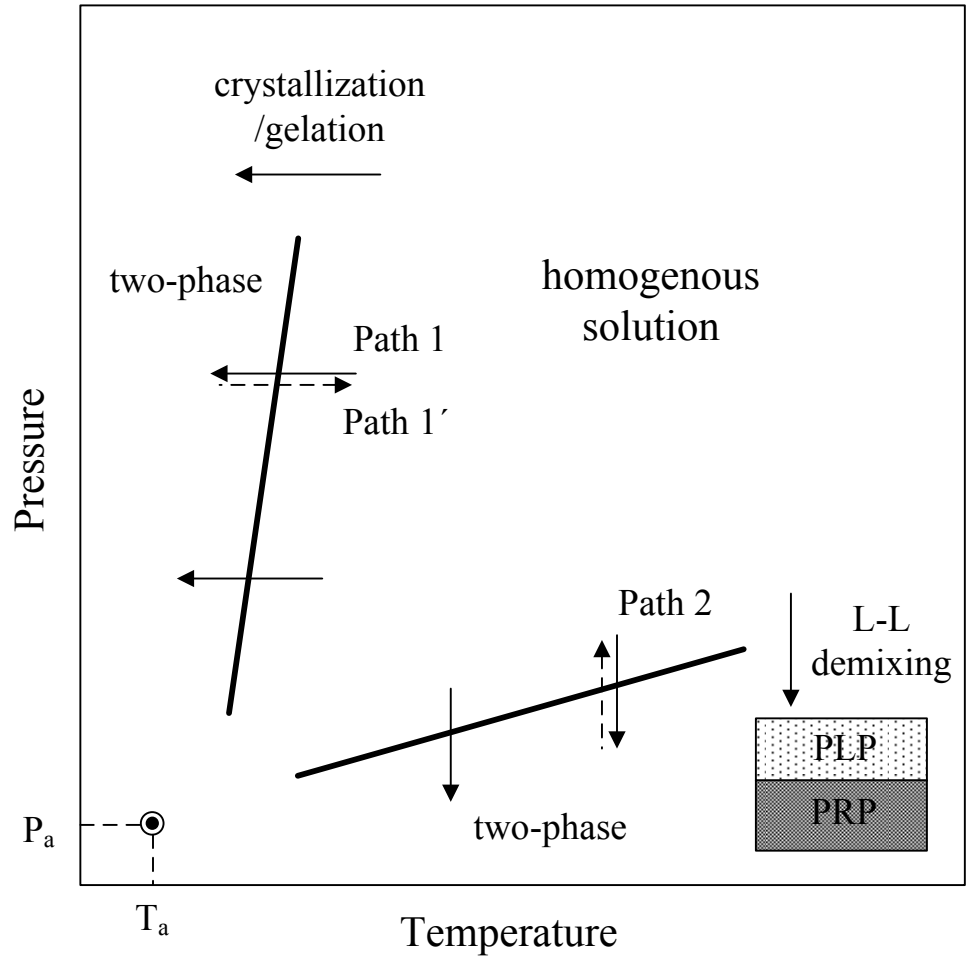

Figure 6.1 Schematic representation of different paths followed to determine the phase boundaries. Ta = ambient temperature; Pa = ambient pressure; PLP = polymer-lean phase; PRP = polymer-rich phase.

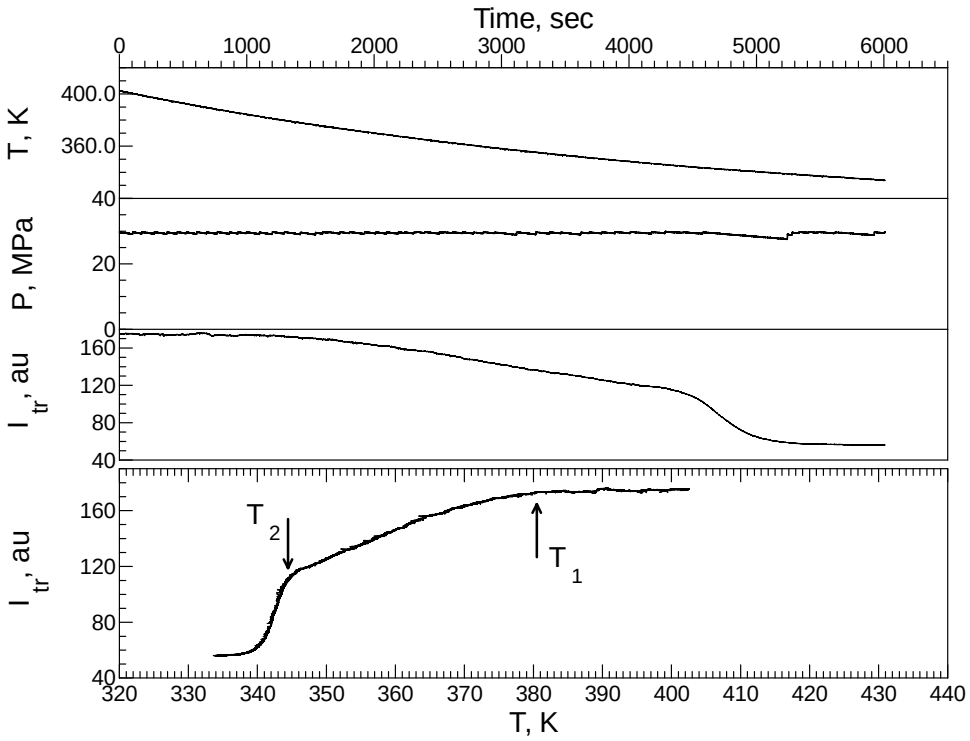

Figure 6.2 Variation of temperature T, pressure P, and transmitted light intensity Itr with time and Itr with temperature along the constant pressure cooling path in 4.8 wt % sPS solution in pure acetophenone at 29.5 MPa.

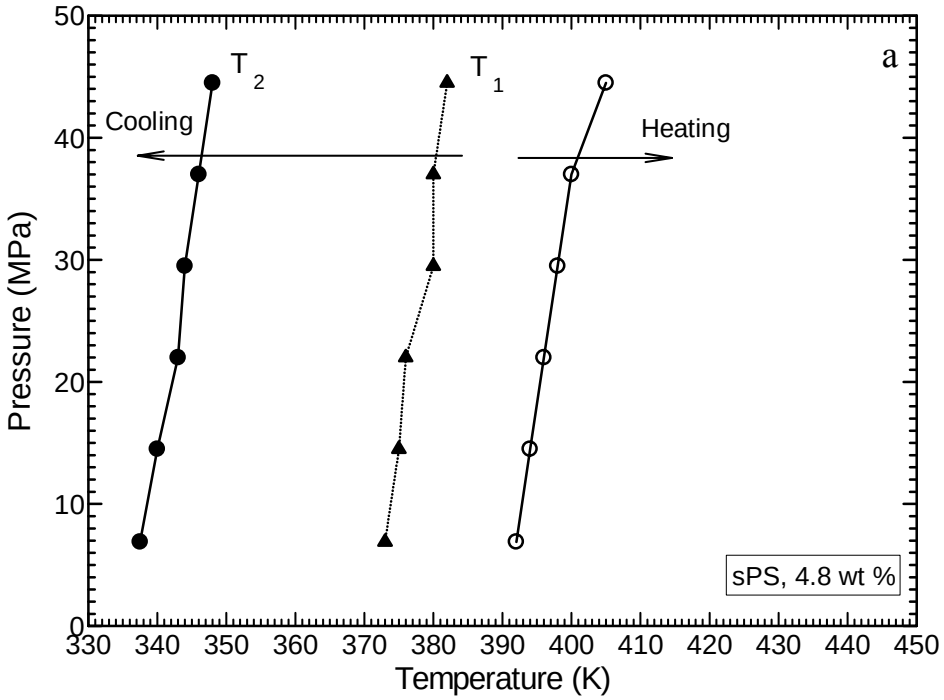

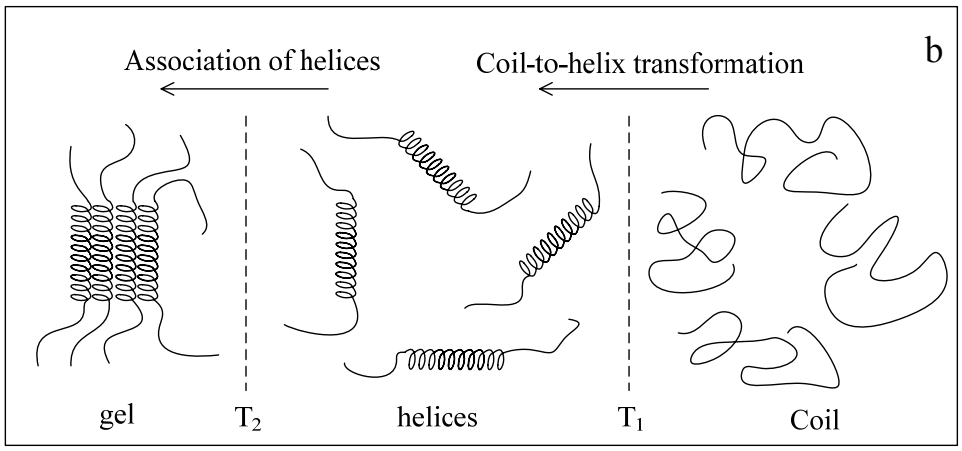

Figure 6.3 (a) The sol-gel phase boundaries for 4.8 wt % syndiotactic polystyrene solutions in pure acetophenone. Filled triangle symbols represent the T_1 upon cooling; Filled circle symbols represent the T_2 upon cooling and opened circle symbols represent the gel melting points upon heating. (b) Schematic representation of coil-to-helix transformation at T_1 and association of helices leading to gelation at T_2.

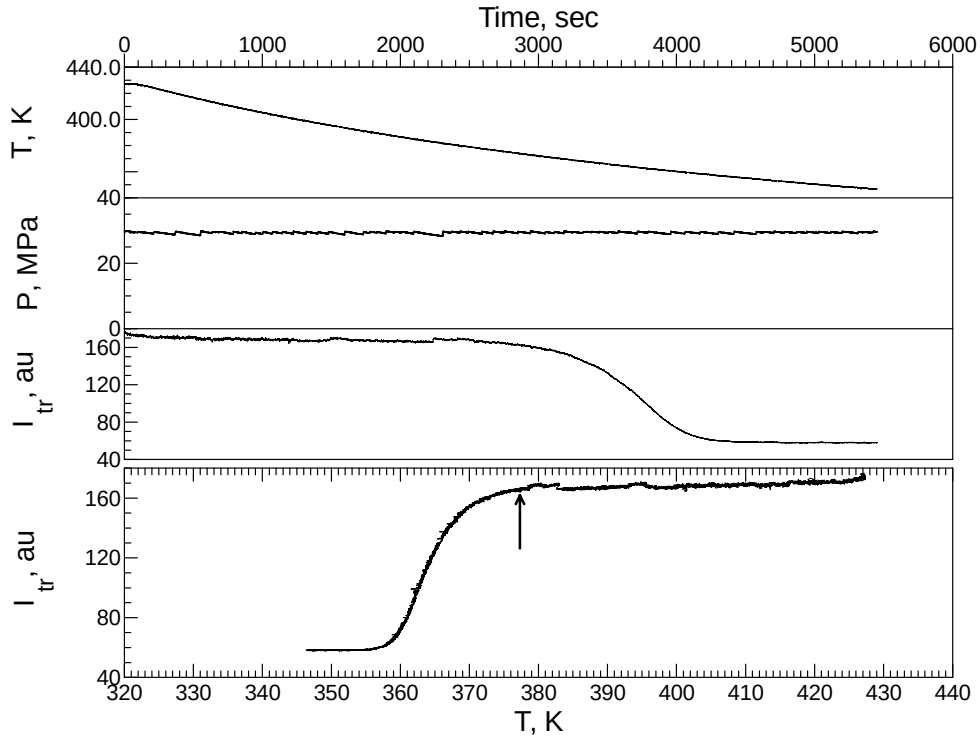

Figure 6.4 Variation of temperature T, pressure P, and transmitted light intensity Itr with time and Itr with temperature along the constant pressure cooling path in 4.9 wt % sPS solution in acetophenone (75) + CO_2 (25) at 29.5 MPa.

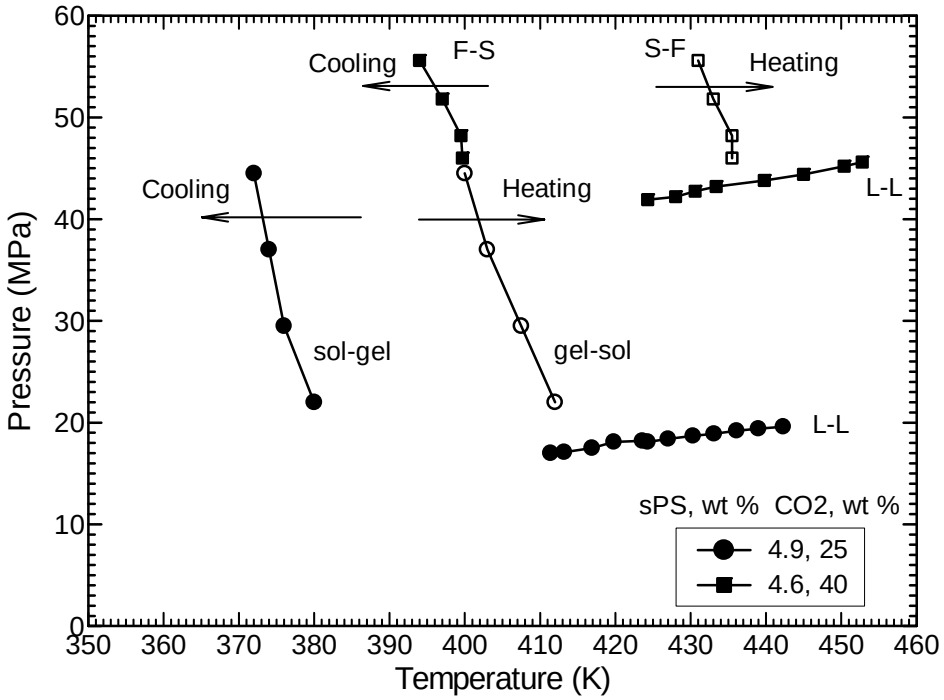

Figure 6.5 The sol-gel or fluid-solid and L-L phase boundaries for syndiotactic polystyrene solutions acetophenone + CO_2 mixture with 25 and 40 wt % CO_2 in the solvent mixture.

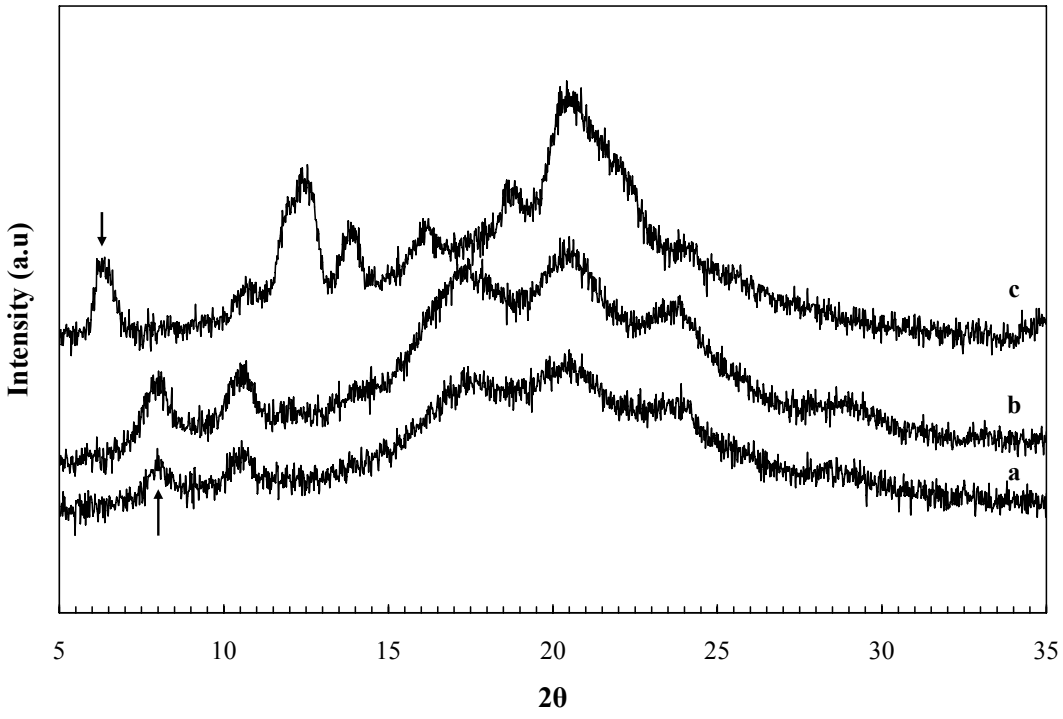

Figure 6.6 X-ray diffraction patterns in the 2θ range 5° - 35° for (a) sPS sample from 4.8 wt % pure acetophenone solution, (b) sPS sample from 4.9 wt % solution in the acetophenone + CO_2 mixture containing 25 wt % CO_2, and (c) sPS sample from 4.6 wt % solution in the acetophenone + CO_2 mixture containing 40 wt % CO_2. The samples are obtained from the constant pressure cooling path at 44.5 MPa for (a) and (b) and 50 MPa for (c).

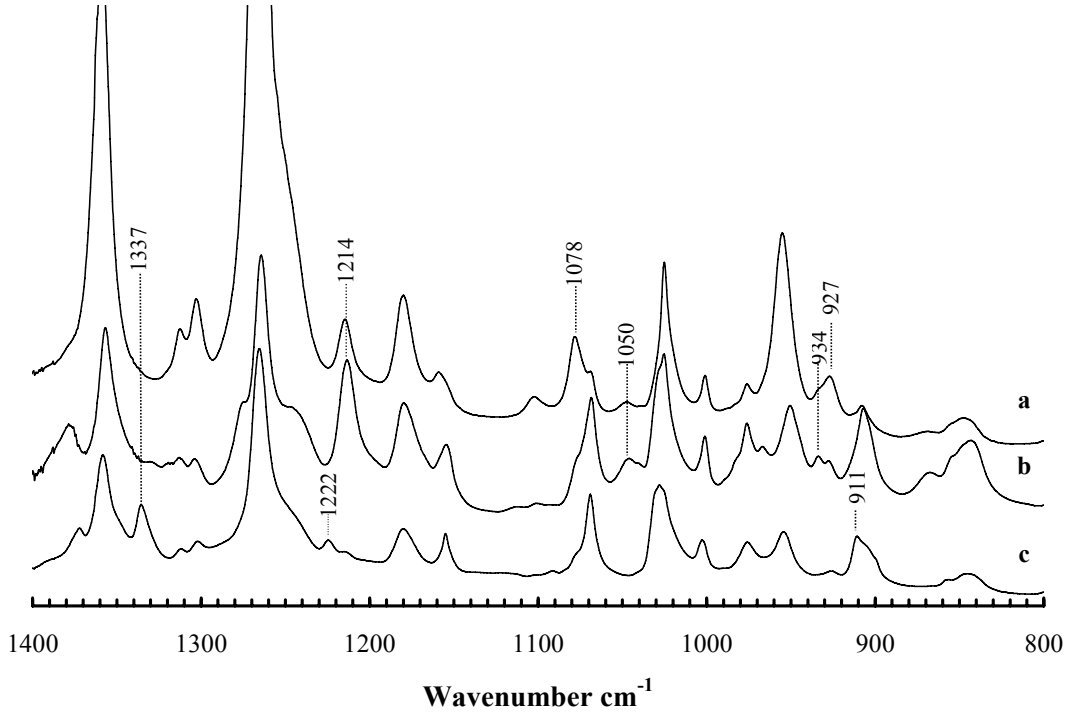

Figure 6.7 FTIR spectra of sPS samples: (a) from 4.8 wt % pure acetophenone solution, (b) from 4.9 wt % solution in the acetophenone + CO_2 mixture containing 25 wt % CO_2, and (c) from 4.6 wt % solution in the acetophenone + CO_2 mixture containing 40 wt % CO_2.

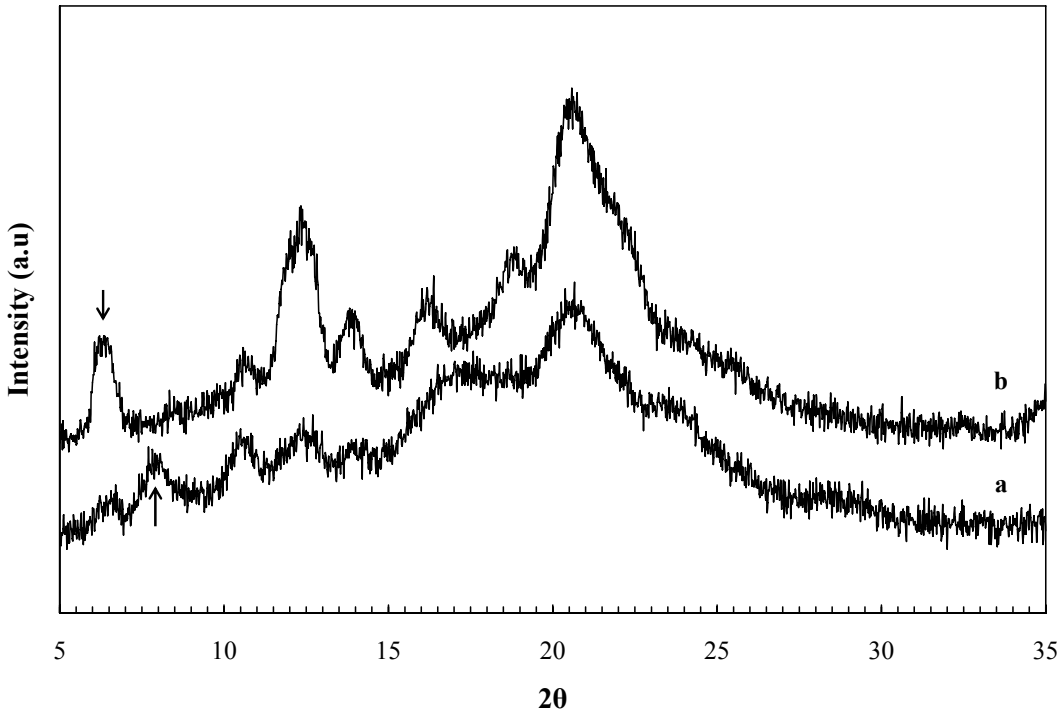

Figure 6.8 X-ray diffraction patterns in the 2θ range 5° - 35° for (a) the polymer-rich phase sample of sPS from 4.9 wt % solution in acetophenone (75) + CO_2 (25), and (b) the polymer-rich phase sample of sPS from 4.6 wt % solution in acetophenone (60) + CO_2 (40).

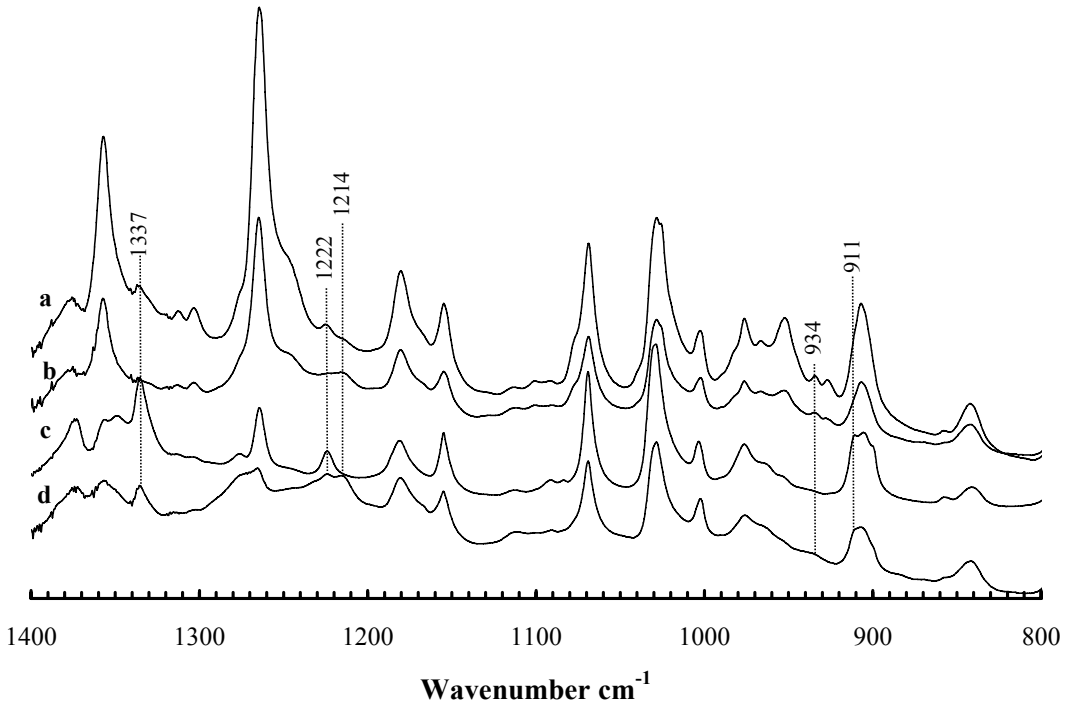

Figure 6.9 FTIR spectra of sPS samples: (a) from polymer-rich phase of 4.9 wt % solution in acetophenone (75) + CO_2 (25), (b) from polymer-lean phase of 4.9 wt % solution in acetophenone (75) + CO_2 (25), (c) from polymer-rich phase of 4.6 wt % solution in acetophenone (60) + CO_2 (40), and (d) from polymer-lean phase of 4.6 wt % solution in acetophenone (60) + CO_2 (40).

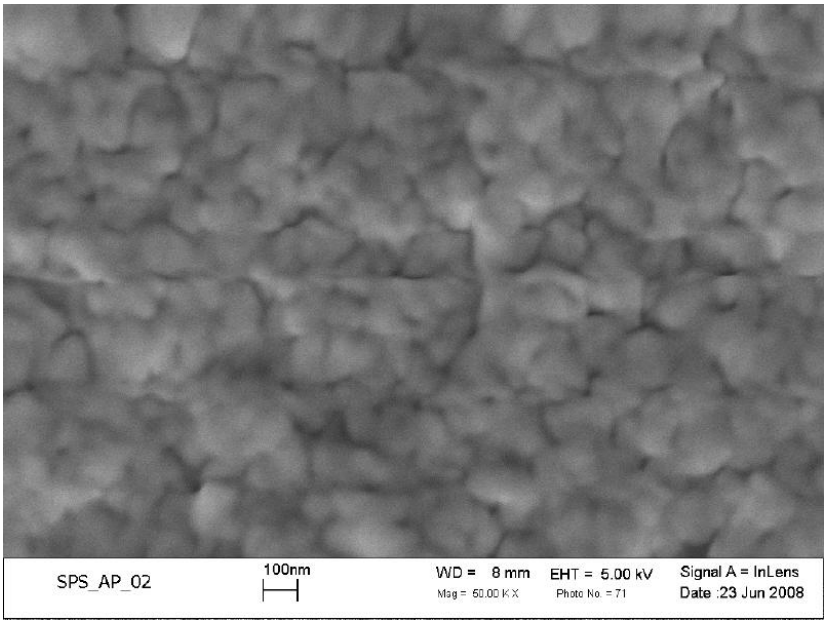
SPS_AP_02
100nm
WD = 8 mm
Mag = 50.00 K X
EHT = 5.00 kV
Photo No. = 71
Signal A = InLens
Date :23 Jun 2008

(a)

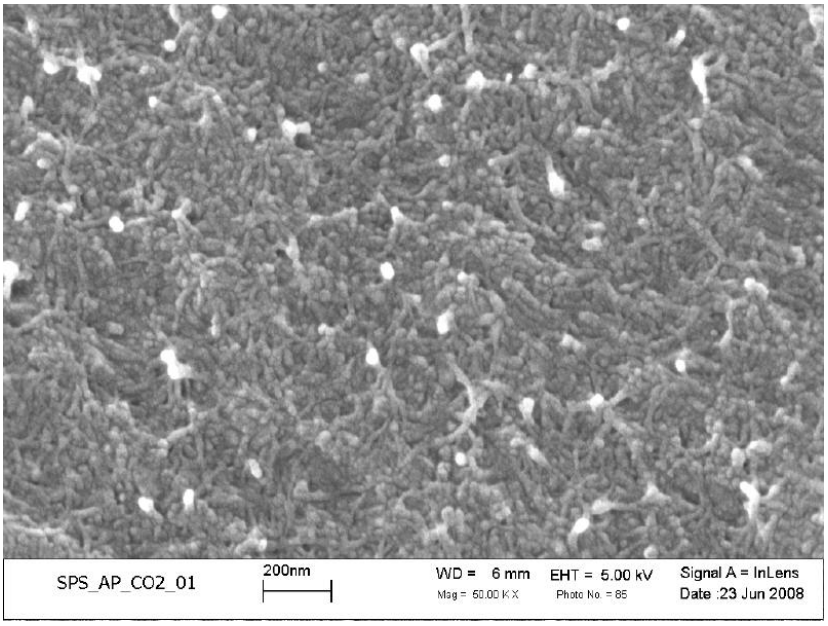
SPS_AP_CO2_01
200nm
WD = 6 mm
Mag = 50.00 K X
EHT = 5.00 kV
Photo No. = 85
Signal A = InLens
Date :23 Jun 2008

(b)

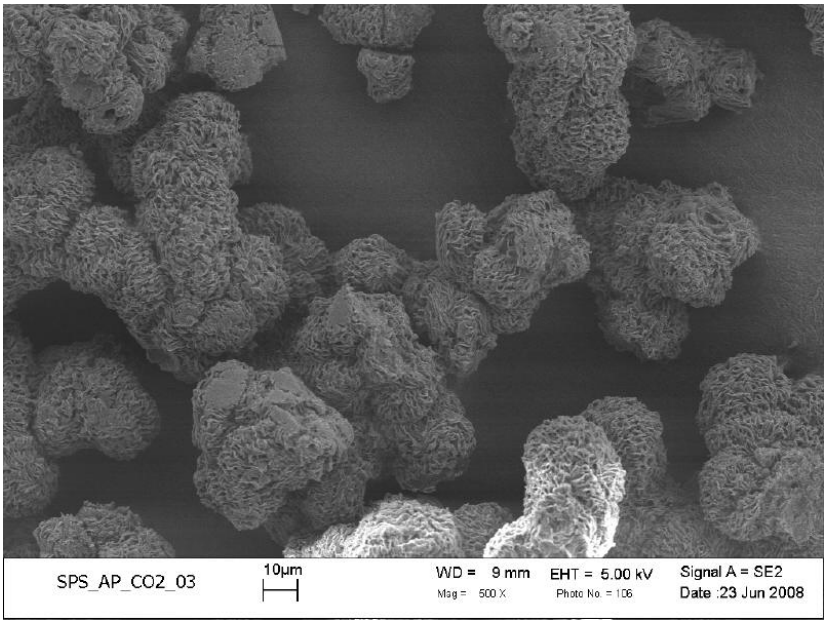

(c)

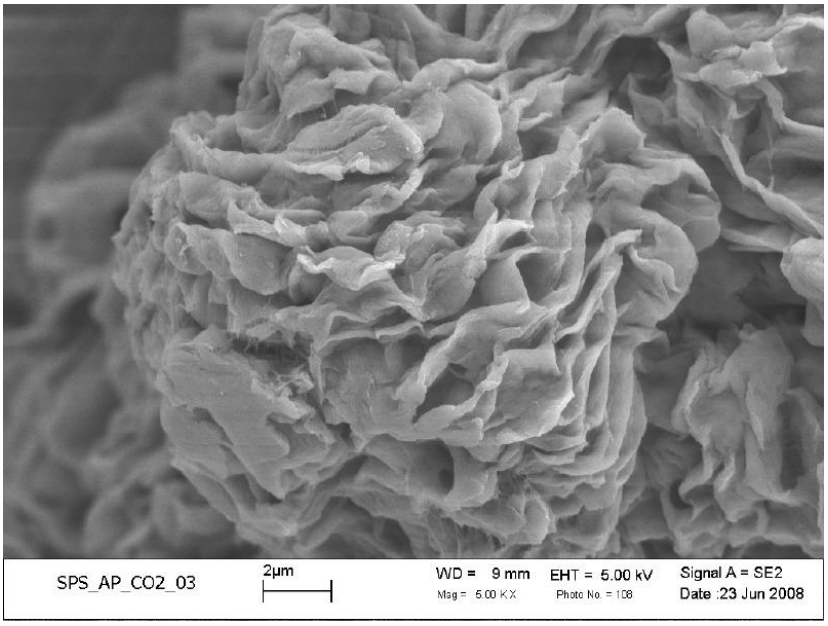

(d)

Figure 6.10 FESEM micrographs of sPS gel samples (a) from pure acetophenone solution, (b) from solution in the acetophenone + CO_2 mixture containing 25 wt % CO_2, and (c) from solution in the acetophenone + CO_2 mixture containing 40 wt % CO_2; (d) detailed morphology of the particles in (c). The scale bars and magnifications are: (a) 100 nm, 50,000 ×; (b) 200 nm, 50,000 ×; (c) 10 µm, 500 ×; and (d) 2 µm, 5,000 ×.

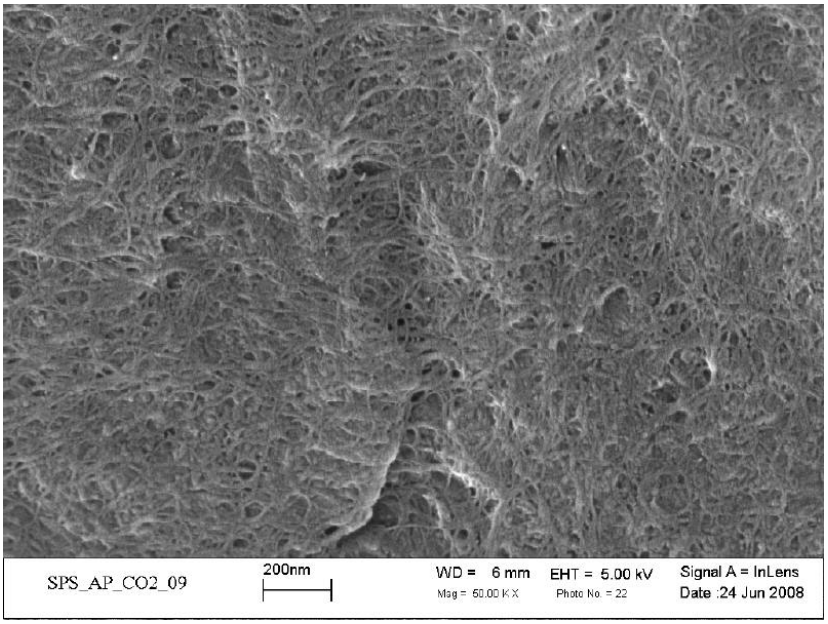

(a)

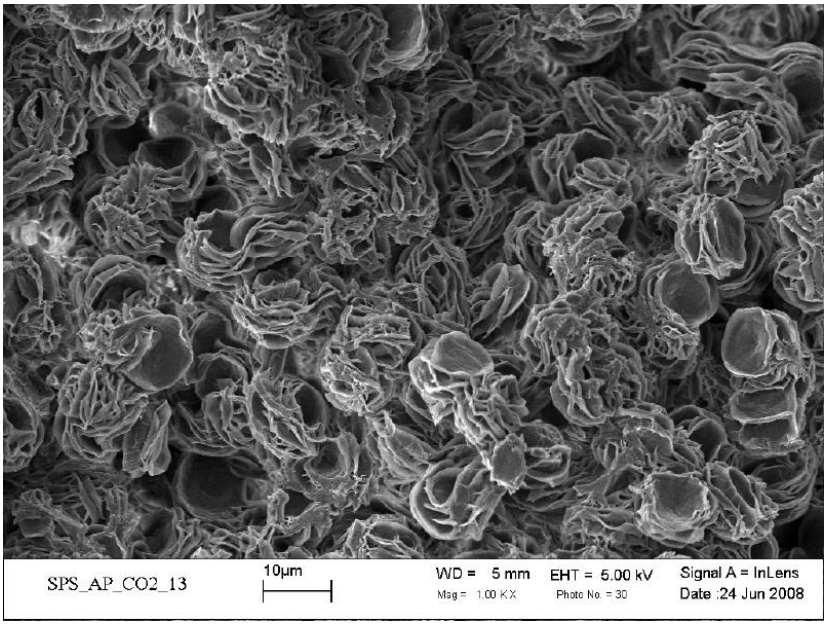

(b)

Figure 6.11 FESEM micrographs of (a) the polymer-rich phase sample of sPS from 4.9 wt % solution in acetophenone (75) + CO_2 (25), and (b) the polymer-rich phase sample of sPS from 4.6 wt % solution in acetophenone (60) + CO_2 (40). The scale bars and magnifications are: (a) 200 nm, 50,000 × and (b) 10 μm, 1,000 ×.

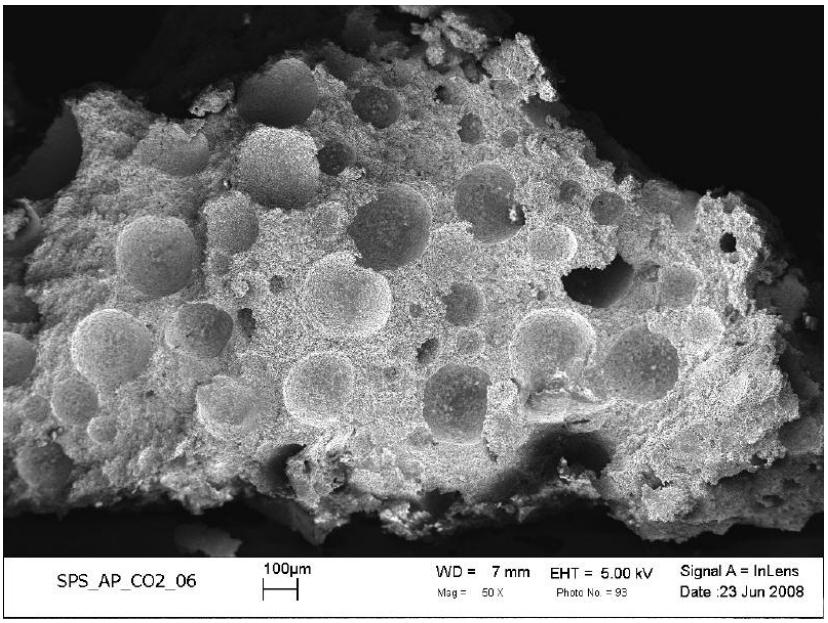
SPS_AP_CO2_06
100µm
WD = 7 mm
Mag = 50 X
EHT = 5.00 kV
Photo No. = 93
Signal A = InLens
Date :23 Jun 2008

(a)

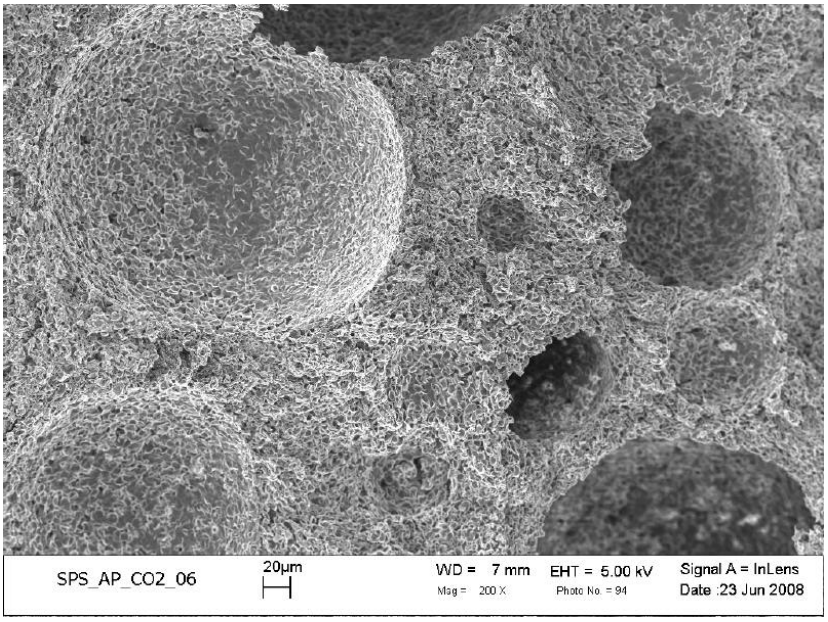
SPS_AP_CO2_06
20µm
WD = 7 mm
Mag = 200 X
EHT = 5.00 kV
Photo No. = 94
Signal A = InLens
Date :23 Jun 2008

(b)

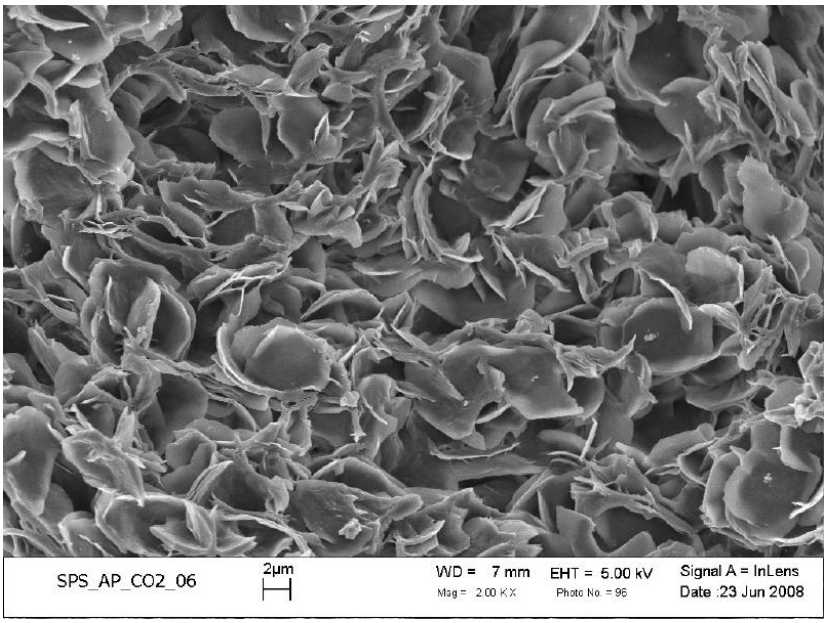

(c)

Figure 6.12 FESEM micrographs of sPS sample after treated in acetophenone (50) + CO_2 (50) at 443 K and 51 MPa, (a) × 50; (b) × 200; (c) × 2K. The scale bars are 100 μm in (a), 20 μm in (b) and 2 μm in (c) respectively.

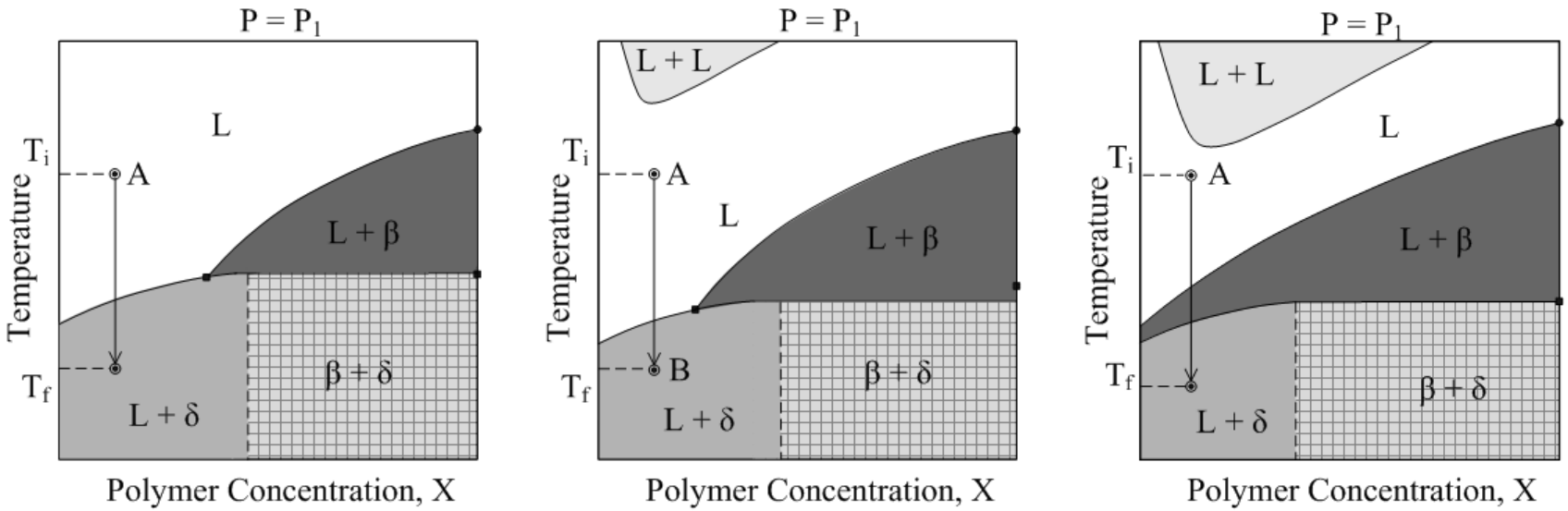

Figure 6.13 Schematic representation of the T-x phase diagrams for sPS in pure acetophenone and acetophenone + CO_2 at high pressures and the consequence of constant pressure cooling path followed on the eventual crystalline forms that are generated in (a) pure acetophenone; (b) acetophenone + CO_2 (less amount) and (c) acetophenone + CO_2 (high amount). L: liquid phase; β: β crystal form of sPS; δ: δ crystal form; P: pressure.

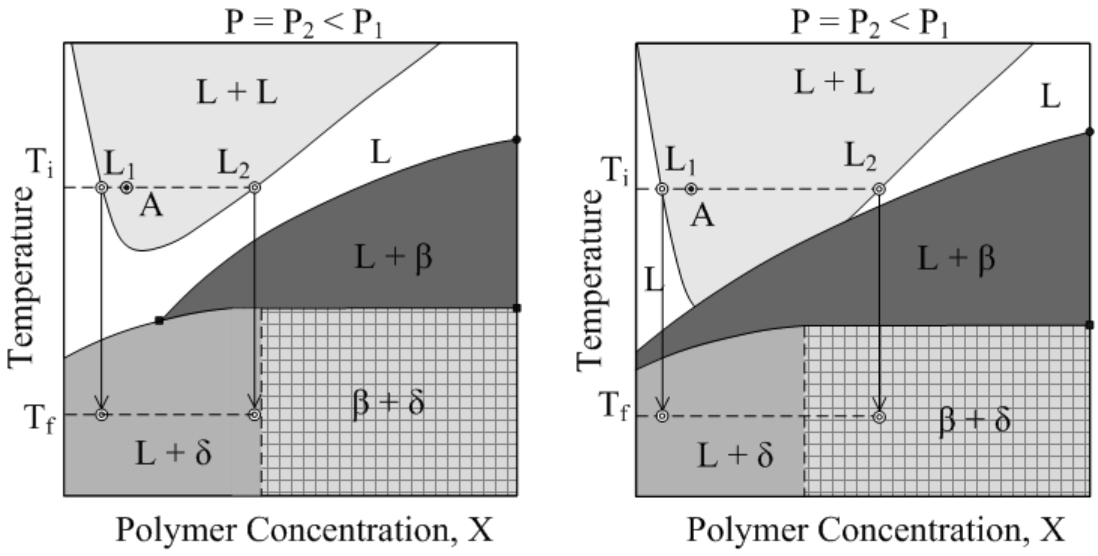

Figure 6.14 Schematic representation of the T-x phase diagrams for sPS in acetophenone + CO_2 at high pressures and the consequence of constant temperature pressure quench path followed on the eventual crystalline forms that are generated in (a) acetophenone + CO_2 (less amount) and (b) acetophenone + CO_2 (high amount). L_1, and L_2: the polymer-lean and the polymer-rich phases. Other symbols are as in Figure 6.13.

Chapter 7

Effect of Carbon Dioxide on Thermoreversible Gelation in Polymeric Solutions

Carbon dioxide influences on the thermoreversible gelation of poly(4-methyl-1-pentene) (P4MP1) solution in n-pentane and syndiotactic polystyrene (sPS) in toluene and acetophenone in two different ways as presented in the early chapters. In P4MP1 solutions in n-pentane, with addition of large amounts of CO_2, the solution was observed to form a gel upon cooling instead of undergoing crystallization. However, with addition of large amounts of CO_2, sPS solutions in toluene were observed to undergo crystallization or form a weak gel by localized crystallization, instead of the strong elastic gel formed in sPS solutions in pure toluene. Carbon dioxide is thus observed to induce the gelation in P4MP1 in n-pentane solutions, while weaken or completely destroy the gelation of sPS in toluene.

In this chapter, the different mechanisms of gelation are proposed that are based on the information of the phase diagrams, crystalline forms that are generated and gel structures observed for these systems. Before presenting the specific mechanism of gelation in these systems, a broad introduction is given on the thermoreversible gels along with a literature review on thermoreversible gelation on synthetic polymer system.

7.1 Introduction

A clear definition of a gel should first be given. However, the definition of a gel is still a matter of debate [Almdal *et al.* 1993], and there is no clear-cut, accurate definition. The famous comment made by Jordan Lloyd in 1926 [Lloyd 1926] that is “The colloidal state, the gel, is one which is easier to recognize than define” still holds. There may exist a continuum from the true gel state to the true liquid state. What is difficulty is where to put

the borderline. Nonetheless, a widely accepted topological definition exists which describes a gel as a "three dimensional network constituted of solid connectedness and mainly swollen by a solvent" [Guenet 1992].

Flory [Flory 1974] subdivided the gel networks into four different types according to their structures:

Type I:	Well-ordered lamellar structures.
Type II:	Covalent polymer networks; completed disordered.
Type III:	Polymer networks formed through physical aggregation; with region of local order.
Type IV:	Particulate, disordered structures.

The soap gels, phospholipids and clays are the examples of the Type I gel. The long-range electrostatic, van der Waals forces as well as dipolar interactions play important role in this type gel formation. The network in the Type II gels is provided by crosslinking of a high molecular weight polymer or by crosslinking reactions in polymerization. Many thermoreversible gels in polymers and biopolymers belong to Type III and the networks are formed by physical interactions, which include crystallization, helix formation, and complex formation. The Type IV of gels includes V_2O_5 gels and globular and fibrillar protein gels.

The gels formed in polymer (as well as biopolymer) are mainly fallen into the Type II (chemical gel) and Type III (physical gel) according to Flory's classification. The processes leading to formation of polymer gels through chemical reactions or physical interactions are summarized in Figure 7.1. In chemical gels, the connectedness usually builds up through covalent bonds by polymerization or the later chemical treatment of polymers. The covalent bonds are very strong links so that these gels are 'heat-irreversible'. Heating this

type of gel eventually cause the breaking up of the covalent bonds, which entails irreversible degradation of the gel and impedes the re-formation of the similar system. In physical gel, the junctions are formed by physical processes in which the energy involved is of the order of κT so that these gels are 'heat-reversible'[Guenet 1992]. Heating this type of gel causes the breaking up of the junctions inside of the gels which can be re-formed by a later cooling process. Therefore, this type of gels is also called "thermoreversible gels".

A common example of physical gelation is the formation of gelatin gels produced by boiling animal bonds in water and cooling the solution. Indeed, early studies on physical gels were focused on the biopolymer which can be extracted from nature. Some excellent reviews on the physical gelation in biopolymers are accessible in the literature [Clark and Ross-Murphy 1987; Guenet 1992; te Nijenhuis 1997]. Recent discovery of gelation in synthetic polymers in organic solvents in the absence of the hydrogen bonding which is the key interaction in the gels of biopolymer in water, has opened up new research field. And the reminder of this chapter is devoted only to the thermoreversible gelation in synthetic polymers that arise from the physical processes depicted in Figure 7.1.

7.2 Literature Review on Gelation in Synthetic Polymers

7.2.1 Liquid-Liquid Phase Separation

The final stable product of the liquid-liquid phase separation is a system of two fluid layers. Obviously, the final stage of liquid-liquid phase separation can not lead to form a gel structure. It is important that, in order to form a gel induced via phase separation, the development of such a stable two layer fluid-stage has to be prevented. Hence, the phase separation has to be arrested at an appropriate stage so that the connectedness can be established throughout the whole system. There are two types of processes by which this can be achieved: vitrification and crystallization, which can arrest phase separation at a stage where the conditions for gel formation can be fulfilled.

7.2.1.1 Combination of Liquid-Liquid Phase Separation and Vitrification

Figure 7.2 shows the schematic phase diagram of polymer (amorphous) solution with UCST type phase boundary and the glass transition temperature depression curve, which is started from T_g of the pure polymer and depressed by addition of the solvent. As shown in Figure 7.2, the binodal and T_g curves intersect each other at C_2. This intersection point is called as "Berghmans Point" [Arnauts and Berghmans 1987] and marked as 'BP' in the figure. The LCST type phase separation in polymer solution, which is induced by heating the polymer solution, seldom leads to form a gel structure.

Consider the situation, as shown in Figure 7.2, where the temperature is lowered from Point A located in the homogenous one-phase region. Upon cooling, the phase separation takes place as soon as the temperature reaches the L-L phase boundary and two liquid phases begin to develop. When point B is reached, the two phases will develop: B_1, polymer lean phase and B_2, the polymer rich phase. In principle, over time, two distinct layers in equilibrium representing the two phases will be formed. The ratio of the two phases is determined by the level rule. With further decrease in temperature, the viscosity of polymer rich phase increases due to the increasing polymer concentration in polymer rich phase. Eventually, the temperature becomes equal to T_g of polymer-rich phase and polymer chains in this phase are solidified. As shown in Figure 7.2, for the deeper temperature quench, the temperature is lowered to point C and the two phases represented as C_1 (polymer-lean phase) and C_2 (polymer-rich phase) are formed. At point C_2, where the binodal and glass temperature curves intersect, the polymer rich phase is in the glassy state and the development of two distinct liquid layers is prevented. And a dispersion of polymer-rich microscopic solidified droplets may develop in the sea of polymer-lean liquid phase. In some cases, parts of polymer chains that are in polymer-lean phase also form part of polymer-rich droplets and thus form the connection between these droplets. Then, a network structure is formed, in which the polymer-rich droplets act as the anchor points for

the whole system. The schematic representation of the type of structure that develops is shown in Figure 7.3(a). Actually, the final gel morphology developed from this mechanism is determined by the initial polymer concentration of polymer solution which, in turn, defines the ratio of polymer-rich phase and polymer-lean phase according to early mentioned level rule. For the low polymer concentration, the vitrified polymer-rich phase is in the form of small droplets inside of polymer-lean phase. For high polymer concentration (close to point C_2 in Figure 7.2, but not higher than that of point C_2), the polymer-lean phase forms the liquid droplets in vitrified polymer-rich matrix, as shown in Figure 7.3(b). For the intermediate polymer concentration, which is close to the critical point of polymer solution where the binodal and spinodal curves merge together, a bicontinuous interpenetrating network arises as a consequence of spinodal decomposition and the development of late stage of spinodal decomposition is prevented due to the vetrified polymer rich phase. The type of the structure is represented as Figure 7.3(c).

This mechanism describes the thermoreversible gelation of atactic polystyrene (aPS). The gelation behavior of solutions of aPS has been the subject of many studies [Wellinghoff *et al.* 1979; Tan *et al.* 1983; Boyer *et al.* 1985; Francois *et al.* 1986; Klein and Guenet 1989; Guenet and Klein 1990; Xie *et al.* 1990; Xie *et al.* 1993; Chen *et al.* 1995; Xie *et al.* 1998; Bui and Berry 2007]. Although the origin of gel is still in dispute, nowadays it is usually assumed that the mechanism of gel formation is a consequence of phase separation. Wellingoff *et al.* [Wellinghoff *et al.* 1979] obtained clear gels in 1 % solutions of aPS in carbon disulfide by cooling the solutions to -94 °C. Both gel formation and gel melting temperatures increased with increasing polymer concentration. In contract to gelation of a semi-crystalline polymer, such as poly(vinyl chloride), the gelation of aPS solutions is not induced by crystallization. Wellinghoff *et al.*[Wellinghoff *et al.* 1979] also reported that no endothermic or exothermic peaks were observed by high-sensitivity DSC measurement and no significant changes in infrared spectra of aPS solution in carbon disulfide were detected

upon cooling to gelation. These authors supposed that a fine dispersion of polymer rich regions developed upon quenching into the two-phase region and the relatively concentrated polymer phase is in solidified glass state which provides the connectedness for the network. The gelation of aPS is found to be hindered in good solvent and encouraged in poor solvents like as carbon disulfide. Berghmans *et al.* [Arnauts and Berghmans 1987; Van den Broecke and Berghmans 1990] show that the phase separation plays a dominant role in gelation behavior of amorphous atactic polystyrene. The gel structures of these aPS gels corresponding to the structures predicted in Figure 7.3 were experimentally obtained by Keller and co-workers [Hikmet *et al.* 1988; Callister *et al.* 1990]. Both the experimental diagram and the gel structures formed from different polymer concentration region in system of aPS/*trans*-decalin reported by Arnauts *et al.*[Arnauts *et al.* 1993] also support the mechanism proposed in Figure 7.2 and Figure 7.3.

It is worth to mention here that there is another view for the gelation of aPS solution in carbon disulfide offered by Guenet and co-workers[Francois *et al.* 1986; Gan *et al.* 1986; Francois *et al.* 1988; Guenet and Klein 1990]. These authors suggested that the gelation probably arises from the formation of polymer-solvent compound. Francosi *et al.*[Francois *et al.* 1988] on the basis of experiments carried out with isotactic samples suggested that the gelation of aPS solution may arise from the syndiotactic sequence in the atactic chain. On this point, the gelation of syndiotactic polystyrene is of prime interest and can provide further insight into the gelation mechanism.

7.2.1.2 Combination of Liquid-Liquid Phase Separation and Crystallization

Some polymers consist of molecules with sufficient regularity in the chain, so that these polymers can crystallize. Depending on the solvent and conditions, these semi-crystalline polymers solution can also form thermoreversible gels. There are usually two ways to lead to the gelation depending on solvent quality: via liquid-liquid phase separation in a poor

solvent or via crystallization in a good solvent. Figure 7.4 shows the two phase diagram with fluid-solid (crystallization) and liquid-liquid phase boundaries. In a good solvent, the fluid-solid phase boundary is far above the possible liquid-liquid two-phase region and the gelation for these systems may directly arise from the crystallization. In a poor solvent, the phase separation temperature and crystallization must be in same region and the fluid-solid phase boundary may intersect with the liquid-liquid phase boundary. In this case, beside the crystallization, the liquid-liquid phase separation also plays an important role in gelation. The section below focuses on the formation of gelation involving the combination of liquid-liquid phase separation and crystallization. The gelation arising only from crystallization will be discussed a later section.

A more detailed phase diagram of the interference between fluid-solid boundary and liquid-liquid phase boundary is shown in Figure 7.5, where the fluid-solid curve intersects with binodal curve. Consider the situation where solution is cooled from Point A. the liquid-liquid phase separation takes place right after entering the two phase region. Upon continuous cooling to Point B, the solution will develop into two phase B_1, polymer-lean phase and B_2, phase-rich phase. An invariant situation is reached at temperature T_i, where a three-phase equilibrium exists and liquid-liquid phase separation leads to crystallization of the polymer. This results in a solid polymer phase and a dilute polymer-lean solution. It has to be emphasized that this is the case when the real thermodynamic equilibrium is reached. In some cases, the development of large crystalline solid polymer phase is prevented and the micro-crystals may act as the connectedness in the system and leads to the formation of thermoreversible gelation.

The effect of kinetics is another important aspect in gelation. Liquid-liquid demixing processes generally start and proceed rapidly in polymer solution even though in small temperature quench. However, in many polymers, high supercooling is needed for

crystallization. Therefore, it is possible that the liquid-liquid phase separated region is reached before crystallization can take place even when the binodal curve is below the crystallization curve. The liquid-liquid demixing can precede crystallization even when the crystallization is favored thermodynamically. Thus, the distance between the crystallization curve and liquid-liquid demixing curve is very important in determining the formation of the final gel structure.

These phenomena involving the phase separation and crystallization have been studied in detail by Llody and co-workers [Lloyd *et al.* 1990; Kim and Lloyd 1991; Lloyd *et al.* 1991; Laxminarayan *et al.* 1994] for solutions of semi-crystalline polymers, such as polypropylene, polyvinylidene fluoride, polychlorotrifluoroethylene and poly(4-methyl-1-pentene). Cho *et al.* [Cho *et al.* 1993] studied the thermoreversible gelation of polyvinylidene fluoride in γ-butyrolactone. They concluded that the gelation in high polymer concentration region arises directly from crystallization, while for low polymer concentration range, liquid-liquid phase separation plays an important role in formation of the thermoreversible gel.

7.2.2 Crystallization

Figure 7.6 represents the crystallization of a polymer from solution. Depending on the initial polymer concentration, the crystallization of polymers from solution can lead to different morphologies: particles, spherulites or even interconnected networks. Many factors influence the crystallization of polymers from solution. The polymer concentration of solution is a particular important parameter. Crystallization of the polymer from the solution with low polymer concentration usually results in the formation of chain folded lamellae and the crystals appear as suspended particles giving rise to a turbid suspension. In some cases, however, these crystals connected by polymer chains can act as junctions and, hence, lead to the formation of gel. At higher polymer concentrations, suspensions of

supramolecular architectures of these lamellae are obtained. The morphology is frequently spherulites or axialites. At sufficiently high concentrations, interpenetrating and interlocking of these lamellae can form and give rise to the formation of the stiff brittle crystalline gels. The formation of this kind of gel can be promoted by stirring the solution or introducing flow, by increasing polymer concentration and by increasing the molecular weight of the polymer [van de Witte *et al.* 1996].

Keller [Keller 1995] postulated that two kinds of crystal can act as a junction point for the gel network. The fringed micelle crystals are formed by interchain aggregation, in which the chain segments forming the crystal are from different chains. The chain-folded crystals are formed predominantly by intramolecular aggregation, and the segments forming the crystal, at least to a large extend, are from one and the same chain. The schematic representation of these two structures is shown in Figure 7.7. In the case of the thermoreversible gel of isotactic polystyrene, wide-angle X-ray diffraction (WAXD) studies reported by Atkin *et al.* [Atkins *et al.* 1977] indicated that the polymer in the fringed-micellar junctions could have an extended chain conformation, such as 12_1 helical chain conformation instead of 3_1 helical chain conformation, which has been later predicted to be feasible by Sundararajan *et al.* [Sundararajan *et al.* 1982]. However, the existence of the long extended 12_1 helix in iPS gel is still in matter of debate. The occurrence of the fringed micelle crystallite in polymer crystal is also questioned by some authors [Domszy *et al.* 1986]. For polyethylene-copolymers, the heat and temperature of fusion of the crystals in the gel have been found to be exactly the same as the chain folded crystal formed from the dilute solutions. This led the authors to conclude that the junctions in copoly(ethylene-butene) gels are still chain folded crystal, and not the fringed micelle crystals [Domszy *et al.* 1986].

It is generally accepted that the junctions for the thermoreversible gel of poly(vinyl

chloride) are tiny crystals according to experimental observation and theoretical calculations. Keller *et al.* [Lemstra *et al.* 1978; Keller 1979; Guerrero *et al.* 1980] proposed the existence of two crystal populations in PVC gel: type A and type B, which show a different orientation under stretching. Type A crystals, which are believed to be lamellar and well developed with less connections in the network, arise from the longer syndiotactic sequence of the chains, while type B crystals are supposed to be fringed micellar crystallites and are responsible for the network formation in the gels. Guenet *et al.* [Mutin and Guenet 1986; Candau *et al.* 1987; Mutin *et al.* 1988] have pointed out the existence of two types of physical links in PVC aggregates: strong link, resulting from the crystallization of syndiotactic sequences, and weak links arising from less stereoregular sequences. The strong links are primarily responsible for the formation of the gel network. From the results of small angle neutron scattering experiments, Guenet and co-works [Abied *et al.* 1990] also concluded that these links are mainly in fiber-like structures. This is in agreement with the electron microscopy observation of Yang and Geil [Yang and Geil 1983]. The authors also suggested that the origin of the thermoreversible PVC gel, at least in its early stage, is due to the formation of interchain hydrogen bonds. Kawanishi *el al*. [Kawanishi *et al.* 1986] mapped out the spinodal curve and the sol-gel transition curve in the system of PVC/γ-butyrolactone. Their results show that there is no direct relationship between the phase separation through spinodal decomposition and the gelation.

7.2.3 Formation of Polymer-Solvent Compound

The term “compound” usually refers to a chemical substance consisting of two or more elements chemically bonded with a well-defined ratio [Guenet 2007]. The compounds of interest here are formed through physical interactions and are not chemically bonded. A compound usually forms between biopolymer and water through hydrogen bonds. Early belief was that hydrogen bonds were required in the formation of a compound involving polymers. Recently, several synthetic polymers have been shown to form the compounds

also by incorporating an organic solvent molecule into the microstructure created by polymer chains without requiring hydrogen bonds. The chains are usually in solvated helical conformation by the formation of the polymer-solvent compound. These helices may aggregate and form three-dimension networks and result in the formation of thermoreversible gels. Guenet [Guenet 1992] defined a class of polymers processing bulky side groups such as: polystyrene, poly(methyl methacrylate), which have the ability of formation of the polymer-solvent compound, as solvent-induced gel polymers. The formation of thermoreversible gel in these polymer systems has been shown to be very sensitive to the solvent type.

From the successful synthesis of the syndiotactic polystyrene in 1986 [Ishihara *et al.* 1986], it has been a good model polymer to study the thermoreversible gel. Syndiotactic polystyrene can form gels in a series of solvents including benzene, chloroform, toluene, [Daniel *et al.* 1995; Daniel *et al.* 1996]. Crystallization from the melt or from solution under well-defined conditions of concentration and temperature, leads to the formation of fold-chain, crystalline lamellae in which polymer chain adopt an all trans, planar zigzag conformation (named as α and β crystalline forms). The polymer chains can also adopt conformations in 2_1 helical structures with formation of δ and γ crystalline forms. Clear evidence from temperature-concentration phase diagram, FTIR and XRD for the participation of the solvent in the formation of δ form (a polymer-solvent compound) has been presented. The polymer-solvent compound is found to be responsible for the formation of transparent, elastic thermoreversible gels, even at very low polymer concentration [Daniel *et al.* 1994].

Figure 7.8 shows schematic views of the various kinds of gel structure discussed in this section. In Figure 7.8(a) and (b), the system first phase separates into two phases, polymer-rich and polymer-lean phases, and the polymer-rich phase may vitrify (a) or

crystallize (b) and act as the connectedness for the gel network. In Figure 7.8(c), micro crystals are responsible for the gel formation. Figure 7.8(d) shows that the helix structure which may be promoted by the formation of polymer-solvent compound is the origin of the gelation.

7.3 Effect of CO_2 in Formation of Thermoreversible Gel

7.3.1 P4MP1/*n*-Pentane

Charlet *et al.* [Charlet *et al.* 1984] studied the gelation of P4MP1 in cyclopentane and cyclohexane solution in which the two types of polymers were employed: a nascent sample (as received) and a sample after recrystallization. The gelation behavior of these two polymer samples is different. Their results have shown that the nascent sample has a stronger ability to form a gel than the recrystallization one. This leads the authors to believe that the structures related to the formation of gel junctions have been formed in the nascent sample and are destroyed by the melting and recrystallization process. Their results also show that the different polymorphic crystalline forms collected from the solutions are not directly related to the formation of gel junctions. These authors finally proposed that the formation of thermoreversible gel of P4MP1 in the two cycloalkanes may arise from intermolecular association between several helical sections and the solvent molecules, which leads to the formation of 'polymer-solvent compound'. Wegsteen and Berghmans [Wegsteen and Berghmans 1998] investigated phase behaviour of the P4MP1 in cyclohexane by mapping out of the temperature-concentration phase diagram through DSC measurements. In low concentration region, the transparent gels are obtained in the polymorphic Form V, whereas in high concentration region, the polymorphic Form I is found to be the more stable form than Form V. From the information provided from phase diagram, the authors concluded that Form V represents a polymer-solvent compound. The From V is found to transfer into Form III during drying. The transformation of Form V into Form III through drying leads us to suspect that the Form V is a real polymer-solvent

compound. The formation of polymer-solvent compound is believed to form by a physical interaction or spatial match between the cavity of helix and shape of the solvent molecule. The polymer-solvent compounds usually decompose through congruent or incongruent melting. However, these polymer-solvent compounds should be still in stable state with evaporation of the solvents. The transformation from solvent-incorporated Form V of P4MP1 into the solvent-free Form III without heating implies that the interaction between polymer chain and solvent molecule is so weak that the incorporated solvent can be vaporized and the pack of the helix can be rearranged. In this case, the Form V may not be recognized as a polymer-solvent compound. The δ form of sPS formed from different solutions has been proved to be a polymer-solvent compound. The δ form can be obtained by direct drying of the solutions without transferring into the solvent-free γ form, which can be obtained by heating the δ form to 135 °C. In addition, the structure of δ form has been found to be slight different with different solvents. Therefore, the δ form of sPS incorporated different solvent molecules into the crystalline structure can be recognized as the true polymer-solvent compound.

Tanigami *et al.* [Tanigami *et al.* 1985] also reported the gelation and crystallization of P4MP1 in cyclohexane solution. Two methods were employed in preparation of gels: ordinary gelation, referring to the gelation directly formed by cooling, and regelation, referring to gelation by reheating the ordinary gel to dissolution temperature and followed by gelation by cooling. The gelation behaviour is observed to be different according to different gel preparation methods. For ordinary gelation, in low polymer concentration region, the gel is transparent at early stage of gelation and soon become turbid due to crystallization. In intermediate polymer concentration region, the white particles of crystallites appear first in homogenous solution, which is followed by the formation of the gels. In high polymer concentration region, large spherulites in the order of micrometer can be observed and these spherulites impinge on each other and give rise to formation of a

semitransparent gel. However, the regenerated gel prepared by regelation method is found to be transparent at early stage of gelation. After 24 hrs storage, four different gels appeared: transparent gel, uncrystallized transparent gel, partly crystallized semitransparent gel, and completely crystallized opaque gel. The authors proposed two types of mechanism of gelation discussed early: solid-liquid phase separation and liquid-liquid phase separation. The gels formed in intermediate and high polymer concentration region by ordinary gelation are induced by solid-liquid phase separation, in which crystallites may act as the link-points for gel network. However, for gelation in the low concentration region by ordinary gelation and the whole region by regelation, the liquid-liquid phase separation plays an important role in early stage of gelation. Gelation is caused by some overlapping of polymer chains in the polymer-rich phase without crystallization. The crystallization is observed after the gelation.

As discussed in Chapter 4, the P4MP1 solution in n-pentane is observed to form a gel with addition of large amount CO_2 (e.g. 40 wt % or 50 wt %) when cooling from one phase region to room temperature, whereas the P4MP1 solution in pure n-pentane or in low amount CO_2 in the fluid mixture is observed to form crystals only, instead of gels. By close look at the phase diagram mapped out for gel formation and gel melting (sol-gel and gel-sol transition) curve, a gel mechanism that combines liquid-liquid phase separation can be proposed. According to the information provided from the temperature and pressure phase diagrams, the sol-gel or gel-sol transition temperature on pressure shows sensitive dependence on pressure. At low pressures, gelation occurs at higher temperatures and at high pressures, the gelation occurs at lower temperatures. These results lead us to conclude that the gel may arise from a UCST-type liquid-liquid phase separation. The temperature-concentration phase diagrams of P4MP1 solution in n-pentane with or without CO_2 are schematically shown in Figure 7.9 with both liquid-liquid phase boundary and fluid-solid phase boundary. As shown in Figure 7.9(a), the binodal curve for liquid-liquid

phase separation is below the crystallization curves for P4MP1. And cooling from point A to point B only leads to crystallization. With addition of CO_2 into the solution, the solvent quality of fluid mixture becomes poorer, resulting in the shrinking of the homogenous region, which is shown as a UCST binodal curve occurring at higher temperature in Figure 7.9(b). The shifting of the binodal curve to higher temperatures causes that the binodal curve intersects with the crystallization curve. Upon cooling from point A to point B, the system enters a two liquid-liquid phase region first. When the temperature at point B is below the crystallization line shown as dashed line inside of two phase regions, the polymer-rich phase can crystallize, and these ordered crystalline structures can act as the anchor points for the formation of three-dimension network.

7.3.2 sPS/Toluene

As mentioned in earlier sections, it is generally accepted that the origin of thermoreversible gel formed from sPS solution in toluene in the low polymer concentration region is the formation of polymer-solvent molecular compound in δ crystalline form. The detailed crystal structure of the δ form of sPS incorporated toluene has been reported by Chatani *et al.* [Chatani *et al.* 1993] The crystal structure viewed along the polymer chain axis is shown in Figure 7.10 [Chatani *et al.* 1993]. As shown in Figure 7.10, the solvent molecule only occupies the isolated holes created by the helix along the **b** axis. While the **a** axis is close-packed and not affected by incorporating of different solvent molecules.

The mechanism for the gelation of sPS in toluene solution is shown in Figure 7.11a. When cooling the sPS solution in toluene, the polymer chains adopt the helical conformation and the incorporated toluene molecules into cavities between the helices enhance the stability of the helical conformation. Each toluene molecule is surrounded by two helices and thus each toluene molecule has the same contribution to stabilizing the both helices. And eventually, the two helices seem to be locked together by toluene molecules entrapped

between them. These bonded helices finally give rise to the formation of high elastic thermoreversible gel even at very low polymer concentration.

The influence of CO_2 on the gelation of sPS solution in toluene is shown in Figure 7.11b. With addition of CO_2 into the system, the formation of sPS-toluene compound is affected by the presence of the second solvent molecule, CO_2. Carbon dioxide is not a good solvent for most polymers including sPS and can destabilize the helical conformation of sPS chain. For the sPS solution in the solvent mixture of toluene and CO_2, the CO_2 competes with toluene molecules to interact with sPS chains. As a result, at relatively low CO_2 concentrations, the sPS-toluene compound can still be formed but at relatively low rate, and at large CO_2 concentration, the strong competition between CO_2 and toluene makes that the formation of stable sPS-toluene compound becomes impossible. In this case, the sPS may form the gel through crystallization or just crystallize without gelation. In the present study, the morphology of sPS samples collected from high CO_2 concentration has been found to be stacked-lamella structures instead of the fibrillar structure collected in pure toluene solvent, as discussed in Chapter 5. The results support the mechanism proposed above.

7.4 Conclusion

In this chapter, the four different gel mechanisms in synthetic polymer solution have been reviewed. The gel in polymer solvent can form through phase separation with the combination of vitrification (amorphous polymers) or crystallization (semi-crystalline polymers). For the semi-crystalline polymers, the gelation can be induced directly by crystallization. In some system, the formation of polymer-solvent compound that promotes the stability of structure of polymer chain eventually leads to gelation. CO_2 has two different effects on the systems of P4MP1 in n-pentane and sPS in toluene due to the different gel mechanism. In P4MP1 solution in n-pentane, the addition of CO_2 moves the L-L phase boundary (UCST) to higher temperatures which intersects with L-S curve

(crystallization) of P4MP1 solution in the mixture of n-pentane + CO_2. At certain conditions, the polymer rich phase in solution formed through L-L phase separation is under crystallization condition in which case, the polymer crystallizes and becomes the anchor points for the networks. However, in the system of sPS solution in toluene, the gelation is induced by formation of a polymer-solvent compound. The addition of CO_2 increases the competition of CO_2 with toluene interacting with the helix and eventually destabilizing the helix. As a result, the whole gel network is destroyed when large amount CO_2 is introduced into the system.

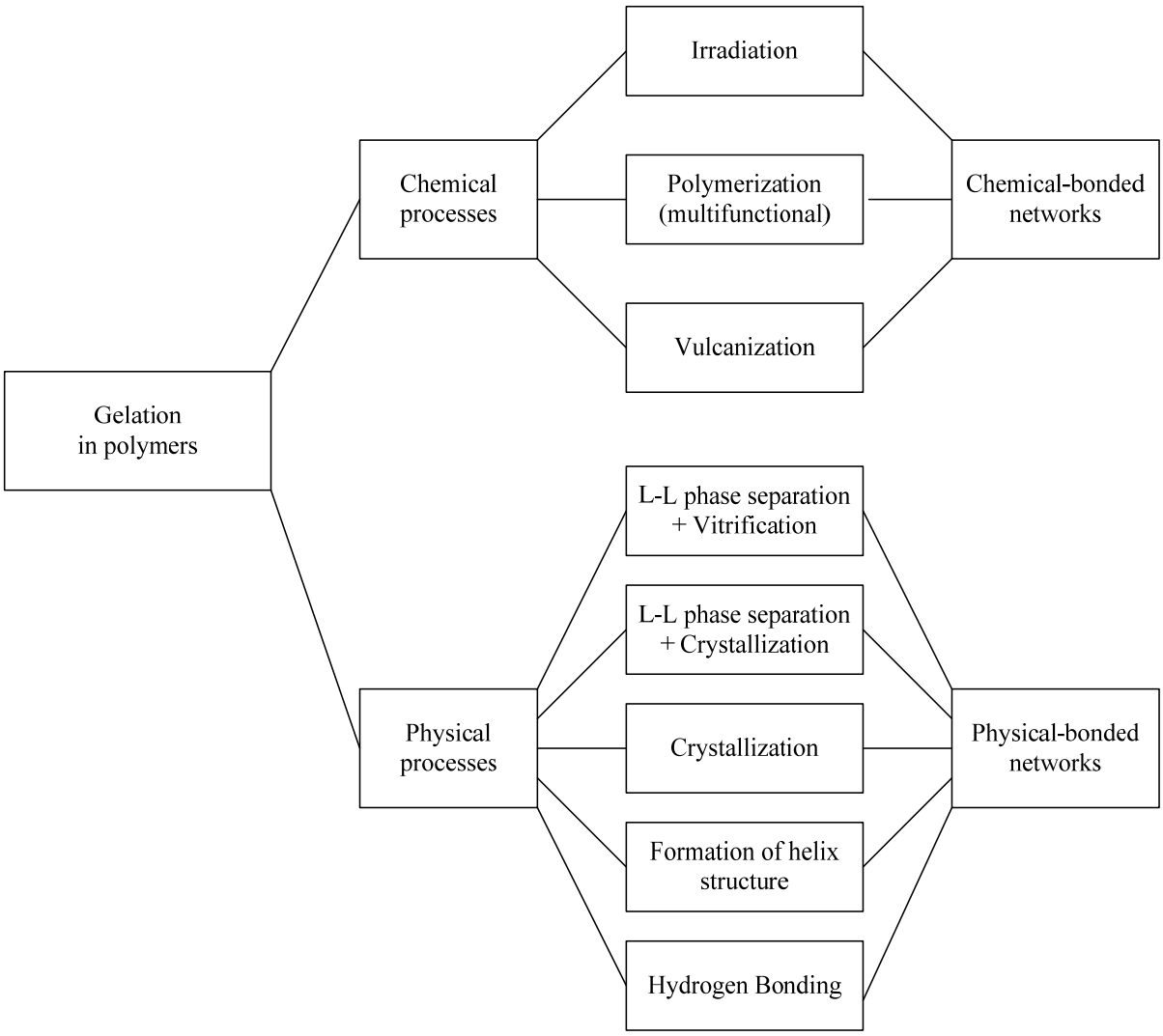

Figure 7.1 The different sources lead to form of junctions inside of polymer gels.

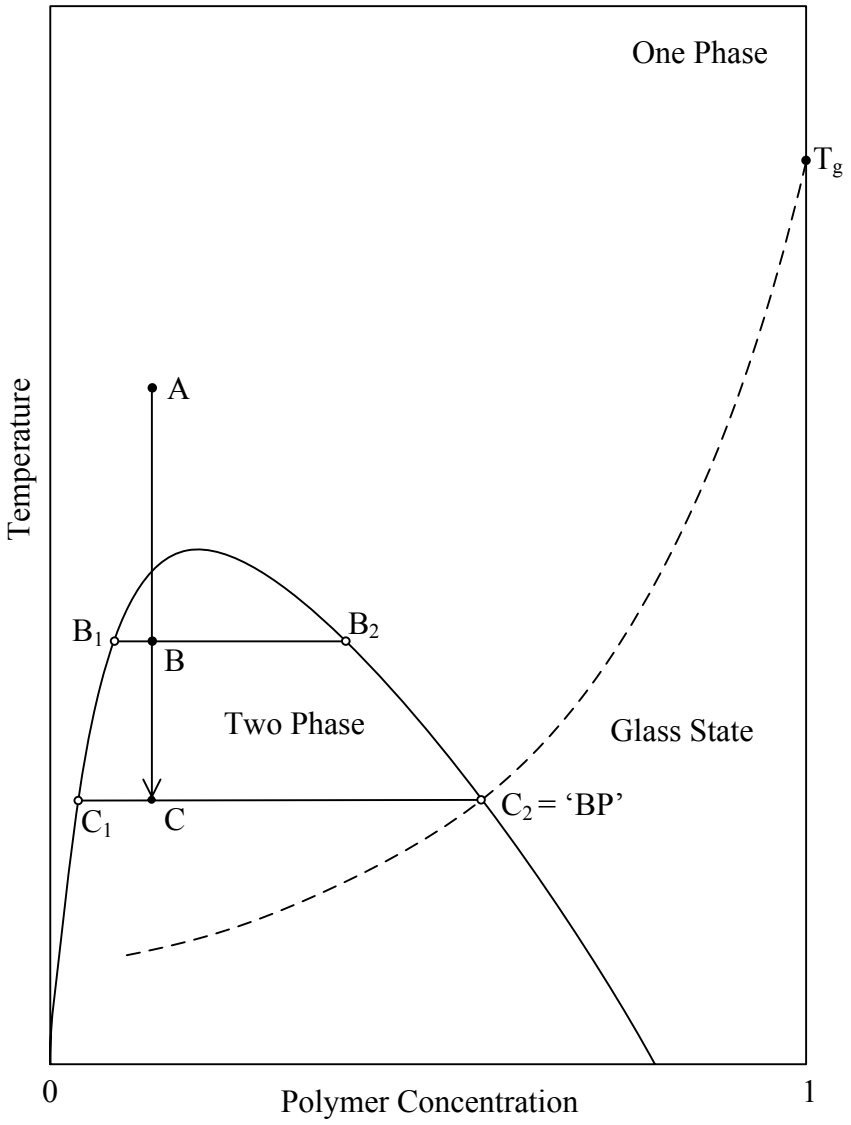

Figure 7.2 The schematic representation of phase diagram of amorphous polymer solution for which the glass transition curve intersects with binodal curve.

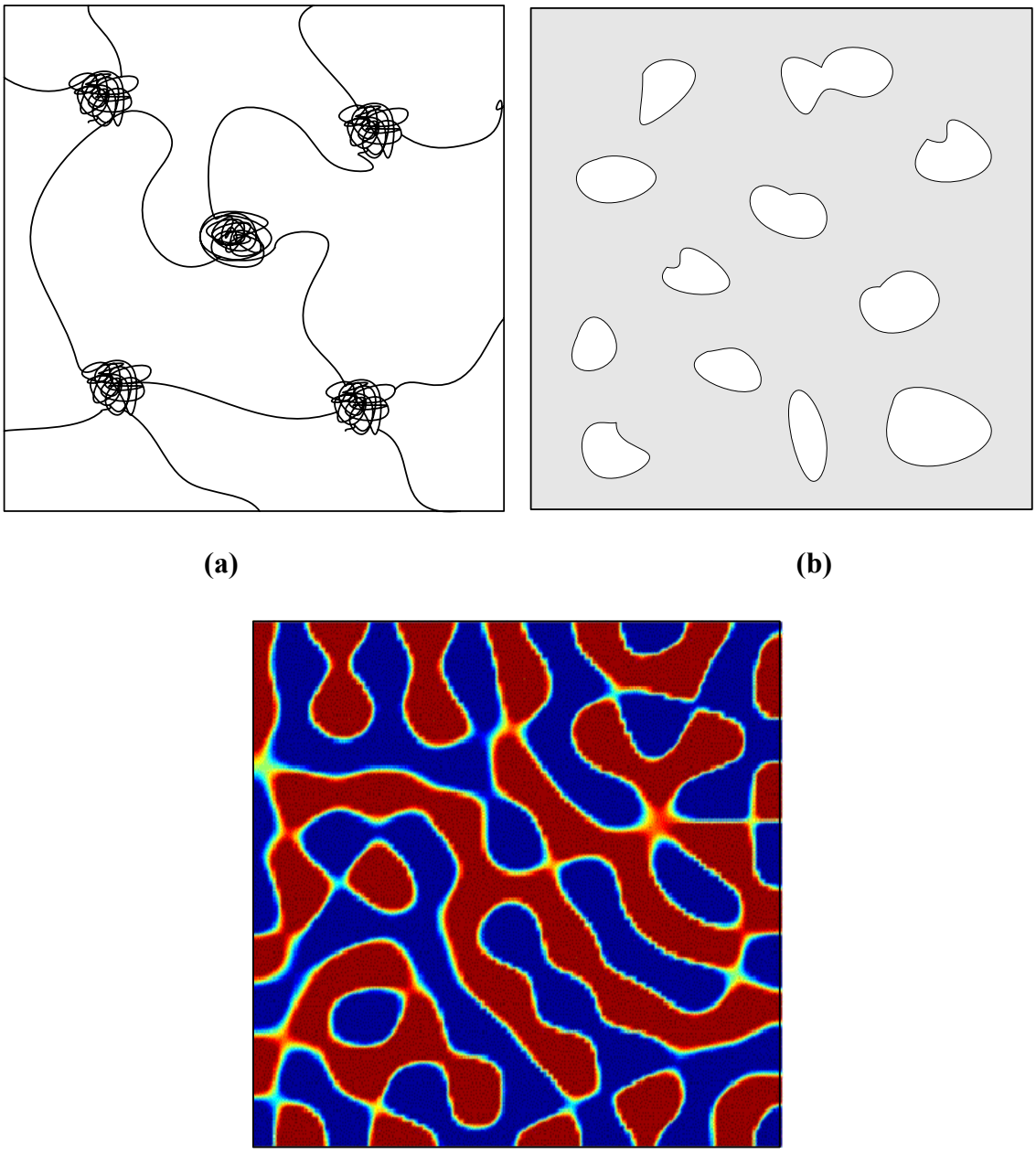

Figure 7.3 Schematic illustrations of the principal classes of gel morphology obtainable by L-L phase separation intercepted by vitrification. (a) Molecularly connected (glassy spheres-polymer rich phase connected by isolated solvated chains), (b) Solid (glassy)-phase connected and (c) Phase-connected bicontinuous. [Keller 1995]

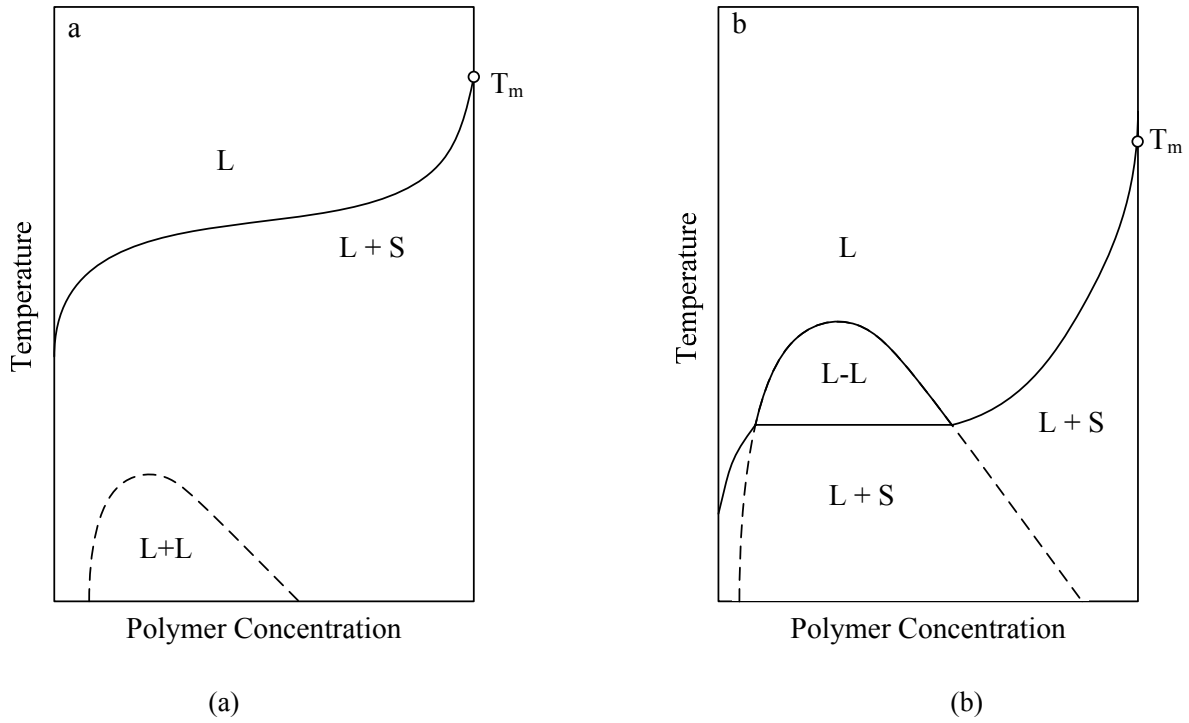

Figure 7.4 Schematic representation of phase diagrams with interference between liquid-solid curve and the binodal liquid-liquid curve: (a) L-L curve is far below the L-S curve; (b) L-L intersects with L-S curve. [te Nijenhuis 1997]

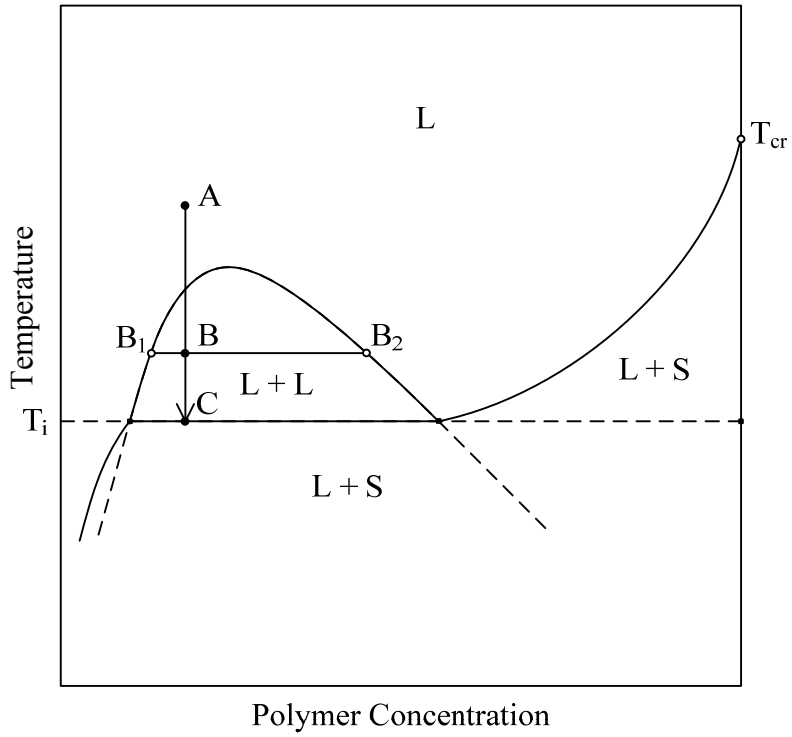

Figure 7.5 Schematic representation of phase diagram of polymer solution with interference between L-L demixing and L-S demixing. [te Nijenhuis 1997]

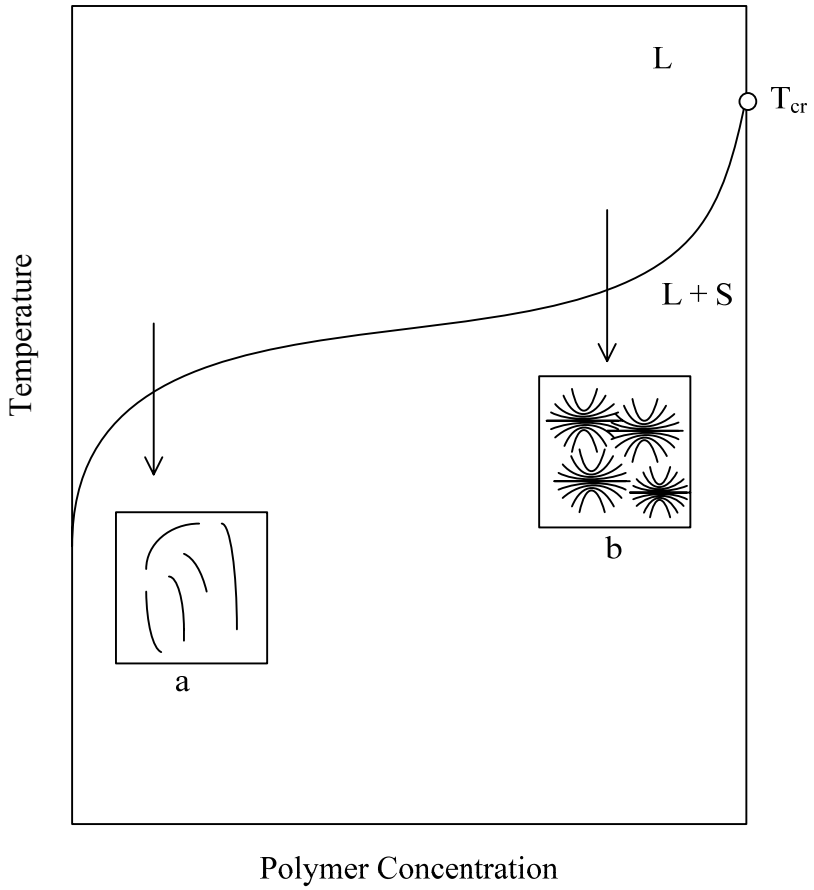

Figure 7.6 Schematic representation of phase diagram with only liquid-solid transition for a semicrystalline polymer solution: (a) at very low polymer concentration: chain-fold lamellae; (b) at high polymer concentration: spherulites.

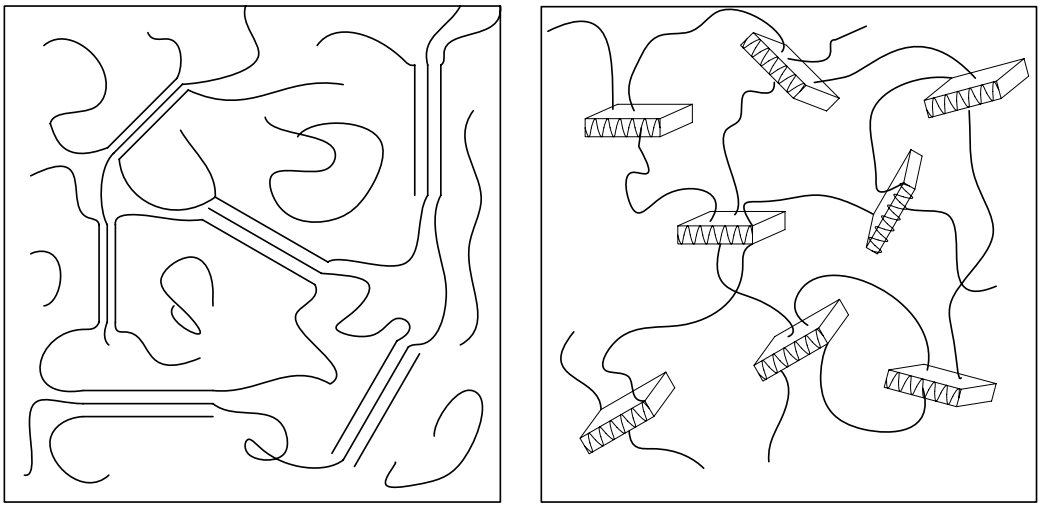

(a) **(b)**

Figure 7.7 Schematic representations of possible gel classes arising from crystallization: (a) the junctions are small bundles, micelles constituted by portions of different chains; (b) the junctions are the chain-folded crystal and the links are interlamellar tie molecules. [Keller 1995]

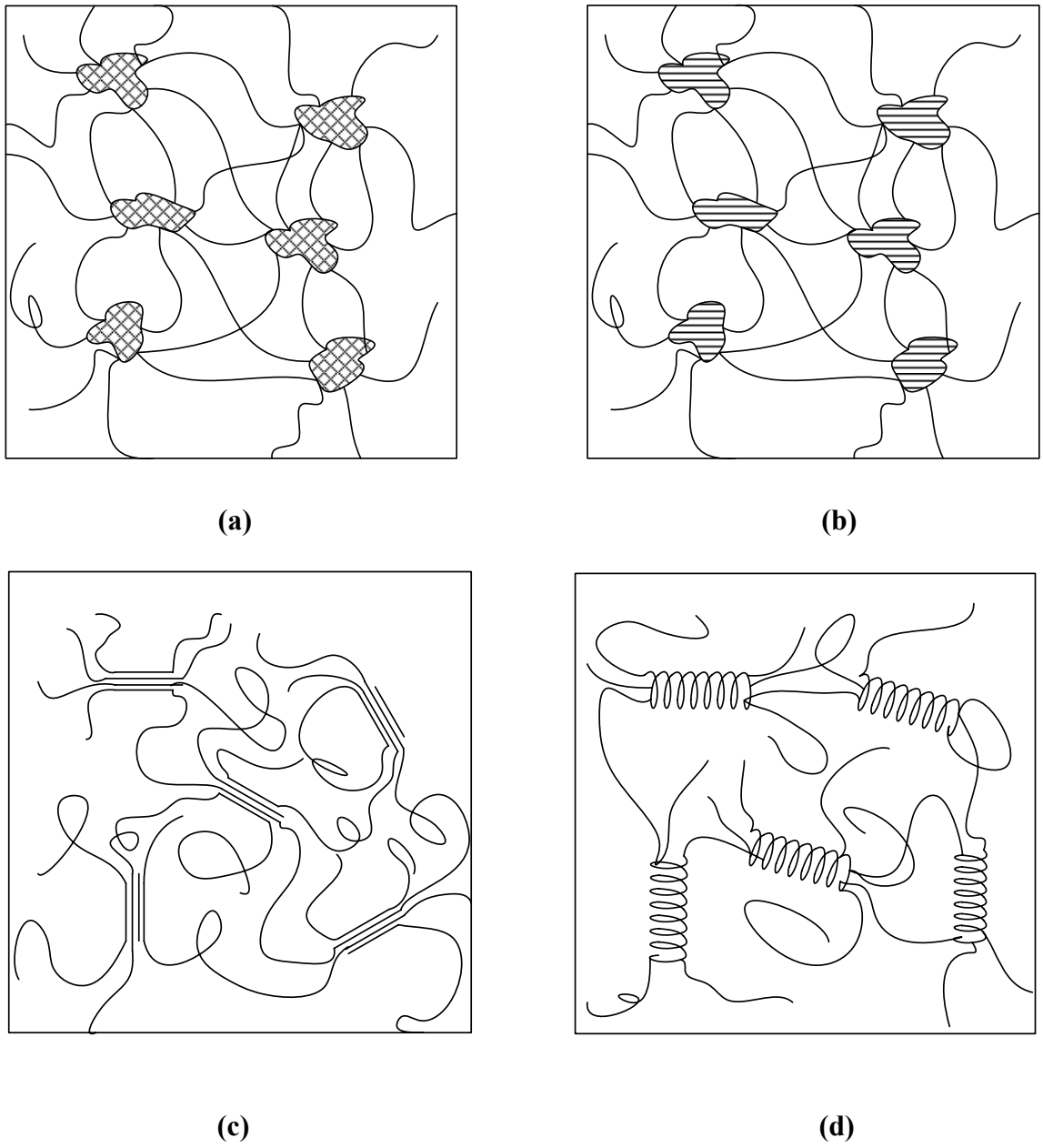

Figure 7.8 Schematic representations of different types of polymer gels: (a) induced by L-L phase separation and vetrification; (b) induced by L-L phase separation and crystallization; (c) induced by crystallization; (d) induced by formation of polymer-solvent compound.

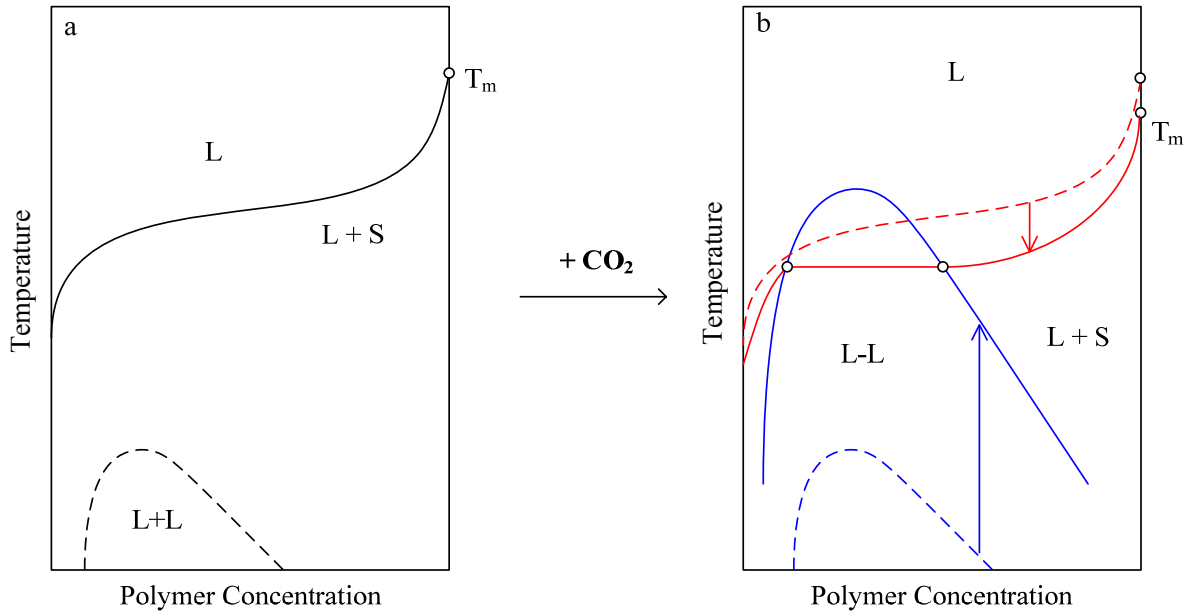

Figure 7.9 Schematic representations of the mechanism of gelation of P4MP1 in n-pentene induced by the addition of CO_2. The gel forms by the combination of L-L phase separation and L-S phase separation.

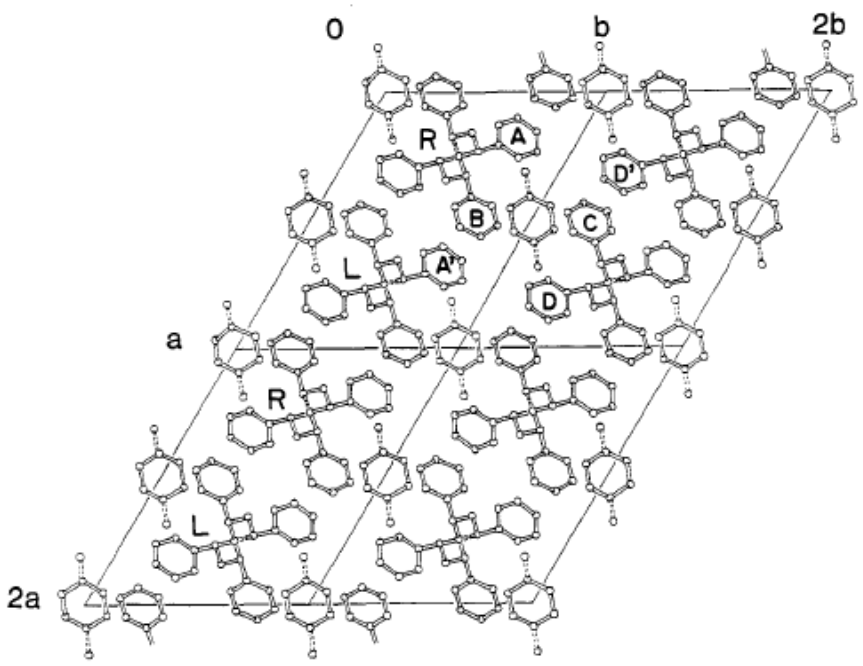

Figure 7.10 Crystalline lattice as seen parallel to the helix axis: monoclinic cell with a = 1.758 nm, b = 1.326 nm, c = 0.771 nm, γ = 121.2°. sPS samples exposed to toluene vapors. [Chatani *et al.* 1993, Polymer; Reprinted with permission from Elsevier]

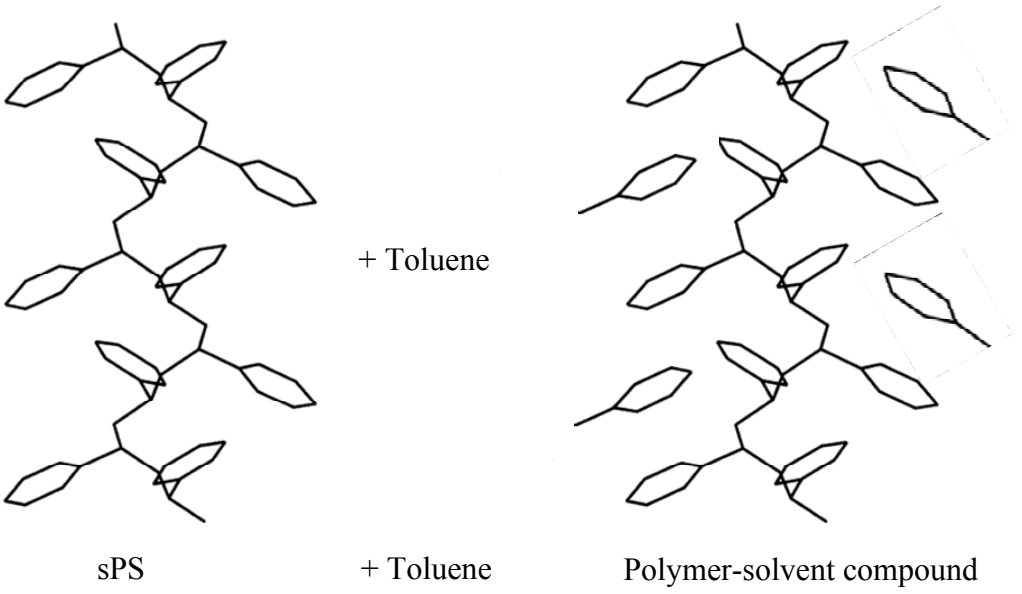

(a)

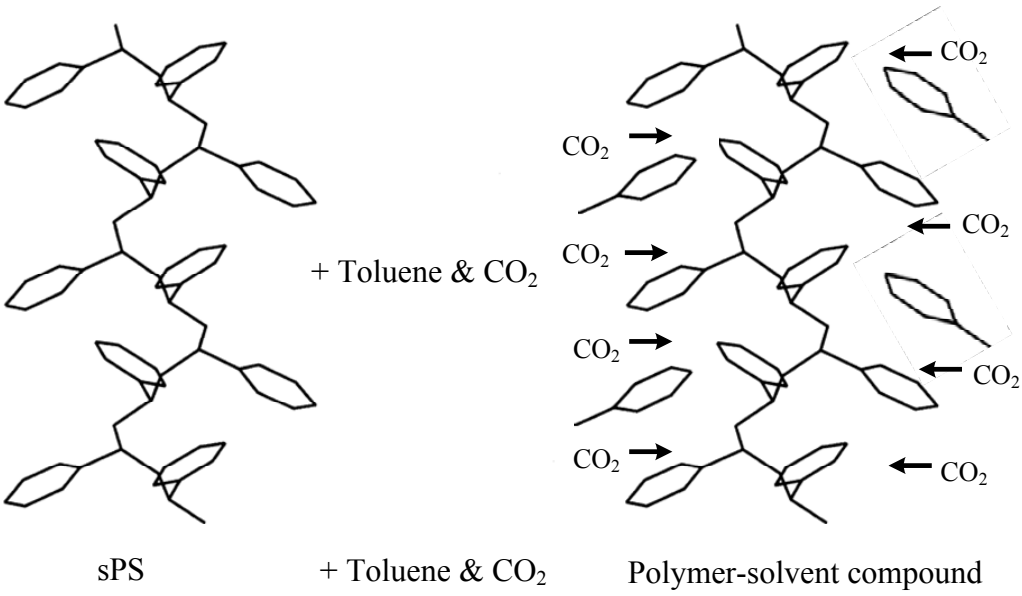

(b)

Figure 7.11 Schematic representation of mechanism of gelation of sPS + toluene by formation of polymer-solvent compound interfered with the addition of CO_2, (a) without CO_2; (b) with CO_2

Chapter 8

Summary and Recommendations

The primary objective of this thesis work was to study the phase separation and phase separation kinetics of polymers in dense fluids with or without CO_2 to get better understanding on the thermodynamic and dynamic aspects of miscibility and phase separation for polymer solutions under high pressure and the influence of pressure and/or fluid composition on polymorphic transformations. The majority of the work was focused on the fluid-solid or sol-gel phase separation in semi-crystalline polymers in fluid mixtures containing CO_2. Specific systems included poly(4-methyl-1-pentene) in n-pentane and in n-pentane + CO_2 and syndiotactic polystyrene in toluene, toluene + CO_2, acetophenone and acetophenone + CO_2. The kinetics of pressure-induced phase separation was also studied in solutions of atactic polystyrene in acetone.

8.1 Summary Observation on the Kinetics of Pressure-Induced Phase Separation

The kinetics of pressure-induced phase separation in atactic polystyrene (M_w = 129,200; PDI = 1.02) in acetone was investigated using a high pressure time- and angle-resolved light scattering system. The key findings are summarized below.

1. In solutions that undergo phase separation by nucleation and growth the scattered light intensities show a continual decrease with angle. The scattered light intensities increase with time at all angles. In solutions that undergo phase separation by spinodal decomposition, the angular distribution of the scattered light intensities goes through a maximum. The mechanism of phase separation depends on the polymer concentration and the depth of the pressure quench imposed. For the polymer investigated, the 11.4

wt % solution was found to undergo spinodal decomposition for both the shallow or deep quenches indication that this concentration corresponds to the critical polymer concentration .At concentrations below this critical concentration phase separation was found to proceed by nucleation and growth for shallow quenches but by spinodal decomposition for deeper quenches.

These experiments that were carried out with different quench depths in the range from 0.1 MPa – 3.0 MPa in 4.0, 5.0, 8.2 and 11.4 wt % solutions permitted mapping the binodal and spinodal envelops for this system. Higher concentrations could not be explored to limitations of the present experimental system for high polymer concentrations.

2. The early stage of spinodal decomposition was found to be relatively short and the stationary wave number $q_m(0)$ where the maximum in the scattered light intensity increases in time without change in the angular position was not captured even after very short time. The angular position of the maximum shifts to lower angles with time.

   The kinetics of spinodal decomposition in intermediate and late stage could be described by power-law scaling models. The characteristic wavenumber q_m corresponding to the scattered light intensity maximum I_m was analyzed by power-law scaling according to $q_m \sim t^{-\alpha}$ and $I_m \sim t^{\beta}$. The results show $\beta \approx 2\alpha$.

8.2 Summary Observation on Phase Behavior

The phase boundaries of P4MP1 in n-pentane and n-pentane + CO_2, sPS in toluene and toluene + CO_2, sPS in acetophenone and acetophenone + CO_2 have been mapped out in the variable-volume view-cell system in the temperature range from 298 K to 443 K and pressures up to 50 MPa. The results are summarized as follows:

The phase boundaries of P4MP1 in n-pentane and n-pentane + CO_2, and the phase boundaries of sPS in toluene, toluene + CO_2, acetophenone and acetophenone + CO_2 were mapped out in the variable-volume view-cell system in the temperature range from 298 K to 443 K and pressures up to 50 MPa. The results are summarized as follows:

1. The fluid-solid phase separation in P4MP1 solutions in pure pentane solutions was a crystallization process. In syndiotactic PS solutions in pure toluene or acetophenone was a gelation process. The phase boundary temperatures were dependent on polymer concentrations, and in P4MP1 solutions in n-pentane increased by about 15 K when the polymer concentration was increased from 1.0 to 6.4 wt %. In solutions of sPS in pure toluene, sol-gel transition temperatures were found to increase by about 25 K when the polymer concentration was increased from 1.6 wt % to 25 wt %. No liquid-liquid phase separation was observed in these solutions under experimental conditions. The solid-fluid or sol-gel phase transition temperatures in these systems are not sensitive with pressure changes. Usually, these boundaries are shown as sharp boundaries in T-P phase diagram.

2. In solutions containing CO_2, the fluid-solid phase separation boundary was found to shift to lower temperatures in the P4MP1 + pentane system for CO_2 addition levels up to 20 wt % CO_2. At CO_2 addition levels of 40 and 50 wt % a unique transformation from crystallization to gelation was observed to take place. In sPS solution a reverse behavior was observed. In pure toluene and acetophenone, and at CO_2 addition levels < 20 wt % phase separation is a gelation process. But at CO_2 addition levels of 40 and 50 wt %, the phase separation process becomes a crystallization process.

3. In P4MP1 solutions in pentane or pentane + CO_2 mixtures no liquid-liquid phase

separation boundary could be detected. In contrast, sPS solutions in toluene + CO_2 with greater than 28 % carbon dioxide and acetophenone + CO_2 solutions with greater than 25 % CO_2 were found to display a liquid –liquid phase boundary. In solutions with even higher CO_2 levels, the L-L boundary was shifted to higher pressures.

8.3 Summary Observation on Polymorphic Structures Transformations

P4MP1 and sPS both show polymorphism. There are five different polymorphic structures reported for each polymer. The polymorphic states observed in polymers regenerated from different solutions at different pressure and or fluid composition conditions are summarized below.

1. The polymorphic structures of P4MP1 were found to display strong dependence of pressure and CO_2 concentration in fluid mixtures. With increasing crystallization pressure in solutions in n-pentane, crystal structure of P4MP1 was found to change from Form III to Form II. The Form II was found to be the most preferred crystal form of P4MP1 under high pressure which is rarely obtained at ambient conditions. For solution containing CO_2, the crystal structure shifts from Form II to Form I with increasing CO_2 in the fluid mixture. These transformations stem from the change of the solvent power which is altered by pressure or addition of CO_2.

2. The pressure was found to have limited effect on the polymorphic structures of sPS during constant pressure crystallization processing. While the polymorphic structures display strong dependence on the amount of CO_2 in the solution. In pure organic solvents (toluene and acetophenone) or with relatively low level CO_2 (i.e. toluene (84) + CO_2 (16) and acetophenone (75) + CO_2 (25)), only the δ crystal form was obtained. In solutions with high CO_2 content (i.e. acetophenone (60) + CO_2 (40)), only the β form

was obtained. At intermediate levels of CO_2 (i.e. toluene (72) + CO_2 (28)), a mixture of δ + β forms is obtained. There is a transformation from the δ to the β crystal form with increasing amount of carbon dioxide in the solutions.

8.4 Summary Observations on Path Dependence Crystal Form and Morphology

In sPS solutions in toluene + CO_2 and in acetophenone + CO_2, the phase separation experiments were carried out either along a constant pressure cooling path or constant temperature pressure-quench path which was then followed by depressurization or further cooling. The constant pressure cooling leads to crossing either the crystallization or gelation boundary first. Constant temperature pressure reduction leads to liquid-liquid phase separation with the formation of a polymer-rich and a polymer-lean phase. The polymers recovered after the systems are brought to ambient conditions following these different paths show distinct difference in their crystal from and morphologies. The results are summarized below.

1. The samples collected after constant pressure cooling in sPS solution in toluene (72) + CO_2 (28) display essentially the δ form with a minor appearance of β form. Only the δ form is obtained from sPS solution in acetophenone (75) + CO_2 (25). However, a mixture of δ + β crystal forms was obtained from sPS solution in acetophenone (60) + CO_2 (40) solutions.

2. Along a constant temperature pressure reduction path, the crystal form and the morphology of the samples from polymer-lean phase and polymer-rich phase show dramatic differences. The polymer-rich phase sample from sPS solution in toluene (72) + CO_2 (28) shows only the β crystal form with a stacked-lamellar morphology, while the polymer-lean phase sample from this solution is a mixture of δ + β crystal form. In

contrast, the polymer-rich phase sample from the acetophenone (75) + CO_2 (25) solution is a mixture of δ + β form and the polymer-lean phase sample shows only the δ form.

3. These observations on the path dependence of crystal structure can be explained in terms of T-x phase diagrams which take into account the change in the location of the phase boundaries with changes in pressure and CO_2 content of the solutions.

8.5 Recommendations

The following suggestions can be considered in future studies:

1. Time limitations did not permit investigation of the kinetics of phase separation in P4MP1 and sPS solutions. The differences in the dynamics of gelation or crystallizations processes could provide new insights and should be considered in a future study.

2. The exploration of phase separation dynamics at high polymer concentrations would also be desirable. This however would require new designs or extensive modifications of the present light scattering system to achieve in-situ homogenization in very viscous systems.

3. The crystallization and gelation processes in polymer solutions in the view-cell under high pressure were only monitored by the transmitted light intensity change. The samples were collected at room conditions and further dried before characterization. These processes may potentially alter the initial structures formed in these samples. To gain insight into the actual gelation mechanism or the crystallization process, in-situ measurement capabilities, such as in-situ FTIR under high pressure would be highly

desirable. The in-situ measurement of IR spectra would give information on the changes of polymer chain conformation during phase transformations. Since sapphire windows are not suitable as IR windows due to sapphire's high absorption in the IR range, other windows are needed. This may present challenges for operation at very high pressures and temperatures with different fluids. Several high pressure IR cells have been reported in several groups. Rigby et al. [Rigby et al. 1970] constructed a IR cell by using CaF2 and KBr as IR window materials. The transparent regions for CaF2 and KBr are 4000-1100 and 4000-400 cm-1. KBr windows, having good transparency in the far IR region, can only hold up to 30 MPa for temperatures below 50 °C. CaF2, as a strong crystal, can withstand high pressures up to 200 MPa, while the low transparency in far IR region limits its application for polymer system, in which the far IR band is dominating. A commercial high pressure autoclave was recently reported [Kamer et al. 2004] in which the windows are made of ZnS, however having a maximum pressure of only 18.5 MPa and temperatures up to 200 °C. The transparent region for ZnS is 17000-833 cm-1. To study the chain conformation information under high pressure, the selected IR windows must have good strength and good transparency in the far IR region. The common inorganic materials as discussed above have limitations and can not meet the requirements. To be transparent in the far infrared region normally requires dielectric materials with heavy, weakly bonded atoms such as zinc sulfide, zinc selenide and germanium. However, gaining far infrared transparency is almost always traded off against mechanical strength [Mollart et al. 2003].

The exception to this general rule is diamond, which has excellent far infrared properties. Therefore, it offers a combination of high strength, thermal conductivity and durability with optical transparency from ultraviolet to far IR region. Diamond anvil cells (DACs) have been used to generate very high static pressures [Xu *et al.* 2006]. But DACs have their limitations with respect to the small sample sizes that are involved.

Recently it has become possible to make large area polycrystalline Type IIa diamond windows with a chemical vapor deposition (CVD) route [Xu *et al.* 2006]. The large planar windows of CVD diamond have been made up to 120 mm in diameter and 2 mm in thickness. Most recently, Hirano and co-workers [Abe *et al.* 2005] have constructed a high pressure cell for IR and Raman spectrometric measurement by using the CVD diamond as windows (5 mm in diameter and 0.5 mm in thickness). Their system can operate at temperatures up to 400 °C and pressures up to 50 MPa. Therefore the CVD diamond could be an ideal window material for a future high pressure IR cell to study details of gelation and crystallization processes as they occur in a view cell. Modification of the view cell by incorporation such windows for IR studies should thus be considered in future studies.

4. The FTIR results of sPS gel sample formed from pure acetophenone solutions show two distinct peaks located at 1214 and 1050 cm^{-1}. The origin of the peaks must relate to the specific interaction between the acetophenone group and the cavity formed in the δ form. Further FTIR studies or NMR measurements on the system is needed for further elucidations. Such studies may provide more information on the nano environment inside the nanoporous cavities in crystalline phase.

5. The recently reported [Rizzo *et al.* 2007] ε form of sPS is described to be a nanoporous crystalline phase similar to the δ form, but with a different pore shape. The ε form is generated by treating the γ form powder in liquid chloroform at ambient pressures for at least 24 h, followed by extraction with supercritical carbon dioxide. The nano pores in the ε form is reported to be "channel" shape instead of cavities which could provide a medium in which aligned reactions such a polymerizations could possibly be carried out to generate special blends. The possibility of forming the ε form of sPS from high pressure solutions should be explored in the future.

6. The present study has focused on the polymorphic transformations in P4MP1, but more so in sPS. Future studies should expand the scope to other stereoregular polymers that show polymorphism. Research should also be directed to better identification of conditions that display coil-to-helix and the association of helices as distinct steps in gelation processes.

References

Abe, J., Hirano, N. and Tsuchiya, N. (2005). "Experimental apparatus for measurement of IR and Raman spectrum at high temperatures and pressures." 3rd International Workshop on Water Dynamics, Sendai, Japan.

Abied, H., Brulet, A. and Guenet, J. M. (1990). "Physical gels from PVC: molecular structure of pregels and gels by low-angle neutron scattering." *Colloid and Polymer Science*, 268, (5), 403.

Addink, E. J. and Beintema, J. (1961). "Polymorphism of crystalline polypropylene " *Polymer*, 2, 185.

Aerts, L. and Berghmans, H. (1990). "Calorimetric investigation of the phase-behavior of the system poly(2,6-dimethyl-1,4-phenyleneoxide)-antracene." *Bull. Soc. Chim. Belg*, 99, 931.

Aerts, L., Kunz, M., Berghmans, H. and Koningsveld, R. (1993). "Relation between phase-behavior and morphology in polyethylene diphenyl ether systems." *Makromol. Chem.*, 194, 2697.

Aharoni, S. M., Charlet, G. and Delmas, G. (1981). "Investigation of solutions and gels of poly(4-methyl-1-pentene) in cyclohexane and decalin by viscosimetry, calorimetry, and X-ray diffraction. a new crystalline form of poly(4-methyl-1-pentene) from gels." *Macromolecules*, 14, 1390.

Aksimentiev, A., Holyst, R. and Moorthi, K. (2000). "Kinetics of the droplet formation at the early and intermediate stages of the spinodal decomposition in homopolymer blends." *Macromolecular Theory and Simulations* 9, (8), 661.

Albunia, A. R., Musto, P. and Guerra, G. (2006). "FTIR spectra of pure helical crystalline phases of syndiotactic polystyrene." *Polymer*, 47, 234.

Almdal, K., Dyre, J., Hvidt, S. and Kramer, O. (1993). "Towards a phenomenological definition of the term ‘gel’ " *Polymer Gels and Networks*, 1, (1), 5.

Arnauts, J. and Berghmans, H. (1987). "Amorphous thermoreversible gels of atactic polystyrene." *Polymer Communications*, 28, (3), 66.

Arnauts, J., Berghmans, H. and Koningsveld, R. (1993). "Structure formation in solutions of atactic polystyrene in trans-decalin." *Makromolekulare Chemie*, 194, (1), 77.

Atkins, E. D. T., Isaac, D. H., Keller, A. and Miyasaka, K. (1977). "Analysis of anomalous x-ray diffraction effects of isotactic polystyrene gels and its implications for chain

conformation and isomeric homogeneity." *Journal of Polymer Science, Polymer Physics Edition*, 15, 211.

Bachmann, M. A. and Lando, J. B. (1981). "A reexamination of the crystal structure of phase II of ploy(vinylidene fluoride)." *Macromolecules*, 14, 40.

Berghmans, H. and Deberdt, F. (1994). "Phase behaviour and structure formation in solutions of vinyl polymers." *Phil. Trans. R. Soc. Lond. A*, 348, 117.

Binder, K., Billottet, C. and Mirold, P. (1978). "Theory of spinodal decomposition in solid and liquid binary-mixtures." *Z. Phys. B*, 30, 183.

Binder, K. and Fratzl, P. (2001). *Phase transformations in materials, Chapter 7*. Weinheim, Wiley-VCH

Boyer, R. F., Baer, E. and Hiltner, A. (1985). "Concerning gelation effects in atactic polystyrene solutions." *Macromolecules*, 18, (3), 427.

Bruckner, S. and Meille, S. V. (1989). "Non-parallel chains in crystalline γ-isotactic polypropylene." *Nature*, 340, 455.

Bruckner, S., Meille, S. V., Petraccone, V. and Pirozzi, B. (1991). "Polymorphism in isotactic polyproplene." *Prog. Polym. Sci.*, 16, 361.

Bui, H. S. and Berry, G. C. (2007). "Moderately concentrated solutions and gels of atactic polystyrene in solvent mixtures of carbon disulfide and tricresyl phosphate." *Journal of Rheology*, 51, (5), 915.

Cahn, J. W. (1959). "Free energy of a nununiform system. II. Thermodynamic basis " *J. Chem. Phys*, 30, 1121.

Cahn, J. W. (1961). "On spinodal decompostion." *Acta Metallurgica*, 9, 795.

Cahn, J. W. (1965). "Phase separation by spinodal decompostion in isotropic system." *J. Chem. Phys*, 42, 93.

Cahn, J. W. and Hilliard, J. E. (1958). "Free energy of a nonuniform system. I. Interfacial free energy." *J. Chem. Phys*, 28, 258.

Cahn, J. W. and Hilliard, J. E. (1959). "Free energy of a nonuniform system. III. Nucleation in a two-component incompressible fluid." *J. Chem. Phys*, 31, 688.

Callister, S., Keller, A. and Hikmet, R. M. (1990). "On thermoreversible gels: their classification, relation to phase transitions and vitrification, their morphology and

properties." *Makromolekulare Chemie, Macromolecular Symposia*, 39, 19.

Candau, S. J., Dormoy, Y., Mutin, P. H., Debeauvais, F. and Guenet, J. M. (1987). " Physical gels from PVC: dynamic properties of dilute solutions." *Polymer*, 28, (8), 1334.

Chan, A. and Radosz, M. (2000). "Fluid-liquid and fluid-solid phase behavior of poly(ethylene-co-octene-1) in sub- and supercritical propane, ethylene, and ethylene+hexene-1." *Macromolecules*, 33, 6800.

Charlet, G. and Delmas, G. (1982). "Modification V of poly(4-methylpentene-1) from cyclopentane solutions and gels." *Polym. Bull.*, 6, 367.

Charlet, G. and Delmas, G. (1984). "Effect of solvent on the polymorphism of poly(4-methylpentene-1): 2. crystallization in semi-dilute solutions." *Polymer*, 25, 1619.

Charlet, G., Delmas, G., Revol, F. J. and Manley, R. S. J. (1984). "Effect of solvent on the polymorphism of Poly(4-methylpentene-1): 1. solution-grown single crystals polymer." *Polymer*, 25, 1613.

Charlet, G., Phung-Nguyen, H. and Delmas, G. (1984). "Thermoreversible gelation of poly(4-methyl-1-pentene) in cyclopentane and cyclohexane." *Macromolecules*, 17, 1200.

Chatani, Y., Shimane, Y., Ijitsu, T. and Yukinari, T. (1993). "Structural study on syndiotactic polystyrene: 3. Crystal structure of planar form I. ." *Polymer*, 34, (8), 1625.

Chatani, Y., Shimane, Y., Inagaki, T., Ijitsu, T., Yukinari, T. and Shikuma, H. (1993). "Structural study on syndiotactic polystyrene: 2. Crystal structure of molecular compound with toluene." *Polymer*, 34, (8), 1620.

Chatani, Y., Shimane, Y., Inoue, Y., Inagaki, T., Ishioka, T., Ijitsu, T. and Yukinari, T. (1992). "Structural study of syndiotactic polystyrene: 1. Polymorphism." *Polymer*, 33, 488.

Chen, S.-J., Berry, G. C. and Plazek, D. J. (1995). "Moderately concentrated solutions of polystyrene. 6. gel formation in carbon disulfide." *Macromolecules*, 28, (19), 6539.

Cho, J. W., Song, H. Y. and Kim, S. Y. (1993). "Thermoreversible gelation of poly(vinylidene fluoride) in .gamma.-butyrolactone solution." *Polymer* 34, (5), 1024.

Clark, A. H. and Ross-Murphy, S. B. (1987). "Structural and mechanical properties of biopolymer gels " *Advances in Polymer Science*, 83, 57.

Cojazzi, G., Malta, V., Celotti, G. and Zannetti, R. (1976). "Crystal structure of form III of isotactic poly-1-butene." *Mackromolekulare Chemie*, 177, 915.

Cook, H. E. (1970). "Brownian motion in spinodal decomposition." *Acta Metallurgica*, 18, 297.

Corradini, P. and Guerra, G. (1992). "Polymorphism in polymers." *Advances in Polymer Science*, 100, 183.

D'Aniello, C., Rizzo, P. and Guerra, G. (2005). "Polymorphism and mechanical properties of syndiotactic polystyrene films." *Polymer*, 46, 11435.

Danch, A. and Gadomski, A. (2000). "On the crystallization-amorphous supermolecular structure of poly(4-methyl-1-pentene) films cast from solution: experimental evidences and theoretical remarks." *J. Molecular Liquids*, 86, 249.

Daniel, C., Alfano, D., Venditto, V., Cardea, S., Reverchon, E., Larobina, D., Mensitieri, G. and Guerra, G. (2005). "Aerogels with a microporous crystalline host phase." *Advanced Materials*, 17, 1515.

Daniel, C., Dammer, C. and Guenet, J.M. (1994). "On the definition of thermoreversible gels: the case of syndiotactic polystyrene " *Polymer*, 35, (19), 4243.

Daniel, C., Deluca, M. D., Guenet, J. M., Brulet, A. and Menelle, A. (1996). "Thermoreversible gelation of syndiotactic polystyrene in benzene." *Polymer*, 37, 1273.

Daniel, C., Menelle, A., Brulet, A. and Guenet, J. M. (1995). "Thermoreversible gelation of syndiotactic polystyrene in toluene and choroform." *Polymer*, 38, 4193.

De Gennes, P. G. (1979). *Scaling concepts in polymer physics*. Ithaca, NY, and London, Cornell University Press.

De Rosa, C. (1996). "Crystal structure of the trigonal modification (a form) of syndiotactic polystyrene." *Macromolecules*, 29, 8460.

De Rosa, C. (1999). "Chain conformation of Form IV of isotactic poly(4-methyl-1-pentene)." *Macromolecules*, 1999, 935.

De Rosa, C. (2003). "Crystal structure of Form II of isotactic poly(4-methyl-1-pentene)." *Macromolecules*, 36, 6087.

De Rosa, C., Borriello, V., Venditto, V. and Corradini, P. (1994). "Crystal structure of form III and the polymorphism of isotactic poly." *Macromolecules*, 27, 3864.

De Rosa, C., Capitani, D. and Cosco, S. (1997). "Solid-State ^{13}C Nuclear Magnetic Resonance Spectra of Four Crystalline Forms of Isotactic Poly(4-methyl-1-pentene)." *Macromolecules*, 30, 8322.

De Rosa, C., Guerra, G., Petraccone, V. and Pirozzi, B. (1997). "Crystal structure of the emptied clathrate form (δe form) of syndiotactic polystrene." *Macromolecules*, 30, 4147.

De Rosa, C., Rapacciuolo, M., Guerra, G., Petraccone, V. and Corradini, P. (1992). "On the crystal structure of the orthorhombic form of syndiotactic polystyrene." *Polymer*, 33, 1423.

De Rosa, C., Rizzo, P., de Ballesteros, O. R., Petraccone, V. and Guerra, G. (1999). "Crystal structure of the clathrate δ form of syndiotactic polystyrene containing 1,2-dichloroethane " *Polymer*, 40, 2103.

De Rudder, J., Berghmans, H. and De Schryver, F. C. (2002). "Gelation mechanism of syndiotactic polystyrene in bromoform." *Macromolecules*, 35, 9592.

De Rudder, J., Berghmans, H., De Schryver, F. C., Bosco, M. and Paoletti, S. (2002). "Gelation mechanism of syndiotactic polystyrene in bromoform." *Macromolecules*, 35, 9529.

Dean, D. M. and Register, R. A. (1998). "Oriented -isotactic polypropylene crystallized at atmospheric pressure." *Journal of Polymer Science, Part B: Polymer Physics*, 36, 2821.

Deberdt, F. and Berghmans, H. (1993). "Phase behaviour of syndiotactic polystyrene-decalin." *Polymer*, 34, 2192.

Deberdt, F. and Berghmans, H. (1994). "Phase behaviour of syndiotactic polystyrene-*o*-xylene." *Polymer*, 35, 1694.

Domszy, R. C., Alamo, R., Edwards, C. O. and Mandelkern, L. (1986). "Thermoreversible gelation and crystallization of homopolymers and copolymers." *Macromolecules*, 19, (2), 310.

Ernesto Reverchon, G. G., Vincenzo Venditto (1999). "Regeneration of nanoporous crystalline syndiotactic polystyrene by supercritical CO_2." *Journal of Applied Polymer Science*, 74, 2077.

Fang, J. and Kiran, E. (2006). "Crystallization and gelation of isotactic poly(4-methyl-1-pentene) in n-pentane and in n-pentane + CO_2 at high pressures." *Journal of Supercritical Fluids*, 38, 132.

Fang, J. and Kiran, E. (2008). "Thermoreversible gelation and polymorphic transformations of syndiotactic polystyrene in toluene and toluene + carbon dioxide fluid mixtures at high pressures." *Submitted to Macromolecules*,

Flory, P. J. (1974). "Introductory lecture." *Faraday discussions of the Chemical Society* 57, 7.

Francois, J., Gan, J., Sarazin, D. and Guenet, J. M. (1988). "Relation between physical gelation and tacticity in polystyrene." *Polymer*, 29, (5), 898.

Francois, J., Gan, J. Y. S. and Guenet, J. M. (1986). "Sol-gel transition and phase diagram of the system atactic polystyrene-carbon disulfide." *Macromolecules*, 19, (11), 2755.

Furukawa, H. (1985). "A dynamic scaling assumption for phase separation." *Adv. Phys.*, 34, 703.

Galdi, N., Albunia, A. R., Oliva, L. and Guerra, G. (2006). "Selective molecular-complex phase formation of syndiotactic polystyrene with a styrene dimer." *Macromolecules*, 39, 9171.

Gambi, A., Giorgianni, S., Passerini, A., Visinoni, R. and Ghersetti, S. (1980). "Infrared studies of acetophenone and its deuterated derivatives." *Spectrochimica Acta, Part A: Molecular and Biomolecular Spectroscopy*, 36A, 871.

Gan, J. Y. S., Francois, J. and Guenet, J. M. (1986). "Enhanced low-angle scattering from moderately concentrated solutions of atactic polystyrene and its relation to physical gelation." *Macromolecules*, 19, (1), 173.

Gekko, K. and Fukamizu, M. (1991). " Effect of pressure on the sol-gel transition of gelatin." *International Journal of Biological Macromolecules*, 13, (5), 295.

George, M., Luo, C., Wang, C., Carretti, E., Dei, L. and Weiss, R. G. (2005). " Chemically and physically induced (reversible) gelation of organic liquids by monomeric and polymeric gelators." *Macromolecular Symposia* 227, 173.

Giles, M. R., Griffiths, R. M. T., Irvine, D. J. and Howdle, S. M. (2003). "The polymerization of functionalized methacrylate monomers in supercritical carbon dioxide." *European Polymer Journal* 39, (9), 1785.

Girolamo, M., Keller, A. and Overbergh, N. (1976). "Gelation-crystallization in isotactic polystyrene solutions and its implications to crystal morphology, to the origin and structure of gels, and to the chemical homogeneity of polyolefins." *J. Polym. Sci., Polym. Phys. Ed.*, 14, 39.

Gomez, M. A., Jasse, B., Cozine, M. H. and Tonelli, A. E. (1990). "High-resolution ^{13}C nuclear magnetic resonance observations of two crystalline model compounds for syndiotactic polystyrene." *J. Am. Chem. Soc.*, 112, 5881.

Gomez, M. A. and Tonelli, A. E. (1990). "Carbon-13 nuclear magnetic resonance study of chain conformation in the solid polymorphs of syndiotactic polystyrene." *Macromolecules*, 23, 3385.

Gomez, M. A. and Tonelli, A. E. (1990). "Carbon-13 nuclear magnetic resonance study of chain conformation in the solid polymorphs of syndiotactic polystyrene." *Macromolecules*, 23, 3385.

Gomez, M. A. and Tonelli, A. E. (1991). "Structural, conformational, and motional studies of the crystalline polymorphs of syndiotactic polystyrene." *Macromolecules*, 24, 3533.

Gowd, E. B., Nair, S. S., Ramesh, C. and Tashiro, K. (2003). "Studies on the clathrate (δ) form of syndiotactic polystyrene crystallized by different solvents using fourier transform infrared spectroscopy." *Macromolecules*, 36, 7388.

Grassi, A., Longo, P. and Guerra, G. (1989). "Solid-state high-resolution carbon-13 NMR spectra of syndiotactic polystyrene. ." *Makromolekulare Chemie, Rapid Communications*, 10, (12), 687.

Greis, O., Xu, Y., Asano, T. and Petermann, J. (1989). "Morphology and structure of syndiotactic polystyrene." *Polymer*, 30, (4), 590.

Gu, M., Zhang, J., Wang, X., Tao, H. and Ge, L. (2006). "Formation of poly(vinylidene fluoride) (PVDF) membranes via thermally induced phase separation." *Desalination*, 192, 160.

Guenet, J. M. (1992). *Thermoreversible gelation of polymers and biopolymers.* London, Academic Press.

Guenet, J. M. (1986). "On the molecular structure of isotactic polystyrene physical gels as revealed by differential scanning calorimetry and neutron diffraction, ." *Macromolecules*, 19, 1961.

Guenet, J. M. (2007). *Polymer-solvent molecular compounds*. Amsterdam, Elsevier.

Guenet, J. M. and Klein, M. (1990). "Structures in polystyrene solutions: their origins and their implications on physical gelation." *Makromolekulare Chemie, Macromolecular Symposia*, 39, 85.

Guerra, G., Musto, P., Karasz, F. E. and Macknight, W. J. (1990). "Fourier-transform infrared-spectroscopy of the polymorphic forms of syndiotactic polystyrene." *Macromolecular Chemistry and Physics*, 191, 2111.

Guerra, G., Vitagliano, V. M., De Rosa, C., Petraccone, V. and Corradini, P. (1990). "Polymorphism in melt crystallized syndiotactic polystyrene samples." *Macromolecules*, 23, 1539.

Guerrero, S. J., Keller, A., Soni, P. L. and Geil, P. H. (1980). " Study of crystal texture in

PVC gels by x-ray diffraction and infrared dichroism." *Journal of Polymer Science, Polymer Physics Edition*, 18, (7), 1533.

Handa, P. Y., Zhang, Z. and Wong, B. (1997). "Effect of compressed CO_2 on phase transitions and polymorphism in syndiotactic polystyrene." *Macromolecules*, 30, 8499.

Hasegawa, R., Tanabe, Y., Kobayashi, M., Tadokoro, M., Sawaoka, A. and Kawai, N. (1970). "Structural studies of pressure-crystallized polymers. I. Heat treatment of oriented polymers under high pressure." *Journal of Polymer Science Part A-2: Polymer Physics*, 8, 1073.

Hashimoto, T. (1992). Self-assembly of polymer blends at phase separation morphology control by spinning of domain growth. *Progress in Pacific Polymer Science*. 175 Y. Imanishi. Berlin, Springer**:** 175.

Hashimoto, T., Itakura, M. and Hasegawa, H. (1986). "Late stage spinodal decomposition of a binary polymer mixture. I. critical test of dynamical scaling on scattering function." *J. Chem. Phys*, 85, 6118.

Hashimoto, T., Itakura, M. and Hasegawa, H. (1986). "Late stage spinodal decomposition of a binary polymer mixture. II. Scaling analysis on $Q_m(\tau)$ and $I_m(\tau)$." *J. Chem. Phys*, 85, 6773.

Hashimoto, T., Kumaki, J. and Kawai, H. (1983). "Time-resolved light scattering studies on kinetics of phase separation and phase dissolution of polymer blends. 1. Kinetics of phase separation of a binary mixture of polystyrene and poly(vinyl methyl ether)." *Macromolecules*, 16, (4), 641.

Hatanaka, M. and Saito, H. (2004). "In-situ investigation of liquid-liquid phase separation in polycarbonate/carbon dioxide system." *Macromolecules*, 37, 7358.

Henderson, I. C. and Clarke, N. (2004). "Two-Step Phase Separation in Polymer Blends. Macromolecules." *Macromolecules*, 37, (5), 1952.

Hikmet, R. M., Callister, S. and Keller, A. (1988). "Thermoreversible gelation of atactic polystyrene: phase transformation and morphology." *Polymer*, 29, (8), 1378.

Hikosaka, M. and Seto, T. (1973). "Order of the molecular chains in isotactic polypropylene crystals. ." *Polymer Journal*, 5, 111.

Holland, V. F. and Miller, R. L. (1964). "Isotactic poly-1-butene single crystals: morphology." *Journal of Applied Physics*, 35, 3241.

Immirzi, A., De Candia, F., Iannelli, P., Zambelli, A. and Vittoria, V. (1988).

"Solvent-induced polymorphism in syndiotactic polystyrene." *Makromolekulare Chemie, Rapid Communications*, 9, 761.

Ishihara, N., Kuramoto, M. and Uoi, M. (1988). "Stereospecific polymerization of styrene giving the syndiotactic polymer." *Macromolecules*, 21, 3356

Ishihara, N., Seimiya, T., Kuramoto, M. and Uoi, M. (1986). "Crystalline syndiotactic polystyrene." *Macromolecules*, 19, 2464.

Kamer, P. C. J., van Rooy, A., Schoemaker, G. C. and Van Leeuwen, P. W. N. M. (2004). "in situ mechaistic studies in rhodium catalyzed hydroformylation of alkenes." *Coordination Chemsitry Reviews*, 248, 2409.

Kanaya, H., Hara, K., Okabe, H., Taki, S., Matsushige, K., Nishimuta, S. and Muguruma, M. (1993). "Optical measurements during gelation process of muscle protein under high pressure." *Journal of the Physical Society of Japan*, 62, (1), 362.

Kaszonyiova, M., Rybnikar, F. and Geil, P. H. (2005). "Polymorphism of isotactic poly(butene-1)." *Journal of Macromolecular Science, Part B: Physics* 44, 377.

Kawanishi, K., Takeda, Y. and Inoue, T. (1986). "The sol-gel transition and the liquid-liquid phase separation in poly(vinyl chloride) solutions. ." *Polymer Journal* 18, (5), 411.

Keith, H. D., Padden, F. J., Jr., Walter, N. M. and Wyckoff, H. W. (1959). "Evidence for a second crystal form of polypropylene." *Journal of Applied Physics*, 30, 1485.

Keller, A. (1979). "Networks and crystallinity." *Polymer*, 20, (11), 1371.

Keller, A. (1995). "Aspects of polymer gels." *Faraday Discuss*, 101, 1.

Kennedy, K. A., Roberts, G. W. and DeSimone, J. M. (2005). "Heterogeneous polymerization of fluoroolefins in supercritical carbon dioxide." A*dvances in Polymer Science*, 175, 329.

Kim, S. S. and Lloyd, D. R. (1991). "Microporous membrane formation via thermally induced phase separation. III. Effect of thermodynamic interactions on the structure of isotactic polypropylene membranes." *Journal of Membrane Science* 64, (1-2), 13.

Kiran, E. (1994). Polymer formation, modification and processing in or with supercritical fluids. *Supercritical Fluids*. 541 E. Kiran and J. M. H. Levelt Sengers. Dordrecht, The Netherlands, Kluwer Academic Publishers**:** 541.

Kiran, E. (2000). *Polymer miscibility and kinetics of pressure-induced phase separation in near-critical and supercritical fluids*. Dordrecht, Kluwer.

Kiran, E. and Liu, K. (2002). "The miscibility and phase behavior of polyethylene with poly(dimethylsiloxane) in near critical pentane." *Korean Journal of Chemical Engineering*, 19, 153.

Kiran, E., Zhuang, W. and Sen, Y. L. (1993). "Solubility and demixing of polyethylene in supercritical binary fluid mixtures: carbon dioxide-cyclohexane, carbon dioxide-toluene, carbon dioxide-pentane." *Journal of Applied Polymer Science*, 47, (5), 895.

Kirby, C. F. and Mchugh, M. A. (1999). "Phase behavior of polymers in supercritical fluid solvents." *Chem. Rev.*, 99, 565.

Kitts, C. C. and Vanden Bout, D. A. (2007). "The effect of solvent quality on the chain morphology in solutions of poly(9,9'-dioctylfluorene)." *Polymer*, 48, 2322.

Klein, M. and Guenet, J. M. (1989). "Effect of polymer chain microstructure on solvent crystallization: implications on polymer solvation and on physical gelation." *Macromolecules*, 22, (9), 3716.

Knez, Z. and Weidner, E. (2003). "Particles formation and particle design using supercritical fluids." *Current Opinion in Solid State & Materials Science*, 7, (4-5), 353.

Kobayashi, M., Nakaoki, T. and Ishihara, N. (1989). "Polymorphic structures and molecular vibrations of syndiotactic polystyrene." *Macromolecules*, 22, 4377.

Kojima, J., Takenaka, M., Kakayama, Y. and Hashimoto, T. (1999). "Early stage spinodal decomposition in polymer solution under high pressure." *Macromolecules*, 32, 1809.

Koningsveld, R. and Stockmayer, W. H. (2001). *Polymer phase diagrams: a textbook*. Oxford, Oxford University Press.

Kusanagi, H., Takase, M., Chatani, Y. and Tadokoro, H. (1978). "Crystal structure of isotactic poly(4-methly-1-pentene)." *Journal of Polymer Science, Polymer Physics Edition*, 16, 131.

Kuwahara, N., Tachikawa, M., Hamano, K. and Kenmochi, Y. (1982). "Phase separation in an unstable system polydimethylsiloxane-diethyl carbonate." *Phys Rev A*, 35, 3449.

Lal, J. and Bansil, R. (1991). "Light-scattering study of kinetics of spinodal decomposition in a polymer solution." *Macromolecules*, 24, 290.

Lando, J. B., Olf, H. G. and Peterlin, A. (1966). "Nuclear magnetic resonance and x-ray determination of the structure of poly(vinylidene fluoride). ." *Journal of Polymer Science, Part A-1: Polymer Chemistry*, 4, (4), 941.

Langer, L. S. (1971). "Theory of spinodal decomposition in alloys." *Ann. Phys.*, 65, 53.

Langer, L. S., Bar-on, M. and Miller, H. D. (1975). "New computational method in theory of spinodal decomposition." *Phys. Rev. A*, 11, 1417.

Laxminarayan, A., McGuire, K. S., Kim, S. S. and Lloyd, D. R. (1994). "Effect of initial composition, phase separation temperature and polymer crystallization on the formation of microcellular structures via thermally induced phase separation." *Polymer*, 35, (14), 3060.

Lee, H. J., Jung, B., Kang, Y. S. and Lee, H. (2004). "Phase separation of polymer casting solution by nonsolvent vapor." *J Membr Sci*, 245, 103.

Lee, K. D., Chan, P. K. and Feng, X. S. (2004). "Morphology development and characterization of the phase-separated structure resulting from the thermal-induced phase separation phenomenon in polymer solutions under a temperature gradient." *Chem Eng Sci*, 59, 1491.

Lemstra, P. J. and Challa, G. (1975). "Crystallization of isotactic polystyrene for dilute solutions." *J. Polym. Sci., Polym. Phys. Ed*, 13, 1809.

Lemstra, P. J., Keller, A. and Cudby, M. (1978). "Gelation crystallization of poly(vinyl chloride)." *Journal of Polymer Science, Polymer Physics Edition* 16, (8), 1507.

Leugering, H. J. and Kirsch, G. (1973). "Effect of crystallization from oriented melts on crystal structure of isotactic polypropylene." *Angewandte Makromolekulare Chemie*, 33, 17.

Li, D., Krantz, W. B., Greensberg, A. R. and Sani, R. L. (2006). "Membrane formation via thermally induced phase separation (TIPS): Model development and validation." *Journal of Membrane Science*, 279, 50.

Li, J. X. and Cheung, W. L. (1999). "Conversion of growth and recrystallization of β-phase in doped iPP." *Polymer*, 40, 2085.

Li, Y. and Xue, G. (1998). "Molecular conformation of syndiotactic polystyrene gel from octadecyl benzoate solution." *Macromolecular Rapid Communications*, 19, 549.

Liao, X., He, J., Zhang, J. and Ma, W. (2007). "Effect of cosolvent on solid phase transition of α to β-form crystal of syndiotactic polystyrene occured in supercritical CO_2 containing solvent." *Journal of Polymer Science: Part B: Polymer Physics*, 45, 1625.

Liu, K. and Kiran, E. (1999). "Kinetics of pressure-induced phase separation(PIPS) in solution of polydimethylsiloxane in supercritical carbon dioxide; crossover from nucleation and growth to spinodal decomposition mechanism." *J Supercrit Fluid*, 16, 59.

Liu, K. and Kiran, E. (2001). "Pressure-induced phase separation in polymer solutions: kinetics of separation and crossover form nucleation and growth to spinodal decomposition in solution of polyethylene in n-pentane." *Macromolecules*, 34, 3060.

Liu, K. and Kiran, E. (2007). "A tunable mixture solvent for poly(ε-caprolactone): acetone + CO_2." *Polymer*, 48, 5612.

Liu, K. and Kiran, E. (2007). "Viscosity, density and excess volume of acetone + carbon dioxide mixtures at high pressures." *Industrial & Engineering Chemistry Research*, 46, (16), 5453.

Lloyd, D. J. (1926). *Colloid Chemistry*. New York, Chemical Catalog Company.

Lloyd, D. R., Kim, S. S. and Kinzer, K. E. (1991). "Microporous membrane formation via thermally induced phase separation. II. Liquid-liquid phase separation." *Journal of Membrane Science*, 64, (1-2), 1.

Lloyd, D. R., Kinzer, K. E. and Tseng, H. S. (1990). "Microporous membrane formation via thermally induced phase separation. I. Solid-liquid phase separation." *Journal of Membrane Science*, 52, (3), 239.

Lopez, L. C., Wilkes, G. L., Stricklen, P. M. and White, S. A. (1992). "Synthesis, structure, and properties of poly(4-Methyl-1-pentene)." *J. Macromol. Sci.-Rev. Macromol. Chem. Phys.*, C32, 301.

Lotz, B. and Thierry, A. (2003). "Spherulite morphology of form III isotactic poly(1-butene)." *Macromolecules*, 26, 286.

Lotz, B., Wittmann, J. C. and Lovinger, A. J. (1996). "Structure and morphology of polypropylene: a molecular analysis." *Polymer*, 37, 4979.

Lovinger, A. J. (1981). "Unit cell of the γ phase of poly(vinylidene fluoride)." *Macromolecules*, 14, 322.

Lovinger, A. J. (1983). "Ferroelectric polymers." *Science*, 220, 1115.

Lovinger, A. J., Chua, J. O. and Gryte, C. C. (1977). "Studies on the a and b forms of isotactic polypropylene by crystallization in a temperature gradient." *Journal of Polymer Science, Polymer Physics Edition*, 15, 641.

Luszczyk, M., Rebelo, L. P. N. and Van Hook, W. A. (1996). "Isotope and pressure dependence of liquid-liquid equilibria in polymer solutions. 5. Measurements of solute and solvent isotope effects in polystyrene-acetone and polystyrene-methylcyclopentane. 6. A continuous polydisperse thermodynamic interpretation of demixing measurements in

polystyrene-acetone and polystyrene-methylcyclopentane solutions. ." *Macromolecules*, 28, (3), 745.

Ma, W., Yu, J. and He, J. (2004). "Direct Formation of γ form crystal of syndiotactic polystyrene from amorphous state in supercritical CO_2." *Macromolecules*, 37, 6912.

Madbouly, S. A. and Ougizawa, T. (2004). "Isothermal crystallization of poly(.epsilon.-caprolactone) in blends with poly(styrene-co-acrylonitrile): Influence of phase separation process." *Macromolecular Chemistry and Physics* 205, (14), 1923.

Malanga, M. (2000). "Syndiotactic Polystyrene Materials." *Advanced Materials*, 12, 1869.

Manfredi, C., De Rosa, C., Guerra, G., Rapacciuolo, M., Auriemma, F. and Corradini, P. (1995). "Structural changes induced by thermal treatments on emptied and filled clathrates of syndiotactic polystyrene." *Macromolecular Chemistry and Physics*, 196, 2795

Mencik, Z. (1972). "Crystal structure of isotactic polypropylene." *Journal of Macromolecular Science, Physics* 6, 101.

Mollart, T. P., Lewis, K. L., Pickles, C. S. and Wort, C. J. H. (2003). "Factors affecting the optical performance of CVD diamond infrared optics." *Semiconductor Science and Technology*, 18, S117.

Morrow, D. R. and Newman, B. A. (1968). "Crystallization of low-molecular-weight polypropylene fractions." *Journal of Applied Physics*, 39, (11), 4944.

Moyses, S. and Spells, S. J. (1999). "Conformationally sensitive infrared vibrations of the syndiotactic polystyrene/ethylbenzene complex." *Macromolecules*, 32, 2684.

Mutin, P. H. and Guenet, J. M. (1986). "Physical gels from PVC: a light-scattering investigation of dilute solutions." *Polymer*, 27, (7), 1098.

Mutin, P. H., Guenet, J. M., Hirsch, E. and Candau, S. J. (1988). "Physical gels from poly(vinyl chloride): behavior with concentration and temperature of aggregates formed in dilute solutions." *Polymer*, 29, (1), 30.

Natta, G. and Corradini, P. (1955). "Crystal structure of isotactic polystyrenes." *Makromolekulare Chemie*, 16, 77.

Natta, G. and Corradini, P. (1960). "Structure and properties of isotactic polypropylene." *Nuovo Cimento*, 15, (1), 40.

Petraccone, V., Ruiz de Ballesteros, O., Tarallo, O., Rizzo, P. and Guerra, G. (2008). "Nanoporous polymer crystals with cavities and channels." *Chemistry of Materials*, 20,

(11), 3663.

Petraccone, V., Tarallo, O., Venditto, V. and Guerra, G. (2005). "An intercalate molecular complex of syndiotactic polystyrene." *Macromolecules* 38, (16), 6965.

Phillips, P. J. and Mezghani, K. (1996). Polymorphism in isotactic polypropylene. *The polymeric materials encyclopedia: synthesis, properties and applications*. CRC press**:** 6637.

Phung-Nguyen, H. and Delmas, G. (1985). "Heat of formation of poly(4-methylpentene-1) gels." *Macromolecules*, 18, 1235.

Point, J. J. and Coutelier, C. (1985). "Linear high polymers as host in intercalates. Introduction and example." *J. Polym. Sci., Polym. Phys. Ed*, 23, 231.

Pradhan, D. and Ehrlich, P. (1995). "Morphologies of microporous polyethylene and polypropylene crystallized from solution in supercritical propane. ." *Journal of Polymer Science, Part B: Polymer Physics*, 33, (7), 1053.

Rapacciuolo, M., De Rosa, C., Guerra, G., Mensitieri, G., Apicella, A. and Del Nobile, M. A. (1991). "Different solvent stability of the crystalline polymorphic forms of syndiotactic polystyrene." *Journal of Materials Science Letters*, 10, 1084.

Rappl, T. J. and Balsara, N. P. (2005). "Does coarsening begin during the initial stages of spinodal decomposition?" *Journal of Chemical Physics*, 122, (21), 214903/1.

Rastogi, S., Goossens, J. G. P. and lemstra, P. J. (1998). "An in situ SAXS/WAXS/Raman spectroscopy study on the phase behavior of syndiotactic polystyrene (sPS)/solvent systems: compound formation and solvent (dis)ordering." *Macromolecules*, 31, 2983.

Ray, B., Elhasri, S., Thierry, A., Marie, P. and Guenet, J.-M. (2002). "Solvent-induced crystallization of syndiotactic polystyrene: thermodynamics and morphology." *Macromolecules*, 35, 9730.

Reynolds, N. M., Savage, J. D. and Hsu, S. L. (1989). "A spectroscopic study of syndiotactic polystyrene." *Macromolecules*, 22, 2867.

Rigby, W., WHyman, R. and Wilding, K. (1970). "A high pressure spectrophotometric cell." *J. Phys. E; Sci. Intrum.* , 2, 572.

Rizzo, P., Albunia, A. R. and Guerra, G. (2005). "Polymorphism of syndiotactic polystyrene: γ phase crystallization induced by bulky non-guest solvents." *polymer*, 46, 9549.

Rizzo, P., Daniel, C., De Girolamo Del Mauro, A. and Guerra, G. (2007). "New host

polymeric framework and related polar guest cocrystals." *Chemistry of Materials*, 19, 3864.

Rizzo, P., Lamberti, M., Albunia, A. R., Ruiz de Ballesteros, O. and Guerra, G. (2002). "Crystalline Orientation in Syndiotactic Polystyrene Cast Films." *Macromolecules*, 35, (15), 5854.

Roels, T., Deberdt, F. and Berghmans, H. (1994). "Solvent quality and phase stability in syndiotactic polystyrene-solvent systems." *Macromolecules*, 27, 6216.

Roels, T., Rastogi, S., De Rudder, J. and Berghmans, H. (1997). "Temperature induced structure changes in syndiotactic polystyrene/cis-decalin systems." *Macromolecules*, 30, 7939.

Saiani, A. and Guenet, J. M. (1997). "On the helical form in syndiotactic poly(methyl methacrylate) thermoreversible gels as revealed by small-angle neutron scattering." *Macromolecules* 30, 966.

Schaefer, J. and Stejskal, E. O. (1976). "Carbon-13 Nuclear Magnetic Resonance of Polymers Spinning at the Magic Angle." *J. Am. Chem. Soc.*, 98, 1031.

Siggia, E. D. (1979). "Late stages of spinodal decomposition in binary mixtures." *Phys. Rev. A*, 20, 595.

Siow, K. S., Delmas, G. and Patterson, D. (1972). "Cloud-point curves in polymer solutions with adjacent upper and lower critical solution temperatures." *Macromolecules*, 5, (1), 29.

Stehling, F. C., Ergos, E. and Mandelkern, L. (1971). "Phase separation in n-hexatriacontane-n-hexatriacontane-d_{74} and polyethylene-poly(ethylene-d4) systems." *Macromolecules*, 4, 672.

Sundararajan, P. R., Tyrer, N. J. and Bluhm, T. L. (1982). "Solvent-dependent conformations in gels of isotactic polystyrene." *Macromolecules*, 15, 286.

Szydlowski, J., Rebelo, L. P. and Van Hook, W. A. (1992). "A new apparatus for the detection of phase equilibria in polymer solvent systems by light scattering." *Review of Scientific Instruments*, 63, (2), 1717.

Szydlowski, J. and Van Hook, W. A. (1991). "Isotope and pressure effects on liquid-liquid equilibria in polymer solutions: H/D solvent isotope effects in acetone-polystyrene solutions." *Macromolecules*, 24, (17), 4883.

Tai, H., Wang, W. and Howdle, S. M. (2005). "Copolymerization of vinylidene fluoride and hexafluoropropylene in supercritical carbon dioxide." *Macromolecules*, 38, (22), 9135.

Takayanagi, M. and Kawasaki, N. (1967). "Mechanical relaxation of poly(4-methyl-1-pentene) at cryogenic temperatures." *Journal of Macromolecular Science, Physics* B1, 741.

Takenaka, M., Kojima, J., Nakayama, Y. and Hashimoto, T. (2005). "Later-stage spinodal decomposition in polymer solution under high pressure - analyses of q_m and I_m." *Polymer*, 46, 10782.

Tan, H., Moet, A., Hiltner, A. and Baer, E. (1983). "Thermoreversible gelation of atactic polystyrene solutions." *Macromolecules*, 16, (1), 28.

Tang, P., Arrighi, V., Higgins, J. S. and Li, G. X. (2004). "Kinetics of phase separation of poly(styrene-co-methyl methacrylate) and poly(styrene-co-acrylonitrile) blends. ." *Polymer International* 53, (11), 1686.

Tanigami, T., Suzuki, H., Yamaura, K. and Matsuzawa, S. (1985). "Gelation and crystallization of poly(4-methyl-1-pentene) in cyclohexane solution." *Macromolecules*, 18, 2595.

te Nijenhuis, K. (1997). "Thermoreversible Networks." *Advances in Polymer Science*, 130, 1.

te Nijenhuis, K. (1997). "Thermoreversible networks: viscoelastic properties and structure of gels." *Adances in Polymer Science*, 130, 1.

Teramoto, G., Takafumi, O., Hiromu, S., Hironari, S. and Fujita, Y. (2004). "Morphology control of polypropylene by crystallization under carbon dioxide." *journal of Polymer Science, Part B: Polymer Physics*, 42, 2738.

Turner-Jones, A. (1963). "Poly-1-butylene type II crystalline form." *Journal of Polymer Science, Part B: Polymer Letters*, 1, 455.

Upper, G., Zhang, W., Beckel, D., Sohn, S., Liu, K. and Kiran, E. (2006). "High pressure crystallization of polyethylene in n-pentane and n-pentane + carbon dioxide fluid mixture." *Industrial & Engineering Chemistry-Research*, (in press),

Utracki, L. A. (1994). Thermodynamics and kinetics of phase separation. . *Interpenetrating polymer networks advances in chemistry*. 77 D. Klempner, L. H. Sperling and L. A. Utracki. Washington DC, American Chemical Society. **239:** 77.

van de Witte, P., Dijkstra, P. J., van den Berg, J. W. A. and Feijen, J. (1996). "Phase separation processes in polymer solutions in relation to membrane formation." *Journal of Membrane Science*, 117, (1-2), 1.

Van den Broecke, P. and Berghmans, H. (1990). "Thermoreversible gelation of solutions of vinyl polymers." *Makromolekulare Chemie, Macromolecular Symposia*, 39, 59.

Vittoria, V., De Candia, F., Iannelli, P. and Immirzi, A. (1988). "Solvent-induced crystallization of glassy syndiotactic polystyrene." *Makromolekulare Chemie, Rapid Communications*, 9, 765.

Vossoughi, S. (2000). "Profile modification using in situ gelation technology - a review. ." *Journal of Petroleum Science & Engineering*, 26, (1-4), 199.

Wegsteen, K. and Berghmans, H. (1998). "Phase behavior and structure formation in solutions of poly(4-methyl-1-pentene) in cyclohexane." *Macromolecular Chemistry and Physics*, 199, 267.

Weidner, E., Wiesmet, V., Knze, Z. and Skerget, M. (1997). "Phase Equilibrium (Solid-Liquid-Gas) in Polyethyleneglycol-Carbon Dioxide Systems." *J Supercritical Fluids*, 12, 139.

Weinhold, S., Litt, M. H. and Lando, J. B. (1980). "The crystal structure of the γ phase of poly(vinylidene fluoride)." *Macromolecules*, 13, 1178.

Wellinghoff, S., Shaw, J. and Baer, E. (1979). "Polymeric materials from the gel state. The development of fringed micelle structure in a glass." *Macromolecules*, 12, (5), 932.

Winter, H. H., Gappert, G. and Ito, H. (2002). "Rigid pore structure from highly swollen polymer gels." *Macromolecules* 35, (9), 3325.

Xie, X.-M., Tanioka, A. and Miyasaka, K. (1998). "Thermoreversible gelation mechanism of polystyrene/CS_2 solutions." *Polymer Journal*, 30, (5), 435.

Xie, X. M., Tanioka, A. and Miyasaka, K. (1990). "Study on the gelation rate of atactic polystyrene/carbon disulfide solutions." *Polymer*, 31, (2), 281.

Xie, X. M., Tanioka, A. and Miyasaka, K. (1993). "Fourier transform infrared spectroscopic studies of gelation and crystallization of polystyrene/carbon disulfide solutions." *Polymer*, 34, (7), 1388.

Xiong, Y. (1998). Kinetics of pressure-induced phase separation in polymer solutions: a time- and angle-resolved light scattering study, University of Maine. PH.D. Thesis.

Xiong, Y. and Kiran, E. (1998). "High-pressure light scattering apparatus to study pressure-induced phase separation in polymer solutions." *Rev. Sci. Instrum.*, 69, 1463.

Xiong, Y. and Kiran, E. (2000). "Kinetics of pressure-induced phase separation (PIPS) in

polystyrene + methycyclohexane solutions at high pressure." *Polymer*, 41, 3759.

Xu, Z., Kapoor, P. N. and Butler, I. S. (2006). "Pressure-tuning infrared and Raman spectra of trans-dichloro-bis[(diperfluoroethyl)phenylphosphine]platinum(II), trans-Pt[PPh(CF_3CF_2)$_2$]$_2$$Cl_2$." *Inorganica Chimica Acta*, 359, 4121.

Yang, Y. C. and Geil, P. H. (1983). "Morphology and properties of PVC/solvent gels." *Journal of Macromolecular Science, Physics*, B22, (3), 463.

Yave, W., Quijada, R., Ulbricht, M. and Benavente, R. (2005). "Syndiotactic polypropylene as potential material for the preparation of porous membranes via thermally induced phase separation (TIPS) process." *Polymer*, 46, 11582.

Yeo, S.-D. and Kiran, E. (2004). "Copolymerization of acrylonitrile with methyl methacrylate and 2-chlorostyrene in supercritical CO_2." *Macromolecules*, 37, (22), 8239.

Yeo, S.-D. and Kiran, E. (2005). "Formation of polymer particles with supercritical fluids: A review." *Journal of Supercritical Fluids*, 34, (3), 287.

Yoshioka, A. and Tashiro, K. (2003). "Infrared bands sensitive to the chain packing mode in crystalline δ, δ_e, and γ forms of syndiotactic polystyrene." *Macromolecules*, 36, 3001.

Zambelli, A., Longo, P., Pellecchia, C. and Grassi, A. (1987). "β-Hydrogen abstraction and regiospecific insertion in syndiotactic polymerization of styrene." *Macromolecules*, 20, 2035.

Zeman, L. and Patterson, D. (1972). "Pressure effects in polymer solution phase equilibriums. II. Systems showing upper and low critical solution temperatures." *Journal of Physical Chemistry*, 76, (8), 1214.

Zhang, W., Dindar, C., Bayraktar, Z. and Kiran, E. (2003). "Phase behavior, density, and crystallization of polyethlyene in n-pentane and n-pentane/CO_2 at high pressures." *Journal of Applied Polymer Science*, 89, 2201.

Zhang, W. and Kiran, E. (2006). "High-pressure crystallization and melting of polyethylene in n-pentane." *Journal of Supercritical Fluids*, 38, 406.

Appendix A

Data Tables of the Phase Behavior

The numerical data on the phase boundaries of syndiotactic polystyrene in toluene and toluene + CO_2, acetophenone and acetophenone + CO_2 at high pressures are included in this section. The numerical data on the phase boundaries of P4MP1 in n-pentane and n-pentane + CO_2 has been presented in Table 4.1 and 4.2. Table A.1 gives the experimental data for sol-gel phase boundaries of sPS in toluene. Table A.2 gives the experimental data for sol-gel or solid-fluid phase boundaries of sPS in toluene + CO_2. Table A.3 presents the experimental data for liquid-liquid phase boundaries of sPS in toluene + CO_2. Table A.4 gives the experimental data for sol-gel phase boundary of 4.8 wt % sPS in acetophenone. Table A.5 and A.6 present the experimental data for sol-gel or solid-fluid phase boundaries and liquid-liquid phase boundaries of sPS in acetophenone + CO_2 respectively.

Table A.1 Experimental data for sol-gel phase separation in syndiotactic polystyrene in toluene solutions.

Polymer Fraction (wt %)	Pressure (MPa)	Gelation T (K)	Dissolution T (K)
1.6	44.5	345.0	389.0
	37.0	343.0	386.5
	29.5	341.5	385.0
	22.0	339.0	382.0
	14.5	336.5	377.5
	6.9	332.0	371.0
2.8	44.5	347.5	391.0
	37.0	345.0	389.0
	29.5	343.5	387.0
	22.0	341.0	384.0
	14.5	338.5	380.0
	6.9	335.5	375.0
4.8	44.5	351.0	393.0
	37.0	348.5	391.5
	29.5	346.5	389.5
	22.0	343.0	386.0
	14.5	341.0	382.0
	6.9	339.0	378.0
12.6	44.5	356.0	398.0
	37.0	354.0	396.0
	29.5	353.0	393.0
	22.0	351.0	390.0
	14.5	348.5	387.5
	6.9	346.5	386.0
25.0	44.5	369.5	412.0
	37.0	367.5	410.0
	29.5	366.0	407.5
	22.0	362.5	403.0
	14.5	360.0	400.0
	6.9	357.5	398.5

Table A.2 Experimental data for gel-sol or solid-fluid transition temperatures in ~ 4.8 wt % syndiotactic polystyrene in toluene + CO_2 solutions with different CO_2 contents.

CO_2 in Fluid Mixture (wt %)	Pressure (MPa)	Gel-Sol Transition	
		Gelation T (K)	Dissolution T (K)
16	44.5	341.0	389.0
	37.0	340.5	388.0
	29.5	339.0	387.0
	22.0	338.0	387.0
	14.5	336.5	386.5
	6.9	336.0	386.0
28	44.5	346.0	399.0
	37.0	347.0	398.0
	29.5	347.0	398.0
	22.0	348.0	400.0
		Solid-Fluid Transition	
		Crystallization T (K)	Melting T (K)
43	52.0	380.0	411.0
	48.5	381.0	422.0

Table A.3 Experimental data for liquid-liquid transition temperatures in ~ 4.8 wt % syndiotactic polystyrene in toluene + CO_2 with different CO_2 contents.

CO_2 in Fluid Mixture (wt %)	Liquid-Liquid Transition	
	Pressure (MPa)	Temperature (K)
28	23.1	430.0
	22.9	426.5
	21.0	418.3
	19.5	412.8
	18.8	408.6
	17.3	403.6
	16.4	397.8
	14.0	393.0
43	49.8	437.3
	48.6	434.0
	48.0	429.1
	47.0	426.0
	46.7	421.4
	46.0	417.9
	45.0	413.8

Table A.4 Experimental data for sol-gel phase separation in syndiotactic polystyrene in acetophenone solutions.

Polymer Fraction (wt %)	Pressure (MPa)	Gelation T (K)		Dissolution T (K)
		T_1	T_2	
4.8	44.5	382	348	405
	37.0	380	346	400
	29.5	380	344	398
	22.0	376	343	396
	14.5	375	340	394
	6.9	373	337.5	392

Table A.5 Experimental data for gel-sol or solid-fluid transition temperatures in ~ 4.8 wt % syndiotactic polystyrene in acetophenone + CO_2 solutions with different CO_2 contents.

CO_2 in Fluid Mixture (wt %)	Pressure (MPa)	Gel-Sol Transition	
		Gelation T (K)	Dissolution T (K)
25	44.5	372.0	400.0
	37.0	374.0	403.0
	29.5	376.0	407.5
	22.0	380.0	412.0
		Solid-Fluid Transition	
		Crystallization T (K)	Melting T (K)
40	55.6	394.0	431.0
	51.8	397.0	433.0
	48.2	399.5	435.5
	46.0	399.7	435.5

Table A.6 Experimental data for liquid-liquid transition temperatures in ~ 4.8 wt % syndiotactic polystyrene in acetophenone + CO_2 with different CO_2 contents.

CO_2 in Fluid Mixture (wt %)	Liquid-Liquid Transition	
	Pressure (MPa)	Temperature (K)
25	17.0	411.4
	17.1	413.2
	17.5	416.9
	18.1	419.8
	18.2	423.6
	18.1	424.3
	18.4	427.0
	18.7	430.3
	18.9	433.1
	19.2	436.1
	19.4	439.0
	19.6	442.3
40	41.9	424.3
	42.2	428.0
	42.8	430.6
	43.2	433.4
	43.8	439.8
	44.4	445.0
	45.2	450.4
	45.6	452.8